공학박사 학위논문

Shear Strength of Ultra-High Performance Fiber Reinforced Concrete I-shaped Beams

강섬유 보강 초고성능 콘크리트 I형 보의 전단 강도

2017 년 8 월

서울대학교 대학원

건축학과

이 지 형

Shear Strength of Ultra-High Performance Fiber Reinforced Concrete I-shaped Beams

지도 교수 홍 성 걸

이 논문을 공학박사 학위논문으로 제출함
2017 년 8 월

서울대학교 대학원
건축학과
이 지 형

이지형의 공학박사 학위논문을 인준함
2017 년 8 월

위 원 장 _____ (인)

부위원장 _____ (인)

위 원 _____ (인)

위 원 _____ (인)

위 원 _____ (인)

Abstract

Shear Strength of Ultra-High Performance Fiber Reinforced Concrete I-shaped Beams

Lee, Ji-Hyung
Department of Architecture and Architectural Engineering
College of Engineering
Seoul National University

Ultra-High Performance Fiber Reinforced Concrete (UHPFRC) shows outstanding durability and workability as well as remarkable mechanical properties. High durability and tensile strength make it possible for the UHPFRC structure being thin and diverse shape of structures with none or much less reinforced rebars. In order to take the advantages, there is a great need to study the in-plane shear behavior without reinforcement. In this study, shear strength of UHPFRC I-shaped beams without stirrups is suggested based on the theoretical and experimental studies.

Existing results indicates that the stress redistribution capacity of UHPFRC in thin web is manifested replacing the traditional reinforced rebar. The shear capacity of UHPFRC beam has been identified as depending on tensile behavior with respect to its post-cracking characteristics. The current recommendations for UHPFRC suggest that shear design strength of UHPFRC is a summation of matrix contribution and fiber contribution. The post-cracking

behavior gives shear strength by fiber contribution and the traditional shear strength for ordinary concrete beams without stirrups is regarded as same as the strength due to matrix contribution. The dominant failure in UHPFRC I-shaped beam without stirrup is found as diagonal crack localization in web.

Shear behavior of UHPFRC I-shaped beam shows the contradictory points. One is that a large range of stress redistribution area comparable to RC beam with stirrup is induced by micro-cracking action. However the final failure occurs abruptly at one opening crack among the dispersed micro cracks while the other cracks close with its own resilience. The diagonal tension failure due to crack localization followed by micro-cracking with a strength increase in a visible region is defined as "Semi-Brittle Fracture" in the frame work of plastic limit analysis and fracture mechanics. Plastic limit analysis gives a solution for the maximum strength determined by UHPFRC failure criterion and fracture mechanics explains the diagonal tension failure with respect to size effect.

Limit analysis and fracture mechanics are adopted to analyze the UHPFRC I-shaped shear beam without stirrup with diagonal tension failure in web. The diagonal tension failure can be defined by semi-brittle fracture composed by a stable strength increase with wide micro-cracking area and a final crack localization. The strength increase due to micro-cracking behavior can be analyzed by limit analysis and the crack localization should be interpreted in terms of concrete fracture mechanics. General assumptions and the major concerns for each methodology is introduced at first. Overview and applications for each approach is identified and compared with respect to pro and cons for UHPFRC shear design. Once the material model for cracked UHPFRC is suggested, a physical model for UHPFRC in-plane elements subjected to shear can be proposed.

Experimental investigations of UHPFRC material characteristics include various type of tensile strength tests, direct shear tests (or push-off tests) on monolithic specimens, biaxial tension-compression strength test on reinforced

panels and 3-point bending test on off-center notched prisms. Several types of tensile strength tests on UHPFRC are performed to define the effective tensile strength and fracture properties such as material characteristic length and fracture energy, and then the simplified UHPFRC tensile behavior with hardening part is suggested. Mohr-Coulomb failure criterion of UHPFRC is established by the friction angle and the effectiveness factor based on push-off test and biaxial panel test.

In the application of the shear strength evaluation, the hardening behavior is analyzed by variable angle truss analogy in limit analysis and the brittleness due to cracking localization is considered by size effect using fracture mechanics. Fiber reinforcement effect is taken into account for Mohr-Coulomb failure criterion with frictional angle. Splitting cracked zone is assumed as a uniform stress field, Rankine zone, of damaged zone with a constant stiffness. The plastic limit analysis gives the lower bound solution for the minimum value of the inclination angle in cracking zone. Size effect in shear beam is suggested by different modelling approaches from a new point of view based on fracture mechanics. Suggested brittleness factor at material level from the ratio of energy release rate is converted into a new brittleness factor at structural level for stress redistribution zone in shear beam. The brittleness factor may explain the size effect of uniform stress field in shear beam. The characteristic length of emerging splitting cracks and the inclination angle of the stress redistribution region of splitting cracks are considered as main parameters for determination of shear strength of UHPFRC I-shaped beams without stirrups. The suggested equation is verified with test results including previous studies.

Keywords : UHPFRC, shear strength, semi-brittle fracture, limit analysis, fracture mechanics, size effect

Student Number : 2012-30151

Contents

List of Tables

List of Figures

Chapter 1. Introduction

1.1 General of UHPFRC

Concrete is the most frequently and easily used building material. However concrete structures have several disadvantages, low tensile strength, high self-weight and maintenance cost. Reinforced concrete structures are designed with the resisting combination of tensile forces on reinforced steel and compressive forces on concrete. The cracking in concrete induces corrosion of reinforced steel and shortening life cycle of the existing structures. The reinforced rebars make the structure thicker and define the shaping of structures. For several decades, various cementitious composites are developed to overcome the disadvantages of reinforced concrete structures.

The origin of Ultra High Performance Concrete (UHPC) can be found to history for development of high-strength cementitious material. Developing of optimum packing density and discovery of suitable superplasticizer and micro filler like silica fume helped the cementitious composites have high strength and good workability with low water-cement ratio around 0.2. Extremely dense microstructure is the most important characteristics of UHPC (Fig. 1-1). This dense microstructure enables UHPC have high compressive strength over 150 MPa and outstanding durability reducing maintenance or repair cost. UHPC is usually used with steel fibers to avoid explosive brittle behavior at failure and balance the initial cracks generated by autogenous shrinkage. In this paper, the micro cracking behavior of UHPC is a main concern, so let it called to Ultra High Performance Fiber Reinforced Concrete (UHPFRC) to emphasize on fiber action. UHPFRC structural members are generally produced as precast concrete

structures, because they needs quality control of fresh concrete rheology to utilize its self-compacting capacity and heat curing to insure hydrated reaction of silica fume for dense microstructure.

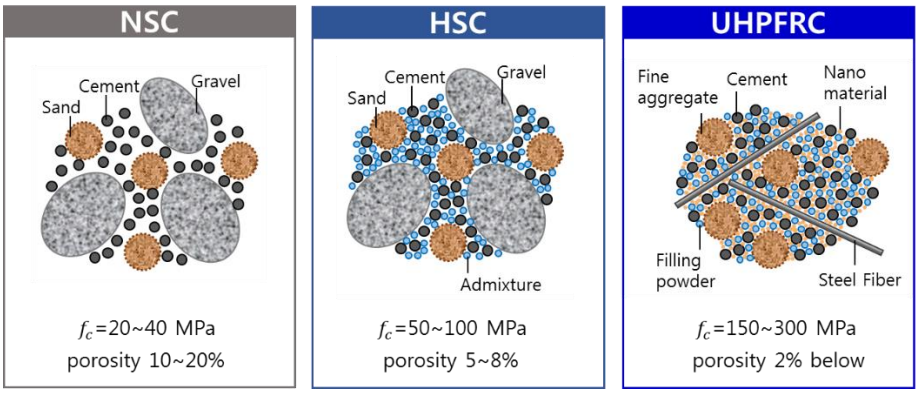

Fig. 1-1. Microstructure of normal strength concrete, high-strength concrete and UHPFRC (or UHPC)

The dense microstructure of UHPFRC allows outstanding tensile behavior induced by micro cracks within 0.1 mm because the bond strength between cement matrix and steel fiber is strong enough to hold steel fibers with a diameter of 0.2 mm. This micro cracking behavior enables a structural member behave hardening behavior with a stable strength increase without conventional reinforced rebars. Tensile strength of UHPFRC is one of the important design parameters, but the existing test methods and design rules are not unified and have been developing in process. An inhomogeneous distribution of the fibers in UHPFRC and the definition and measurement of tensile strain of inhomogeneous material are challenging tasks. The first design rules for UHPFRC were published in France in 2002 and the recent revision was updated in 2013. Japan's first guideline appeared in 2004. South Korea also published the first guideline in 2012 for UHPFRC with a design compressive strength of 180 MPa and a design tensile strength of 9 MPa.

Fig. 1-2. UHPFRC applications for bridge; (a) Seonyu 'Bridge of Peace' in Seoul and (b) KICT cable-stayed footbridge between two buildings

Fig. 1-3. UHPFRC applications for building structures; (a) façade to MuCEM building (Marseille, France) and (b) precast UHPC balconies (Hi-Con, Denmark)

To optimize the given material characteristics, a UHPFRC structure tends to be slender like steel structures. High durability and tensile strength make it possible for the UHPFRC structure being thin and diverse shape of structures with none or much less reinforced rebars. There are many completed projects in bridge and building structures in Europe, Japan, Canada and South Korea. UHPFRC bridges are suitable being exposed to harsh environment and repetitive external loading because of extraordinary durability and low self-weight due to thinner member (Fig. 1-2). Slender columns, stairs, balconies and diverse shape of façade and roofs in a building are also good applications using

UHPFRC material (Fig. 1-3). Strengthening of existing structures, especially for the thin slabs under the pavement of the bridges and roads, is one of the prospective applications (Fig. 1-4).

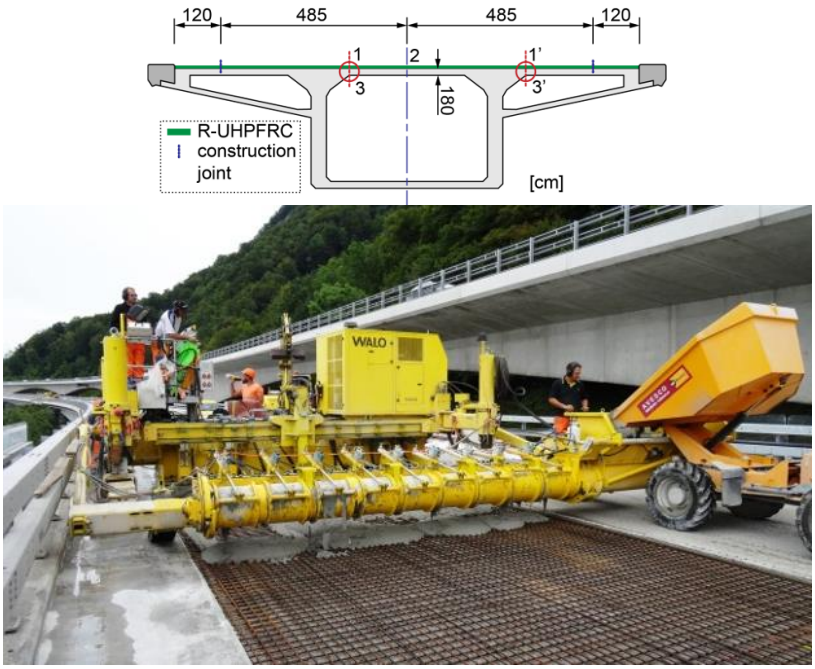

Fig. 1-4. Chillon viaducts strengthening, adapted from; (a) box girders cross section and (b) UHPFRC casting machine (Masse and Brüheiler, 2016)

The cost of UHPFRC per m^3 has been four or five times that of a conventional reinforced concrete. However, comparison should take place on the basis of entire projects. An example of Sakata Mirai, a Japan footbridge. The self-weight of this bridge is only 20% of that of a conventional bridge, so the costs of the foundations were much lower. In future, design will be based primarily on the design life. Moreover, sustainability considerations will play an ever greater role. The UHPFRC solution causes only 40% of the CO_2 emissions of a normal concrete bridge. What this means is that the new construction material UHPFRC has a good chance of achieving a breakthrough (Fehling et al., 2013).

1.2 Problem Statements

UHPFRC contains steel fibers in order to achieve superior post-cracking behavior and stress redistribution ability which gives a ductile failure in compression and tension. For UHPFRC structural member, thinner cross section is preferred in practice due to high cost and outstanding strength and durability, rather than rectangular section which is normally applied in ordinary reinforced concrete. Existing researches and applications has focused on I-shaped shear beam without stirrup. The test results indicates that the stress redistribution capacity of UHPFRC in thin web is manifested replacing the traditional reinforced rebar. The shear capacity of UHPFRC beam has been identified as depending on tensile behavior with respect to its post-cracking characteristics. The Association Francaise de Genie Civil (AFGC) recommendation (2013) suggests that shear design strength of UHPFRC is a summation of matrix contribution and fiber contribution. The post-cracking behavior gives shear strength by fiber contribution and the traditional shear strength for ordinary concrete beam without stirrup is regarded as same as the strength due to matrix contribution. Lots of researches tried to evaluate fiber contribution with tests by demonstrating the direct effect of fiber volume ratio on UHPFRC tensile behavior (Yang et al., 2012; Baby et al., 2014). The dominant failure in UHPFRC I-shaped beam without stirrup is found as diagonal crack localization in web.

The post-cracking shear strength increase contributes to the shear strength by fiber with the sum of the traditional shear strength for an ordinary concrete beam without stirrups. The fiber contribution is quantified by the UHPFRC tensile strength, and the tensile strength is usually regarded as a residual tensile strength considering the strength reduction as a form of the K factor caused by fiber distribution and orientation. Previous studies including this

recommendation tend to consider that the fiber orientation problem in a structural member belongs to the design strength of UHPFRC tensile behavior. K factor is an empirical reduction factor based on test results, and numerous fiber reinforced concrete models employ a probabilistic approach on fiber distribution at a structural level based on bond strength between a single fiber and the cement matrix. The shear strength equation misses some points of the physical mechanics of diagonal tension failure, such as the size effect.

Shear behavior of UHPFRC I-shaped beam shows the contradictory points. One is that a large range of stress redistribution area comparable to RC beam with stirrup is induced by micro-cracking action. However the final failure occurs abruptly at one opening crack among the dispersed micro cracks while the other cracks close with its own resilience. The diagonal tension failure with splitting cracked zone in failure of UHPFRC shear beam can be postulated as 'semi-brittle' failure. In this research, a physical model for shear behavior of UHPFRC beam is proposed by the limit analysis in the framework of the theory of plasticity and fracture mechanics instead of a decomposition of matrix and fiber contribution as in most research. Splitting cracked zone is assumed as a uniform stress field of damaged zone with a constant stiffness and analysed by plastic limit analysis. Following the limit analysis, the energy dissipated all when any deformation occurs by material failure criteria with flow rule, which is appropriate for a structural element with ductile failure. Therefore the failure with a crack localization should be interpreted by fracture problem. Fracture mechanics concerns brittle failure which depends on crack propagation characteristics due to inherent heterogeneity of UHPFRC. Size effect induced by failure with crack localization can also be explained.

The characteristic length of emerging splitting cracks and the inclination angle of the stress redistribution region of splitting cracks are considered as main parameters for determination of shear strength of UHPFRC I-beam. The plastic limit analysis gives the lower bound solution for the minimum value of

the inclination angle in cracking zone. Size effect in shear beam is suggested by different modelling approaches from a new point of view based on fracture mechanics. Existing researches on size effect are interpreted by UHPFRC tensile behavior in flexural members, and size effect in shear behavior hardly discussed because the effective depth of a structural element in ordinary reinforced concrete is a representative characteristic length governed by flexural behavior. Suggested brittleness factor at material level from the ratio of energy release rate is converted into a new brittleness factor at structural level for stress redistribution zone in shear beam. The brittleness factor may explain the size effect of uniform stress field in shear beam.

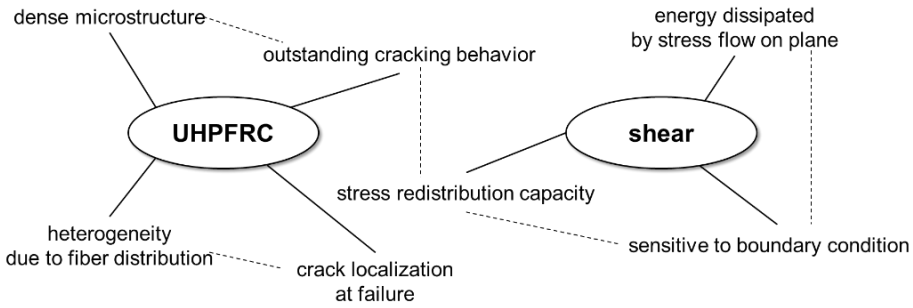

Fig. 1-5. Problem statements

1.3 Research Scope and Objectives

UHPFRC shows superior compressive and tensile strength to ordinary concrete. Cracked UHPFRC also develops a stable increase in strength due to fiber action with large deformation comparable to ordinary reinforced concrete. For UHPFRC shear behavior in I-beams without stirrups, diagonal tension failure by crack localization in web is one of controlling failure modes observed in experimental researches. To understand the shear strength of UHPFRC I-beams, it is first necessary to investigate shear transfer along failure surface and to interpret the reduced strength in terms of effectiveness factors for the limit analysis in the framework of the plasticity theory. The explanation of diagonal tension failure with crack localization in thin web of I beams needs to rely on fracture mechanics approach. A brittleness factor newly defined in this paper is suggested to combine a critical displacement value at material level with size effect at structural level. Characteristic length at material level is from the ratio of pre-peak fracture energy to post-peak energy release rate. Characteristic length at structural level is interpreted as the length of concrete tension tie of splitting crack zone of uniformly tension-compression stressed field. The capacity of splitting crack zone is controlled by the behavior of cracked zone and the configuration of the stress field. The shear strength model of thin webbed I-beams in diagonal tension failure mode is proposed from the limit analysis with new interpretation of characteristic length of brittle material at structural levels.

The research focus on structural failure due to crack localization, so concrete tensile strength with respect to its cracking behavior comes up as an important parameter for UHPFRC in-plane elements. The tensile strength of UHPFRC is dependent on fiber volume ratio rather than the compressive strength because the cracking mechanism in UHPFRC is governed by bond

strength between fiber and cement matrix. The tensile behavior due to fiber reinforcement has to be analyzed to be investigated the physical mechanism with the framework of limit analysis and fracture mechanics. Thus, the research scope is limited to shear strength in a thin web of UHPFRC I-shaped beams without stirrups and the UHPFRC with tensile hardening behavior having the fiber volume fraction of more than 1 % is targeted.

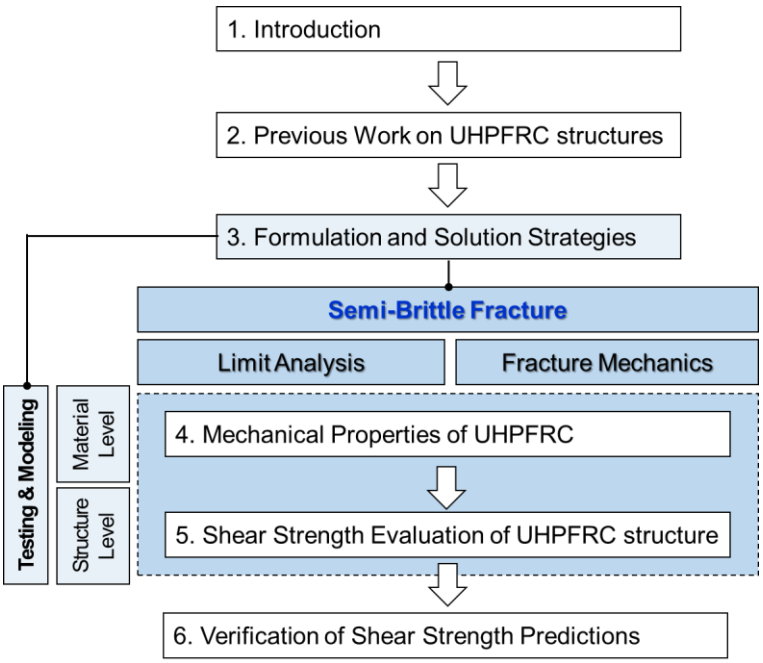

Fig. 1-6. Structure of the thesis

Fig. 1-6 shows the flow chart of the entire thesis. In chapter 2, current design codes and previous studies of UHPFRC shear beams are reviewed. The experimental investigations describes the characteristics of shear failure for UHPFRC structures in order to define the problem statements clearly. Chapter 3 deals with the main approach for UHPFRC shear behavior with the framework of limit analysis and fracture mechanics. Basic assumptions of the

two approaches are introduced and compared. The methodology to combine the two approaches is investigated with respect of the multiscale approaches based on fracture mechanics. Brittleness number and size effect are suggested to explain the UHPFRC shear behavior and the previous studies of size effect on RC structures are reviewed. Based on the framework suggested in chapter 3, the material properties of UHPFRC are investigated by several tests and defined regarding to the limit analysis and fracture mechanics approaches in chapter 4. Shear strength evaluation of UHPFRC I-shaped beams without stirrups is proposed and then the proposed shear strength equation is verified in chapter 5 and 6.

Chapter 2. Previous Work on UHPFRC elements subjected to Shear

2.1 General

It has to be noticed which criteria for previous works are applied to select. First, definition of the UHPFRC tensile strength is an important design parameter for shear strength, so previous work in this chapter deals with the recommendations and the researches about the tensile strength of UHPFRC as well as shear strength. Shear failure, especially diagonal tensile failure is governed by concrete tensile strength. In ordinary concrete, the tensile strength is considered as being dependent on the compressive strength. On the other hand, fiber reinforced concrete (FRC) considers its tensile strength to evaluate shear strength of structural member directly, so classification and definition of FRC also has to be pointed out. Secondly, the code and recommendations for FRC is dealt with in this chapter. Most of the existing codes and recommendations are established for FRC which mainly behaves softening behavior on post-cracking behavior.

The tensile strength including the crack width and the tensile strain is the key parameter to design shear strength for FRC. The primary design factor to determine the tensile behavior of FRC is known for fiber volume ratio and its geometry. The tensile behavior of UHPFRC is greater than that of FRC, because the bond strength between cement matrix and steel fiber is much greater than that of ordinary FRC and the outstanding capability on self-compacting and high flow ability enable to mix lots of bulk ratio of steel fiber into the UHPFRC fresh concrete. The preferred fiber volume ratio in UHPFRC is over 1.5% to

ensure its tensile hardening behavior. The tensile hardening behavior induces the shear strength increase directly and broaden stress redistribution region. In other words, the effect of fiber reinforcement replaced the reinforcement of steel reinforcement rebar. On the other hand, compressive strength of UHPFRC is relatively independent on the fiber volume ratio and the steel fiber acts to increase ductility preventing extreme brittle failure regarding to high compressive strength above 150 MPa.

In this chapter, at first, shear behavior of UHPFRC I-shaped beams are reviewed based on the existing recommendations and the experimental researches. The recommendations and the researches dealing with UHPFRC insufficiently exists, so the literature review includes general FRC tensile behavior and shear strength. The existing physical models for the evaluation of FRC shear strength and the existing proposal equations for shear strength of UHPFRC beams are investigated with respect to the crack pattern and the failure mode. The code provisions are introduced from RC shear beams without stirrups, FRC shear beams without stirrups, to UHPFRC shear beams without stirrups including recent studies for evaluating shear strength of UHPFRC shear beams. At the end, the existing experimental investigations are searched for UHPFRC I-shaped beams in order to find out the characteristics of UHPFRC shear behavior in an in-plane elements. The previous experimental studies are categorized by shear design parameters and the findings give hints for solution to evaluate shear strength of UHPFRC beams without stirrups.

2.2 Shear Strength for UHPFRC structures

2.2.1 Code Provisions for RC

Shear strength without transverse reinforcement has been developed as a form of empirical equation (Table 2-1). Each recommendation gives a different equation, and there is no consensus yet. The key parameters for shear strength of reinforced concrete (RC) beams without stirrups are the tensile strength of concrete, the longitudinal reinforcement ratio, the shear span ratio and the effective depth. Size effect is generally accepted except for Zutty's model and the ACI code, but the formulations are various.

The main reason for this controversy topic comes from diverse failure modes depending on diverse design parameters. There are four types of mechanisms that can transfer the shear force in a cracked concrete beam since 1970s (ACI-ASCE Committee 445, 1998); (1) Shear stress in the uncracked concrete zone, (2) Aggregate interlock caused by tangential displacement of the crack faces, (3) Residual tensile stress occurring at limited normal opening of the cracks, (4) Dowel action caused by the longitudinal reinforcing bars. However, each contribution of the mechanisms is not clarified and the significant contribution of shear strength can be attributed to the loading scenario, member geometry.

The definition of concrete contribution to shear strength $V_{Rd,c}$ is also disputable. For instance, the ACI 318-11 code adopts a 45° truss model, and the Eurocode is based on variable angle truss model or stress field, where the inclination is optimized in order to obtain the maximum shear strength. Besides the truss model with an inclination of less than 45°, but with a fixed angle according to the principal stress direction in the web before cracking.

Table 2-1. Empirical equations for predicting shear strength beams without stirrups (Lim, 2012)

Investigator	Equation	Size effect
Zsutty	$v_{cr} = 2210\left(f_c \ \rho \ \frac{d}{a} \right)^{1/3}$, f_c in MPa	$v_{cr} \sim d^0$
CSA code	$v_{cr} = \frac{245}{1275 + s_e}\sqrt{f_c}$, f_c in MPa $s_e = \frac{35 s_x}{(d_{agg} + 16)}$ $s_x = 0.9d$ (beam with reinforcement at bottom tension layer only) d_{agg} =maximum aggregate size of concrete d and d_{agg} in mm	$v_{cr} \sim d^{-1}$
JSCE code	$v_{cr} = 64 \times (f_c \times \rho)^{1/3} \times d^{-1/4} \times \left(0.75 + 1.4\frac{d}{a} \right)$ f_c in MPa, d in m	$v_{cr} \sim d^{-1/4}$
BS8110	$v_{cr} = \frac{790}{\gamma_m}(100 \times \rho)^{1/3} \times \left(\frac{0.4}{d} \right)^{1/4} \times \left(\frac{f_c}{25} \right)^{1/3}$ γ_m =safety factor (=1.25) $100\rho < 3$ (ρ is a number, not a percentage) f_c in MPa, $f_c < 40$ MP, d in m	$v_{cr} \sim d^{-1/4}$
CEB-FIP model code	$v_{cr} = \frac{180}{\gamma_m}\left(1 + \sqrt{\frac{0.2}{d}} \right)\left(\frac{3d}{a} \right)^{1/3} \times (100\rho)^{1/3} \ f_c^{1/3}$ γ_m =safety factor (=1.2) f_c in MPa, d in m	$v_{cr} \sim 1 + d^{-1/2}$
ACI 318-11	A simple form : $v_{cr} = 2\sqrt{f_c}$ A complex form : $v_{cr} = \left(1.9\sqrt{f_c} + 2500\rho\frac{Vd}{M} \right) \le 3.5\sqrt{f_c}$ where $Vd / M \le 1$ f_c in psi, V: total shear force, d in m	$v_{cr} \sim d^0$
Bazant	$v_{cr} = \beta\left(\frac{f_c}{1 + d / d_0} \right)^{1/3}$, f_c in MPa β_0 and d_0 are two constants	$v_{cr} \sim d^{-1/2}$

2.2.2 *fib* Model Code 2010 for FRC

There are general rules for FRC structures in *fib* model code. According to the structures with a degree of redundancy easier the stress redistribution occurs, easier the strain localization occurs. In addition for thin walled structure like shells may be influenced by the casting direction due to wall effect. Fig. 2-1 shows typical load-displacement curve for a FRC structure. The code defines the ultimate displacement δ_u, the displacement at the maximum load δ_{peak} and the displacement at the maximum service load δ_{SLS}, and the conditions to ensure FRC structures without the minimum conventional reinforcement are suggested.

When the structure is able to significantly redistribute the applied load at failure, a factor K_{Rd}, that takes into account favourable effects due to redistribution, can be assumed:

$$P_{Rd} = K_{Rd} \cdot P\left(f_{Fd}\right) \tag{2-1}$$

$$K_{Rd} = \frac{P_{max,k}}{P_{max,m}} \cdot \frac{f_{Ftum}}{P_{Ftuk}} \leq 1.4 \tag{2-2}$$

$P\left(f_{Fd}\right)$ is the resistant load computed taking into account the design strength of FRC. K_{Rd} is mainly affected by the volume of the structure involved in the crack propagation process at failure (V), with respect to that used in the material identification procedure of the post-cracking residual strengths (V_0) as shown in Fig. 2-2. K_{Rd} can be computed by a structural analysis that takes into account a random redistribution of the mechanical characteristics. When a statistical distribution of P_{max} is obtained starting from an assumed standard deviation of the mechanical conventional law, the factor

K_{Rd} can be computed as Eq. (2-2).

The proposed design equation as below are validated for the shear strength of FRC members with conventional longitudinal reinforcement and without shear reinforcement, but not including UHPFRC.

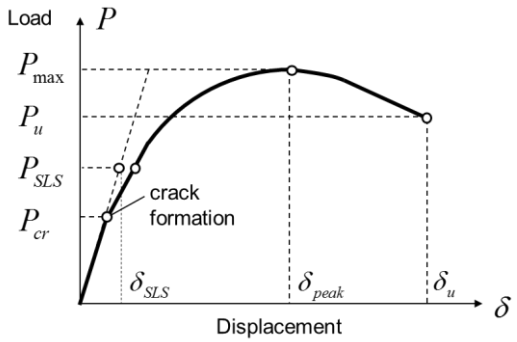

Fig. 2-1. Typical load (P) – displacement (δ) curve for FRC structure (fib, 2012)

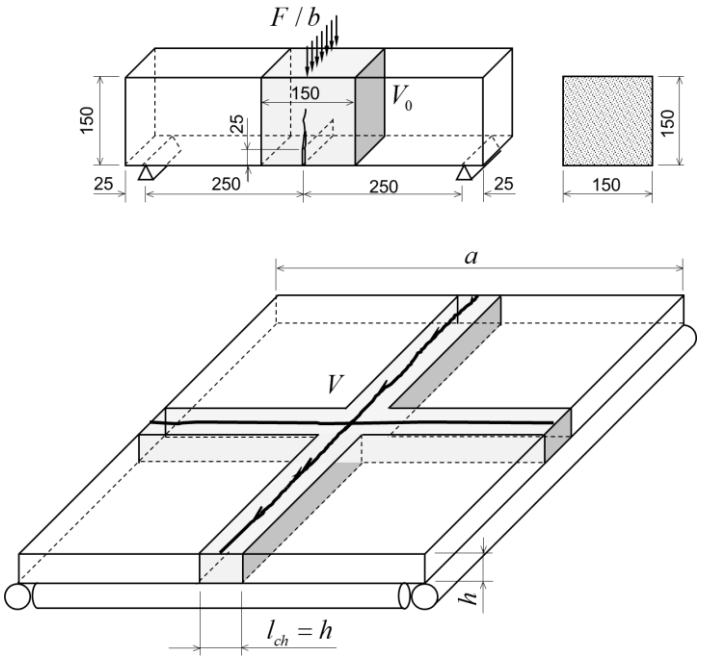

Fig. 2-2. Volume involved in the failure for the classification test (V0) and for a structure (V) (fib, 2012)

$$V_{Rd,F} = \left\{ \begin{array}{l} \dfrac{0.18}{\gamma_c} \cdot k \cdot \left[100 \cdot \rho_l \cdot \left(1 + 7.5 \cdot \dfrac{f_{Ftuk}}{f_{ctk}} \right) \cdot f_{ck} \right]^{1/3} \\ +0.15 \cdot \sigma_{cp} \end{array} \right\} \cdot b_w \cdot d \qquad (2\text{-}3)$$

$$V_{Rd,F\,min} = \left(v_{min} + 0.15 \cdot \sigma_{cp} \right) \cdot b_w \cdot d \qquad (2\text{-}4)$$

$$\text{where} \quad v_{min} = 0.035 \cdot k^{3/2} \cdot f_{ck}^{1/2}$$

There is an additional term corresponding to the tensile strength of FRC in Eq. (2-3) comparing to the Eurocode 2. f_{Ftuk} is the characteristic value of the ultimate residual tensile strength for FRC by considering w_u =1.5 mm. f_{ctk} is the characteristic value of the tensile strength for the concrete without fibers. Another point is that there is no limitation for longitudinal reinforcement ratio ρ_l unlike the ordinary reinforced concrete structures in Eurocode 2.

The commentary of *fib* model code suggests another approach to shear described in RC equations proposed by *fib* model code.

$$V_{Rd,F} = \frac{1}{\gamma_F} \left(k_v \sqrt{f_{ck}} + k_f \, f_{Ftuk} \cot\theta \right) z b_w \qquad (2\text{-}5)$$

$$k_v = \frac{0.4}{1 + 1500\varepsilon_x} \cdot \frac{1300}{1000 + k_{dg} z} \quad \text{for} \quad \rho_w < 0.08\sqrt{f_{ck} / f_{yk}} \qquad (2\text{-}6)$$

$$k_v = \frac{0.4}{1 + 1500\varepsilon_x} \quad \text{for} \quad \rho_w \geq 0.08\sqrt{f_{ck} / f_{yk}} \qquad (2\text{-}7)$$

$$k_{dg} = \frac{32}{16 + d_g} \geq 0.75 \qquad (2\text{-}8)$$

$$\theta_{min} \leq \theta \leq 45^\circ \qquad (2\text{-}9)$$

$$\theta_{min} = 29^{\circ} + 7000\varepsilon_x \tag{2-10}$$

$$w_u = 0.2 + 1000\varepsilon_x \geq 0.125 \text{ mm} \tag{2-11}$$

Eq. (2-5) assumes that fiber contribution is great enough so the tensile strength of FRC f_{Ftuk} with k_f =0.8 can substitute the strength f_{ywd} of shear reinforcement rebar. θ denotes the inclination of the compressive stress field. The minimum inclination of the compressive stress field for FRC, 29°, is larger than that of RC, 20° and the recommendation for the ultimate crack width w_u is given.

The shear strength in *fib* model code is basically applicable to SFRC with tensile-softening behavior, not tensile-hardening material like UHPFRC. However, the commentary and design principles mentions that the tensile-hardening behavior in FRC structures and the stress redistribution ability of FRC structures should be considered with respect to the volume unit corresponding to the structure geometry and material characteristics. The increase of strength and deformation in UHPFRC has to be verified based on theoretical explanation. Moreover the test method and definition of material tensile strength should be reconsidered at the same time corresponding to the shear strength evaluation. Two dimensional elements has to be also investigated with respect to the fiber contribution due to wall effect.

2.2.3 RILEM TC 162-TDF for SFRC

The shear strength in RILEM recommendation is divided as two types. The $\sigma - w$ method for normal strength SFRC evaluates the shear strength defined by the mean design residual stress at the crack width w_m proportional to the strain of longitudinal reinforcement. The diagonal crack is assumed to be 45° (Casanova and Rossi, 1997). The $\sigma - \varepsilon$ method for high strength SFRC evaluates the shear strength defined by the design value τ_{fd} of the increase in shear strength considering the inclination of the compression strut θ. τ_{fd} is lower value than usual than the maximum tensile strength. The design value is applied when the SFRC structure fails with the inclination θ. $f_{R,4}$ is the residual tensile strength for a *CMOD* of 3.5 mm.

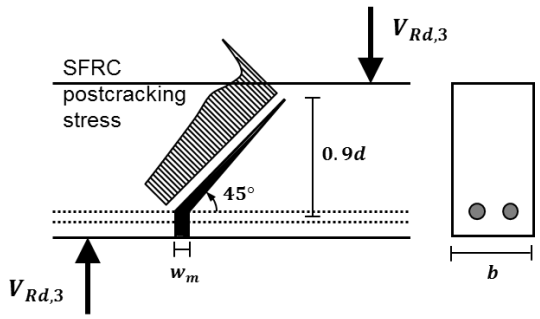

Fig. 2-3. Assumed crack geometry in a beam with conventional longitudinal reinforcement loaded to the ultimate shear loading capacity, $V_{Rd,3}$. The crack is assumed to extended under 45°, and the crack opening at the rebar is limited to w_m

The ultimate shear load carrying capacity V_R is taken to be the sum of the contributions of the member without shear reinforcement V_{cd}, of the stirrups and inclined bars V_{wd} and the steel fibers V_{fd}. For strain-softening FRC, the fiber contribution V_{fd} is calculated from the design stress-crack opening relationship using the mean design residual stress at the crack width w_m as shown in Fig. 2-3. The inclination of the crack is assumed to 45°. A

definition of w_m is necessary to quantify the ultimate load-carrying capacity of the beam failing in shear. According the experimental results, the spacing of these cracks is roughly equal to the inner lever arm of the height of the beam.

$$V_{Rd,3} = V_{cd} + V_{fd} + V_{wd} \tag{2-12}$$

$$V_{fd} = b \cdot z \cdot \bar{\sigma}_{p,d}\left(w_m\right)$$
$$\text{with} \quad \bar{\sigma}_{p,d}\left(w_m\right) = \frac{1}{w_m}\int_0^{w_m} \sigma_{w,d}\left(u\right) du \tag{2-13}$$

The design for $\sigma - \varepsilon$ method is valid for SFRC with compressive strength of up to 50 MPa. The fundamentals is same as the design of normal reinforced concrete in Eurocode 2. The fiber contribution V_f consists of an integration of shear strength due to fibers on the critical shear cracks where θ is the inclination of the compression strut and k_f is a factor taking into account the flange contribution in a T-section. Especially the fiber contribution is defined by τ_{fd}, the design value of the increase in shear strength due to steel fibers, not the tensile strength directly.

$$V_{fd} = k_f \cdot k \cdot \cos\theta \cdot \tau_{fd} \cdot b_w \cdot d \cdot \cot\theta \tag{2-14}$$

$$k_f = 1 + n \cdot \left(\frac{h_f}{b_w}\right) \cdot \left(\frac{h_f}{d}\right)$$
$$\text{with} \quad n = \frac{b_f - b_w}{h_f} \le 3 \quad \text{and} \quad n \le \frac{3 \cdot b_w}{h_f} \tag{2-15}$$

$$k = 1 + \sqrt{\frac{200}{d}} \le 2.0 \tag{2-16}$$

$$\tau_f = \frac{0.18}{\gamma_c} \cdot f_{R,4} \tag{2-17}$$

2.2.4 AFGC-SETRA Recommendation for UHPFRC

The first design rules for UHPC were published in France in 2002. The AFGC recommendation is the most frequently referred recommendation to design UHPFRC structures. The shear strength V_{Rd} is given as the sum of concrete contribution $V_{Rd,c}$, shear reinforcement contribution $V_{Rd,s}$ and fiber contribution $V_{Rd,f}$. The contribution of concrete $V_{Rd,c}$ is given by Eq. (2-19). k takes into account the effect of an axial force, $k>1$ for compression or $k<1$ for tension. The design value for the part of the shear capacity $V_{Rd,f}$ provided by the fibers is given by two types of equations. In the case of strain-softening or low strain-hardening UHPFRC, the strength is given by Eq. (2-21) ~ (2-23). The minimum value of θ =30° is recommended. On the basis of the model proposed by Casanova (1997), the residual tensile strength of the cross-section $\sigma_{Rd,f}$ is defined as the average residual strength within the crack width w_{lim}. w_u is the ultimate crack width attained at the ultimate limit state for bending combined with axial forces and w_{max} is the maximal admissible crack width, 0.3 mm.

$$V_{Rd} = V_{Rd,c} + V_{Rd,s} + V_{Rd,f} \le V_{Rd,max} \tag{2-18}$$

$$V_{Rd,c} = \frac{0.21}{\gamma_c} \cdot k \cdot \sqrt{f_{ck}} \cdot b_w \cdot d \tag{2-19}$$

$$V_{Rd,s} = z \cdot \frac{A_{sw}}{s} \cdot \frac{f_{swk}}{\gamma_s} \cdot \frac{sin(\alpha+\theta)}{sin(\theta)} \tag{2-20}$$

$$V_{Rd,f} = \frac{\sigma_{Rd,f}}{\gamma_f} \cdot \frac{1}{tan\theta} \cdot b_w \cdot z \tag{2-21}$$

$$\sigma_{Rd,f} = \frac{1}{K} \cdot \frac{1}{w_{lim}} \cdot \int_0^{w_{lim}} \sigma_f(w) \cdot dw \tag{2-22}$$

$$w_{lim} = max(w_u, w_{max}) \tag{2-23}$$

$$V_{Rd,max} = 2 \times 1.14 \cdot \frac{\alpha_{cc}}{\gamma_{cf}} \cdot b_w \cdot d \cdot f_{ck}^{2/3} / (\cot\theta + \tan\theta) \tag{2-24}$$

In case of high strain-hardening UHPFRC, the expression $\sigma_{Rd,f}$ becomes Eq. (2-25). ε_u is the ultimate strain attained as the ultimate limit state for bending combined with axial forces under the moment exerted in the section. ε_{max} is equal to ε_{lim} and it can be regarded as 0.0025 in design.

$$\sigma_{Rd,f} = \frac{1}{K} \cdot \frac{1}{\varepsilon_{lim} - \varepsilon_{el}} \cdot \int_{\varepsilon_{el}}^{\varepsilon_{lim}} \sigma_f(\varepsilon) \cdot d\varepsilon \tag{2-25}$$

$$\varepsilon_{lim} = max(\varepsilon_u, \varepsilon_{max}) \tag{2-26}$$

Except for small elements, the value of K used will be K_{global}=1.25. It can be considered that an element is very small for calculating the shear if the width b_w and the height h are both less than $5 l_f$, where l_f is the fiber length. Safety factor for concrete γ_f should be considered separately and the value is equal to 1.5.

The physical model for SFRC is adopted for strain-softening or low strain-hardening UHPFRC in Eq. (2-13). The differences compared to the existing FRC model are the inclination of compressive strut and the fiber orientation factor K. The residual tensile strength $\sigma_{Rd,f}$ is similar to each other. It can be regarded as the average strength of post-cracking behavior within the ultimate tensile strain or crack width. The AFGC recommendation suggests that the maximum admissible crack width is 0.3 mm and the maximum tensile strain is 0.0025 for UHPFRC with fiber volume content of 2-%.

2.2.5 Review of Previous Researches

Most of investigations for UHPFRC shear strength is limited to experimental researches and the researches to evaluate shear strength is not unified yet. The existing recommendations focus on the tensile strength of UHPFRC within the critical crack opening. The crack opening behavior is suitable to explain the ultimate limit state defined by the localized critical crack, but the strength increase due to micro-cracking has to be explained by different point of view considering energy dissipation per unit volume. The stress redistribution represented as strain-hardening behavior should be evaluated based on an appropriate physical model. In this chapter, state of arts which deserve to be studied are introduced and the implications are pointed out.

(1) Sato and Walraven (Delft University of Technology, 2007)

At TU Delft in 2007 a series of shear tests was carried out by Pansuk (2007). The research program contained a series of three beams. The concrete contained 0, 0.8 and 1.6 vol.-% of straight steel fibers 13/0.16 mm. The different failure loads given in Fig. 2-4 and their associated crack patterns revealed that the fibers had a considerable influence on the shear behavior. The shear capacities were compared with the theoretical capacities calculated with Eurocode 2 which uses the variable strut inclination method to calculate the shear capacity of beams with shear reinforcement. According to this method, any strut inclination θ in the range of $1 < cot\theta < 2.5$ may be chosen. The shear reinforcement activated at this angle contributes to the shear capacity in Eq. (2-27). The following approach may be used when employing fibers as shear reinforcement as shown in Eq. (2-28).

$$V_u = b_w d \cdot \cot\theta \cdot \frac{A_{sw}}{t} f_y \quad \text{where} \quad 1 \le \cot\theta \le 2.5 \tag{2-27}$$

$$V_u = b_w h \cdot \cot\theta \cdot \sigma_{pf} \quad \text{where} \quad 1 \le \cot\theta \le 3 \tag{2-28}$$

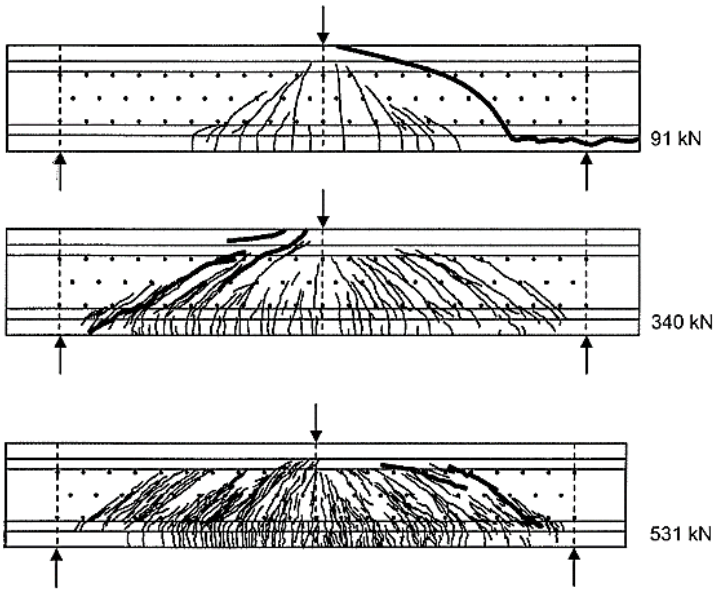

Fig. 2-4. Crack patterns of UHPFRC beams with fiber reinforcement (Sato et al., 2008)

For the shear strength of UHPFRC, the full depth h is taken into account, because the fibers are at the level below the tensile reinforcement are expected to contribute to the shear. The post cracking plastic fiber strength σ_{pf} is formulated as αf_{ct}. The simplification turns out to be advantageous when calculating the crack width and the crack distance. A post cracking reduction factor α =0.72~0.88 was found from the centric tests on dog-bone specimens. In addition, since the fibers are expected to add to the redistribution capacity it is assumed that the limits of strut rotation can be widened to $1 < \cot\theta < 3$.

(2) Qi et al. (Nanjing University, 2016)

A research group in Nanjing University developed a theoretical method, termed the mesoscale fiber-matrix discrete model (MFDM) for estimating the shear contribution of steel fibers and calculating shear strength of UHPFRC beams. The proposed model suggests an effective fiber distribution region (EDR) in Fig. 2-5 along the critical diagonal shear crack, where fibers are efficient at providing shear resistance. The width of the EDR w_e is calculated by either probability theory or the pull-out load slip relationship.

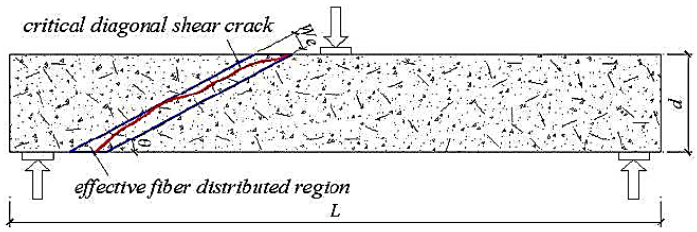

Fig. 2-5. Effective fiber distributed region (EDR) in a beam (Qi et al., 2016)

Assumptions for MFDM are made as follows; The distribution of fibers is uniform inside the beam. All fibers pull out from the side of the crack width a shorter embedment length. Deformation induced by elastic strains is neglected because of the relatively small value compared to slip between the fibers and matrix, as well as the bending stiffness of a fiber. Plane section remain plane. To define the failure mechanism of the compression zone subjected to the combined stress, Rankine's failure criteria are used (Eq. (2-30)). The shear strength is the summation of concrete, shear reinforcement and fiber contribution (Eq. (2-29)).

$$V_n = V_c + V_s + V_f \tag{2-29}$$

$$V_c = \frac{2}{3} b_{ef} c \sqrt{f_t \left(f_t + 0.425 f_{cu} \right)} \tag{2-30}$$

$$V_s = \rho_v f_v b d \cot\theta \quad \text{where} \quad \theta = 29^\circ + 3500\varepsilon_s \tag{2-31}$$

$$V_f = \frac{n}{n_c} \sum F_y \cos\theta = \frac{8\rho_f b d F w_e \cot\theta}{\pi^2 l_f d_f^2} \tag{2-32}$$

All efficient fibers in EDR only provide a resultant force perpendicular to the critical diagonal shear crack and no additional force along the propagation direction of the critical diagonal shear crack. To determine the width of EDR w_e for fiber contribution in Eq. (2-32), two methods are proposed. The first method is based on the probability theory with the consideration of fibers' geometrical dimensions and orientation. A hypothetical mathematical model is introduced to determine the average bond strength between a single fiber and the matrix. Assume that there are n fibers with various embedded depths ranging from 0 to $l_f / 2$ in the matrix. Then the bond strength can be calculated by Eq. (2-33) and the width of the effective fiber distributed area can be obtained by Eq. (2-34). $\bar{P}$ is the average probability for fibers across the critical diagonal shear crack in a beam and approximately equals to $1/\pi$. The second method is based on the assumption that half of the critical width of the critical diagonal crack is equal to the slip corresponding to the maximum shear stress in the fiber pull-out test. The equation can be simplified into Eq. (2-35).

$$F = \lim_{n\to\infty} \frac{1}{n} \sum_{i=1}^{n} F_i = \frac{\tau_b \pi d_f l_f}{4} \tag{2-33}$$

$$w_e = 2 l_f \bar{P} \approx 0.64 l_f \tag{2-34}$$

$$w_e = l_f - \sqrt{\frac{2Q l_f}{\pi d_f \tau_H}} = l_f - \sqrt{\frac{0.48 l_f}{d_f}} \tag{2-35}$$

2.2.6 Remarks

The recommendation and existing researches assume that the UHPFRC shear beams without shear reinforcement fails by the critical diagonal shear crack. Diagonal tension failure is common failure mode in RC shear beams without shear reinforcement. The most important point in differences between UHPFRC shear beams and RC shear beams is strength increase due to micro-cracking behavior before the critical crack localization. The strength increase due to the fiber contribution represented as tensile strength and inclination of compressive strut θ.

The RILEM and AFGC recommendations take into account the term for the fiber contribution adding to the existing RC shear strength equation. The *fib* model code suggests the unified term for the concrete and fiber contribution, but the equation can be applied to SFRC structures except UHPFRC structures. The typical fiber contribution in SFRC shear strength assumes that the inclination of the critical crack is assumed to 45° and the average tensile strength within the ultimate crack width w_m resists the crack surface (Casanova, 1997). However, UHPFRC with low or high strain-hardening behavior should be investigated with respect to the stress redistribution capacity in a shear beam.

Walraven suggests that the UHPFRC shear beams without shear reinforcement can be considered as RC shear beams with shear reinforcement, so the variable strut inclination method is adopted for UHPFRC shear beams. The research group in Nanjing university proposed an effective fiber distribution region along the critical shear crack assuming the uniform distribution of fibers. These proposal indicate that the stress redistribution due to strain-hardening behavior with micro-cracking should be analyzed regarding to in-plane shear strength as well as tensile strength on the critical crack.

2.3 Previous Experimental Studies

2.3.1 Fiber Reinforcement Effect

It has been the biggest questions for researches whether fiber reinforcement can play a role instead of conventional shear reinforcement or not from the beginning of a UHPFRC development. In addition, tensile behavior of UHPFRC is very important design parameter, and tensile stress-strain relationship is found to be primarily determined. The geometry of structural elements, mechanical properties and content of steel fiber strongly influences the tensile behavior of UHPFRC in a material level and shear behavior of UHPFRC structures, and those have been main parameters for experimental studies.

Among the several series of tests performed at the University of Kassel, UHPC I-shaped beams are focused on this paper. The shear bearing behavior of UHPC beams with combined shear reinforcement of stirrups and fibers is investigated. Eight beams with an I-shaped monitoring area and a shear span ratio of 4 were tested in three-point bending tests (Fig. 2-6). In every test beam, the shear failure took place within the web. To show the influence of fibers on the shear bearing behavior, different shear reinforcement was arranged: stirrups with a diameter of 5 mm and a distance of 105 mm, a steel fiber content of 1% by volume, a combination of these two shear reinforcements, and no shear reinforcement at all. During the tests, the crack initiation and propagation, the inclination of the compression strut, and the shear load bearing capacity were identified. Shear cracks occurred in the monitoring area, which were initiated by already developed cracks due to shrinkage and temperature. When stirrups were arranged, they ruptured. After reaching the ultimate load, the load bearing capacity dropped to a plateau, reflecting the strong influence of the bending reinforcement on the shear bearing capacity. The end of the test was either

characterised by a damage of the compression chord of the damage of the bond of the bending reinforcement near the support.

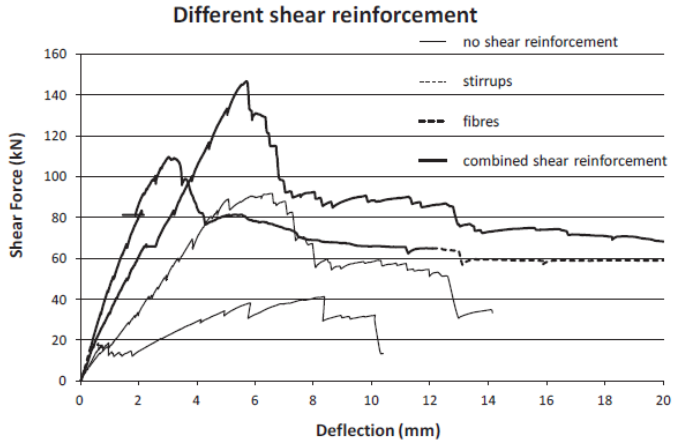

Fig. 2-6. Shear force-deformation of beams with different shear reinforcement (Fehling and Thiemicke, 2012)

Voo and Foster conducted lots of UHPFRC shear beams since 2000. Seven beams were tested in order to investigate the shear behavior of UHPFRC prestressed members without transverse reinforcement. The principal parameters distinguishing the specimens were the fiber type and content and the pre-tensioning force intensity. The members had an I-shaped cross section of 650 mm depth and a length of 4500 mm. The concrete compressive strength was in the range of 150 to 170 MPa. The content of steel fibers varied from 1.25 to 2.5%. All beams exhibited a shear failure. The analysis and conclusion were the following; in terms of prestressing effect, the comparison indicates a 15 percent variation in strength due to the effect of prestressing. The quantity and type of fibers used in the concrete mixture did not significantly affect the cracking load but had a significant influence on the rate of crack propagation and on the failure loads. At the peak load, many fine cracks were performed in the web, with the cracks well distributed through the shear spans. The failure loads were more than twice the cracking loads.

2.3.2 Conventional Design Parameters on RC Shear Beams without Stirrups

Representative design parameters for RC shear beams without stirrups are shear span ratio, effective depth ratio and longitudinal reinforcement ratio. Concrete strength is excluded in this chapter because it is related to the fiber reinforcement effect in previous chapter. Japanese (JSCE, 2008) and German research group (Hegger et al., 2012) conducted extensive experimental investigation regarding to various shear design parameters with prestressed UHPFRC I-shaped beams.

The Japanese group investigated the shear strength of I-shaped UHPFRC shear beams without stirrups regarding to shear span ratio, effective depth, longitudinal reinforcement ratio and prestressing grade. Based on the test results, FEM analysis also investigated. The size effect and shear span ratio are clearly found in Fig. 2-7.

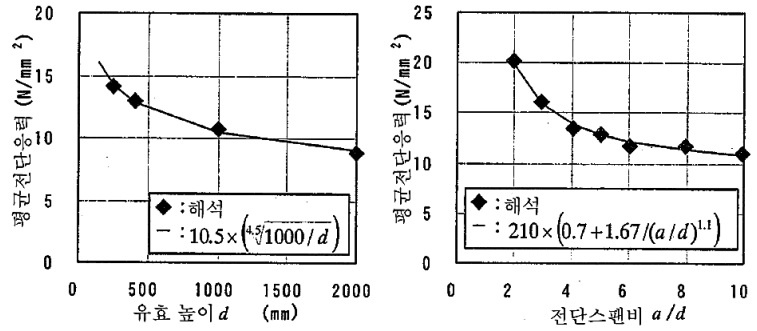

Fig. 2-7. Nonlinear FEM analysis results regarding to design parameters and the corresponding predicted equations (JSCE, 2008)

The research group of RWTH Aachen University in Germany carried out sixty shear tests on pre-tensioned beams between 2006 and 2011. Main

parameters were the prestressing grade, the shear slenderness, the number and position of web openings, the opening diameter and additional shear reinforcement including the amounts of fibers. Stiff load-deformation behavior was observed in all the shear tests. The angle of the failure cracks was between 20° and 24°. Besides increasing the load-carrying capacity, ductile failure and advance warnings of failure are the main advantages of adding steel fibers.

The verified parameters were the fiber content, the prestressing grade, the shear span ratio as well as the position and amount of web openings in the beams. The amount of steel fibers has a significant influence on the shear carrying capacity. With increasing the fiber ratio the failure becomes more and more ductile. Without fibers, single hairline cracks in the anchorage zone were observed. One test with a shear span ratio a / d =4.4 leads to the assumption, that a higher fraction of arch action seems to be present when a / d =3.8.

To compare the results with different cross sections, the shear forces were normalized on the shear stress where d =317 mm, 617 mm and 917 mm. The shear stresses of the 617 mm high effective depths were decreased down to about 70% compared to the values of 317 mm high effective depths. Fig. 2-8 shows that the web thickness seems to have a minor impact on the shear stress, but the beam height shows a significant effect.

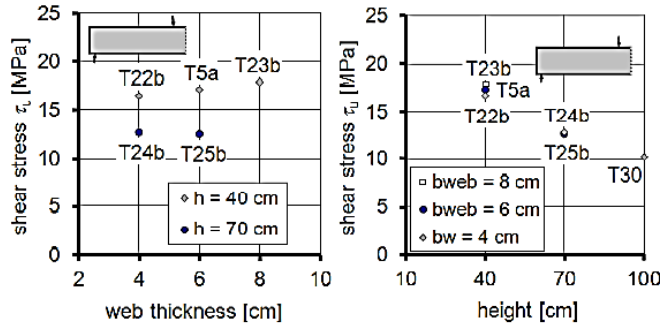

Fig. 2-8. Influence of the web thickness and the beam height on the ultimate shear stresses of beams without opendings (Hegger et al., 2012).

2.3.3 Shear reinforcement ratios and Prestressing Effect

This experiments were performed at the French institute of science and technology for transport, development and networks IFSTTAR. In a four-point bending configuration, shear test have been conducted on eleven 3-m long and 380 mm high I-shaped girders with varied types of shear reinforcement (stirrups and/or fibers, or neither), combined with longitudinal prestressing or mild steel reinforcing bars (Baby et al., 2012). The concrete compressive strength was in the range of 160 to 200 MPa. The different UHPFRC mixes were composed of straight steel fibers with a volume ratio of 2% for the UHPFRC-A and 2.5% for the UHPFRC-B. The shear span ratio was 2.49.

The results of the shear tests on prestressed concrete beams have demonstrated the influence of the material strain corresponding to crack localization on the overall shear behavior. This strain corresponds to the end of the global pseudostrain-hardening behavior. The reinforced beams in UHPFRC without stirrups had a shear failure at a load level two times higher than the beam without fibers. Part of the UHPFRC reinforced beams with stirrups exhibited a flexural failure with large plastic deformations and yet a fully developed critical shear crack. The load tests highlighted that the contributions of fibers and stirrups can be summed.

To identify the contribution of the fibers to the shear response, prisms have been extracted horizontally, vertically, at 30 and 45° in both undamaged ends of the beams to determine the effective orientation factor. In accordance with the tests at different scales, the beam shear-capacity has been quantitatively identified as depending not only on an ideal UHPFRC tensile behavior but also on the effect of fiber orientation, prestressing force, and shape of the cross section in so far as these features influence the shear-crack control.

2.3.4 Remarks

From the experimental investigation for I-shaped UHPFRC shear beams without stirrup, the controlling failure mode is diagonal tension failure due to crack localization in web. In ordinary reinforced concrete, the diagonal tension failure is usually considered as the cracking load because RC shear beams without stirrup fails with a brittle manner right after the critical crack arises. However UHPFRC shear beams without stirrup have an increase of strength due to micro-cracking after initial cracking before the crack localization and the increase is more than twice of the cracking load. The increasing is stable with a constant stiffness but the final failure is governed by a crack localization which is brittle failure.

Cracking behavior in web has to be analyzed regarding to structural design parameters and UHPFRC material characteristics. The location of initial diagonal crack, cracking pattern with additional micro-cracks in web and the crack localization at failure can be defined by the given stress field and UHPFRC stress redistribution capability. The diagonal tension failure is analyzed comparing with RC shear beam without shear reinforcement and the stress redistribution capability is defined by UHPFRC material.

Existing researches reported that diagonal tension failure is the controlling failure mode for shear failure in web of I-shaped UHPFRC beam with or without stirrup. These phenomenon indicates that bond stress between UHPFRC and reinforced rebar is much greater than that of ordinary concrete, and the tensile characteristics of UHPFRC governs its structural failure. Existing recommendations for UHPFRC consider that tensile strength is one of the shear design parameters instead of compressive strength. Hence, defining post-cracking behavior of UHPFRC as well as the tensile strength is important to understand the structural behavior. Whether fiber reinforcement in UHPFRC

substitutes for conventional reinforced rebar or not is one of the following problems.

It has been a challenging problem to evaluate shear strength of concrete structures. Shear behavior of reinforced concrete is more dependent to concrete material characteristics especially cracking behavior. Cracks in concrete structures subjected to shear force usually occur overall structures and the critical crack in lots of microcracks determine the structural failure. Dependent on the resisting force across an opening cracks due to the given structural geometries, the critical crack can be discovered at diverse locations with different failure mode, which is why shear behavior is difficult to deal with. For such a reason, there are lots of design parameters to control a shear behavior of concrete structures, whereas general RC structures caused by yielding of steel reinforcement takes into account of one failure mode with simplified assumptions.

Based on the previous researches, the features of UHPFRC I-shaped beam subjected to shear force distinguished from RC shear beam are summarized as follows:

1) Tensile behavior of UHPFRC material has to be defined to analyze structural shear behavior. Resistant force due to fiber reinforcement can be quantified by tensile strength according to the crack opening width. UHPFRC tensile behavior shows hardening behavior in case of the fiber content of more than 1.0% volume ratio. The tensile hardening behavior in a material level and cracking behavior in a structural level should be analyzed simultaneously because these components mainly attributes the increase of shear strength in UHPFRC structures.

2) Most experimental investigations in previous works focus on I-shaped UHPFRC beam without shear reinforcement in order to

save the construction cost with slender cross section and get advantages of UHPFRC materials. For UHPFRC material with tensile hardening behavior, the shear beam without transverse reinforcement shows stable increase after initial cracking being comparable with RC shear beam with transverse reinforcement.

3) UHPFRC I-shaped beam with or without transverse reinforcement subjected to shear force was found out failing by diagonal crack localization in web. The structural behavior of UHPFRC I-shaped beam can be classified by two phases based on previous test results. Microcracks arises with gradually decreased inclination after initial diagonal crack with 45° inclination and the microcracking area broadens. In the microcracking phases, the strength increase is stable with a constant stiffness. At one point, the crack localization occurs in the middle of microcracking area accompanying abrupt decrease of strength. Microcracking phase is similar to cracking phase of RC shear beam with transverse reinforcement, but macrocracking phase is comparable rather than RC shear beam without transverse reinforcement which is collapsed by diagonal tension failure.

The general approaches are considered to solve the UHPFRC I-shaped shear beam without transverse reinforcement. Diagonal tension failure in web due to crack localization is the only consideration and UHPFRC cracking behavior is the main issue to quantify the fiber reinforcement effect at the following chapter.

Chapter 3. Formulation and Solution Strategies

3.1 General

Diagonal tension failure in web is the controlling failure mode in I-shaped UHPFRC shear beams without stirrups. Previous researches indicate that UHPFRC shear beams behave stable increase in shear strength after an initial diagonal crack like RC shear beams with stirrups. However the ultimate limit state of the structure is controlled by a crack localization. The crack localization has to be interpreted by material and structure level simultaneously considering concrete tensile behavior. The UHPFRC cracking behavior should be defined by combination of micro-cracking behavior with hardening behavior and macro-cracking or crack localization with softening behavior. And then, a physical model considering the crack localization in a structure can be suggested by the appropriate design parameters based on the assumptions for material model.

It is necessary to define the applicable range for material and structure model considering the cracking characteristics of UHPFRC. In this chapter, a hierarchy for approaches on the thesis is suggested with respect to the existing approaches for RC structures. General approaches and previous researches to specify the solution strategies for UHPFRC shear behavior are reviewed and then the necessary explanations to give an evaluation of UHPFRC shear strength are clarified. The original definition for UHPFRC shear behavior is suggested in this chapter.

First of all, general approaches dealing with local failure and global failure of RC shear beam are studied. Limit analysis is the representative theory which

explains a global failure of RC structures. Therefore, global failure is usually regarded as failure of RC structures determined by yielding of steel reinforcement. In addition, fracture mechanics explains local failure of crack localization due to inherent heterogeneity of concrete composed of cement paste and aggregates. The former model is suitable to analyze RC shear beam with transverse reinforcement and the latter model is applicable to explain the size effect in RC shear beam without transverse reinforcement. And then, the UHPFRC shear behavior with global and local failure at the same time can be explained by each approach. In this dissertation, the a definition of shear behavior of UHPFRC I-shaped beam is suggested taking into account an adequate frame work for limit analysis coupled to fracture mechanics. In this regard, UHPFRC cracking behavior has to be analyzed in material and structural level (Fig. 3-1). Previous researches concentrated on material level with meso-mechanism, bond strength between cement matrix and a single steel fiber, but macro-mechanism in a range of structural level should be proposed considering structural design parameters.

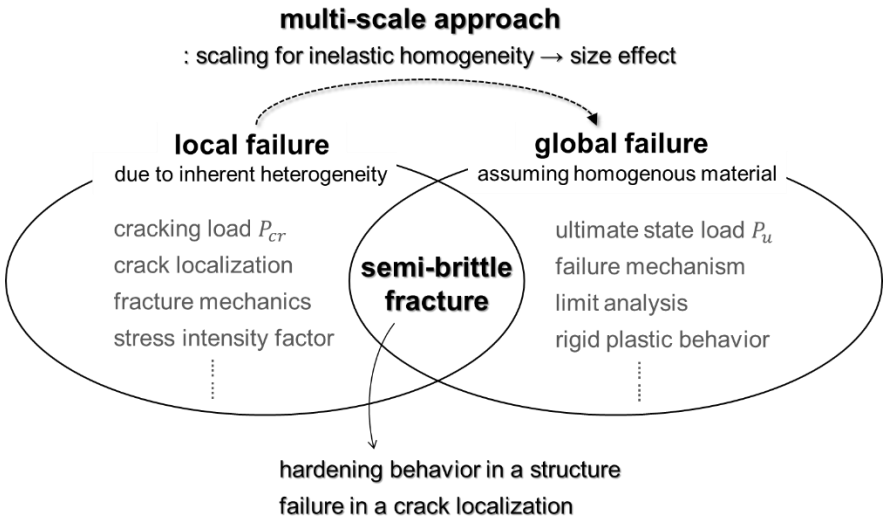

Fig. 3-1. Analysis framework for UHPFRC semi-brittle fracture

3.2 Basic Approaches on Physical Behavior of Concrete structures

3.2.1 Limit Analysis and Concrete Plasticity

The theory of plasticity deals with materials that can deform plastically under constant load when the load has reached a sufficiently high value. Such materials are called 'perfectly plastic materials', and the theory dealing with the determination of the load-carrying capacity of structures made of such materials is called 'limit analysis' (Nielsen and Hoang, 2011). In most RC structures, the maximum strength is attributed to yielding of reinforcement steel which can be assumed to be perfectly plastic materials. In case of the structural member failed by concrete crushing, not steel yielding, concrete should be compensated by using effectiveness factors, because concrete is not a perfectly plastic material, but exhibits a significant strain softening. The assumption for plastic material and discontinuities is too simplified, but it has the advantage to evaluate the ultimate strength logically in terms of the global failure of structures. The load carrying capacity at the ultimate limit state can be obtained with statistically or kinematically admissible state, possible collapse mechanisms of the structure.

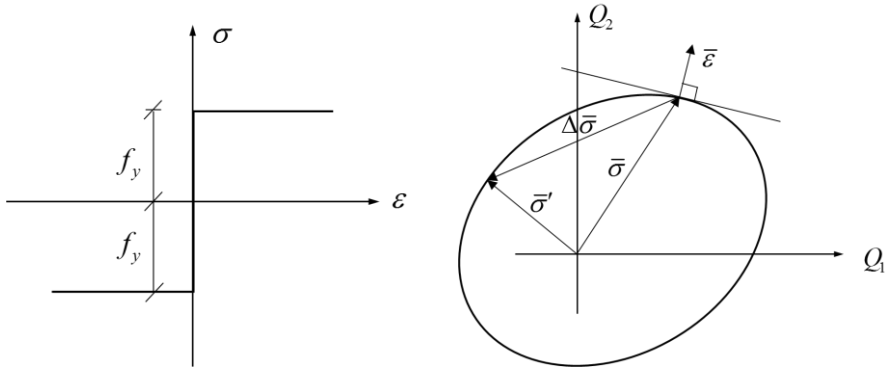

Fig. 3-2. General assumptions for limit analysis: (a) uniaxial stress-strain relation for a rigid-plastic material, (b) maximum work hypothesis (Nielsen and Hoang, 2011)

A rigid-plastic material is defined as a material in which no deformations occur at all for stresses up to a certain limit, the yield point (Fig. 3-2 (a)). For stress f_y at the yield point, arbitrary large deformations are possible without any change in the stresses. This assumption is applicable to the materials of which the plastic strains are much larger than the elastic strains. For arbitrary stress fields with a set of generalized stresses Q_i and the corresponding strains q_i, the yield point is assumed to be determined by a yield condition in Eq. (3-1).

$$f\left(Q_1, Q_2, \ldots, Q_n\right) = 0 \tag{3-1}$$

Von Mises's hypothesis on maximum work can give the stresses according to a homogeneous strain field in a rigid-plastic body. The dissipation energy D in a rigid-plastic body to the given strains can be expressed by W, the work per unit volume, area or length. The stresses corresponding to a given strain field assume such values that W becomes as large as possible. The principal implies that of all stress combinations satisfying the yield condition, we should find the stress field rendering the greatest possible work W. In a Q_i coordinate system like Fig. 3-2 (b), the surface $f = 0$ denotes the yield surface. Then W is equal to the scalar product of a vector of stresses $\bar{\sigma}$ and a vector of strains $\bar{\varepsilon}$. The principle of maximum dissipation has been derived from convexity of the yield surface and normality of the plastic strain rates. It is seen that W is stationary ($\delta W = 0$) only when Eq. (3-2) is satisfied where λ is an indeterminate factor. Thus $\bar{\varepsilon}$ becomes an outward-directed normal to the yield surface, which is called the normality condition or flow rule.

$$q_i = \lambda \frac{\partial f}{\partial Q_i}, \qquad i = 1, 2, \ldots, n \tag{3-2}$$

It is important to note that the flow rule only determines the strains, with the exception of a nonnegative factor in correspondence with the properties of

the material in the uniaxial case. In other words, only the ratios between the strains can be determined. The application of flow rule enables us to use the upper bond technique in a way that is consistent with the yield conditions (Nielsen and Hoang, 2011).

Defining yield condition of plastic rigid material is important to apply the limit analysis. Most failure criteria as hypotheses have been proposed from tests. In 1776, Coulomb advanced the frictional hypothesis. It is based on the observation that failure often occurs along certain sliding planes or yield planes, the resistance of which is determined by a parameter termed the cohesion and an internal friction, the magnitude of which depends on the normal stress in the sliding plane. Rankine and Lamé advanced the hypothesis that failure occurs when the greatest or smallest principal stress, respectively, assumes certain characteristic values. In 1868, Tresca suggested that for mild steel a failure condition could be used that requires only knowledge of the maximum value of the shear stress.

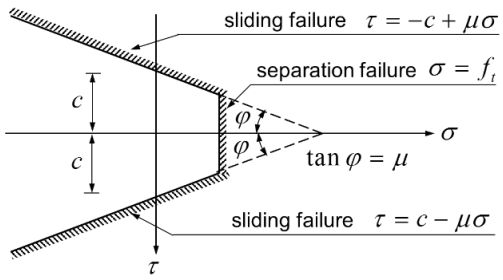

Fig. 3-3. Failure criterion for a modified Coulomb material

In 1882, a more general theory was advanced by Mohr, who assumed that failure occurs when the stresses in a section satisfy the condition $f(\sigma, \tau) = 0$ where σ and τ are the normal stress and the shear stress in the section. If this condition is illustrated in a σ, τ-coordinate system, Mohr's failure envelope, is obtained (Fig. 3-3). While the criterion adequately represents the

behavior of concrete for moderate compressive stresses, the concrete tensile strength is typically overestimated. Therefore, it was supplemented by a tension cut-off, resulting in the modified Coulomb failure criterion.

$$|\tau| + \sigma \tan\varphi - c = 0 \quad \text{and} \quad \sigma - f_{ct} = 0 \tag{3-3}$$

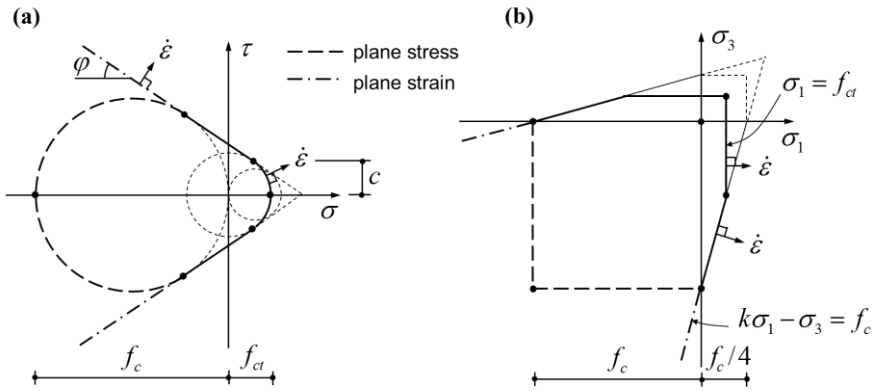

Fig. 3-4. Modified Coulomb failure criterion for concrete: (a) stress plane; (b) principal stress space. Note: tanφ=0.75. (Kaufmann, 1998)

Fig. 3-4 (a) illustrates the modified Coulomb failure criterion in the stress plane. The sliding criterion can be expressed in terms of the principal stresses as

$$k\sigma_1 - \sigma_3 = f_c$$
$$\text{where} \quad k = \frac{1+\sin\varphi}{1-\sin\varphi} \quad \text{and} \quad f_c = \frac{2\cos\varphi}{1-\sin\varphi} \tag{3-4}$$

Here f_c and f_{ct} are the uniaxial compressive and tensile concrete strengths, and c and φ denote the cohesion and the angle of internal friction of the concrete. The resulting six equations with five additional equations corresponding to Eq. (3-4) define the Coulomb yield surface, an irregular hexagonal pyramid in the principal stress space. The pyramid is cut by three

planes corresponding to Eq. (3-3), and the projection and section of which with the (σ_1, σ_3)-plane are shown in Fig. 3-4 (b).

The modified Coulomb failure criterion is a special case of a Mohr failure envelope. The dissipation per unit volume of the concrete can be expressed as Eq. (3-5) for any isotropic material.

$$dD = \dot{\sigma} \cdot \dot{\varepsilon} = c' \cdot \cot\varphi' \cdot \varepsilon_{(1)} \quad \text{where} \quad \varepsilon_{(1)} = \varepsilon_1 + \varepsilon_2 + \varepsilon_3 \tag{3-5}$$

Application of the principal of virtual work to a perfectly plastic body obeying the theory of plastic potential yields the basic theorems of limit analysis established:

(1) Lower bound theorem : Any load corresponding to a statistically admissible state of stress everywhere at or below yield is not higher than the ultimate load. The stress satisfies equilibrium and yield condition and the load will not be able to cause collapse of the body.

(2) Upper bound theorem : Any load resulting from considering a kinematically admissible state of deformation and setting the work done by the external forces equal to the internal energy dissipation is not lower than the ultimate load. Because it is not certain that the external load corresponding to the flow rule corresponds to the strain.

(3) Uniqueness theorem : Any load for which a complete solution, i.e. a statically admissible state of stress everywhere at or below yield and a compatible, kinematically admissible state of deformation can be found, is equal to the ultimate load.

For coinciding lower- and upper- bound solutions a uniqueness theorem was expressed. The lower-bound theorem of limit analysis remains valid for

statistically admissible states of stress containing discontinuities if the equilibrium conditions are fulfilled for elements on the stress discontinuities.

Consider the displacement discontinuity in Fig. 3-5, where the n-axis is perpendicular to the plane of the discontinuity and the displacement vector δ lies in the (n, t)-plane, forming the angle α with the t-axis parallel to the discontinuity. The displacement components u_n and u_t in the directions n and t, are assumed to vary linearly across the narrow failure zone of thickness w_i. This corresponds to constant strains within a zone of homogeneous deformation and then at the limit of w_i tending to zero, the strains tend to infinity.

$$u_n = \frac{|\delta| n \sin\alpha}{w_i} \quad \text{and} \quad u_t = \frac{|\delta| n \cos\alpha}{w_i} \tag{3-6}$$

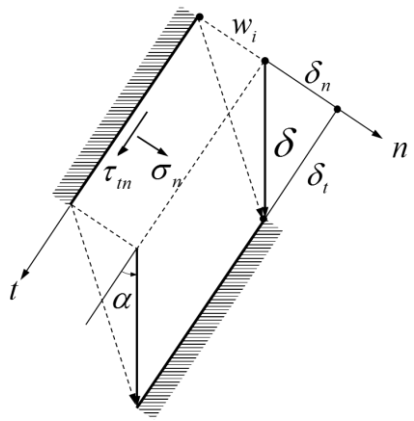

Fig. 3-5. Failure line based on displacement discontinuity: (a) narrow zone of homogeneous deformation; (b) Mohr's circle of strains

The upper-bound theorem remains valid for discontinuous states of strain if the dissipation in the discontinuities is taken into account when calculating the internal energy dissipation. Any yield condition of an isotropic material can be substituted by its associated Mohr envelope without loss of generality when

considering failure surfaces. The dissipation in displacement discontinuities can be established by explicitly calculating the scalar product of the stress and the strain vectors. Chen and Drucker showed that the dissipation per unit area of a failure surface in a material obeying a modified Coulomb failure criterion is equal to

$$dD \cdot w_i = \dot{\sigma} \cdot \dot{\varepsilon} \cdot w_i = \frac{\delta}{2}\left[\sigma_1\left(1+\sin\alpha\right) - \sigma_2\left(1-\sin\alpha\right)\right] \qquad (3\text{-}7)$$

It is very important to define the failure condition for concrete considering the appropriate failure mode such as separation failure and sliding failure with friction angle. Compressive strength of concrete is regarded as the crucial factor and the reduction factor for compressive strength of concrete compensates for cracking effect.

3.2.2 Fracture Mechanics in Concrete Structures

The term ‘fracture’ describes the local detachment of material cohesion in a solid body. It concerns a process that either partically disrupts the body which leads to the development of incipient cracks or entirely destroys it. Fracture of a structure is inevitably connected to the propagation of one or more cracks which can eventually lead to entire rupture and loss of its load carrying capacity. That is why particular emphasis is placed on the temporal and spatial progress of crack propagation. In fracture mechanics it is assumed that a macroscopic crack exists. This crack may be present from the very beginning due to a material defect or due to the component manufacturing. The macroscopic mechanical aspect of fracture can be categorized with respect of the load and fracture progression as follows (Kuna, 2013):

(1) Type of loading : Fracture process under static load are typical for load-bearing constructions in civil engineering. Mechanical loading is one important cause, but other physical loadings such as differential drying, temperature gradients, and chemical attack may also lead to severe cracking and deterioration of structures.

(2) Orientation of a crack in relation to its principal stresses : Failure is in most cases controlled by the local stress which is clearly determined by the principal stresses. Depending on the material, either hypotheses of the maximum principal stress (Rankine), the maximum shear stress (Coulomb) or extended mixed criteria (Mohr) are used. A distinction is being made between the normal-planar crack or cleavage fracture and the shear-planar crack or shear fracture.

(3) Stability of crack propagation : An important feature of fracture is the stability of the crack propagation. The fracture process is then marked

as unstable if the crack grows abruptly without the need to increase external loading. The critical condition is exceeded for the first time and persists without any additional energy supply.

(4) Magnitude of inelastic deformations : Depending on the amount of inelastic deformations or accumulated plastic work in the body that precede or accompany crack growth, distinctions are made between deformation-poor or brittle failure and deformation-rich or ductile failure.

Fatigue and dynamics of the fracture process such as subcritical crack growth and crack grow rate are another important issues, but fracture mechanics of concrete structures subjected to static loading is the primary subject in this chapter. Quasi-brittle material like concrete should be analyzed by non-linear elastic fracture mechanics. To introduce the terminology of fracture mechanics, the classical fracture mechanics approaches are explained in a historical development.

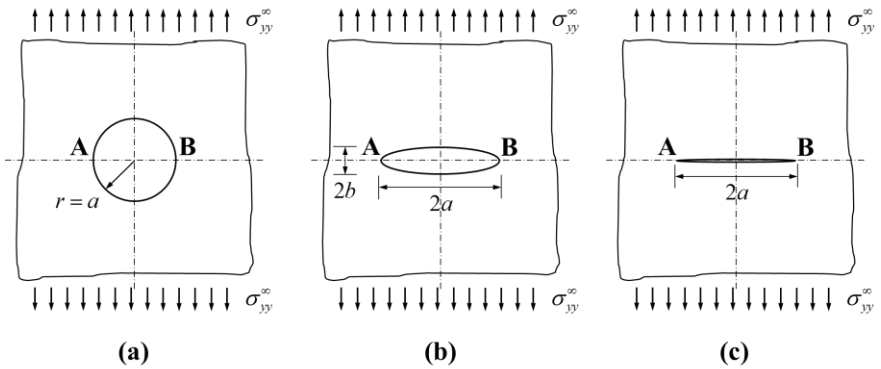

Fig. 3-6. Plate with (a) perfectly circular hole; (b) elliptical hole; and (c) slit

Stress approach by Kirsch (1898) and Inglis (1913) derive the local stress field at the hole in Fig. 3-6 (a). Semi-inverse method coupled with the Airy

stress function was applied to the body. When the shape of the hole is changed to elliptical, the stress concentrations become more severe (Fig. 3-6 (b)). The flatter the ellipse, the higher the stress concentrations, and the lower the measured failure stress of the plate will be. For a slit, that is when $b \to 0$ (Fig. 3-6 (c)), the tangential stress at the tip will become infinitely large. The stress approach is preferred to calculate the local stress, strain and displacement field in the presence of a line-crack.

Energy approach by Griffith (1921) derive the local stress field at the line-crack tip. It considers the body as a global perspective and energy balance. Fracture begins when there is a change in the total energy (Eq.(3-8) ~ (3-10)). Griffith applied the idea of progressive crack extension to ideally brittle material.

$$\Delta\Pi = U + W_s = -\frac{\pi\sigma^2 a^2}{E} + 2 \cdot \gamma_s \cdot 2a \tag{3-8}$$

$$\frac{d\left(\Delta\Pi\right)}{da} = 0 \tag{3-9}$$

$$\sigma_c = \sqrt{\left(\frac{2E\gamma_s}{\pi a}\right)} \tag{3-10}$$

where σ=remote stress or applied stress, σ_c=the critical stress for the onset of fracture, a=half of the crack length, U=the elastic energy released in an area of radius $2a$, W_s=the total surface energy needed to create the new crack area $2a$ and γ_s=the specific surface energy of the material.

After the failure of a Liberty ship at dockside attributed to damage at square-shaped hatches in 1943 during the Second World War, a series of experimental studies on crack propagation behavior was started. Irwin (1957) introduced the strain energy release rate, G_c. Irwin fracture criterion of Eq.

(3-11) is the basis for an energy-based fracture model for all material in a quasi-brittle manner. The value G_c is relatively easy to obtain by performing the fracture experiment of the material. Eq. (3-12) shows that the energy approach represented by G_c and the stress approach represented by K_c are equivalent.

$$\sigma_c = \left(\frac{2E\left(\gamma_s + \gamma_p\right)}{\pi a} \right)^{1/2} = \left(\frac{EG_c}{\pi a} \right)^{1/2} \tag{3-11}$$

$$K_c^2 = \sigma_c \sqrt{\pi a} = EG_c \tag{3-12}$$

where γ_p =the surface plastic energy of the material, G_c =strain energy release rate (=crack extension energy [J/m^2]) and K_c =stress intensity factor or fracture toughness [MPa$\sqrt{m}$].

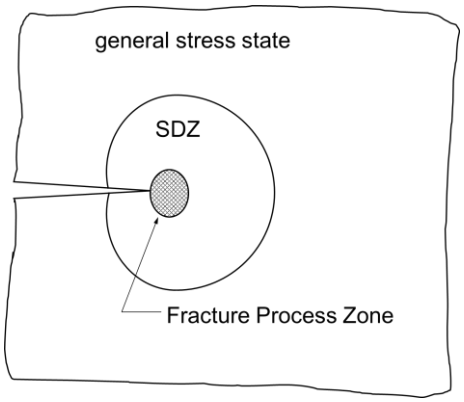

Fig. 3-7. LEFM conditions apply if the fracture-process zone is fully contained in the singularity-dominated zone (SDZ) (Sanford, 2003)

William (1952) used the Airy stress function to solve the problem of a wedge of arbitrary apex angle, 2α , and obtained general solution to a particular singular problem, which becomes a base in the development of LFEM theory. The formula for calculating the displacement, strain, and stress

near a crack tip becomes the same functional form regardless of crack size, specimen geometry, and loading system. Only the parameter $\sigma\sqrt{\pi a}$ changes with the applied stress and crack size. Irwin (1957) substituted Stress Intensity Factor K [MPa$\sqrt{m}$] for $\sigma\sqrt{\pi a}$. Fracture mechanics concerns the level of singularity near the sharp cracks in elastic bodies and there is no governing equation. LEFM condition is applied of the fracture process zone is contained in the singularity dominated zone (Fig. 3-7).

Irwin (1960) predicted the existence of plastic zone ahead of crack tip. Plastic zone at the crack tip is not small enough, stress intensity factor K is not applicable. Non-linear and elastoplastic fracture mechanics has been developed based on energy approach. Rice (1968) adapted the principal of conservation of energy momentum to 2D non-linear elastic body containing a singularity and suggested an integral form which called as J-integral (Fig. 3-8 and Eq. (3-13)). Energy release rate for non-linear elastic bodies can be defined by J-integral.

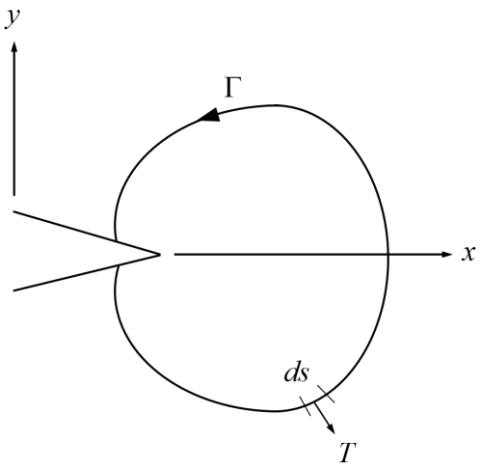

Fig. 3-8. A J-integral integration path

$$J = \frac{d\Pi}{da} = -\int_{\Gamma} W dy + \int_{\Gamma} T \frac{\partial u}{\partial x} ds \qquad (3\text{-}13)$$

where Π = potential energy of body, Γ =the path of the integral which enclose the crack, $W = \int \sigma_{ij} d\varepsilon_{ij}$ =the strain energy per unit volume due to loading, T =the outward traction (stress) vector acting on the contour around the crack, u =the displacement vector, ds =an increment of the contour path, x, y =the rectangular coordinate and $T(\partial u / \partial x) ds$ =the rate of work input from the stress field into the area enclosed by Γ .

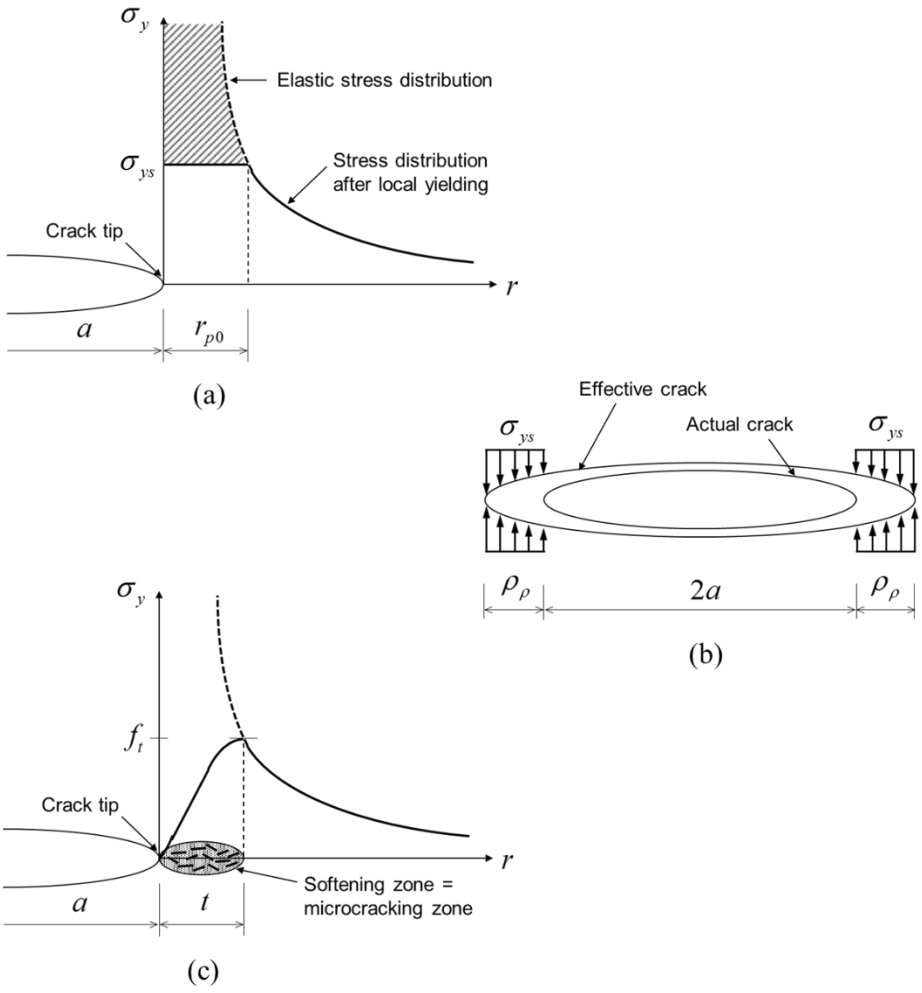

Fig. 3-9. Principal of (a) the plastic crack-tip model; (b) closing pressure at crack tips; and (c) similarity of the fictitious crack model

Barenblatt (1962) devised a cohesive crack model that served as a basis for subsequent developments in concrete fracture mechanics. In Fig. 3-9 (a), (b) the principal of the plastic crack-tip model is shown. The size of the plastic zone is t, advancing in front of the stress-free crack with length $2a$. The LEFM analysis should lead to a stress singularity at the tip of the stress-free crack, but through the assumption of the cohesive zone, also referred to as the process zone, the maximum stress is limited to the yield stress σ_y.

In 1976, Hillerborg, Modéer, and Petersson proposed an extension of the aforementioned plastic crack-tip model for concrete fractures. The so-called 'Fictitious Crack Model' included a process zone similar to the plastic crack-tip zone, although the stress distribution would not be uniform, the maximum 'yield stress' was much smaller, namely equal to the uniaxial tensile strength of concrete (Fig. 3-9 (c)).

The specific fracture energy G_f and the characteristic length l_{ch} are used to try to quantify the brittleness of concrete in the fictitious crack model. The specific fracture energy G_f is defined as the amount of energy needed to create one unit crack area and is equal to the area under the softening curve of stress and crack opening relationship. The fracture energy can be written as Eq.(3-14). Higher specific fracture energy would mean a more ductile material. The characteristic length l_{ch} of the material defined as Eq. (3-15).

$$G_f = \int_0^{w_c} \sigma(w) dw \tag{3-14}$$

$$l_{ch} = \frac{EG_f}{f_t^2} \tag{3-15}$$

where $\sigma(w)$ =stress in separation with crack opening w, w_c =the maximum crack opening and f_t = the tensile strength

Hillerborg and coworkers proposed that the characteristic length is a measure of the brittleness of the concrete. However the brittleness of a material may differ when the structural condition change (Elfgren, 1989). Eq. (3-16) shows a brittleness number as the quotient of the elastic energy U stored in the structure and the fracture energy W_s. The suggested brittleness number is a measure for the size of the structure.

$$\frac{U}{W_s} = \frac{L^3 f_t^2 / E}{L^2 G_f} = \frac{L f_t^2}{E G_f} = \frac{L}{l_{ch}} \tag{3-16}$$

Failure of concrete structures typically involves stable growth of large cracking zones and the formation of large fractures before the maximum load is reached. The typical characteristics of plastic failure is that the structure develops a single-degree-of-freedom mechanism such that the failure in various parts of the structure proceeds simultaneously, in proportion to a single parameter. Such failures are manifested by the existence of a long yield plateau on the load-deflection diagram. If the load-deflection diagram lacks such a plateau, the failure is not plastic but brittle (Fig. 3-10).

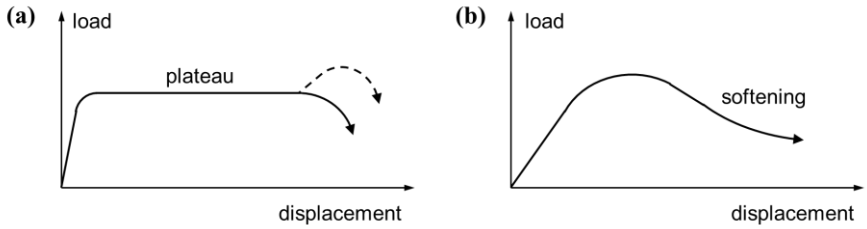

Fig. 3-10. Load-deflection curves with and without yielding plateau (adapted from ACI committee 446, 1992)

When there are no significant geometric effects (such as the $P-\Delta$ effect in bucking), the absence of a plateau implies the existence of softening

in the material due to fracture, cracking, or other damage. This further implies that the failure process cannot develop a single-degree-of-freedom mechanism but consists of propagation of the failure zones throughout the structure (Bazant, 1998). The failure is nonsimultaneous and propagation (Fig. 3 11).

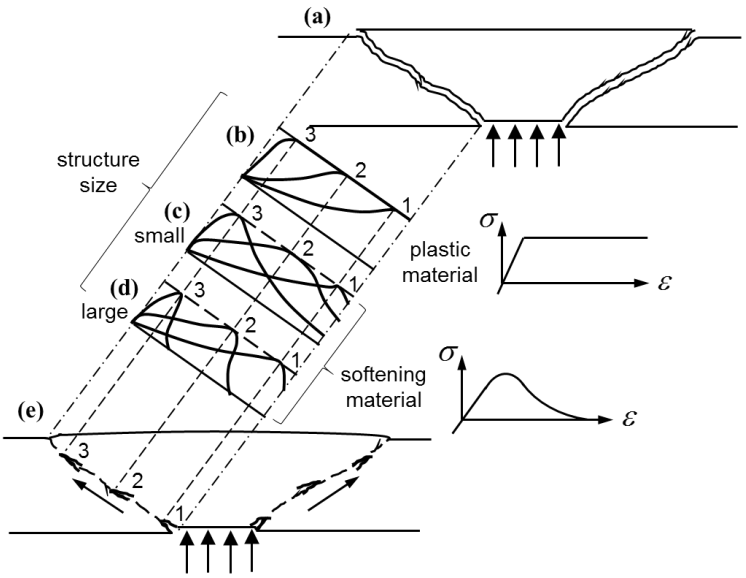

Fig. 3-11. Influence of the structure size on the length of the yielding plateau in a punched slab (adapted from ACI committee 446, 1992)

3.2.3 Comparison of Basic Approaches on Cracked Concrete

Limit analysis is suitable to explain ductile failure of rigid-plastic material and fracture mechanics deals with brittle failure which arises from the abrupt crack propagation. The field covered by two approaches is located opposite. However concrete is quasi-brittle material and inelastic behavior due to micro-cracking is observed. Concrete cracking behavior is the key to alleviate the drastic ductile or brittle failure. The concrete failure usually belongs to the area between limit analysis and LEFM (Fig. 3-12). Assumptions for Concrete cracking is directly related to the failure mode and failure criterion. The assumptions for dissipation energy along the crack faces according to the given failure mode determines the maximum strength of concrete structures. Hence it has to be clarified that the assumptions for concrete cracking in limit analysis and fracture mechanics before setting a framework for two approaches.

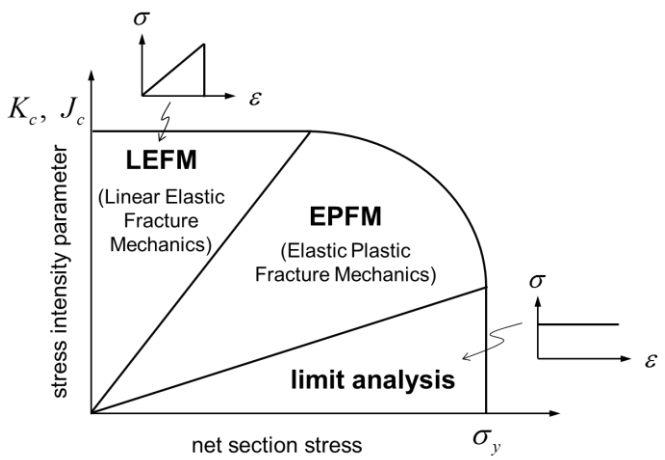

Fig. 3-12. Failure analysis diagram for a ductile material or quasi-brittle material

Ordinary concrete which have a compressive strength less than 40 MPa must at least be treated as a two-phase material, cement paste and aggregate

particles. Concrete is inherently heterogeneous as composite material with lots of pores in cement and irregular shape of aggregate. The surface of cement and aggregate is usually weaker than the strength between cement itself, so cracks occur along the aggregate in normal strength concrete. Microcracks are present even before loading due to shrinkage of the cement paste. Application of a simple isotropic failure condition like the modified Coulomb criterion is approximate.

Fracture mechanics considers that concrete cracking is primarily caused by the material's low tensile resistance. There are three types of fracture modes distinguished in classical fracture mechanics. Fig. 3-13 depicts the three fracture modes: The opening mode or mode I, in-plane shear or mode II and out-of-plane shear or mode III. However, brittle failure in concrete structures usually occurs without steel reinforcement and most of facture model for concrete concerns the tensile cracking behavior of mode I. Mode II and mode III are usually neglected.

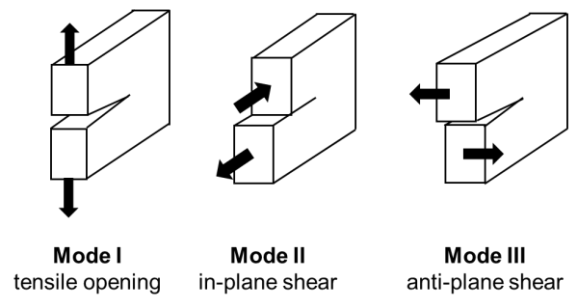

Fig. 3-13. Sketches of the three pure modes in fracture mechanics

Non-linear fracture mechanics for mode I quasi-brittle material like concrete, a nonlinearity beyond the proportional limit f_y exits before the maximum stress (Fig. 3-14 (a)). After the proportional limit, randomly distributed microcracks are formed. At some point of before the peak stress, microcracks begin to localize into a macrocrack that critically propagates at the

peak stress. It is noted that the tensile strength f_t is different than the conventional concrete strength obtained from a regular tensile test. The tensile strength is a material fracture parameter which does not depend on the size, geometry of the tested specimen and the testing procedure.

Distribution of the tensile stresses on the newly formed crack surfaces depends on the definition of the fracture process zone ahead of the initial crack tip (Fig. 3-14 (b)). The fracture behavior of concrete is greatly influenced by the fracture process zone. The physical mechanisms in the fracture process zone are modelled by a cohesive pressure acting on the crack surfaces. The inelastic fracture response due to the presence of the fracture process zone may be taken into account by a cohesive pressure acting on the crack faces.

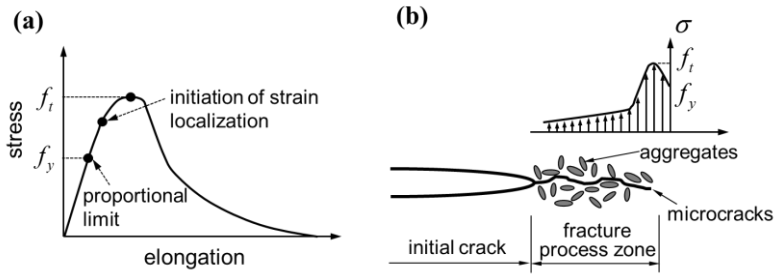

Fig. 3-14. General description of quasi-brittle fracture: (a) tensile stress-elongation curves, and (b) sketch of concrete and fracture process zone including effect of crack-tip microcracks (Shah et al., 1995)

Limit analysis assumes a rigid-plastic material, so basically failure criteria explains the physical behavior. The crack surfaces are regared as a complete discontinuity and called as failure line. All energy dissipates at the failure line and the stresses and displacements are determined by the failure criteria. Depending on the material, either hypotheses of the maximum principal stress (Rankine), the maximum shear stress (Coulomb) or extended mixed criteria (Mohr) are used (Fig. 3-15).

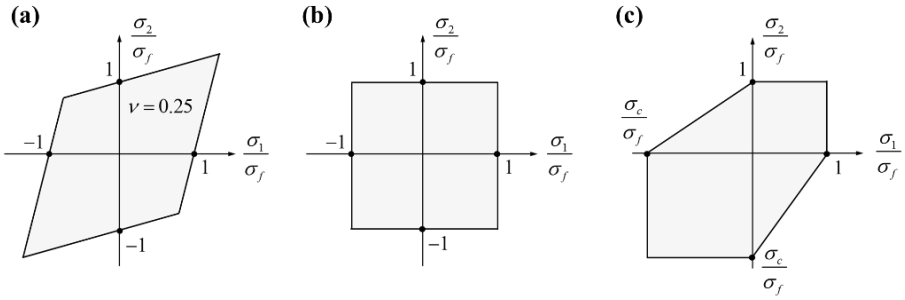

Fig. 3-15. Failure loci in plane stress for three common brittle failure theories: (a) Saint Venant failure theory (Maximum normal strain), (b) Rankine failure theory (Maximum normal stress), and (c) Mohr-Coulomb failure theory (Largest principal stress) (Sanford, 2003)

A distinction for failure theories is being made between the normal-planar crack of mode I and the shear-planar crack of mode II as shown in Fig. 3-13. The failure line or discrete crack can be considered same and failure criteria for the material can be suggested by one theory. The difference is a major concern. Fracture mechanics focuses on the stability of crack propagation at the crack tip and limit analysis concentrates on the yield strength at failure.

Limit analysis adopts the Mohr-Coulomb failure criterion as shown in Fig. 3-16, Fig. 3-17 and Fig. 3-19. There are two types of failure mode: (1) separation failure governed by tensile strength, and (2) sliding failure governed by compressive strength, confined strength and friction angle. Fig. 3-16 ~ Fig. 3-20 shows the failure line according to the separation failure and sliding failure determined by pure compression, tension and shear strength. Either pure compression, tension or shear tests gives the parameters to define Mohr-Coulomb criterion.

The compression failure condition will be satisfied in all sections that are tangent planes to the set of conical surfaces having the top angle $90^\circ - \varphi$ and axis parallel with the direction of force. The corresponding conical failure is often experienced in tests using cylindrical test specimens (Fig. 3-16).

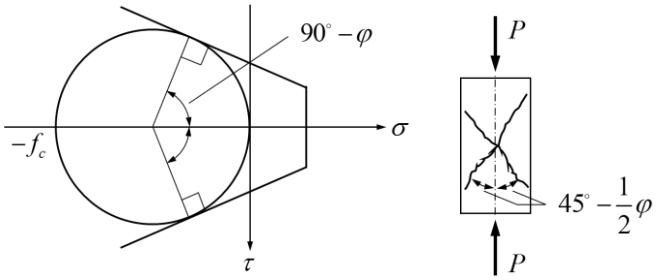

Fig. 3-16. Mohr's circle and failure section at pure compression

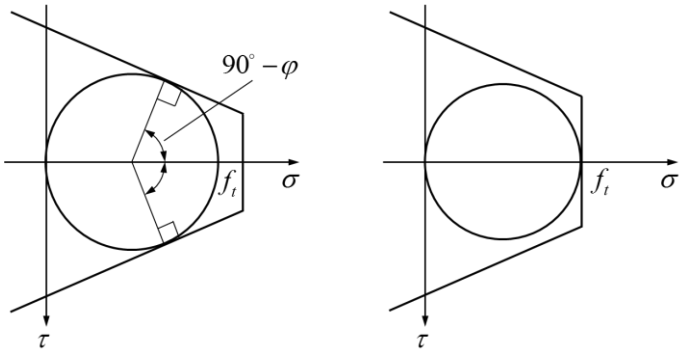

Fig. 3-17. Mohr's circle at pure tension

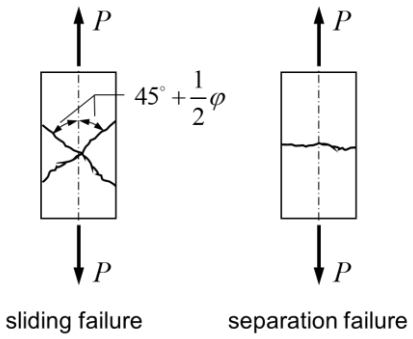

Fig. 3-18. Failure section at pure tension

The tensile test holds the possibility of sliding failure as well as separation failure. By the sliding failure we may get failure in two sets of sections forming the angle $90^\circ-\varphi$ with each other and the angle $45^\circ+\varphi/2$ with the direction

of force. By separation failure the failure section is perpendicular to the direction of force (Fig. 3-17 and Fig. 3-18).

The shear strength of the material f_v is determined by a test and the test also holds the possibility of sliding failure as well as separation failure. At sliding failure, the failure section will form an angle $\varphi/2$ with the x- and y- directions, respectively, and at separation failure, the failure will take place in the section that forms an angle of 45° with the x- and y- directions (Fig. 3-19 and Fig. 3-20).

Following the assumptions of the rigid-plastic material and the flow rule, once the failure section occurs, the maximum strength is determined and the direction of deformation along the failure line obeys the perpendicular to the failure criteria at the critical point.

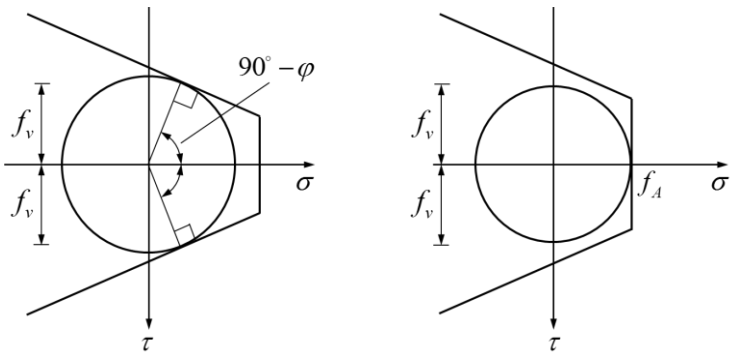

Fig. 3-19. Mohr's circle at pure shear

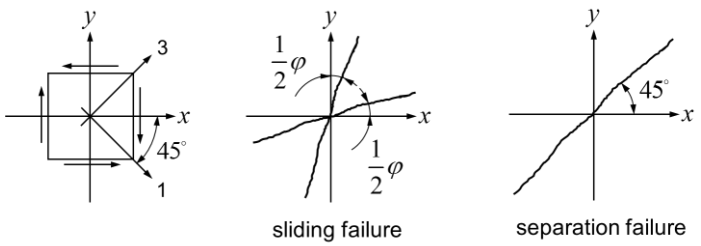

Fig. 3-20. Failure section at pure shear

Application of a simple isotropic failure condition like the modified Coulomb criterion is approximate. The application of plastic theory is that the strength parameters normally are lower than the standard values. The main reason is that the concrete is cracked, and cracking reduces the strength. The effective strengths has to be defined by giving the effectiveness factor for the strength. In addition, the softening behavior of concrete in compression and tension after the peak value exists. Since the theory of perfectly plastic materials is unable to take into account the softening in a rational manner, this phenomenon must be dealt with by effectiveness factors as well.

The strength reduction due to cracking might be subdivided into (1) strength reduction due to microcracking present even before any load is applied, (2) strength reduction due to load-induced microcracking, and finally (3) strength reduction due to macrocracking. While the microcracking present before loading may be assumed to lead to an isotropic material, load-induced microcrackin and macrocracking will cause anisotrophy. It consists of either considering cracked concrete to be isotropic with the effective strength parameters or by dealing with the strength parameters only in certain selected directions depending on the crack system. In tests with approximate homogeneous stress fields, cracking is the main concern.

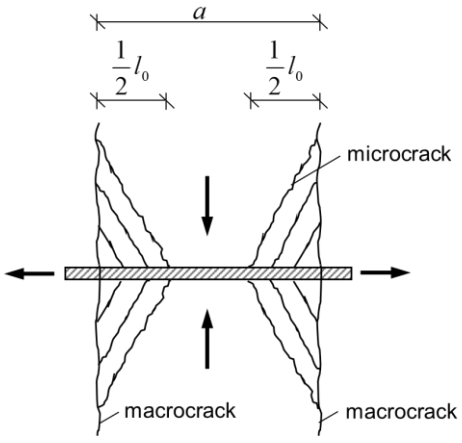

Fig. 3-21. Formation of microcracks between two macrocracks

It is likely that load-induced microcracking is a main cause of the strength reduction always found in shear problems. Particularly if, after the formation of a macrocrack, reinforcement crossing the cracks is stressed, the transfer of shear stresses from reinforcement to concrete and the resulting bursting stresses in regions near the cracks may give rise to a substantial increase in microcracking. Fig. 3-21 shows two parallel macrocracks, which are acrossed by a reinforcement bar perpendicular to the cracks. The reinforcement bar is stressed in tension. The microcracks are shown schematically in the figure.

The failure condition for a macrocrack may also be formulated by using modified Coulomb failure condition. The cohesion is strongly reduced to about 50% of that of the virgin material, but the friction angle seems to be unchanged. Cracks strictly parallel to the load direction will not change the strength even if the cracks have no strength at all. However, if the cracks have an inclination to the load direction, strength may be reduced (Fig. 3-22).

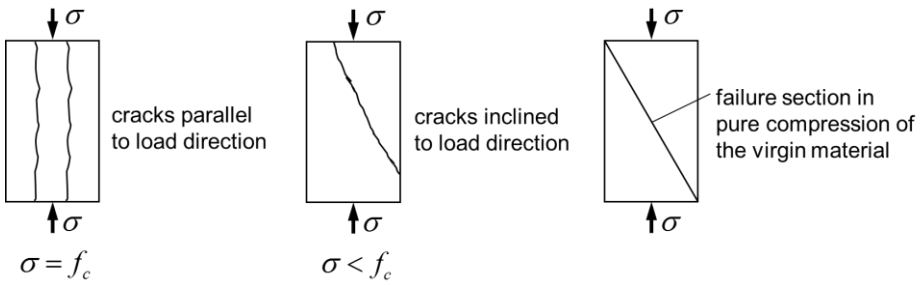

Fig. 3-22. Influence of cracks on compressive strength

Where sliding in cracks plays an important role is the shear failure of orthotropic panels reinforced in two perpendicular directions with different reinforcement ratios. The initial cracks will be formed under 45° with the sections with pure shear, and this initial crack direction sill be roughly independent of the reinforcement. However, if the reinforcement ratios in the two reinforcement directions are different, the final compression direction will

be different from the initial one. This means that the final compression direction in the concrete might be as shown in Fig. 3-23. Such a reduced compressive strength has been measured by Vecchio and Collins (1986) and they measured the strains.

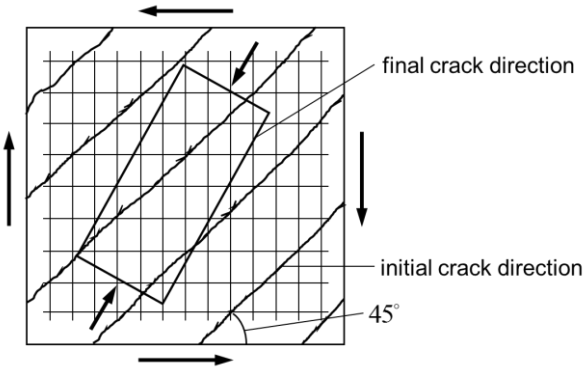

Fig. 3-23. Orthotropic panel in pure shear

Heterogeneity of ordinary concrete inevitably comes from physical behavior of two different particle composites, cement paste and aggregates. Whereas fracture mechanics interests tensile behavior of concrete, concrete cracking behavior in limit analysis focuses on compressive cracking behavior subjected to confining pressure given by steel reinforcement. Comparison of the assumptions for two mechanical approaches is noted in Table 3-1. Fracture mechanics have no governing equations and the size of the fracture process zone and the shape of softening curve at the fracture process zone determines the dissipated elastic and surface energy on the discrete crack face. These characteristics influences the structural capacity depending on the structure size when the failure is caused by the critical crack. On the other hand, limit analysis gives the solutions in the form of the maximum strength and the cracking behavior of concrete compensates for the strength reduction factor directly. These methods are simple and easy, but has to be supported by empirical evidences. In case of in-plane shear failure in uniform stress field, the cracking

problems take an important role.

In a RC structure, the interaction between concrete and steel reinforcement determines the cracking behavior within the serviceability limit state. Bond shear stress-slip relationship is idealized from pull-out test results. The bond strength is expressed in terms of concrete tensile strength and it is usually assumed that the crack width is controlled by the strain of steel reinforcement. At the ultimate limit state, once tension stiffening of steel reinforcement and compression softening behavior of concrete in cracked RC structures are evaluated, equilibrium and compatibility conditions with a constant crack spacing gives the maximum strength in a structural element subjected to shear. Crack spacing in RC structures is controlled in a structural level with a range of 200 ~ 500 mm. On the other hand, UHPFRC is fiber reinforced concrete. The microstructure is extremely dense, so able to withstand bond stress between cement matrix and steel fiber in a range of half of fiber length within 10 mm. Therefore, the cracking behavior of UHPFRC has to be investigated in a material level first.

Table 3-1. Application Criteria of Basic Mechanical Approach for Ordinary Concrete

	Limit Analysis	Fracture Mechanics
Applicable Failure	Ductile failure	Brittle failure
Governing Rule	Flow rule, Normality rule	Brittleness number
Major Concern	Maximum strength problem	Stability problem after crack initiation
Appropriate Solution for	Maximum strength P_u on failure mechanism with large deformation	Cracking strength P_{cr} on abrupt failure by crack localization
Equilibrium Eq.	Energy conservation	Energy release rate at crack initiation
Basic Assumptions	Tensile strength is resisted by steel reinforcement only. (Tensile strength of concrete is usually neglected.)	Stress redistribution zone is determined by shape of softening curve in material tensile behavior.
Application	Usual structural elements	Shear beam without stirrup Flexural beam with lightly longitudinally reinforcement
Failure Criterion	Steel yielding with Flow rule Concrete Crushing with Mohr-Coulomb criterion (frictional failure)	Critical stress intensity factor Critical energy release rate
Theory for linear behavior	Rigid-plastic material	LEFM
	Energy dissipated all when any deformation occurs according to material failure criteria with flow rule	Energy dissipated all at the crack tip. Energy dissipation limits to singularity problem represented as stress intensity factor K_I
Theory for nonlinear behavior	Strength reduction factor	Damage mechanics
	Strength reduction factor compensates the characteristics of nonlinear structural response due to cracking effect like compression softening behavior.	Energy is dissipated continuously after crack propagation. FPZ exists along the crack. FPZ is represented by intrinsic size based on energy release rate G_I .

LEFM = linear elastic fracture mechanics, FPZ = fracture process zone

3.3 Multiscale Approach based on Fracture Mechanics

3.3.1 Consideration of UHPFRC Material Characteristics

UHPC is an almost homogeneous cementitious composite based on reactive powder. The composition of fine aggregates of less than 0.5 mm particle size and fillers make UHPC high density and low porosity, which cannot provide the aggregate interlocking usually obtained in ordinary concrete. UHPC has a high compressive strength greater than 150 MPa, but extremely brittle behavior is observed at the same time. Fiber reinforcement in UHPFRC gives outstanding ability of stress distribution as well as high tensile strength and release the brittleness of UHPC effectively. The material characteristics of UHPFRC can be summarized by high strength concrete and fiber reinforcement effect.

Compressive strength of UHPFRC is slightly affected by the amount of fiber content and fiber reinforcement effect is usually neglected. The ductility of compressive behavior increases with the higher content of fiber volume, but the elastic modulus and the peak strength is mainly determined by the mix composition of UHPC, not fiber content. On the other hand, tensile behavior of UHPFRC has outstanding post-cracking behavior and the mechanical properties of cracked UHPFRC is determined by the contribution of fiber reinforcement.

In a UHPFRC structure, fiber reinforcement acts effectively and the fiber reinforcement can contribute as the replacement of the conventional reinforcement rebars. The physical mechanism of fiber contribution can be explained by passive confinement in Fig. 3-24. Mixing fibers in concrete can have the same effect as applying external confinement. The biaxial failure envelops, more specifically, the biaxial compression regime, expended when

fibers were added to the concrete, indicating that the fibers restrain crack growth in the free (unconfined) direction. Thus, like adding a small confining stress in the third direction, fibers will help to restrain crack growth. The two mechanisms thus appear to be similar.

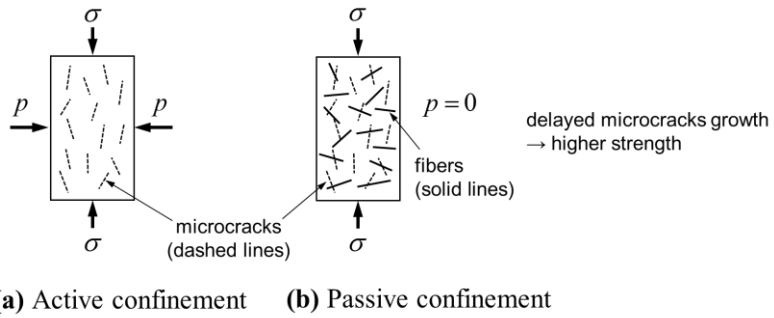

Fig. 3-24. Delayed microcrack growth in general leads to a higher strength. Either active (external) confinement (a) or adding fibers to the concrete (b) is an effective measure (van Mier, 2012)

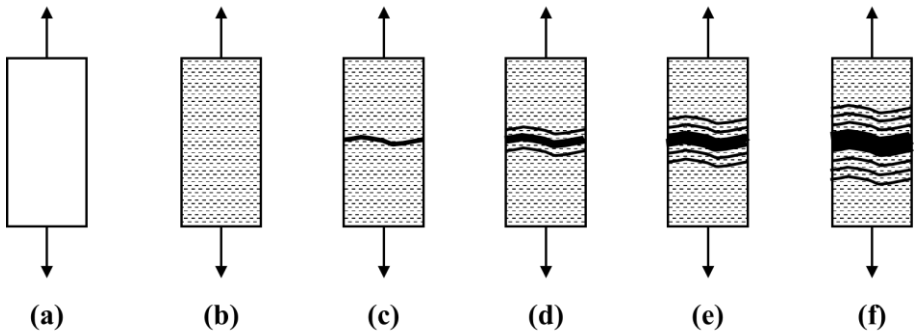

Fig. 3-25. Multiple cracking sequence, as assumed in the analytical model of multiple cracking (Markovic, 2006) :
(a) initial state; (b) microcracks; (c) the first through-crack; (d) the creation of second and third through-crack; (e) and (f) only the first through-crack continues to open, as other through-cracks are only being created, up to a certain saturation level

The cracking characteristics of UHPFRC is the key issue to analyze shear behavior of UHPFRC in-plane members. The stable microcracking behavior occurs in a wide range and the strength and deformation increase due to

microcracking is large enough to induce tensile hardening behavior. The previous works focused on uniaxial tensile behavior according to the cracking phase and Fig. 3-25 shows a typical cracking behavior of UHPFRC.

Modelling of multiple cracking based on fracture energy: The energy based analytical model for the multi cracking sequence was developed by Tjiptobroto and Hansen (1992) for cementitious composites with discontinuous randomly oriented fibers (Fig. 3-25). The main assumption of their analytical model is that the first formed macrocrack in a concrete specimen, will also be the dominant failure crack. It was also assumed in this model, that the change of the initial tensile stiffness corresponds to the formation of this first through-crack. It is supposed that other through-cracks should be only created. Therefore, the energy terms will be different for different types of cracks. For the opening of the first through-crack, both the fracture energy needed to debond the fibers and to pull them out will be taken into account. (Markovic, 2006).

The exiting model is based on pull-out test of single fiber, so the physical model is scaled in a range of length of steel fibers. However, the cracking behavior is different to the size and boundary condition of the structural member. The material with softening strain behavior under direct tensile test can show the hardening deflection behavior under bending test. Scaling for inelastic homogeneity region is needed according to the member size.

In this chapter, the representative previous theoretical models dealing with interaction between single fiber and cement matrix in UHPFRC are introduced first, and then the limitations of the models are pointed out. To overcome the shortcomings of the previous models, an appropriate macro-mechanism for UHPFRC cracking behavior is also investigated. We can get a hint from the macro-mechanism model for ordinary concrete.

3.3.2 Meso-mechanism for Concrete and UHPFRC Material

Cracking behavior of concrete has been developed by theories dealing with composition of heterogeneous cement particles. Hence, the mechanical scale they focused on lies in a range of particle sizes, and the model parameters are also related with the particle sizes. Nevertheless the physical mechanisms on the macrocrack faces called as meso-mechanism in this dissertation are important with respect to a structural behavior. The separation behavior between the cracks determines tensile behavior and the sliding behavior between the cracks determines shear transfer ability. The physical behavior of separation and sliding behavior between cracks is one of the important assumptions for limit analysis and fracture mechanics, and the structural capacity of a concrete structure is derived from these assumptions. The representative analytical models dealing with meso-mechanism of concrete and UHPFRC is depicted in Fig. 3-26.

Ordinary concrete is a composite of cement paste and aggregate and macrocrack arises along the lines of aggregate and cement paste. According to the van Mier (2007), the fracture process of concrete loaded in tension, begin by the formation of numerous fine microcracks in the interfacial zone around aggregated grains. If the tensile load continues to increase, these microcracks connect with each other and form larger cracks, which subsequently leads to failure (Fig. 3-26 (a)). Hence, the maximum size of aggregates is usually considered as the key parameter to determine the cracking characteristics of concrete. The previous researches on concrete fracture is mainly about the shape of softening curve in tensile stress-crack width relationship in a meso-scale. Size effect approach applies to a concrete structure when a critical crack governs the collapse of the structure, but the theory basically based on statistical research in a structural scale. Application to the RC structures, the aggregate interlocking (Walraven, 1980) plays a role when reinforcement rebars crosses

the cracks, and theoretical models such as modified compression field theory (Vecchio and Collins, 1985) explains the compression softening behavior in a uniform stress field using the stress on the crack faces according to the crack width.

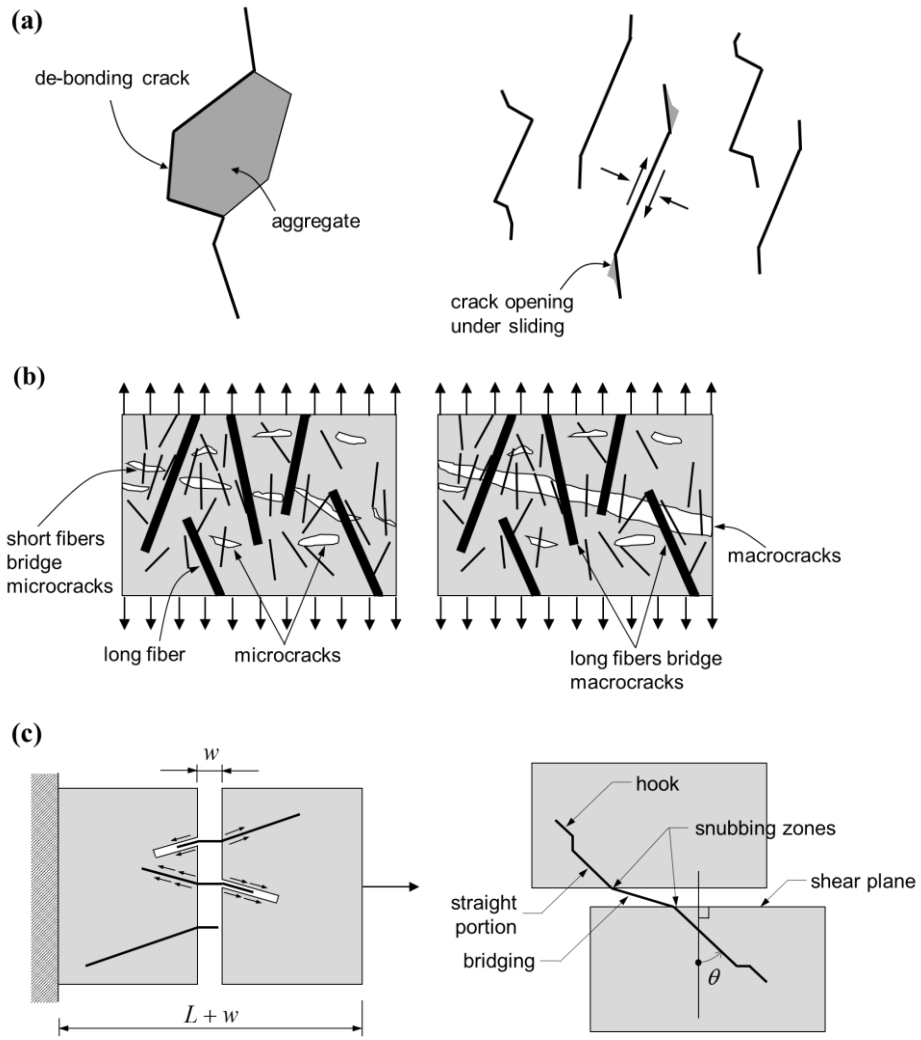

Fig. 3-26. Meso-mechanisms in various type of concretes: (a) the internal splitting cracks developed in soft cement matrix along the stiff aggregate particles (van Mier, 2013); (b) the influence of short thin fibers and long thick fibers on the bridging cracks (Markovic, 2006); (c) bond stress between matrix and fibers (Foster et al., 2008)

Cracking behavior of UHPFRC has been developed with respect to the material mix composition and most researches take an attention to the interaction of steel fiber and cement matrix. These theoretical and mechanical investigation considers that the macro-scaled cracking mechanism is the summation of individual fiber action. It grounds the empirical evidence which is that the shape, volume content of fiber mainly affects the tensile behavior of UHPFRC, whereas the compressive strength hardly changes its peak value regardless of fiber effect. The recommendations on UHPFRC structural design, such as AFGC (2013) and *fib* bulletin (2011), use the fiber orientation factor as a quantified value of fiber efficiency.

Markovic (2006) found a basic principles of the mixture design of Hybrid-Fiber Concrete, and the theory explains well how a typical fiber bridging acts on crack faces. Assumptions are following as below:

1) The application of short and long steel fibers together in one same concrete mixture.

2) To ensure that all these fibers are homogeneously distributed in each part of the structure element on the structure level.

3) To ensure that all these fibers are as effective as possible in crack bridging on the material level.

The idea of the utilization of short and long fibers together is given in Fig. 3-26 (b). Short fibers can bridge microcracks more efficiently, because they are very thin and their number in concrete is much higher than of that of the long thick fibers, for the same fiber volume quantity. Taking into account that microcrack formation and crack bridging by fibers, occurs in the first phases of tensile loading, the short fibers can have a significant influence on the increase of the tensile strength. As microcracks grow and join into larger macrocracks, the long hooked-end fibers become more active in crack bridging. In this way,

primarily the ductility can be improved, and partly also the tensile strength. Long fibers can provide a stable post-peak response. Short fibers will be less and less active, because they are being more and more pulled out, as the crack width increases.

Variable Engagement Model (VEM) is the most acceptable theory to explain the cracking behavior of UHPFRC in a meso- and macro-scale simultaneously (Fig. 3-26 (c)). The model is developed by integrating the behavior of single, randomly oriented fibers over 3D space with both fiber pull-out and fiber fracture considered. Based on quantifiable material and mix parameters, the model is shown to be capable of capturing the stress versus crack opening displacement response for both plain and deformed steel fiber reinforced composites in both the pre- and post-peak stage (Voo and Foster, 2004). Assumptions are following as below:

1) Behavior of FRC in tension is equal to the superposition of the individual components.

2) The geometric centers of the fibers are uniformly distributed in space and all fibers have an equal probability of being oriented in any direction.

3) All fibers pull-out from the side of the crack with the shorter embedded length while the longer side of the fiber remains rigidly embedded in the matrix.

4) Displacements due to elastic strains in the fibers are small relative to displacements resulting from slop between the fibers and the matrix.

5) Energies from fibers bending are small, relative to pull-out components, and can be neglected.

For mechanically anchored fibers after the adhesion between the fibers and

matrix is broken, slip between the matrix and the fibers must occur before the anchorage is engaged. The cracking opening displacement w in Fig. 3-26 (c) for which the fiber becomes effectively engaged is termed the engagement length w_e defined by Eq. (3-17).

$$w_e = \alpha \tan\theta \tag{3-17}$$

w_e is the crack opening displacement of the fiber and α is a material constant measured by pull out test of a single fiber and has the units of length. θ is an arbitrary value of a single fiber and this value plays a role as a fiber orientation factor by integrating the engaged fibers with the uniform probabilistic assumption. Given a random distribution of fibers with equal probability that any given fiber crossing a crack has a shorter embedded length of between zero and the half of fiber length, the average value of the local orientation factor for all engaged fiber can be found. Multi fiber strength can be defined by global orientation factor, aspect ratio of fiber, volumetric ratio of fibers and fiber-matrix bond strength.

As mentioned introduction in this chapter, VEM also considers that the tensile behavior of UHPFRC is a summation of two different components, cement matrix and fiber. The model is reasonable and powerful, but in the process of probabilistic integration from material characteristics of a single fiber, the physical behavior of composites can be missed. In addition, VEM drives the stress-crack opening displacement relationship using mechanical properties of fiber, without tensile strength test and it can be vulnerable to application of UHPFRC structural design in field.

3.3.3 Macro-mechanism for Compressive Concrete Behavior

Macro-mechanism in this dissertation concentrates on the structural geometry related to the material cracking behavior, whereas the meso-mechanism, such as aggregate interlocking and VEM, is investigated in a range of particle size, such as the maximum size of aggregate or the geometry of steel fiber. The most differential assumption for two approaches is about concrete characteristics. Meso-mechanism assumes that concrete is a heterogeneous cementitious composites combined with two different particles, but macro-mechanism assumes that concrete is homogeneous material and cracked concrete is homogeneous and anisotropic material. The assumption for macro-mechanism is usually applied to concrete structure design. In spite of the given assumption, stress and crack opening width perpendicular to the crack faces are still important for both approaches.

The existing analytical cracking model for fiber reinforced cementitious composites are focused on tensile softening response as explained in previous chapter. However, tensile hardening behavior is observed in UHPFRC with greater than 1.5% fiber volume content (Wille et al., 2011; Voo and Foster, 2004) and the strain hardening behavior has to be investigated with respect to macro-scale. In a strain hardening behavior, energy dissipates by unit volume and concrete cracking characteristics has to be analyzed with different respect view rather than crack opening behavior. We also need to analyze the cracking behavior using inelastic fracture mechanics, not LEFM.

The representative phenomenon due to tensile hardening behavior is micro-crack propagation and the consequent macro crack at in-plane shear members. Tensile softening curve explains the interaction between the existing macrocrack assuming energy dissipates on a crack surface, so the opening behavior governs the interactions. However tensile hardening behavior affects

crack inclination, especially when the specimen is subjected to shear forces. Hence, the key issue for inelastic behavior and shear problem of UHPFRC structures can be mode II behavior which can be represented as inclination of crack propagation, and this effect has to be quantified as a substitution of conventional steel reinforcement. An analysis will always start by calculating the inclination of the mode II crack. This qualification seems correct because it propagates in a straight line. No rotations are caused by the loading system which would turn the situation toward a mixed-mode crack (Fig. 3-27).

Fig. 3-27. Pulled-out fibers on the fracture surfaces of a UHPFRC member

There is no analytical model to investigate inelastic behavior of UHPFRC in tensile stress-strain relationship. Instead of it, we can find a hint for inelastic behavior of UHPFRC from compressive behavior of concrete regarding to the following points: (1) noticeable inelastic hardening behavior and softening behavior (2) failure represented by combination of various failure mode. In comparison to tensile failure, compressive fracture is at least one step up in the degree of complexity. Shear, and probably also buckling instabilities close to the surface of specimens/structures subjected to compression are two additional mechanisms that cannot be neglected. When shear fracture occurs (mode II and mode III) and confinement is large enough to prevent local tensile fracture, frictional restraint in cracks starts to become more important and may eventually have an effect on the fracture process (van Mier, 2013).

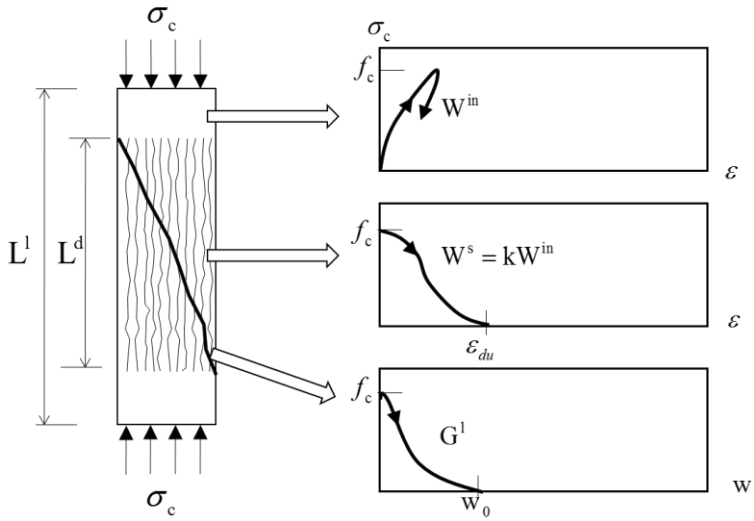

Fig. 3-28. Illustration of the CDZ model on a specimen loaded in uniaxial compression (Markeset and Hillerborg, 1995)

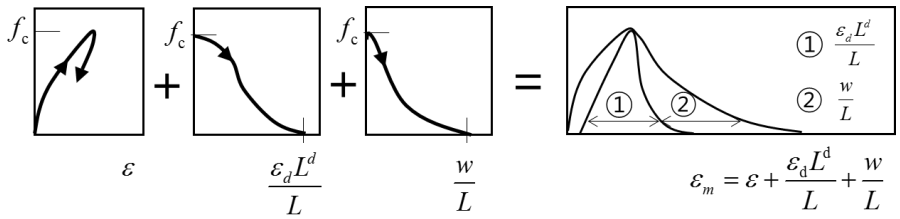

Fig. 3-29. Composition of the complete stress-strain curve (Markeset and Hillerborg, 1995)

Markeset (1995) extended the fictitious model to compressive behavior of the material with Hillerborg. The model, named the Compressive Damage Zone (CDZ) model, is based on the hypothesis of compressive failure within a zone of limited length. In this damage zone, the failure mode is a combination of distributed axial splitting and localized deformation. Within the damage zone the post-peak behavior is described by means of two curves, one related to the distributed splitting cracking and one to the localized deformation. The compressive strain caused by the axial splitting cracks is assumed to be

proportional to the tensile fracture energy G_I. It is shown through compressive tests of specimens of different length and width that the proposed failure hypothesis is realistic.

In the CDZ model, it is assumed that failure of relatively slender concrete specimen takes place within a damage zone of limited length L^d, whereas the parts outside this zone are unloaded during failure. The deformation of the specimen under centric compression is described by means of three curves shown in Fig. 3-28.

The first curve is the stress-strain curve for the material loaded up to the compressive strength f_c and then unloaded. This curve is valid for the concrete material in the whole specimen.

The second curve shows the relationship between the stress and the average additional strain ε_d within the damage zone, related to the formation of longitudinal cracks and a corresponding additional lateral strain within this damage zone.

The third curve is a stress-deformation curve, related to localized deformations. These deformations are in Fig. 3-28 illustrated as shear deformation in an inclined shear band, but they may also take place in other ways.

The total deformation of the specimen shown in Fig. 3-29 is

$$\Delta L = \varepsilon L + \varepsilon_d L^d + w \tag{3-18}$$

$$\varepsilon_m = \varepsilon + \varepsilon_d \frac{L^d}{L} + \frac{w}{L} \tag{3-19}$$

This equation, which is valid for L greater than L^d, is illustrated in Fig. 3-28. For a specimen length L equal to or less than the damage zone length

L^d the average strain becomes

$$\varepsilon_m = \varepsilon + \varepsilon_d + \frac{w}{L} \tag{3-20}$$

Concrete nonlinear behavior has focused on compressive failure. Tensile characteristics of ordinary concrete is usually disregarded or dependent to the compressive strength. Cracking strength of concrete hardly governs the failure of RC structures, and the cracks had been formed are confined by crossed reinforcement in a structure. That is why the structural capacity of RC members is determined by strength and elongation of the steel reinforcement.

UHPFRC has to be investigated regarding to tensile failure. Tensile strength of UHPFRC plays a similar role to analyze UHPFRC structural behavior. It can pay attention to UHPFRC tensile behavior with micro-cracking behavior before peak load and macro-cracking of softening behavior in the similar way of the compressive behavior of ordinary concrete with softening phenomenon. Fracture mechanics approach is a major part with respect to the multiscale approach, because the failure of a UHPFRC structure is assumed to be caused by crack localization which belongs to brittle failure. The failure due to crack localization is determined by the characteristics of concrete cracking.

A multiscale approach is concluded by determining the criterion for applicable scales of proposed model and test results. Design criteria for combined action is determined by limit analysis and the characteristics of brittle failure due to cracking phenomenon of UHPFRC is specified by fracture mechanics. The failure due to crack localization is determined by the characteristics of concrete cracking. Existing researches on concrete cracking belongs to brittle failure analyzed by fracture. For example, there are cohesive crack models for semi-brittle materials derived from localization of damage coupled to plasticity (Larsson and Runesson, 1995)

3.4 Semi-Brittle Fracture and Size Effect in UHPFRC structures

3.4.1 Definition of Semi-Brittle Fracture

From the previous experimental studies, the controlling failure mode of UHPFRC I-shaped shear beams without stirrups has been found out as diagonal tension failure in web. The diagonal tension failure is usually observed in RC shear beams without stirrups and the failure arises with a brittle manner with a brittle manner right after the critical crack emerges. Despite the final failure mode is same as the diagonal tension failure, UHPFRC members collapses differently rather than RC members, in case the contribution of fiber reinforcement is large enough to substitute conventional shear reinforcement in a range of inelastic behavior before the peak load. It has to be assumed that UHPFRC has tensile hardening behavior with sufficient fiber content. In this paper, let this kind of UHPFRC shear failure be called as "semi-brittle fracture".

Here is typical shear behavior of UHPFRC I-shaped beams without stirrups, which fails as semi-brittle fracture :

1) After an initial crack is observed in a web, microcracks due to fiber reinforcement spreads in a wide area with stable strength increase.

2) While new microcrack forms and the microcracks broaden its area without crack opening, the stiffness of the UHPFRC member remains constant. The shape of microcracking area corresponds to the relatively uniform compression field in web.

3) At some point, either a particular diagonal crack or cracks opens increasingly and then the other microcracks close. The particular crack is called as the critical crack, and we name the process of the critical

crack formation the crack localization.

4) When the opening width of the critical crack is reached to the certain value, the shear member has its peak load and then collapses instantly. In other words, the crack localization occurs in a short time, and the post-peak behavior is very brittle.

Previous experimental studies reported that UHPFRC shear beams without stirrup have an increase of strength due to micro-cracking after initial cracking before the crack localization and the increase is more than twice of the cracking load. Fig. 3-30 shows wide microcracking region in web and the critical crack pattern which induces the structural capacity as explained above. Based on these empirical evidences, semi-brittle fracture can be defined, with respect to an analytical view point of limit analysis and fracture mechanics, as follows :

1) The microcracking behavior in web is similar to the cracking behavior of RC shear beams with stirrups after initial crack occurs in terms of strength-displacement relationship and cracking patterns. After the microcracks are formed, they still resists the applied forces stably and the resistance increase is stable with a constant stiffness. The contribution of fiber reinforcement can be represented by UHPFRC tensile strength and the microcracking area in web can be regarded as uniform compression field. Hence, the variable angle truss analogy based on limit analysis can be applied.

2) The process of crack localization and the final failure mode is similar to the diagonal tension failure of RC shear beams without stirrups. The kind of failure belongs to fracture in a brittle manner, but the inelastic behavior including pre- and post-peak behavior is more ductile than that of RC members. Therefore, the peak strength of UHPFRC I-shaped shear beams without stirrups is explained by fracture mechanics, especially inelastic fracture theory.

Following the chapter, it will be discussed how two approaches of limit analysis and fracture mechanics combines each other, especially regarding to the terminology and assumptions applicable to the major premise. In addition, the technical methods which is needed to analyze semi-brittle fracture will be suggested conceptually.

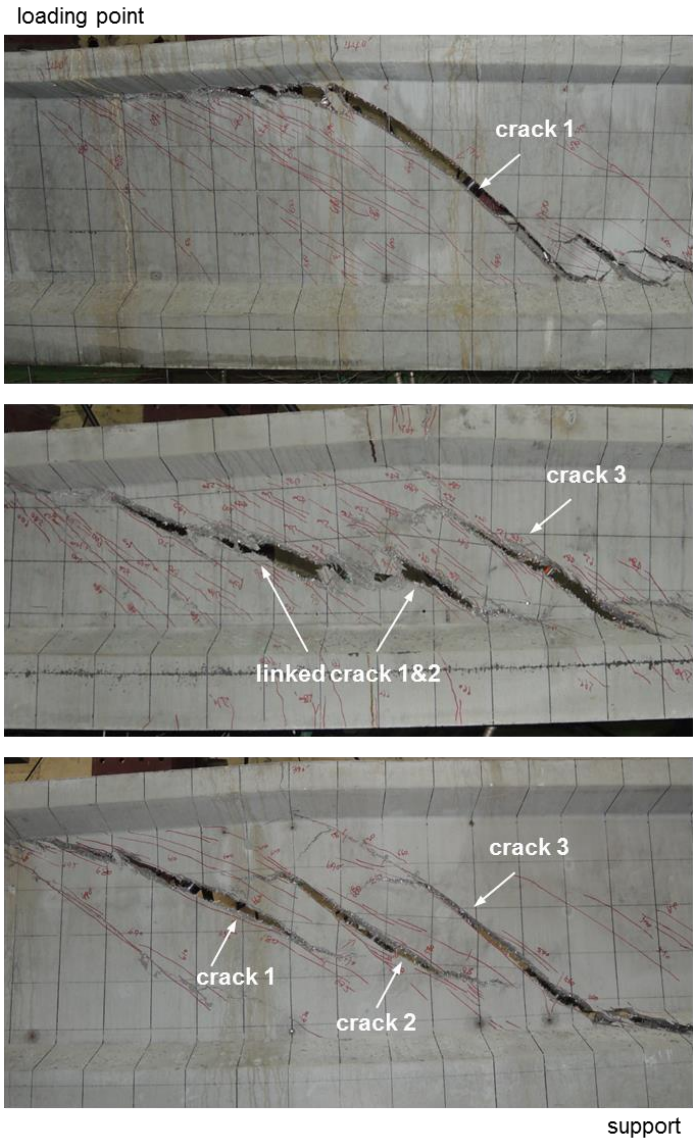

Fig. 3-30. Typical crack pattern in UHPFRC I-shaped shear beams without stirrups at the ultimate state (Localized major cracks are indicated in the figures.)

3.4.2 Framework for Limit Analysis coupled to Fracture

From the definition of semi-brittle fracture, we can get a hint of solution for UHPFRC in-plane shear problems. Final failure is caused by crack localization, which usually occurs after the initial cracking in RC shear beams without stirrups, and has been considered to belong to fracture mechanics. However the inelastic part of UHPFRC microcracking contributes to the strength increase dominantly, so the microcracking behavior has to be analyzed how this behavior induces the strength increase and the crack localization.

The other important issue to be pointed out is that tensile strength of UHPFRC determines the structural capacity. The tensile stress and strain relationship of UHPFRC is a resultant of fiber reinforcement effect. The previous studies on UHPFRC tensile behavior such as VEM (Voo and Foster, 2004) consider that UHPFRC is the composites of cement matrix and fiber and the tensile strength is a summation of individual fiber's bond strength taking into account fibers' distribution like fiber orientation factor (AFGC, 2013; Fehling et al., 2014; Voo and Foster, 2004). These meso-scale approaches are questionable to apply its result to design strength directly. The probabilistic method which they adopted cannot give any perception of physical mechanisms in a macro-scale.

In this dissertation, limit analysis instructs that the physical behavior of microcracking and the resulting maximum strength of UHPFRC in-plane shear members are suggested, and fracture mechanics gives the strength degradation for the maximum strength due to the crack localization with respect to macro-mechanisms of UHPFRC heterogeneity. Basically fracture mechanics deals with the stability problem and does not give a governing equation. Thus, the method of coupled to limit analysis and fracture mechanics has been introduced by previous studies.

Two kinds of formulas are possible to obtain the load capacities corresponding to nonlinear fracture mechanics is to exploit the size effect law (Bazant and Planas, 1998). One can start from the formula based on plastic limit analysis which now exists in the code, and introduce in it a correction due to the size effect law. Alternatively, one can set up the ultimate load formula based on LEFM, and introduce into it a correction according to the size effect law.

First one is suitable to structures of normal sizes exhibit failures that are closer to limit analysis approximately applies. The accuracy of the type of correction would decrease with increasing size, as the behavior is getting more brittle and more remote from the size to which plastic limit analysis approximately applies. For very large structures of for certain types of failure (anchor pullout, diagonal shear), the failure is known to be very brittle, actually closer to LEFM than to plastic limit analysis. In that case, the second kind of formula must be expected to give a more realistic result. The error of this correction increases with a decreasing structure size and is the smallest for large sizes close to the LEFM asymptote (Bazant and Planas, 1998).

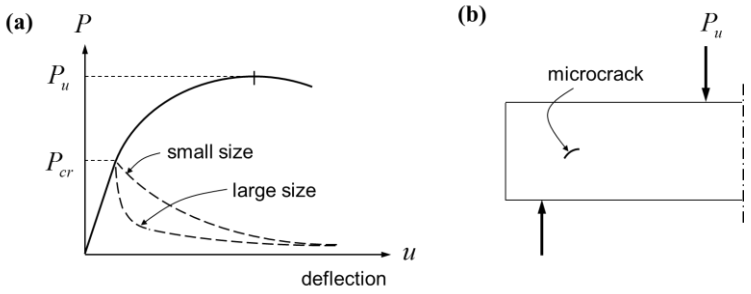

Fig. 3-31. (a) Load-deflection curves for a relatively ductile structure (solid line), and for a brittle structure that fails at first cracking (dashed line). (b) A brittle structure failing at crack initiation, the crack at maximum load still being microscopic. (Bazant and Planas, 1998)

The main line will be to develop solutions using plastic theory based on the modified Coulomb failure conditions. These solutions are then modified by

the effective strength parameters determined on the basis of the tests available. It is believed that such as approach will be the most useful one for the engineering profession at the present stage of development. It will be far more useful than a completely empirical approach, which is still dominating many areas of the concrete field (Nielsen and Hoang, 2012). The plastic solutions will be found using the notations f_c and f_t for the strength parameters. In applications, f_c and f_t are then replaced by effective strength.

Table 3-2. Terminology applied to two Mechanical Approaches

	Limit Analysis	Fracture Mechanics
Material Characteristics	Homogeneous material with ductile behavior	Heterogeneous material with inherent imperfection
Material strength	Effective strength considering microcracking effects	Material constant
	Experimental result	Characteristic value
Maximum strength of a structure	Yield strength	Cracking strength
Governing equation	Lower bound approach & Upper bound approach	(none)
Stability problem	(always stable)	Stability problem as boundary of fracture criteria
Energy dissipation	Energy density per unit Volume	Energy release rate per unit crack Surface (Area)
Crack surface (assumption for discontinuity)	Failure line (complete discontinuity)	Crack propagation (in a way of mode I, II, III)
Application for concrete structures	Strength at ULS	Size effect
Method for reflecting inelasticity	Strength reduction factor for material strength	FPZ and damage mechanics

mode I=crack opening, mode II=in-plane shear, mode III=out-of-plane shear, ULS=ultimate limit state, FPZ = fracture process zone

Before suggesting framework for limit analysis and fracture mechanics, the terminology used in each approach should be unified with appropriate assumption for UHPFRC members. Table 3-2 identifies the terminology of two approaches in accordance with the unified criteria. Based on the given criteria, the basic assumptions can be derived in order to apply two approaches at the same time.

The application field of two approaches seems to be opposite, so the assumptions have to be constructed carefully considering the empirical evidences and reasonable logic development ;

1) The material strength is determined by experimental results. Tensile strength directly applies to design equation as the effective strength based on limit analysis. UHPFRC material is assumed to be homogeneous without ductile behavior, and the fiber orientation factor does not taken into account. At this point, test methods to measure the tensile strength are the important issue and the effective strength and the relevant safety factor should be analyzed differently depending on the test method.

2) The failure criterion of UHPFRC follows the Mohr-Coulomb criterion, not Rankine criterion. Fiber reinforcement in UHPFRC activate as a form of passive confinement and this confinement turns out to be as effective as the conventional reinforcement. The characteristic phenomenon of frictional failure is that the yielding failure is determined by the given pressure, which is usually explained by confinement effect. The Mohr-Coulomb criterion can explain two physical failure mechanism, separation failure and sliding failure. The frictional failure due to fiber reinforcement is essential to analyze the shear behavior of UHPFRC members.

3) Microcracking in a UHPFRC structure is analyzed by limit analysis.

It is assumed that the stiffness of load-displacement relationship is constant and the shear strength can be evaluated using variable truss analogy. The crack opening as well as the inclination of the compression field are subjected to certain limits. Responsible for these limits are the deformations, especially the crack widths necessary to reach ultimate resistance, yielding of longitudinal and stirrup reinforcement in RC members (Grob and Thürlimann, 1976), but UHPFRC material in this case. The yield strength based on limit analysis is the upper limit in case of UHPFRC members, because the value can be obtained by the assumption of material ductility but UHPFRC ductility is not enough for the assumption.

4) Crack localization is a phenomenon of a result of stress concentration and has to be analyzed in a different way from ductile yielding. The post-peak behavior of UHPFRC tensile strength is neither ductile nor extremely brittle, so the crack localization should be analyzed by inelastic fracture mechanics. The energy release rate which determines the brittleness of a structure can be expressed by size effect.

In summary, UHPFRC material with tensile hardening behavior due to microcracking is assumed to be homogeneous. The tensile strength is an effective strength and the value is already reflected the heterogeneity due to fiber distribution. Fiber reinforcement effect is taken into account for Mohr-Coulomb failure criterion with frictional angle. In the application of the shear strength evaluation, the hardening behavior is analyzed by variable angle truss analogy in limit analysis and the brittleness due to cracking localization is considered by size effect using fracture mechanics. The brittleness of UHPFRC structures comes from an anisotropy due to microcracking behavior and a lack of ductility. The fracture toughness of UHPFRC will be investigated in a macro-level.

3.4.3 Brittleness and Size Effect in Structural Design

One of the simplest ways to incorporate fracture mechanics into design practice is though the size effect, or modification of structural strength with the size of the structure (Fig. 3-32). The size effect is the most compelling reason for adopting fracture mechanics. The load capacity predicted by plastic limit analysis or any theory in which the material failure criterion is expressed in terms of stress or strain are said to exhibit no size effect. The size effect represents the deviation from such a prediction. The size effect on the structural strength is the deviation, engendered by a change of structure size, of the actual load capacity of a structure from the load capacity predicted by plastic limit analysis (van Mier, 2013).

The size effect is defined through a comparison of geometrically similar structures of different sizes. It is conventionally characterized in terms of the nominal strength. According to the classical theories, such as the elastic analysis and plastic limit analysis, the nominal strength is constant independent to the structure size for any structural geometry. On the other hand, failures governed by LEFM exhibit a strong size effect. The concrete structures exhibits transitional behavior as depicted by solid curve in Fig. 3-32 (b). This curve approaches a horizontal line for the strength criterion if the structure is very small, and an inclined straight line if the structure is very large.

The size effect on ductility of structures is characterized by the deformation at the failure point (Fig. 3-33). Failure occurs closer to the peak as the size increases. For loading in which the load is controlled, structures become unstable at the maximum load, while for loading in which the displacement is controlled, structures fail in strain-softening range. This effect is predicted by fracture mechanics, and it can be explained by that strain energy is available to drive the propagation of the failure zone in a larger structure.

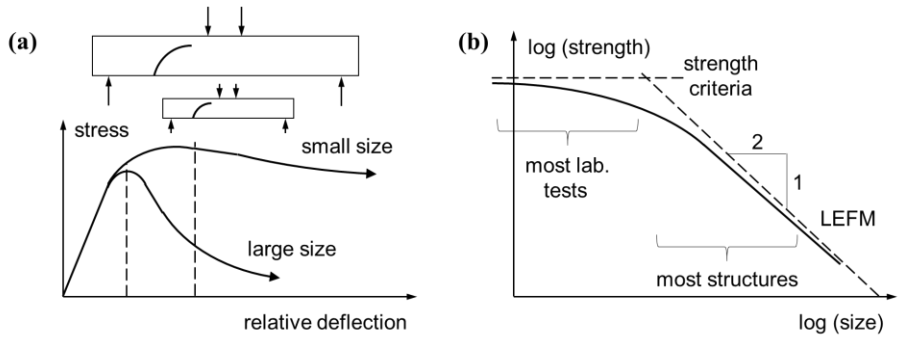

Fig. 3-32. Size effects: (a) on the curves of nominal stress vs. relative deflection, and (b) on the strength in a bilogarithmic plot (adapted from ACI committee 446, 1992)

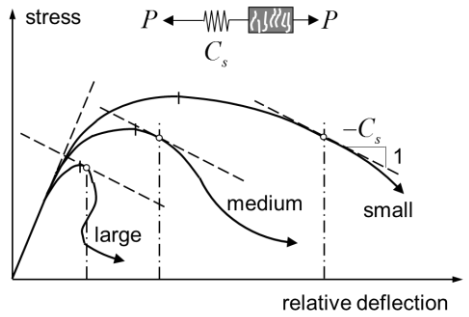

Fig. 3-33. Size effect on structural ductility (adapted from ACI committee 446, 1992)

There are different types of size effect (Bazant and Planas, 1998) as below :

1) Boundary layer effect, also known as the wall effect. This effect is due to the fact that the concrete layer adjacent to the walls of the formwork has inevitably a smaller relative content of large aggregate pieces and a larger relative content of cement and mortar than the interior of the member. Therefore, the surface layer, whose thickness is independent of the structure size and is of the same order of magnitude as the maximum aggregate size, has different properties. The size effect is due to the fact that in a smaller member, the surface layer occupies a large portion of the cross-section, while in a large member, it occupies

a small part of the cross-section. In most situations, this type of size effect does not seem to be very strong.

2) Statistical size effect, which is caused by the randomness of material strength and has traditionally been believed to explain size effects in concrete structures. The theory of this size effect, originated by Weibull (1939), is based on the model of a chain. The failure load of a chain is determined by the minimum value of the strength of the links in the chain, and the statistical size effect is due to the fact that the longer the chain, the smaller is the strength value that is likely to be encountered in the chain. This explanation, which certainly applies to the size effect observed in the failure of a long concrete bar under tension, is described by Weibull's weakest-link statistics. However, on closer scrutiny this explanation is found to be inapplicable to most types of failures of reinforced concrete structures. In contrast to metallic and other structures, which fail at the initiation of a macroscopic crack, concrete structures fail only after a large stress redistributions and a release of stored energy, which, in turn, causes a much stronger size effect, dominating over any possible statistical size effect. At the same time, the mechanics of failure restricts the possible locations of the decisive crack growth at the moment of failure to a very small zone. This causes the random strength values outside this zone to become irrelevant, thus suppressing the statistical size effect. We will also see that some recent experiments on diagonal shear failure of reinforced concrete beams contradict the prediction of the statistical theory.

3) Fracture mechanics size effect, due to the release of stored energy of the structure into the fracture front. This is the most important source of size effect, and will be examined in more detail.

A size effect occurs in RC elements when the failure by yielding of longitudinal steel bars is excluded in advance (brittle failure takes then place in a compressive concrete zone). Comprehensive investigation on a size effect were carried out by Walraven and Lehwalter (1994) for different RC beams. The size effect is applied to shear strength of RC members without stirrups in euro code.

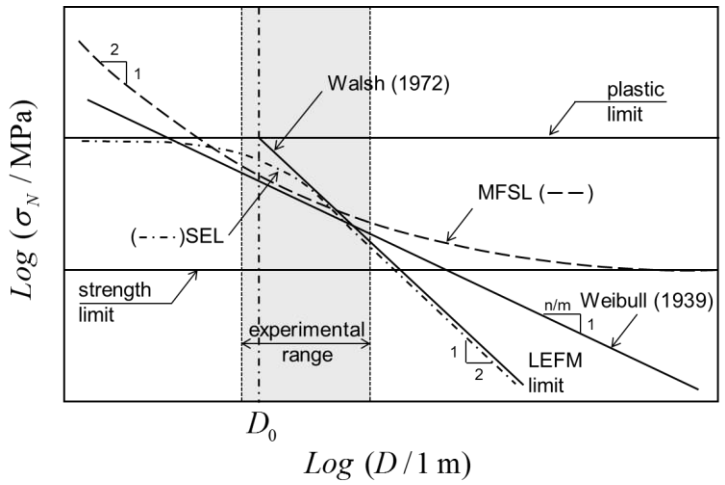

Fig. 3-34. Comparison of the various size effect models (van Mier, 2013)

There are various models to explain the size effect. Classical approaches include Weibull's weakest link theory, and the size effect law (SEL) by Bazant (1984) and the multifractal scaling law (MFSL) developed by Carpinteri (1994) are two phenomenological size effect models. SEL is partly based on cohesive softening models and contains elements derived from the length of the FPZ. MFSL is based on considerations about the fractal structure of concrete and its effect on mechanical behavior. The nominal strength of a structure suggested by each model is represented in Eq. (3-21) for SEL and Eq. (3-22) for MFSL. Fig. 3-34 shows that various size effect models and the experimental range is shown as a grey-shaded area. Although the differences in asymptotic behavior

of SEL and MFSL, the assumption in SEL was confirmed by experiments. Bazant (2004) verifies that the double-logarithmic scale in Eq. (2-21) fits the behavior of concrete structures.

$$\sigma_N(D) = \frac{Bf_t'}{\sqrt{1+D/D_0}} \tag{3-21}$$

$$\sigma_N(D) = f_t\sqrt{1+\frac{l_c}{D}} \tag{3-22}$$

There are several issues, such as the slope of LEFM, the upper or lower limit and the type of brittleness number, to define a suitable size effect model. The decrease of nominal strength with increasing characteristic size takes a certain slope, which depends both on the material and on the dimensionality. The Weibull theory explains the nominal strength is proportional to the $D^{-n/m}$, where n is the number of dimensions and m is a Weibull modulus as the material constant. Table 3-3 shows shear strength models of RC rectangular beams without stirrups based on fracture approaches. The slope of LEFM is in a range of -1/4 and -1/2.

The following issue is the different horizontal asymptote between SEL and MFSL. SEL has the upper limit as a plastic limit for small-scale members, but MFSL has the lower limit as a strength limit for large-scale members. In case of SEL there is uncertainty about the length of the fracture process zone, where in MFSL the same is true for the characteristic length and the limit value of the tensile strength for infinite size. The range of available experimental data is shown as a grey-shaded area. In reality, the horizontal asymptote for large sizes should be a slope, at least similar to Weibull. The SEL formulation is more generally accepted, so Eurocode 2 modified the formula of SEL greater than 1 which has the lower bound.

Table 3-3. Shear strength of RC beams based on fracture approaches

Researcher	Equation
Eurocode 2	$v_{Rd,c} = C\left(100\rho_l f_{ck}\right)^{1/3} \cdot \left\{1+\left(d/200\right)^{-1/2}\right\}$
Konig et al. (1993)	$v_u = Cf_{ct}\left(d/l_{ch}\cdot\rho_l\right)^{-1/3},\ l_{ch} = EG_f / f_{ct}^2$
Gustafsson and Hillerborg (1988)	$f_v = kf_t\left(d/l_{ch}\right)^{-1/4},\ l_{ch} = EG_f / f_{ct}^2$
Bazant-Kim-Sun (1984, 1987)	$v_u = v_u^p\left(1+D/D_0\right)^{-1/2},\ D_0 = 25d_a$

$v_{Rd,c}$, v_u, f_v, v_u =shear strength, f_{ct}, f_t =tensile strength, d, D =effective depth of the RC member, D_0, l_{ch} =characteristic material size, ρ_l =longitudinal reinforcement ratio, d_a =maximum diameter of aggregates.

Table 3-4. Brittleness numbers in Fracture mechanics

Researcher	Equation	Geometry dependence
Carpinteri (1982)	$s_c = \dfrac{G_F}{Df_t}$	Irrelevant
Bazant (1987)	$\beta_n = \dfrac{\bar{D}}{c_f} = \dfrac{D}{D_0}$	
Planas and Elices (1989, 1991)	$\beta_p = \dfrac{\bar{D}}{l_{ch}}\quad(\beta_p > 0.04)$	
ASTEM E399	$\beta_k = \dfrac{Df_t^2}{K_{Ic}^2}\quad(\beta_k \geq 2.5)$	Relevant (dependent on structural type and loading)
Hillerborg	$\beta_k = \dfrac{D}{l_{ch}},\ l_{ch} = \dfrac{K_{Ic}^2}{f_t^2} = \dfrac{EG_F}{f_t^2}$	

s_c, β_n, β_p, β_k =brittleness number, f_t =tensile strength, D, $\bar{D}$ =characteristic structural dimension, D_0, l_{ch} =characteristic material size.

Third issue is the concept of brittleness of structural failure. The brittleness of RC structures has a long history, but the definition of brittleness has not stabilized (Table 3-4). One of the fundamental reasons is that the apparent brittleness depends simultaneously on the material, the geometry of the structure and loading, and the size of the structure. The general form is as below.

$$\sigma_{Nu} = f_t \times f\left(\frac{D}{l}, \text{geometry}\right) \tag{3-23}$$

The ratio D/l appears in the SEL, and any variable proportional to it is a good candidate to be a brittleness number. In this dissertation, the size effect follows the general form in Eq. (3-23) and the brittleness number of UHPFRC shear beams is newly suggested in chapter 4 and 5.

For RC structures, the Bazant model is generally used. However, the specific formula is different from each other, especially regarding to the slope of LEFM and the upper or lower limit (ACI committee 446, 1992; CEB, 2004). The asymptote for large-scale RC members is unrealistic, which comes from the assumption of that the shape of the crack band remains constant. It is assumed that the critical crack propagates accompanying the crack band with similar figure of the initial crack band. Despite of these disadvantages, the size effect of UHPFRC I-shaped shear beams without stirrups is evaluated based on Bazant model. The number of test results is not enough even in the moderate size and the insufficient test results are preferred to be verified by theoretical approach rather than empirical approach.

Chapter 4. Mechanical Properties of UHPFRC

4.1 General

The composition of UHPFRC has several scientific and engineering rules. The maximum grain size should be less than that of traditional concrete mixes and an optimum packing density for the aggregate is important to avoid stress concentrations on contact surfaces. The amount of cement should be used for that the water is fully bound. Fine steel fibers should be added to the concrete in order to guarantee a ductile behavior (Fehling et al., 2014).

The typical mix compositions of UHPFRC used in this dissertation are indicated in Table 4-1. Water binder ratio is around 0.2, and the powder combines cement, silica fume, filler and shrinkage reducing agent. The maximum diameter of fine aggregates is less than 0.5 mm. Liquid superplasticizer is adopted to secure the fluidity with an amount varying with respect to the required fluidity and environment conditions. Steel fiber is admixed at a volume fraction of 1.0~1.5% relative to the whole volume.

Mix composition and the type of steel fiber determine the tensile characteristics of UHPFRC. There are diverse type of fibers, for instance, hooked steel fiber, twisted steel fiber, Polyvinyl alcohol (PVA), etc.. Fibers mentioned ahead are widely used in FRC to satisfy the required capacity with efficient cost. However UHPC matrix is much more homogeneous than FRC and high-strength straight steel fiber is usually used to exhibit hardening tensile behavior. The yield strength of steel fiber in UHPFRC is basically higher than 2000 MPa. The diameter of fiber is 0.2 mm and the length is selected appropriately as the values of 16 mm and 20 mm according to the tensile

strength required for UHPFRC. This type of steel fiber is classified as micro-steel fiber and has to be distinguished from macro-steel fibers used in FRC.

The early curing is conducted during 24 hours under wet condition at around 20°C, and then high temperature wet curing is conducted to exhibit high strength in a short time and reduce shrinkage and creep. High temperature wet curing is performed at around 90°C during 48 hours.

Table 4-1. Mix composition of UHPFRC (used in this dissertation)

Material ID	W/B	Mass unit (kg/m^3)						
		Water	Premix binder	Fine aggregates	Steel fiber		Super-plasticizer	Air-entraining agent
					16 mm	20 mm		
1	0.20	197.1	1269.5	867.4	39	78	18.1	0.5
2	0.20	196.9	1287.8	866.4	39	78	24.4	0.9
3	0.23	221.3	1258.7	846.8	-	78	17.7	0.7

Premix binder = cement, Zr, BS, filler, expansion agent, shrinkage reducing agent premix

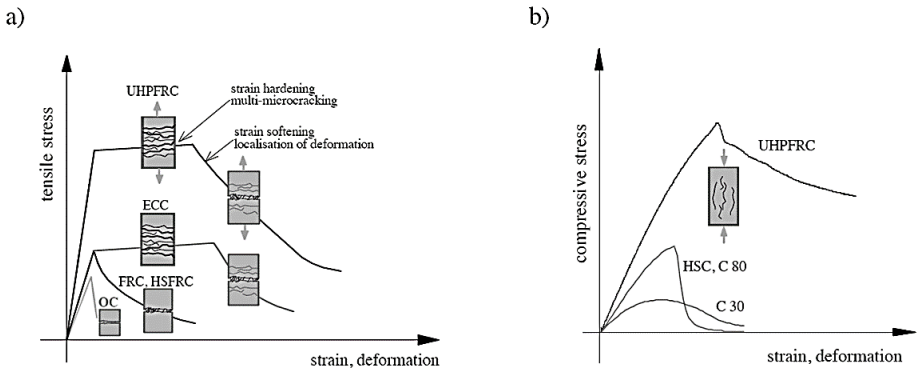

Fig. 4-1. Typical response of UHPFRC in uniaxial stress state in comparison to ordinary and high-strength concrete (HSC), fiber-reinforced normal or high-strength concrete (FRC, HSFRC), and engineered cementitious composites (ECC) : a) uniaxial tension; b) uniaxial compression (Li, Fischer 2002)

UHPFRC shows outstanding durability as well as high compressive and tensile strength. The compressive strength of UHPFRC is 160~170 MPa and the ultimate compressive strain is about 0.004 in this research. Tensile strength is over 10 MPa and the ultimate crack mouth opening displacement (CMOD) is about 0.2~0.4 mm. Fig. 4-1 shows compressive stress-strain curve and tensile stress-CMOD curve of UHPFRC with strain-hardening resisted by creating number of micro cracks. To define cracking behavior of UHPFRC, it is important to distinguish whether the response of the composites is strain-hardening or strain-softening in tension, and whether it is deflection-hardening or deflection-softening (Naaman et al., 2014). Deflection-hardening composites defined by bending test are useful in structural applications dominated by flexural behavior, but in this research, strain-hardening UHPFRC will be confined for distinct and specific physical model. A strain-hardening composites generates multiple micro-cracking and a crack localization with strain-softening behavior occurs after the peak point as shown in Fig. 4-1.

The experimental investigations of UHPFRC material characteristics include various type of tensile strength tests, direct shear tests (or push-off tests) on monolithic and pre-cracked specimens, biaxial tension-compression strength test on reinforced panels and 3-point bending test on off-center notched prisms. Several types of tensile strength tests on UHPFRC are performed to define the effective tensile strength and fracture properties such as material characteristic length and fracture energy, and then the simplified UHPFRC tensile behavior with hardening part is suggested. Mohr-Coulomb failure criterion of UHPFRC is established by the friction angle and the effectiveness factor based on push-off test and biaxial panel test.

4.2 Uniaxial Tensile behavior of UHPFRC

4.2.1 Test and Analysis Methods for Uniaxial Tension

The ordinary concrete tensile strength is usually evaluated by means of indirect tests such as the bending or modulus of rupture test, the double punch test, or the split cylinder test. For most purpose, an estimate of the tensile strength based on the uniaxial compressive strength is sufficient (Kaufmann, 1998).

Fiber reinforcement effect has to be quantified by the tensile strength in UHPFRC, so the tensile strength of UHPFRC should be analyzed with respect to the stress-strain response. The approach for ordinary concrete does not work. Fig. 4-2 shows the stress-strain relationship of UHPFRC with tensile hardening behavior. Microcracks which occurred in an overall specimen enable to increase the strength with ductility. The peak strength is governed by a crack localization and, so the deformation at the peak strength is also measured by the crack width.

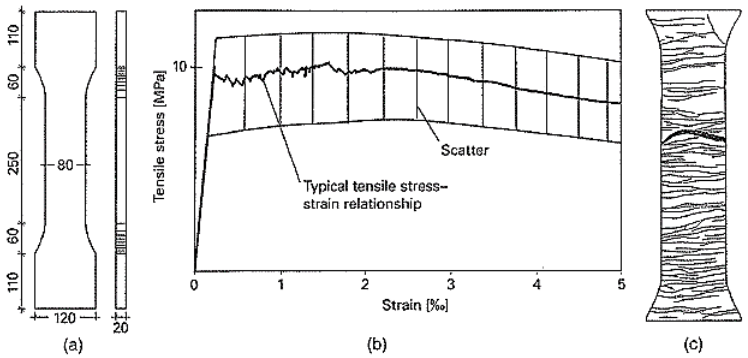

Fig. 4-2. Stress-strain diagram for axial tension for UHPC containing fibers with an initially strain hardening behavior (Fehling et al., 2013): (a) dimensions, (b) stress-strain diagram, (b) crack pattern. (Note: ε=1‰ corresponds to approx.. 0.2 mm elongation)

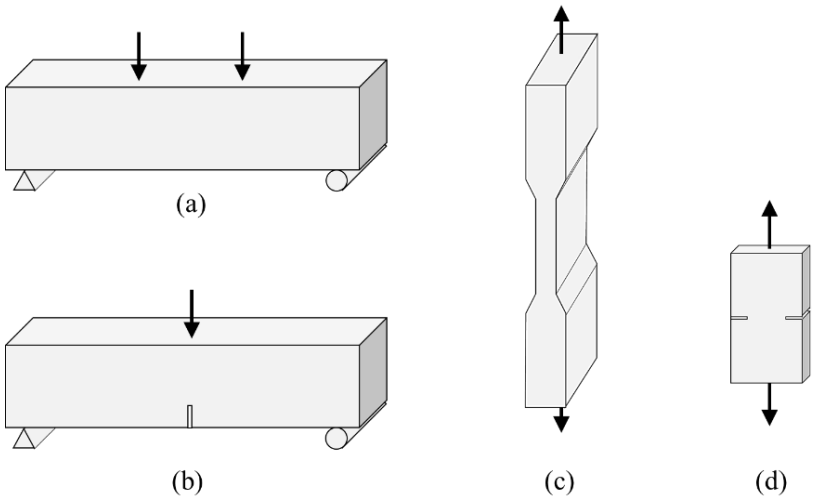

Fig. 4-3. Representative tension test on UHPFRC specimens: (a) four-point bending test, (b) three-point bending test on notched prism, (c) direct tension test, (d) direct tension test on notched plate

Direct tension test is the confident test method to get the strength-strain response, but it is difficult to perform the test. The test results are influenced by the boundary condition severely, and the crack localization easily occurs at the supports, not in the middle of the valid range.

Diverse test methods to measure stress-strain or crack width relationship of UHPFRC are performed in fields as shown in Fig. 4-3, and there are arguments which is the most proper test method among them. Bending test on prism is easy to conduct, but the test results should be analyzed by inverse analysis. The French recommendation for UHPFRC adopts four-point bending test on unnotch prism, and Euro code and *fib* model code adopt the three-point bending test on notched prism. In this chapter, the tension test and corresponding analysis methods in recommendations are investigated and the compared the advantages and disadvantages.

4.2.1.1 Four-Point Bending Test on Unnotched Prism

AFGC has been published a pioneering and widely-used recommendation for UHPFRC. In comparison to *fib* model code, the characteristics for strain-hardening behavior of UHPFRC is defined in detail. First of all, there are fiber orientation factor K which applies to the post-cracking part of the tensile law. There is same factor in *fib* model code, but in general an isotropic fiber distribution is assumed, so that the fiber orientation factor K =1.0. Instead of that, partial safety factor γ_F is considered as 1.5 in the model code. Secondly, tensile constitutive law of UHPFRC is categorized by three types; strain-hardening material, low strain-hardening material and strain-softening material. Comparing to *fib* model code, low strain-hardening material is defined differentially. Strain-softening material and low strain-hardening material obeys a $\sigma - w$ law and high strain-hardening material obtain $\sigma - \varepsilon$ law. Finally, thick and thin elements are distinguished and the corresponding post-cracking relationships and computing methods are different. In the following sections, the different types of tensile constitutive law depending on the different types of structure are explained.

For thin elements ($h \leq 3l_f$) the recommendation comments that the constitutive law will thus be similar to that of a high strain-hardening UHPFRC. A $\sigma - \varepsilon$ constitutive law can be assumed in this case. A back analysis based on 4-point bending test results or direct tensile test results can be carried out to get the constitutive law. The standard test should be carried out on a specimen where the cross sectional height is smaller than $3l_f$. By choosing a standard bending test specimen with such a small thickness, the stress-strain relation obtained includes implicitly the effect of the fibers' alignment with the boundary conditions, which is expected to occur in the structural elements as well (Fig. 4-4).

In case of thick elements ($h > 3l_f$), $\sigma - w$ law for strain-softening and low hardening material is distinguished from $\sigma - \varepsilon$ law for high strain-hardening material. Basically the post-cracking response is determined from 3-point bending tests on notched prisms to establish $\sigma - w$ law. A multi-linear stress-crack width $\sigma(w)$ post-cracking relationship is determined on the basis of an inverse analysis on prisms test results. When the material is strain-softening in pure bending (4-point bending tests carried out during characterisation), the same $\sigma - w$ laws as for thick elements must be used. However, this case can theoretically not occur, given the material minimum ductility condition (Fig. 4-5).

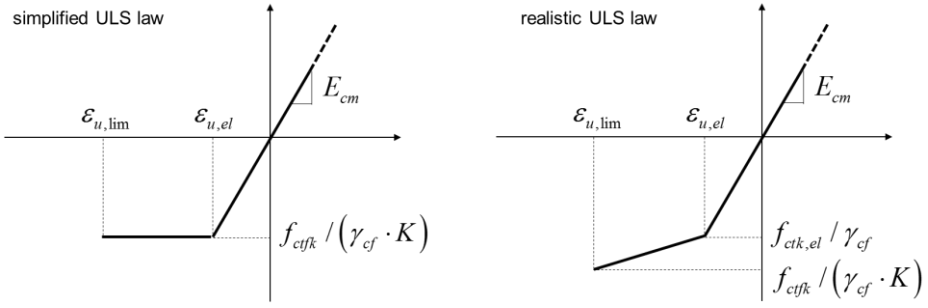

Fig. 4-4. Tensile strength for thin cross sections ($h \leq 3l_f$) (AFGC, 2013)

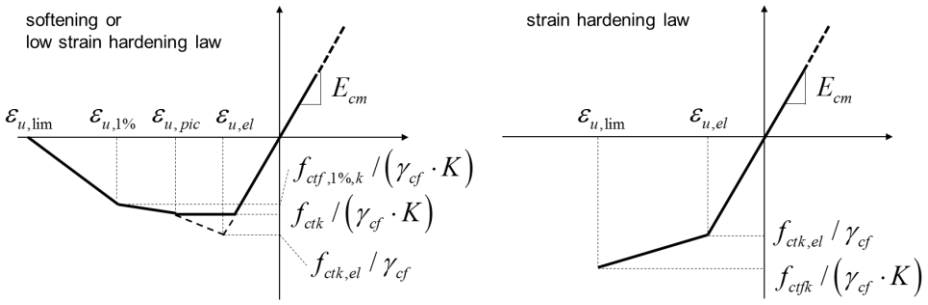

Fig. 4-5. Tensile strength for thick cross sections ($h > 3l_f$) (AFGC, 2013)

A partial safety factor γ_{cf} for fiber reinforced concrete under tension has been introduces in ultimate limit state (ULS) verifications in order to take

manufacturing defects into account. For durable situations, γ_{cf} is 1.3 and for accidental situations, γ_{cf} is 1.05. In addition, the fiber orientation factor K is to be taken into account. This factor is determined experimentally from tests on prototype or in preliminary design computation, K is assumed equal to 1.25 for global effects and to 1.75 for local effects. The given value is applied for thick elements, and in case of thin element K can be 1 when a $\sigma-\varepsilon$ law is used.

Typical UHPFRC applicable to AFGC recommendation has a compressive strength over 150 MPa and a tensile strength of 9 MPa with a tensile strain of 0.0025. The tensile characteristics of UHPFRC usually belongs to low strain-hardening behavior for thick elements and high strain-hardening behavior for thin elements. The AFGC recommendation suggests back analysis based on 4-point bending test results and direct tensile tests are admitted to get tensile stress-strain relation. Recent revision of the AFGC recommendation suggests that strain-hardening behavior needs two types of test methods, direct tensile tests under cyclic loading and 3-point bending tests on notched prism under static loading. Because strain-hardening behavior should be defined with respect of inelastic behavior represented by reduced compliance compared to the elastic behavior.

The recommendation explains the methods for inverse analysis from 4-point bending tests on unnotched prism and 3-point bending tests on notched prism at an appendix in detail. Inverse analysis based on cohesive model is dealing with residual stress in a structure and needs computational calculations. Meanwhile it is possible for test results expressed by $\sigma-w$ relationship to convert $\sigma-\varepsilon$ relationship using the characteristic length l_c . The characteristic length l_c is used for strain softening or low strain-hardening. The value of l_c depends on the cross-section. For rectangular or tee cross-section, a value of $l_c = 2h/3$ can be used, where h is the depth of the cross-section. This method is simple, but the existing physical basis is not enough yet.

4.2.1.2 Three-Point Bending Test on Notched Prism

The *fib* mode code 2010 gives recommendations for material properties of FRC including SFRC, UHPFRC, but the rules are based most of all on experience with SFRC. The recommendation concentrates on explaining how modelling tensile stress-crack width or tensile strain from the given test results. The code includes classification, constitutive law and stress-strain relationship for general tensile behavior of FRC.

Depending on their composition, FRC can show hardening or softening behavior under uniaxial tension (Fig. 4-6). In the case of softening behavior (a) the deformation localize in one crack. In the case of hardening behavior (b) multiple cracking occurs before reaching the peak value. The relationship between strain softening behavior in tension can correspond to hardening behavior in bending and a softening material in bending can result in a monotonically increasing load in the surface (Fig. 4-7). Shifting the characteristics of tensile strength depending on specimen geometry means that the post-cracking behavior of FRC subjected to external force is substantially affected by its boundary condition. For structural use of FRC a hardening behavior in bending is necessary (*fib*, 2012).

Post-cracking behavior of FRC should be characterized by the strength according to the crack width. However, it is not easy to measure the crack width properly and define the representative values from test results. The relationship between tensile strain and crack width is a struggling issue because they are different properties depending on how energy dissipates in a structure. In case of hardening behavior, multiple cracking is represented by tensile strain where energy dissipates by unit volume. In case of softening behavior, a major crack width which localized within cracking zone has to be measured where energy dissipates by unit crack surface.

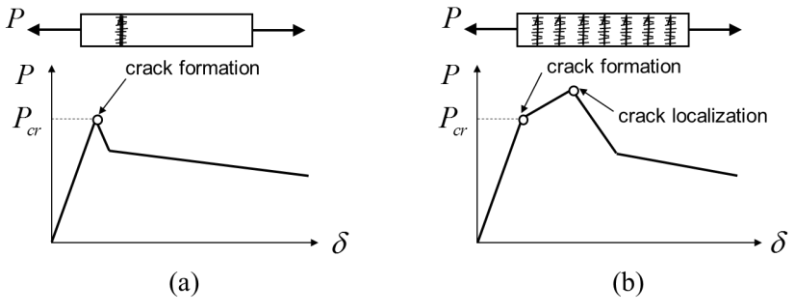

Fig. 4-6. (a) Softening and (b) hardening behavior in axial tension (*fib*, 2012)

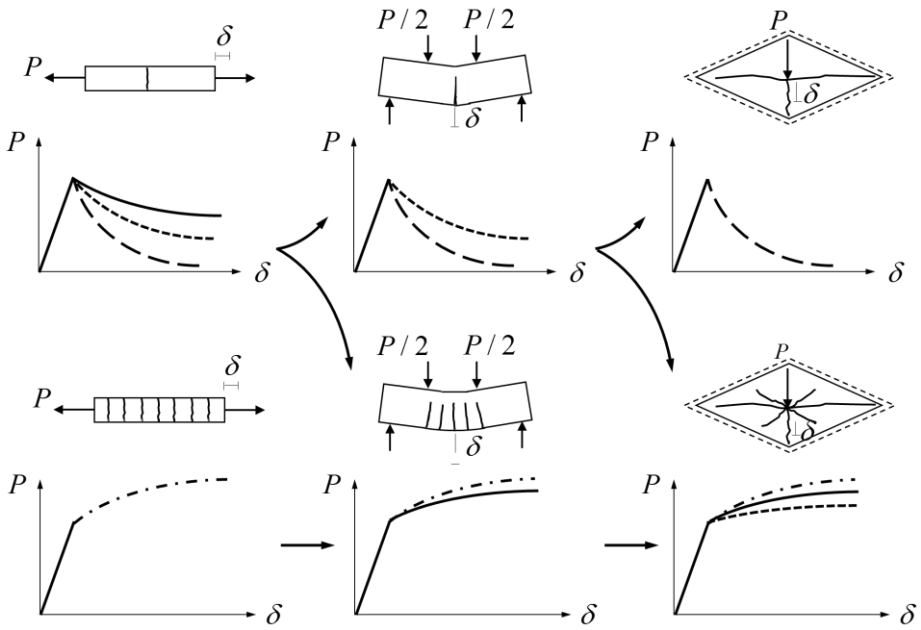

Fig. 4-7. Different of response of structures made of FRC having a softening or hardening behavior under uniaxial and bending loads (fib, 2012)

In comparison to bending or wedge splitting tests, uniaxial tensile tests directly provide material tensile behavior over elastic, strain hardening and softening stages without the need of high computational effort for backward calculation of the material tensile response. However, direct tensile tests are challenging to perform. Difficulties in obtaining evenly distributed stresses

throughout the cross section and controlling a stable load versus crack opening response has limited the number of researchers performing direct tensile tests on cementitious materials and composites. Specimen shapes, which can be distinguished into dogbone shape, unnotched and notched prisms or cylinders, and the type of gripping system (fixed or rotating boundary condition) significantly influence the test results. (Wille et al., 2014) Due to the difficulties in performing uniaxial tensile test, bending tests with small notched beams are best candidates to be a standard test method for the FRC classification. Since bending behavior is markedly different from uniaxial-tension behavior, it may happen that softening materials in tension present a hardening behavior in bending. (Prisco, 2009)

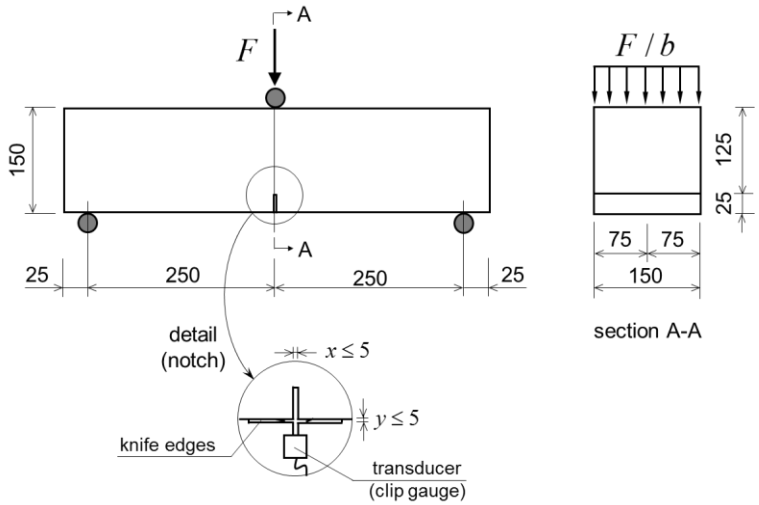

Fig. 4-8. Test set-up required by EN 14651 (dimensions in [mm])

According to the *fib* model code 2010, two simplified stress-crack relationships in tension are identified from the 3-point bending test on notched prism which are performed according to the standards EN 14651 (Fig. 4-8). Parameters, f_{Rj} , representing the residual flexural tensile strength, are evaluated from the applied force F ad crack mouth opening displacement

$CMOD$ relationship, as follows:

$$f_{R,j} = \frac{3F_j l}{2bh_{sp}^2} \tag{4-1}$$

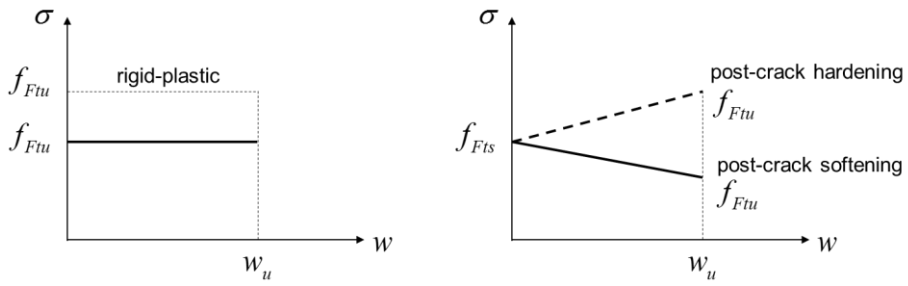

Fig. 4-9. Simplified post-cracking constitutive laws: stress-crack opening (continuous and dashed lines refer to softening and hardening post-cracking behavior, respectively) (fib, 2012)

A first constitutive law, rigid-plastic model (Fig. 4-9 (a)) is defined as follows:

$$f_{Ftu} = \frac{f_{R3}}{3} \tag{4-2}$$

A second constitutive law is defined through a softening linear post-cracking model or a hardening one (Fig. 4-9 (b)). f_{Fts} represents the serviceability residual strength and f_{Ftu} represents the ultimate residual strength. They are defined as follow:

$$f_{Fts} = 0.45 f_{R1} \tag{4-3}$$

$$f_{Ftu} = f_{Fts} - \frac{w_u}{CMOD_3}\left(f_{Fts} - 0.5 f_{R3} + 0.2 f_{R1}\right) \geq 0 \tag{4-4}$$

where f_{R1} and f_{R3} are the residual strength defined from Eq. (4-1) and w_u is the maximum crack opening accepted in structural design representing the ductility of a structure.

For numerical analysis, the *fib* model code 2010 recommends more advanced constitutive laws. To define the stress-strain laws, the crack width and the corresponding structural characteristics length, l_{cs}, of the structural element. In elements with conventional reinforcement (rebars), l_{cs} may be the minimum value of the mean distance between cracks and the distance between the neutral axis and the tensile side of the cross section. Then the strain is assumed equal to:

$$\varepsilon = w / l_{cs} \tag{4-5}$$

The ultimate strength f_{Ftu} in the linear model depends on the required ductility that is related to the allowed crack width. The ultimate crack width can be calculated as $w_u = l_{cs} \cdot \varepsilon_{Fu}$, by assuming ε_{Fu} equal to 2% for variable strain distribution along the cross section and 1% for constant tensile strain distribution along the cross section. In any case, the maximum crack width may not exceed 2.5 mm. When considering hardening materials, ε_{Fu} is equal to 2% for variable strain distribution along the cross section and 1% for constant tensile strain distribution along the cross section. A material is considered as strain hardening when it shows a hardening behavior in tension up to a ε_{Fu} =1% (*fib*, 2012).

For serviceability limit state (SLS) the same constitutive relationship for plain concrete is adopted up to the matrix strength f_{ct}. In the post-cracking stage, a bilinear relation defined by f_{Fts} and f_{Ftu} is applied .

4.2.1.3 Direct Tensile Test

The test setups and specimen geometries in previous studies shows the wide range of variation in direct tensile testing and the lack of a standardized method. Pinned end conditions facilitate specimen alignment and even stress distribution prior to cracking, but do not support an even crack opening throughout the cross section in comparison to a fixed boundary condition. In order to capture strain-hardening behavior, the fiber bridging forces beyond matrix cracking strength need to be transferred into the attachment. Therefore, top-glued specimens without increased cross-sectional area at the end are not suitable for investigating strain-hardening behavior (Wille et al., 2014).

The recommendations of AFGC, JSCE and KCI allow the direct tension test, and the specification given by KCI (Fig. 4-10) was performed in this dissertation. UHPFRC with tensile hardening behavior allows the investigation of multiple cracking and average crack spacing, notched specimens facilitate the investigation of the material softening.

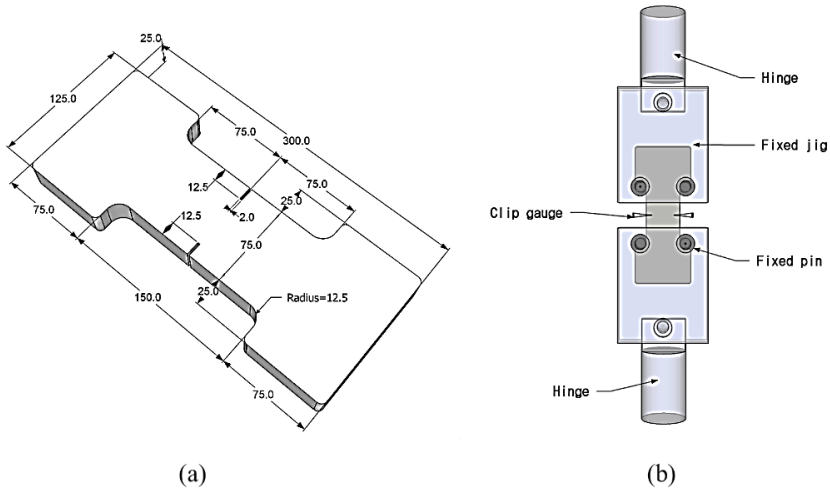

Fig. 4-10. Direct tension test on notched speicmen (KCI, 2012) : (a) specimen dimension (mm), (b) test setup

4.2.1.4 Discussion

Several problem statements from the tension test methods and analysis in previous studies are summarized as follows.

1) Strength and displacement response from each test methods has to be analyzed in a different way. Tensile hardening behavior in a bending test does not ensure the tensile hardening behavior in a direct tension test (Fig. 4-11). Which one is suitable method to determine the effective strength applied in a member design strength should be studied regarding to each material properties.

2) Notched specimen is basically proper to a material with tensile softening behavior, and the inverse analysis in recommendations is based on cohesive model which is also proper to investigate softening curve after the peak strength. Hence, another test methods is needed to investigate the tensile hardening behavior of UHPFRC.

3) Fiber orientation factor plays a role as a reduction factor due to material heterogeneity, and the physical evidence to define the factor is vague. The scattered test results and the brittleness due to crack localization should be analyzed with respect to physical mechanism in a structural scale.

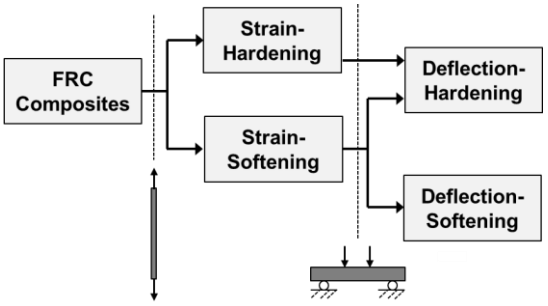

Fig. 4-11. Classification of FRC composites based on their tensile response

4.2.2 Definition of UHPFRC Tensile Behavior

To investigate microcracking behavior in a distributed deformation and local effects of crack opening, two different test series has to be analyzed (Jungwirth and Muttoni, 2004, 2006). Direct tension tests are conducted on dogbone shaped specimens fixed with glue and notched rectangular specimens. The unnotched specimens are subjected to cyclic loading before the peak load decreases to measure the compliance of force-displacement relationship at each cycle. Fig. 4-12 is schematic behavior of UHPFRC tensile element (Jungwirth, 2006). The stress-strain diagram is composed of the elastic phase 1 and the multiple micro-cracking phase 2 and the crack opening phase 3. The elastic and hardening behavior and the softening behavior are classified depending on the energy dissipation type. $G_{F,a,nr}$ is denoted in a fiber activation phase of n_r meso-cracks throughout component dissipated energy, and $G_{F,lr}$ is the fracture energy of fiber pull-out phase in a crack (Fig. 4-13).

A similar definition as typical tensile properties of UHPFRC is suggested (Wille and Naaman, 2010). The notation for fracture properties in this dissertation is followed by the definition as below.

1) *strain based elastic part*, determined by the initial tensile behavior up to the cracking strength σ_{cc}, which is defined as a fictitious point of transition from ideal linear elastic to best fitted linear strain-hardening behavior, and determined by the associated strain ε_{cc} and the elastic modulus E_{cc}.

2) *strain based strain hardening part*, determined by the dissipated energy per unit volume $g_{f,A}$, 99% of the tensile strength of the composite σ_{pc}, its associated strain ε_{pc} and ε_{soft}, hardening modulus E_{hc} and the residual strain ε_{res}.

3) *crack opening based softening part*, which is characterized by the dissipated energy per crack surface area $G_{f,B}$.

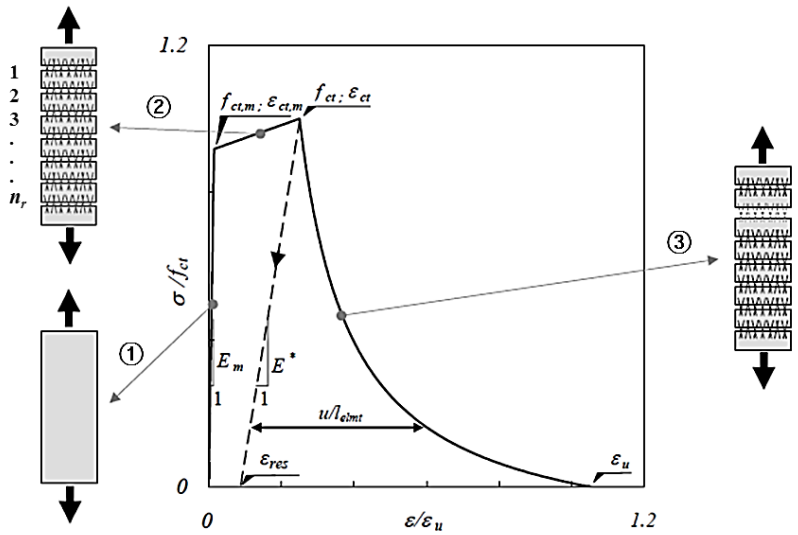

Fig. 4-12. Linage of load phase and crack opening in a behavior for a concrete tension member (Jungwirth, 2006)

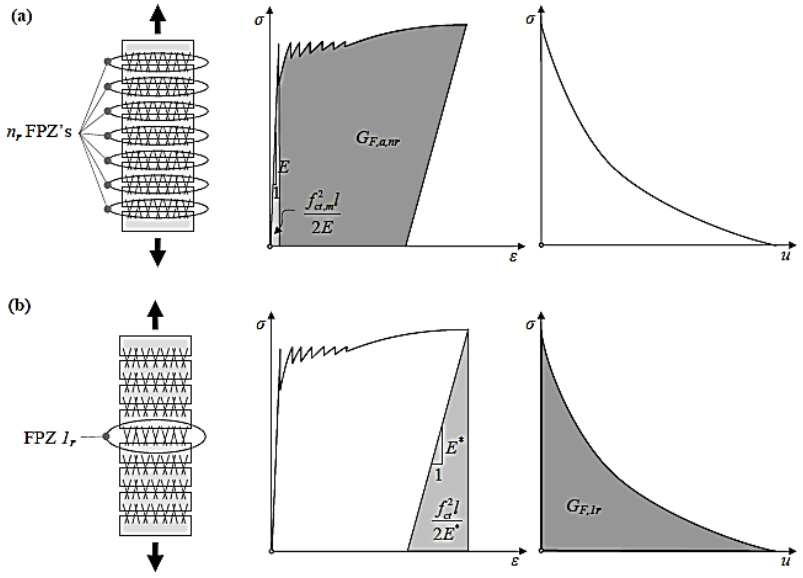

Fig. 4-13. (a) tension element with multiple FRZ, (b) discrimination of different fracture energies (Jungwirth, 2006)

4.2.3 Uniaxial Tensile Test Results of UHPFRC

The material tensile strength of UHPFRC is a key parameter of shear design. In normal strength concrete with large aggregate, the maximum tensile strength is almost immediately developed after cracking, whereas the steel fiber reinforced concrete has a much higher softening behavior after reaching maximum strength and nonlinear section after cracking. The tensile stress - strain relationship is important because the behavior after cracking greatly affects the behavior of the member. The average tensile strength of the part from the crack initiation point to the critical crack width (w_u) in the tensile strength-crack width relationship occurring along the tensile strength at the time of reaching the maximum strength. A direct tensile test and a flexural tensile test were carried out at the same time, and a notched specimen was applied to investigate the residual tensile stress according to the crack width. In Eurocode and JCI, the material tensile strength of SFRC is determined by three-point load test of rectangular parallelepiped beam with notch. The notched specimen is defined as the notch width as the crack opening displacement (CMOD) and is analyzed by the tensile strength and the post crack behavior through residual stress after cracking through the load and CMOD relationship. Generally, the method of deriving the material tensile strength-CMOD nonlinear function through inverse analysis by finite element analysis is widely used, but it is difficult to apply the method with difficulty of convergence. In this study, the tensile strength of the material was obtained from the load-displacement relationship proposed in the European model code (*fib* model code 2010). The *fib* model assumes the load-displacement relation for the FRC material exhibiting tensile hardening or softening behavior to be linear with respect to the critical crack width and obtains the service tensile strength (f_{Fts}) and the ultimate tensile strength (f_{Ftu}). In this case, the residual bending tensile strength against the specific CMOD is shown in EN 1465116.

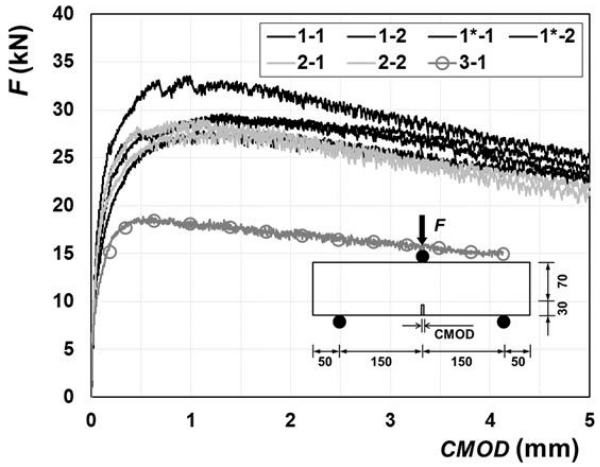

(a)

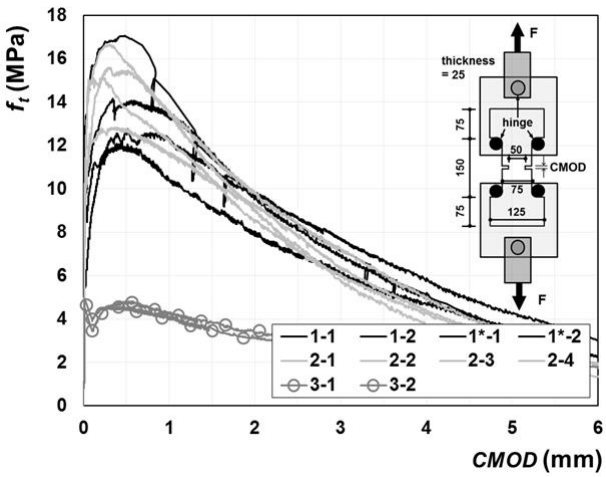

(b)

Fig. 4-14. Tensile test results of UHPFRC from (a) 4-point bending test on notched prism and (b) direct tension test on notched plate

On the other hand, in order to directly obtain the material tensile strength without inverse analysis, a direct tensile test is required. However, the tensile test method has a variety of methods, and the resultant values for the sample size and constraint are large. In this study, both ends of the notched specimen were applied as a hinge according to the Guideline 21 for designing ultra-high-performance concrete K-UHPC. The results are shown in Fig. 4-14.

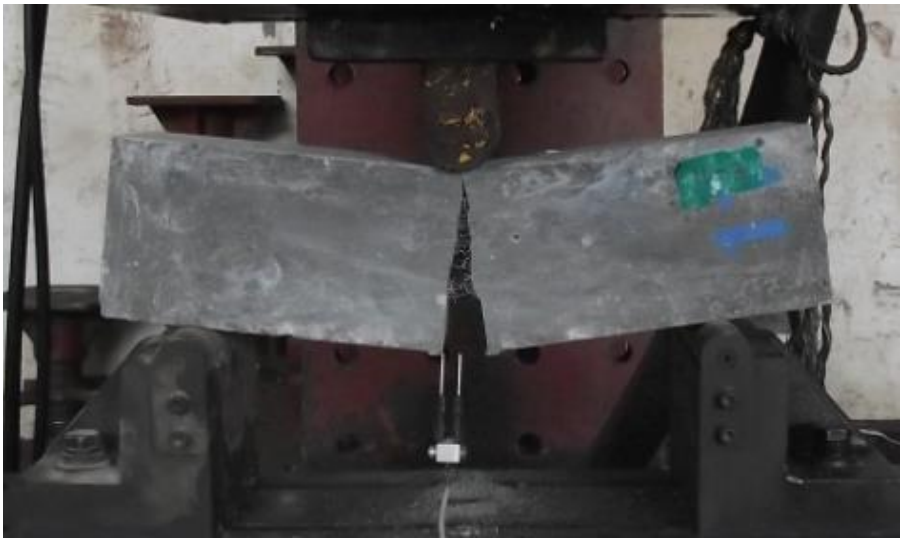

(a)

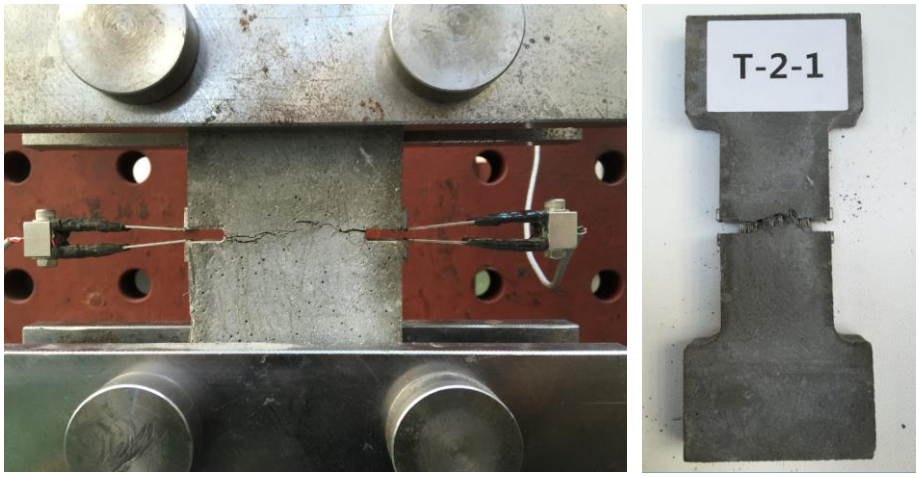

(b)

Fig. 4-15. Tensile test results of UHPFRC from (a) 4-point bending test on notched prism and (b) direct tension test on notched plate

Fig. 4-14 is the load-CMOD graph obtained from the flexural tensile test according to EN 14651. This value is assumed to be 0.03 mm. The results of direct tensile test are stable for each material and specimen, while the results of bending test are stable. As a result of the direct tensile test, the tensile strengths

of Formulations 1 and 2 of 1.5% by volume of the steel fiber showed similar tensile hardening behavior, while Formulation 3 of 1.0% of the steel fiber volume did not exhibit tensile hardening behavior. However, in the flexural tensile test, Curing behavior. The compressive behavior increases linearly up to the maximum load and the strength is similar in all three formulations to 160-170 MPa.

In AFGC, the residual strength used for the shear strength in the tensile strength-CMD graph is defined as the average of the range from the limit to the crack width, taking into account the coefficient according to the steel fiber effect. Use 1.25 for general structures.

Table 4-2. Comparison of test results of direct tension test and 3-point bending test on notched specimen

Material ID	Cylinder test	Characteristic value of linear model given by *fib* model code 2010 (EN 114651)					Direct tension test results			
	f_c [MPa]	f_{R1} [MPa]	f_{R3} [MPa]	w_u [mm]	f_{Fts} [MPa]	f_{Ftu} [MPa]	f_{cr} [MPa]	f_{ct} [MPa]	w_u [mm]	$\sigma_{Rd,f}$ [MPa]
1	160.1	25.41	25.77	0.30	11.44	11.00	9.45	12.99	0.51	8.98
2	162.4	24.37	24.00	0.30	10.97	10.51	11.23	14.23	0.35	10.18
3	169.9	16.86	16.23	0.30	7.59	7.20	5.31	5.35	0.40	4.26

The design tensile strength shown in Table 4-2 can be compared with the design residual tensile strength by direct testing. The design tensile strength may be either of the residual tensile strength and the result obtained from the bending tensile test results, but the present invention is applied based on the following. The fracture energy in the load-displacement linear relationship is similar to the fracture energy value in the flexural tensile test. This means that the difference in strength between specimens is directly related to the difference

in the critical crack width. f_{Ftu} is defined as the design tensile strength assuming 0.3 mm. The main external resistance mechanism in steel fiber reinforced concrete is the stress redistribution effect by steel fiber, which is defined as the limit crack width, not the maximum strength. Since the critical crack width in the member behavior is affected by various design parameters such as flexural reinforcement ratio and shear span ratio, it is desirable to define the design tensile strength based on the limit crack width of 0.3 mm. In addition, the difference in value between the case 3 and the case 3 can be interpreted as a result of the softening behavior of the material tensile stress-strain relationship and the curing behavior of the bending strength-deflection relationship. In the case of these materials, if the constraining force is sufficient even after the main crack is generated in the member design, the curing behavior after cracking is shown. Therefore, when the compression band and the bending tensile steel are designed to be sufficiently large, it meets tensile strength.

4.3 Failure Criteria of UHPFRC

4.3.1 Biaxial Loading on Reinforced UHPFRC

4.3.1.1 Tension Stiffening Behavior of reinforced UHPC elements

The structural behavior of tension members in reinforced UHPFRC shows that several visible cracks with spacing form before the peak load is achieved, and one macrocrack opens up due to the failure of the reinforcing bars after the peak load, as represented by crack localisation (Jungwirth and Muttoni 2004; Jungwirth 2006; Walraven 2009; Leurbecher and Fehling 2004, 2012; Leurbecher 2007; Fischer and Li 2002). It has been indicated that the contribution of the fibers starts to decrease (softening branch) for strain levels at which steel reinforcement is already in its yielding plateau, and the ultimate tensile strain of UHPFRC can be larger than the yielding point of the reinforcement (Redaelli 2006). In addition, the fact that the material characteristics of UHPFRC govern the behavior of reinforced tensile members implies that the bond stress between the reinforced rebar and UHPFRC is very high. A schematic of crack formation and the internal stresses in reinforced ordinary concrete (R/C) and reinforced engineered cementitious composites (R/ECC) suggested by Fischer and Li (2002, 2007) shows that, due to the uniform stress in the cracked matrix, the damage induced by local slipping and an excessive interfacial bond stress between the reinforcement and the matrix is prevented, and the composite load-deformation response is significantly improved.

Specimens on the tensile loading stage can be considered to be axial members under tension only. The responses of the bare bar and the reinforced concrete specimens are compared in this figure. Experimental data on the tension-stiffening behavior of the three types of specimens, NF, VF and VN,

are given within the elastic range of the reinforced rebar. The applied tensile strain measured on the external reinforcement is distributed between 0 and 0.003. As a result, the actual tensile strain measured on the plane of the panel is recorded between 0 and 0.002. The maximum value of the applied tensile strain is limited by the elastic limit of the steel rebar reinforcement. Once the reinforcement yields outside of the specimen, stress is redistributed along the horizontal reinforcements and it becomes impossible for the measured tensile stress to be applied to the specimen. The rebar has an elastic modulus of 182 GPa and a nominal yield strength of 600 MPa, so the maximum applied tensile strain is determined to be 0.003.

One or two hair cracks are observed in the VF and NF specimens under tensile loading, whereas three or four major cracks are observed in the VN specimens. Ten reinforcements applied on tensile loading are each assumed to have the same tensile stress, so the representative value of the applied tensile stress is defined as an average of the measurements. The dotted lines denote the bare steel stress–strain relationship outside of the specimen, and the irregular solid grey line denotes the measured average value in the specimen's interior. The bold solid line is the tension-stiffening proposal, which has been simplified based on the specimen's measurement results. The VF and NF series maintain almost same stress–strain relationship regardless of the mixing composition, but the VN series shows slightly different behavior. Fig. 4-16 shows the tension-stiffening behavior of a reinforced UHPFRC member neglecting shrinkage.

The response of the UHPC panels without fiber (VN series) is similar to that of normal-strength concrete, which is characterised by a crack-formation stage with a constant cracking strength N_{cr} and a stabilised cracking stage with concrete softening behavior (*fib*, 2012). On the other hand, the responses of the UHPFRC panels (VF and NF series) show remarkable tension-stiffening behavior defined by strain differences $\Delta\varepsilon_{ts}$ between the concrete and

reinforced bars at load N in the stabilised cracking stage. The slight difference between the tension-stiffening behavior of the VF and NF series can be explained by the fact that the earlier cracking along the vertical reinforcement of the VF series induces a decrease in the bond stress between the rebar reinforcement and UHPFRC.

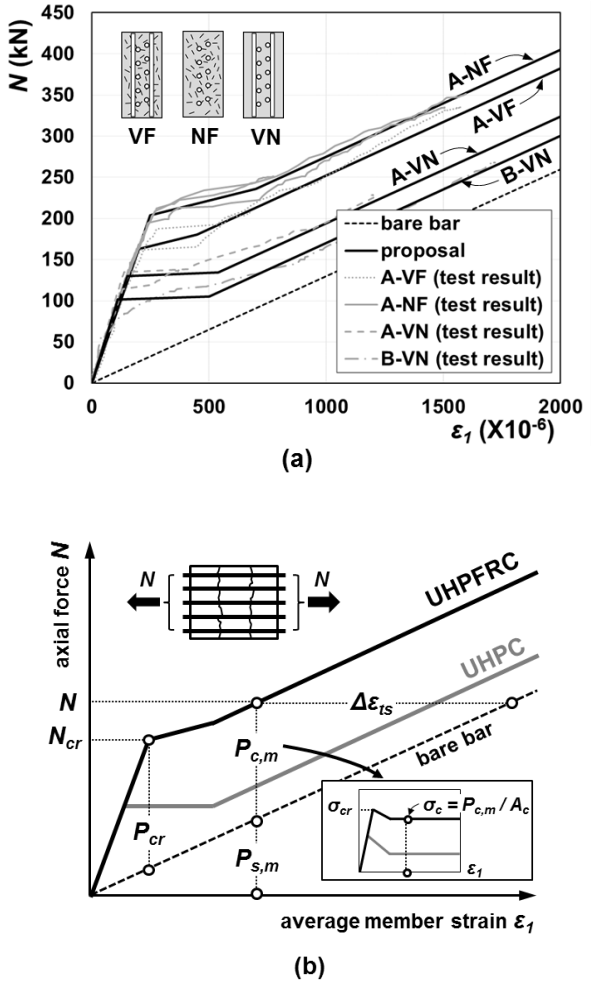

Fig. 4-16. Tension-Stiffening behavior of UHPC with and without fiber: (a) test results and proposal for each specimen type, (b) schematic tension stiffening behavior

The tension-stiffening behavior of UHPC axial members with and without

fiber is schematised in Fig. 4-16 (b). After initial cracking, the UHPC axial members show a distinct crack-formation phase like ordinary concrete, but the UHPFRC axial member shows a brief crack-formation phase with a slight increase in the axial force leading to a definite crack-stabilisation phase. To compare the tension-stiffening behaviors of UHPC and UHPFRC, a tension-stiffening factor should be identified as an index. In this study, the tension-stiffening bond factor β is defined as Eq. (4-6) below (Bischoff 2003).

$$\beta = P_{c,m} / P_{cr} \tag{4-6}$$

While the tension-stiffening factor χ_{ts} suggested by Branson (1997) is defined by tensile strain, the bond factor β is defined by the average force carried by the cracked concrete $P_{c,m}$ and the cracking force carried by the concrete P_{cr}. The details of the tensile behavior of a reinforced member are shown in Table 3. The test results show that the tension-stiffening bond factor β of UHPFRC panels is almost twice that of UHPC panels, and that the contribution of UHPFRC to tension after initial cracking remains constant over the elastic range of the reinforced rebar. The differences between A-VN and B-VN can be explained by compressive strength in case of UHPC without fiber. Fields and Bischoff (2004) reported that the tension-stiffening behavior of high-strength concrete increases with an increase in tensile strength.

The contributions of UHPC and UHPFRC to the tension defined as σ_c are characterised by χ_{ts} and $\sigma_{c,m}$ the axial forces carried by the concrete. The similarity of the characteristic value $\sigma_{c,m}$ and tensile strength considering the bond factor $\beta \cdot f_t$ implies that the bond factor is a suitable index for explaining the tensile behavior of the material. Leutbecher and Fehling et al. (2012, 2014) suggested the contribution of the concrete as Eq. (4-7), which is affected by shape factor β_t from the distribution of the bond stress between concrete cracks:

$$\sigma_{c,m} = \beta_t \cdot \sigma_{cr} + \left(1 - \beta_t\right) \cdot 0.8 f_t \qquad (4\text{-}7)$$

β_t can be interpreted as the bond factor of plain concrete and $\left(1-\beta_t\right)$ can be interpreted as a bond factor considering the fiber reinforcement effect. In this case, $0.8 f_t$ is the contribution of the concrete in the cracked member. The value of β_t is suggested by 0.4, assuming a parabolic distribution of bond stress (Leutbecher and Fehling 2012; Fehling et al. 2014). Bischoff (2003) suggested a concept similar to that of Eq. (4-7), but without representation of the tensile strength of the material. The reported bond factor is 0.4 for plain concrete and 0.65 for fiber-reinforced concrete.

The tension-stiffening bond factor is an index of assessment of the serviceability limit of reinforced concrete under tensile stress. The effective moment of inertia is directly related to the tension-stiffening factor and indicates that a greater tension-stiffening effect brings greater initial stiffness and smaller flexural deflection (ACI 2011). The outstanding tension-stiffening behavior given by the fiber-bridging action ensures that the UHPFRC member has excellent durability and good performance at the serviceability limit state.

4.3.1.2 Reduction in Compressive Strength

Vecchio and Collins (1986) and Belarbi and Hsu (1995) proposed compressive strength formulas based on their own tests. They found the strength reductions down to about 20–30% of the cylinder strength for very large tensile strains. Fehling et al. (2008), on the other hand, proposed a lower limit of about 50% strength reduction when the transverse strain exceeds approximately 0.008. Quite differently, Kollegger and Mehlhorn (1987) worked with a lower limit of 80% of the cylinder strength. These proposals are applicable to normal-strength concrete using coarse aggregates.

All specimens are shown to have compressive failure under different

transverse tensile loadings. Typical failure modes of the panels are shown in Fig. 4-17. Shear sliding failure and vertical splitting failure are observed randomly in the UHPFRC panels among the VF and NF specimens, and concrete spalling failure is observed on the UHPC panels in all VN specimens.

The reduction in the compressive strength of UHPFRC can be considered in terms of high compressive strength and the effect of the reinforced fiber. The shear-transfer mechanism of normal-strength concrete is known for aggregate interlocking, which needs two requisites. One is the existence of a clamping force normal to the crack plane (which is usually provided by transverse reinforcement) and the other is that a crack is formed along the aggregates. In high-strength concrete including UHPC, cracks pass through the aggregates, so that the aggregate interlocking is much less than that of normal-strength concrete. Furthermore, UHPC is composed of fine aggregates only. Meanwhile, the fiber reinforcement relieves the reduction in the compressive strength of cracked concrete, whereas the high-strength-concrete strengthens the reduction, as mentioned above. How these contradictory tendencies affect the reduction of UHPFRC compressive strength has been rarely studied.

(a) Shear Sliding failure | **(b) Vertical Splitting failure** along the horizontal reinforcement | **(c) Concrete Spalling failure** with buckling of steel reinforcement

Fig. 4-17. Typical failure modes (a), (b) and (c) as a result of compressive loading

Fehling et al. (2004, 2008) studied the biaxial tension-compression strength of UHPFRC with a compressive strength of 150 MPa. Although Vecchio and Collins (1986) and Belarbi and Hsu (1995) suggested that this strength is inversely proportion to the principal tensile strain, Fehling separately suggested that the linear function of the principal tensile strain limited by the minimum and maximum values of the reduction factor. The proposal that there is a lower limit on the reduction seems to be reasonable from the following viewpoints. Hoang et al. (2012) pointed out that a significant increase in a strain beyond the yield strain will cause further strength reduction (corresponding to the yield stress of the reinforcement), even though the transverse tension remains practically unchanged. In addition, the lower limit of the reduction suggests a design value for structural members resisted by concrete struts. In this study, the reduction factor of the compressive strengths of UHPC and UHPFRC is suggested in Eq. (4-8) and (4-9), which represents a modification of the proposed equations of Fehling et al. (2008).

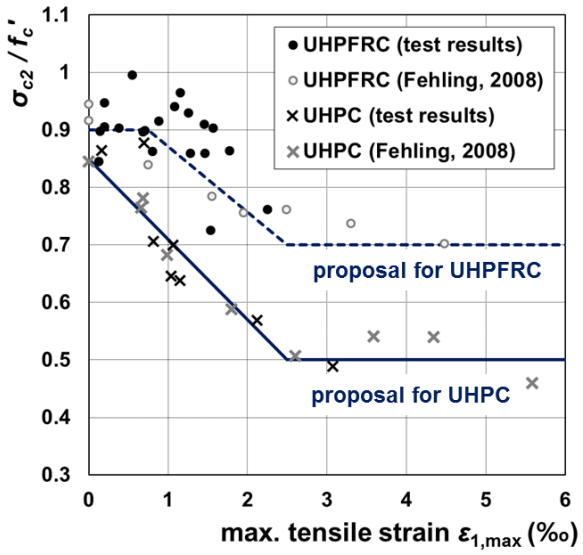

Fig. 4-18. Test results of tension-compressive loading and proposed reduction of compressive strength of UHPC with and without fiber according to transverse tensile strain

for UHPFRC

$$0.7 \le 1.0\left(1.0 - 115 \cdot \varepsilon_{1,max}\right) \le 0.9 \tag{4-8}$$

for UHPC

$$0.5 \le 0.85\left(1.0 - 165 \cdot \varepsilon_{1,max}\right) \le 0.85 \tag{4-9}$$

Fig. 4-18 shows a comparison among the test results in this study, the results from the literature and the above-proposed equation for the reduction in compressive strength of UHPC and UHPFRC. The proposal shown by the dotted line for UHPC matches well with both test results. The proposal shown by the solid line for UHPFRC seems to be conservative for tensile-hardening behavior; nevertheless, it evaluates the reduction value well.

The lower bound of UHPC reduction can be used as the reduction factor for compressive strut failure strength in structural elements such as a strut-tie model and as the shear strength of web-crushing failure. The test results in this study support the value of 0.5 for UHPC without fiber and 0.7 for UHPFRC proposed by Fehling et al. (2008). The value of 0.5 is also the same as that proposed by plastic analysis regardless of the concrete-compressive strength, and has been already adopted in structural standards such as the Eurocode (CEN 2004). The other proposals also lead to a similar conclusion for the lower bound of the reduction. The reduction trends given by Vecchio and Collins (1986) and Belarbi and Hsu (1995) are suggested by biaxial strength test results of ordinary concrete with a compressive strength of 30–40 MPa. The slope of decrease for the UHPC reduction factor is much greater than that for ordinary concrete, but the lower limit of the reduction converges at 0.5. On the other hand, the value of 0.7 for UHPFRC must be verified in a wide range of transverse strains and for diverse rebar and fiber reinforcements.

In ordinary concrete, it is assumed that reinforcements yield after cracking, after which the tensile strain of the structural element entirely relies on the

reinforcement during the stabilised cracking stage. It can be explained that the existing cracks widen and the concrete struts divided by the cracks lose their compressive strength. On the other hand, the ultimate tensile strain of UHPFRC can be larger than the strain at the yielding point of reinforced steel depending on the various mechanical properties of the steel. It means that the softening behavior of UHPFC should be analysed in the crack-formation stage represented by post-cracking behavior. In summary, the correlation between the tensile behavior and compression-softening behavior of UHPFRC is much stronger than that of ordinary concrete due to the outstanding post-cracking behavior of UHPFRC. From this viewpoint, it can be concluded that the test setup by tension-compression sequential loading is suitable for analysing the overall in-plane behavior under biaxial strength, especially for UHPFRC.

4.3.1.3 Schematic failure criteria of UHPC

By reference to the failure criteria of UHPFRC subjected to compression-compression loading (Speck 2007), the schematic failure criteria are proposed. The material properties of the reference indicate a cylinder compressive strength of 150–180 MPa with straight steel fiber of 0.9% and 2.5% volume ratio. The mechanical properties of the reference are similar enough to be categorised as the same material considering that the results are normalised by the compressive strength of the concrete cylinder. The tension-tension strength is considered to be a constant with different values depending on the fiber content.

Various failure criteria are illustrated in Fig. 4-19 and Fig. 4-20. The solid line represents the failure criteria proposed by Kupfer et al. (1969). The coefficients of Eq. (4-10) and (4-11) are adjusted to fit the test results of UHPFRC:

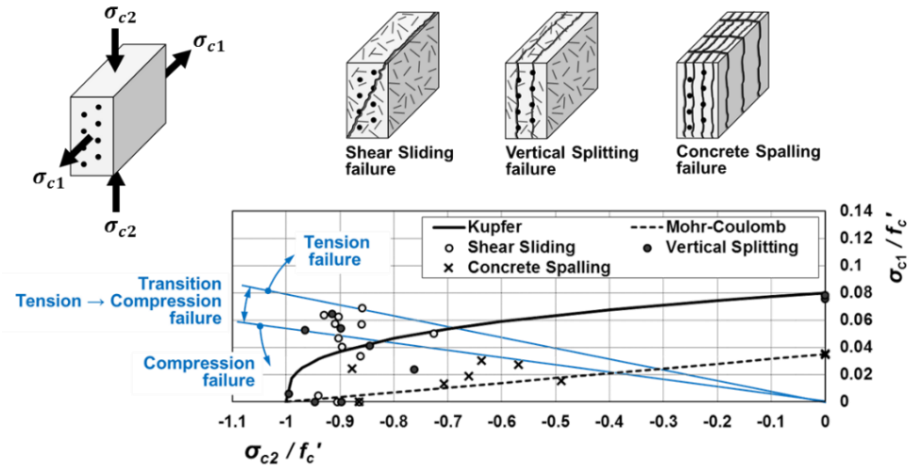

Fig. 4-19. Ultimate strength envelopes under Tension-Compression for UHPC with and without fiber

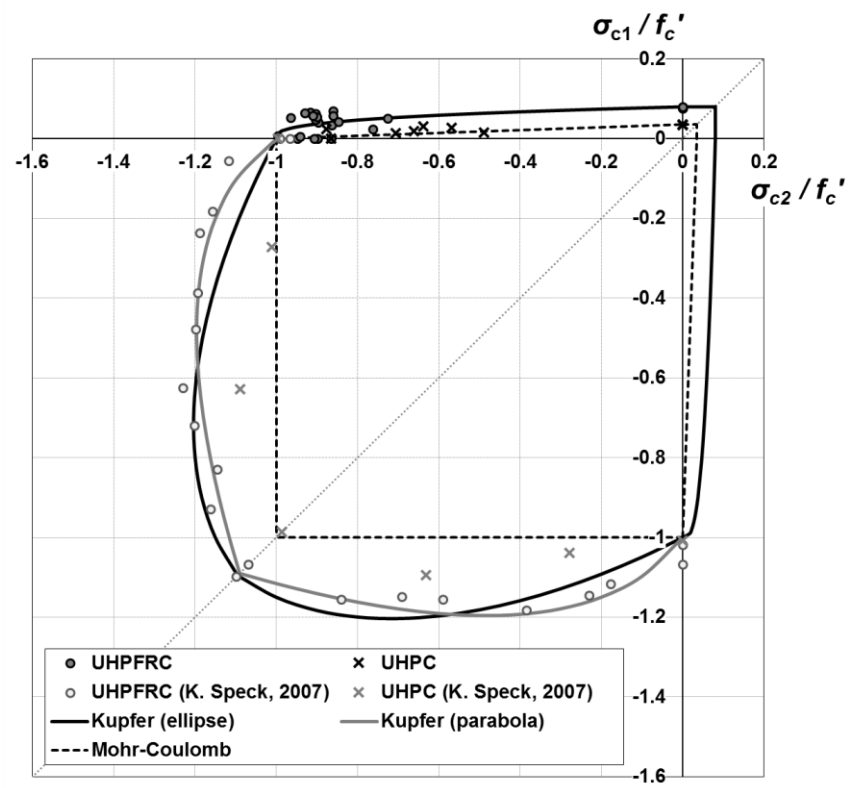

Fig. 4-20. Proposed biaxial failure criteria of UHPC with and without fiber

Compression-compression failure criterion by Kupfer et al. (1969)

ellipse

$$\left(\frac{\sigma_1}{f_c'}\right)^2 - 1.26 \cdot \frac{\sigma_1}{f_c'} \cdot \frac{\sigma_2}{f_c'} + \left(\frac{\sigma_2}{f_c'}\right)^2 - 1 = 0 \quad (4\text{-}10)$$

parabola

$$\left(\frac{\sigma_1}{f_c'} + \frac{\sigma_2}{f_c'}\right)^2 + \frac{\sigma_1}{f_c'} + 3.36 \cdot \frac{\sigma_2}{f_c'} = 0 \quad (4\text{-}11)$$

Compression-tension failure criterion by Kupfer et al. (1969)

$$\frac{\sigma_1}{f_c'} = 0.8\sqrt[3]{1 + \frac{\sigma_2}{f_c'}} \quad (4\text{-}12)$$

The dotted line represents the Mohr–Coulomb failure criteria linearized by plastic analysis. Each part of the envelope is composed of straight lines only, without consideration of the confinement and compression-softening effects. Kupfer's function seems to be suitable for explaining the failure criteria of UHPFRC, and the Mohr–Coulomb failure criteria represent the lower boundary of the concrete or UHPC, which is extremely brittle. The expanded area between the dotted and solid lines can be interpreted by fiber contribution. The fiber reinforcement of UHPC induces ductility due to outstanding post-cracking behavior, despite increased rigidity due to high compressive strength, as explained by the tension-stiffening and compression-softening behaviors of UHPFRC.

The failure criteria of UHPFRC proposed in this study have almost the same envelope curve as that of normal concrete. The actual strength is much greater than that of normal concrete, but the overall mechanical properties of UHPFRC are appropriate for use as a construction material in the field. The failure criteria of UHPC are close to the Mohr–Coulomb failure criteria.

4.3.2 Mohr-Coulomb Failure Criteria

4.3.2.1 Experimental investigation : Push-off test

The tests were carried out on push-off specimens with internal restraint bars (Fig. 4-21). Three transverse reinforcements are arranged with same spacing using different size of the bar. Specimen details are shown in Table III. The specimens were supported on roller bearings and were loaded by a vertical load, applied on top via a knife hinge. With this method of loading, shear without bending moment is produced in the shear plane. The head and the sides of the specimens were reinforced in order to avoid premature failure due to secondary cracks.

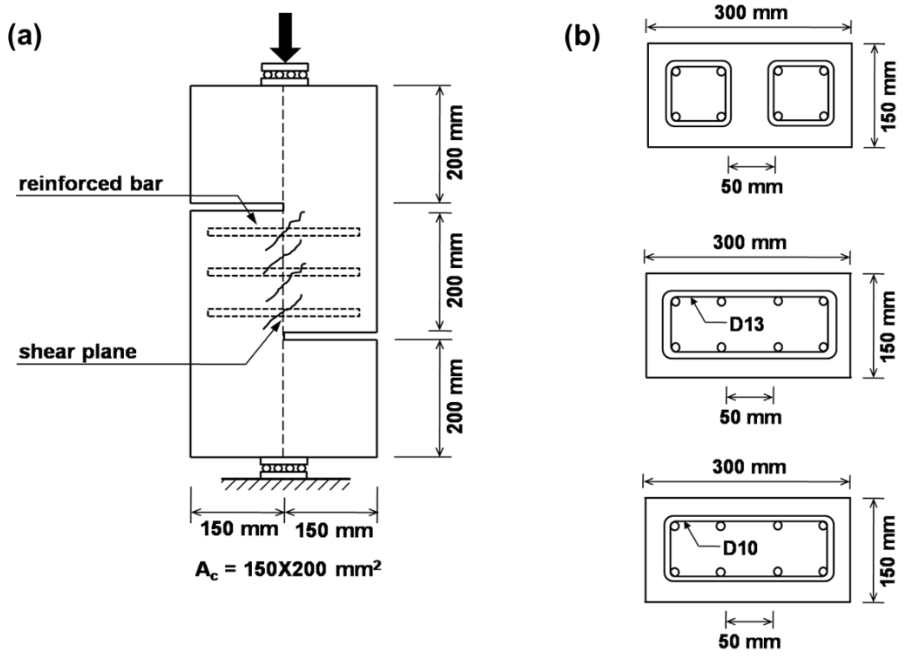

Fig. 4-21. Specimen geometries for tests; (a) test specimen with reinforced bars, (b) specimen dimension and arrangement of bar

Measurements of the crack width and the shear displacement were performed at the center of the specimen on the front and rear faces by means of diagonal LVDT. The vertical external load was measured by a load cell. The passive restraint force normal to the crack plane was determined using strain gauges attached to the internal bars. During the actual shear test, the specimens were subjected to a monotonically increasing load. The shear displacement rate was 0.01 mm/sec. The test were stopped when the shear displacement had reached a value of 2 mm.

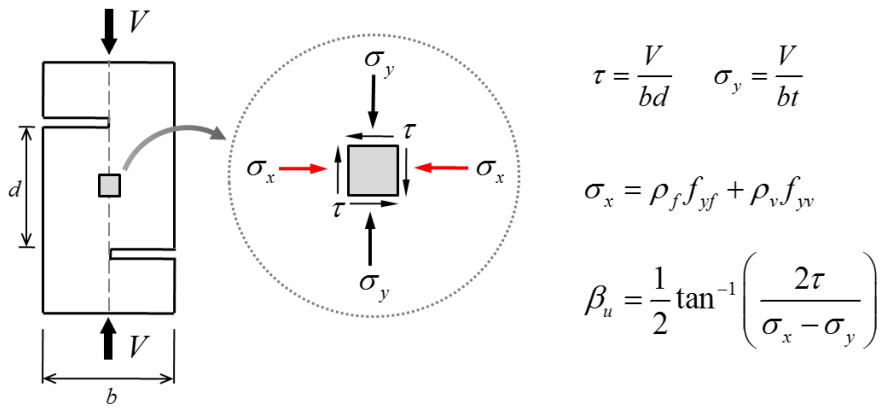

Fig. 4-22. Construction of relationship between shear strength τ, and the reinforcement parameter ρf_y

Consider a push-off specimen, thickness b, and with a shear plane of length d. The stresses acting on a small element of concrete lying in the shear plane will be as shown in Fig. 4-21. Shear stresses τ on all faces, normal stress σ_x, due to the restraint provided by the transverse reinforcement, and normal stresses σ_y. Failure of all specimens occur on the shear plane. Typical failure crack pattern is shown in Fig. 4-23. Higher reinforcement ratios, more inclined crack is observed and accompanied by concrete crushing at the notched edge. Shear stress τ means average value corresponded with Fig. 4-22. First of all, the maximum shear stress clearly increases according to increase of fiber volume

ratio regardless of transverse reinforcement ratio. However, specimen with transverse reinforcement of D10 and D13 makes slight differences with maximum shear stress. The higher transverse reinforcement ratio contributes increase of ductility rather than increase of shear strength. Vertical displacement and horizontal displacement relationship shows dowel action of transverse reinforcement clearly. Specimens without transverse reinforcement maintain constant slope until maximum shear strength, but specimens with transverse reinforcement have increasing its slope until ultimate strength point. These behavior can be explained by inclination of final failure crack and concrete crushing, too.

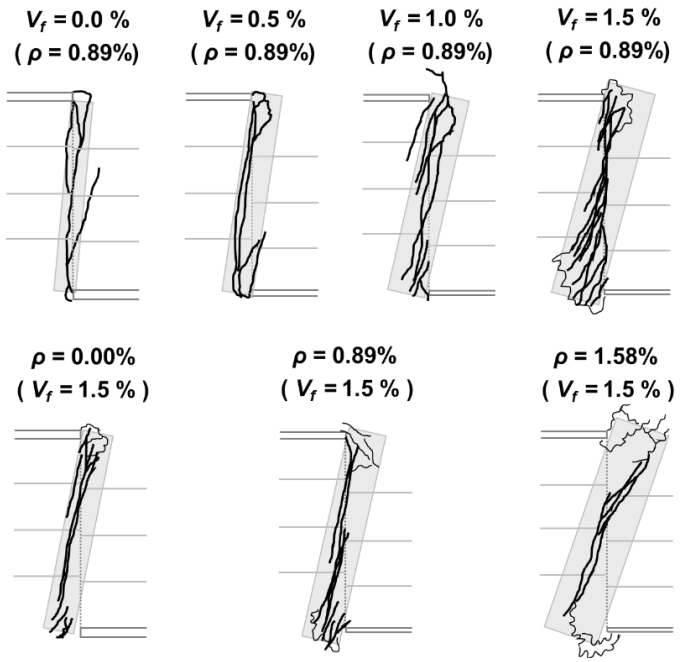

Fig. 4-23. Typical failure crack pattern of push-off tests

4.3.2.2 Analytical investigation

The first analysis based on the theory of plasticity was performed by B.C. Jensen. A theory of less general character but rendering similar results is the

shear-friction theory developed by Mattock and associates. In this research, the failure criteria of reinforced concrete based on plasticity theory is explained, and then the UHPFRC failure criteria will be presented. Basically the theoretical expectation based on modified Coulomb material is almost same, but the characteristic value for monolithic concrete should be verified by test results.

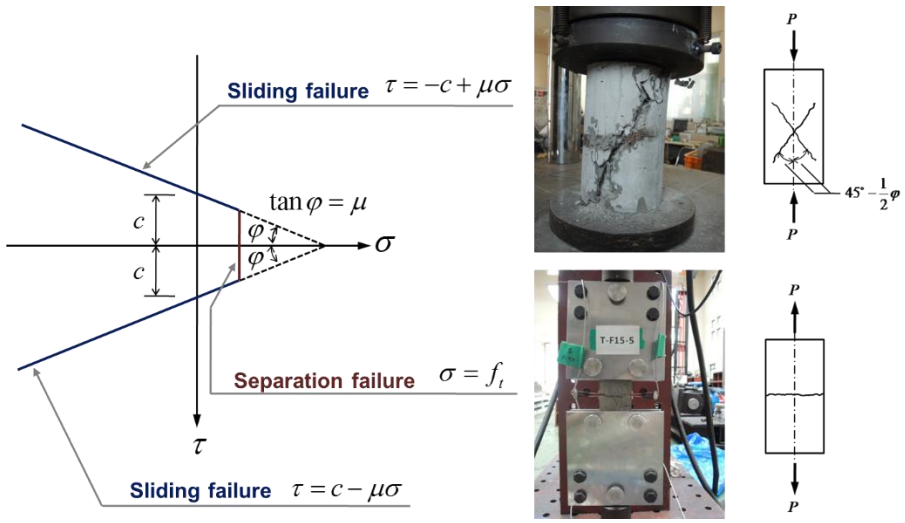

Fig. 4-24. Failure criteria of Modified Coulomb material

The resulting failure criteria makes it natural distinguish between two failure modes, sliding failure and separation failure. At sliding failure there is motion parallel to the failure surface, while motion at separation failure is perpendicular to the failure surface. The condition for sliding failure is $|\tau| = c - \mu\sigma$. One contribution is cohesion, denoted c. The other contribution stems from a kind of internal friction and equals fraction μ of the normal stress σ in the section. The parameter μ is called the coefficient of friction. An angle φ given by $tan\varphi = \mu$ is called the angle of friction. Separation failure occurs when the tensile stress σ in a section exceeds the separation

resistance f_t, when $\sigma = f_t$. Three material constants, c, μ, and f_t must be known for a modified Coulomb material. The material characteristics of UHPFRC coincides with the modified Coulomb material as shown in Fig. 4-24. The compression failure will always involve sliding failure and the pure tensile failure will involve separation failure.

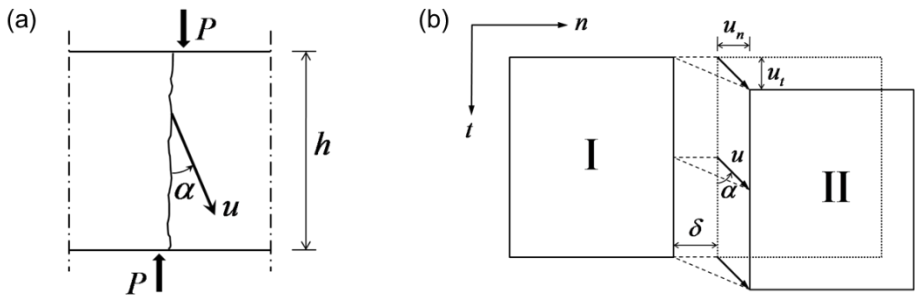

Fig. 4-25. Force set of initially cracked specimen; (a) specimen subjected to shear, (b) failure mechanism in specimen subjected to shear

$$\text{for } \alpha = \varphi, \quad \frac{\tau}{f_c} = \frac{1-\sin\varphi}{2\cos\varphi} + \psi\tan\varphi = \frac{c}{f_c} + \psi\tan\varphi \qquad (4\text{-}13)$$

$$\text{for } 0 < \alpha < \varphi, \quad \frac{\tau}{f_c} = \frac{1-\sin\alpha}{2\cos\alpha} + \psi\tan\alpha \geq \sqrt{\psi(1-\psi)} \qquad (4\text{-}14)$$

$$\text{for } \alpha = 0, \quad \frac{\tau}{f_c} = \frac{1}{2} \qquad (4\text{-}15)$$

In most cases, the strength of a joint can be treated as a plane strain problem. Consider a failure mechanism in the form of a yield line along the line of loading. The relative displacement of the right-hand part to left-hand part is u, forming the angle α to the yield line (Fig. 4-25). The external work is $W_E = Pu \cdot \cos\alpha$. The dissipation consists of two parts, one from the concrete and one from the reinforcement. The reinforcement bars are perpendicular to the yield line. As before, the dowel effect of the reinforcement is neglected, which

means that the dissipation in the reinforcement is $D_R = A_s f_y u \cdot \sin\alpha$, where is the reinforcement area and the yield stress. From the concrete the contribution is $D_C = W_l h$, where h is the length of the yield line, and W_l is given as a function of by the formulas, plane stress problems. The load-carrying capacity determined by Eq. (4-13), (4-14) and (4-15) for virgin material, which can be applied to UHPFRC at the same time.

Assumption for the limit analysis includes neglecting dowel effect of reinforcement because shear friction factor indicates the characteristics of UHPFRC itself. As shown in Fig. 4-25, sliding failure occurs on the shear plane of the specimen and relationship of normal and shear displacement along the crack defines the angle α. The inclination of the two displacements includes dowel effect of reinforcement, so it is not easy to find shear friction factor based on the displacement results directly. Therefore it is necessary to define the restricted forces clamping the crack precisely assuming fiber reinforcement contribution. Let us fiber reinforcement contribution the hardening region of tensile strength. Fiber bridging action reveals between macro crack, which represents $f_t - f_{cr}$. f_t is maximum tensile strength of UHPFRC and f_{cr} is cracking strength of UHPFRC. Considering this term, normal stress between the crack defines as $\rho f_y + f_t - f_{cr}$. Applying the definition of friction factor, the rate of shear stress to normal stress shown in Fig. 4-26 can be identified as 1.4 and friction angle φ is 55°. Dotted line Fig. 4-26 represents failure criteria of UHPFRC material. The comparison of effectiveness factor for RC and UHPFRC is noted at Table 4-3.

Table 4-3. Effectiveness factors for monolithic RC and UHPFRC by limit analysis

	Cohesion factor c	Friction angle φ	Effectiveness factor v	Clamping stress on shear plane
RC	0.17	37°	0.67	ρf_y
UHPFRC	0.08	55°	0.5 (0.7)	$\rho f_y + f_t - f_{cr}$

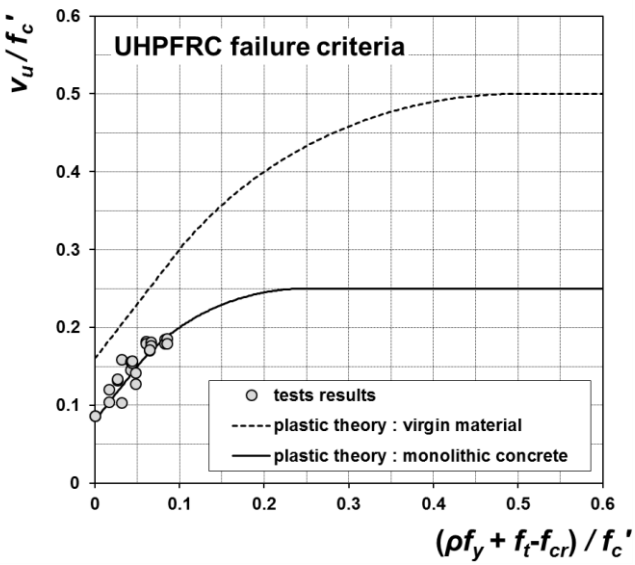

Fig. 4-26. UHPFRC failure criteria by energy method

Effectiveness factor is found fitting the curve to the test results. Solid line in Fig. 4-26 represents failure criteria of UHPFRC for monolithic concrete considering softening and cracking. The effectiveness factor of UHPFRC is ν =0.5, which is much smaller than normal concrete. The important role of effectiveness factor limits the upper bound for the highly reinforced structural element. The failure of web crushing is one of the application. The effectiveness factor of high strength concrete above 100MPa is hardly known, so this value is important for further research.

The analytical and experimental investigation of shear transfer strength for UHPFRC can be summarized as follows.

1) The ultimate shear strength of shear transfer is governed by the tensile strength rather than transverse reinforcement ratio. The transverse reinforcement is much more effective to ductility of structural element.

2) The limit analysis by plasticity theory explains the shear transfer

mechanism of UHPFRC well. The assumption for sliding failure defined by modified Coulomb material is applicable for UHPFRC.

3) The fiber reinforcement contribution $f_t - f_{cr}$ restricts widening crack width and acts as transverse reinforcement. The contribution of fiber reinforcement implies that UHPFRC without transverse reinforcement resists shear friction solely.

4) From the push-off test results, contribution of cohesive c , friction factor μ , and effectiveness factor v is defined and shear transfer strength using the defined variables is represented and verified by test results.

4.4 Fracture Properties of UHPFRC

4.4.1 Mode I Fracture Properties and Material Characteristic Length

Hillerborg introduced the 'fictitious crack model' which is capable of describing the failure of concrete in tension. After the peak load, has been reached, the parts of the member away from the crack unload, and the deformations of the member localize at the crack or in its vicinity, the so-called fracture process zone. This development is called strain localization. Considering a fictitious crack, a fracture process zone of zero initial length, fracture behavior can be described by a stress-crack opening relationship. The area below the stress-crack opening curve represents the specific fracture energy in tension G_f, dissipated per unit area of the fracture process zone until complete separation of the specimen has occurred. Fracture energy G_f is defined as the amount of dissipated work W needed to generate a unit crack with two completely separated crack surfaces, where the new crack area or fracture area. Fig. 4-27 illustrates a simplified response of tensile behavior of ordinary concrete and strain-hardening UHPFRC. Besides the tensile strength, the crack opening displacements w_1 and w_c which are dependent on the fracture energy (*fib*, 2012) are key parameters to define concrete post-cracking behavior.

For UHPFRC stress-strain curves with pre-peak inelasticity, the energy dissipation consists of two terms. The first one corresponds to the energy dissipated in the pre-peak range, which is proportional to the volume, and the second one corresponds to the energy dissipated after peak which, in the cases of localization in a single band, is proportional to the area of the crack band. The pre-peak energy dissipation by volume is $g_{f,A}$ and the postpeak energy dissipation by crack surface is $G_{f,B}$ (Wille and Naaman, 2010). Therefore, the

problem is identical to that for the cohesive crack with bulk dissipation, which related to characteristic length of a material. Table 4-5 shows the reported fracture energy values.

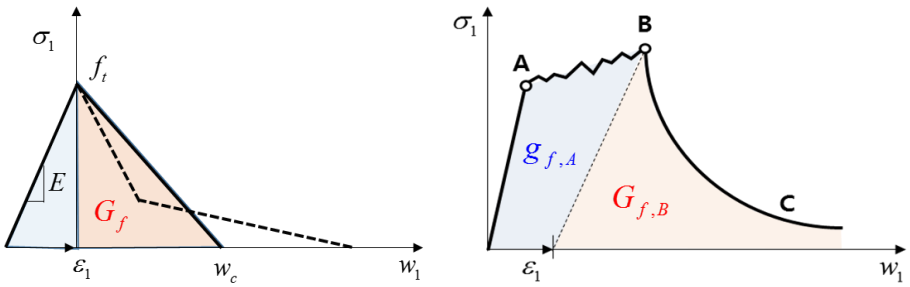

Fig. 4-27. Concrete tensile behavior defined by fracture properties; (a) Ordinary Concrete, (b) UHPFRC

Within nonlinear fracture mechanics, a characteristic length may be defined through a relation between the pre-fracture properties of the material and its post-fracture tensile softening properties. The load-carrying capacity may be dependent only on f_t and a ratio between the steepness of the $\sigma-\varepsilon$ curve and the steepness of the $\sigma-w$ curve (Gustafsson and Hillerborg, 1988). For ordinary concrete, the softening curve is assumed as equivalent linear curve as shown in Fig. 4-27 (a). The critical length $l_{cr}=2\left(EG_f / f_t^2\right)$ is the ratio of the slope of elastic part to that of softening part, which can be interpreted as the equivalent length to transfer elastic energy to surface energy when crack localization occurs. Considering experimental results, the realistic characteristic length is the value of bilinear softening curve with kink point (*fib*, 2012) depicted by dotted line in Fig. 4-27 (a), and the value is about half of the critical length, EG_f / f_t^2, which is generally known for the characteristic length of concrete. Likewise critical length of UHPFRC is defined as $G_{f,B} / g_{f,A}$, the ratio of dissipated energy of pre-peak range to that of post-peak range. Characteristic length is the ratio of dissipated energy release rate which can be

interpreted as the slope of curve. UHPFRC has lower steepness in the inelastic range and higher steepness in the crack localization phase than ordinary concrete. Assuming that the slope in micro cracking phase is almost twice of the slope of equivalent linear elastic phase and the softening curve is linear, the characteristic length of UHPFRC is $2G_{f,B} / g_{f,A}$. The characteristic length is a measure of the brittleness of the concrete. The brittleness of a material has to be changed considering the condition of stress field for brittleness of a structure.

$$l_{ch} = \frac{2G_{f,B}}{g_{f,A}} \tag{4-16}$$

Table 4-4 is fracture properties analyzed by the definition in previous chapter. The tensile stress and strain relationship can be obtained using the given fracture properties (Fig. 4-28).

Table 4-4. Fracture properties based on test results

Material ID	G_f [N/mm]	$G_{f,B}$ [N/mm]	$G_{f,A}$ [N/mm]	s_{rm} [mm]	$g_{f,A}$ [N/mm^2]
2	41.7	39.4	2.3	13.5	0.17472
3	28.0	26.6	1.4	14.25	0.10046

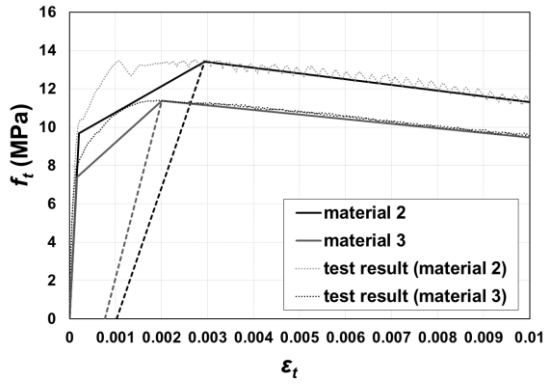

Fig. 4-28. Tensile stress and strain relationship analyzed by fracture properties

Table 4-5. Reported fracture energy values of UHPFRC or high performance cementitious composites

Researcher	Fiber type	Material properties	Test methods	Calculation methods	Fracture energy (kJ/m^2)		
					G_f	$G_{f,A}$	$G_{f,B}$
Wille and Naaman (2010)	2.5% steel fibers (l=13mm, d=0.2mm)	f_c=192 MPa f_{ct}=14.2 MPa ε_{ct}=0.0024	Double bell shaped uniaxial tensile test	Summation of unit volume energy $g_{f,A}$ and the crack surface area energy $G_{f,B}$	25.1	0.18	25.1
Jungwirth and Muttoni (2006)	2.5% steel fibers (l=20mm, d=0.3mm)	$f_{ct,m}$=8.5 MPa f_{ct}=10 MPa ε_{ct}=0.0025	Dogbone shaped specimens	proposed equation considering $G_{f,a,nr}$ in hardening phase and $G_{f,lr}$ in softening phase	21.2	1.9	20.6
			Notched specimens for uniaxial tensile test			0.3	22.2
Benson and Karihaloo (2005)	Mix I : 6% steel fibers 5% (l=6mm, d=0.16mm) 1% (l=13mm, d=0.16mm)	f_c=184 MPa f_{ct}=12 MPa	Dogbone shaped specimen for uniaxial tensile test	traditional fracture energy	17	-	-
	Mix II : 6% steel fibers 4.5% (l=6mm, d=0.16mm) 1.5% (l=13mm, d=0.16mm)	f_c=219 MPa f_{ct}=13.5 MPa			20.5	-	-
Habel et al. (2006)	6% steel fibers (l=10mm, d=0.2mm)	f_c=175 MPa f_{ct}=13.0 MPa ε_{ct}=0.0027	Notched specimens for uniaxial tensile test	traditional fracture energy	24.2	-	-
Maalej et al. (1995)	4% PE(Spectra) fibers	f_{ct}=4~5 MPa	Uniaxial tension and DCB specimens	Steady-state total fracture energy J_c	34	-	-

With respect to the size effect of structural elements, material characteristic length is a kind of the critical point dividing two failure criteria, the plastic limit and the LEFM limit. For RC structures, fracture properties including material characteristic length is determined by the maximum diameter of aggregates in concrete. For example, Bazant-Kim-Sun's formula assumes the characteristic length as $25 d_a$ as shown in Table 3-3. The reason why the diameter of aggregates is the important parameter to determine the fracture properties is associated with concrete cracking behavior. The microcracks in normal strength concrete easily propagates along the surface of aggregates and the macro cracks are the results of integrated microcracks.

The cracking behavior of UHPFRC is mainly caused by bond strength between cement matrix and fiber, so the mix composition and the fibers determines the fracture properties of UHPFRC. Fiber volume fraction and fiber type are key parameters, and the fiber factor χ_f shown in Eq. (4-17) which is a parameter to evaluate whether the workability of the mix. The factor is defined as the product of volume fraction V_f and fiber aspect ratio l_f / d_f.

$$\chi_f = V_f \times l_f / d_f \tag{4-17}$$

Note that a value of $\chi_f \approx 2.5$ was suggested by Markovic (2006) as an upper limit for the straight steel fibers used in his study, which are same as the steel fiber used in this dissertation. However, Wille and Naaman (2011) investigated the workability of UHPFRC with different fiber volume fractions and suggested $\chi_f \approx 2.0$ as an upper limit.

The suggested material characteristic length of UHPFRC of Eq. (4-16) is clear to define, but it is not easy to get the fracture energy of UHPFRC from test results. It might be required to define the characteristic length using fiber factor or typical material properties verified by test results.

4.4.2 Mixed Mode Fracture Properties and Fracture Process Zone

UHPFRC has outstanding post-cracking behavior which is explained by hardening part due to micro cracking and softening part after crack localization. Fracture characteristics of UHPFRC should be analyzed considering its large fracture process zone because flexural and shear elements with conventional reinforcements fail with major crack. Classical fracture mechanics distinguished three types of fracture modes depending the physical behavior at the crack tip: opening mode or mode I, in-plane shear or mode II, and out-of-plane shear or mode III. For ordinary concrete, mode II behavior is usually negligible in comparison with mode I behavior, on the other hand, UHPFRC has different crack bridging effect of material heterogeneities due to bond strength between fibers and matrix. In this research, three point bending test on off-center notched prism was conducted and flexural shear behavior was analyzed with respect to the mixed mode fracture characteristics for different height and same proportional geometry (Fig. 4-29).

Fig. 4-29. Off-center notched specimens of 3-point bending test

RILEM TC89-FMT suggested three types of mixed mode fracture test: three point bending beam with off-center notch, four point shear specimens, and quadratic double-edge-notched specimen. Among the given method, the first test method was conducted in this research to investigate flexural shear behavior, not pure in-plane shear behavior. This method gives stable crack growth and can be analyzed by two parameter fracture model, which indicate characteristic fracture properties for nonlinear fracture materials. (Shah and Carpinteri, 1991).

The tensile behavior is the most important parameter in this research. There are two types of mix compositions A and B with different volume ratio. Material A(=material 1) with fiber volume fraction of 1.5% is expected to show tensile hardening behavior and material B with fiber volume fraction of 0.5% is expected to show tensile softening behavior. For each material, the beam size and initial crack location on flexural shear behavior depending on the material type is planned to investigate size effect and the influence of mode II behavior for UHPFRC. It can be regarded as that pure mode I with zero off-set ratio and mixed-mode tests with 1/3, 1/2 and 2/3 off-set ratio can be performed using similar specimens and same testing setup. In addition, to investigate the size effect on the flexural shear behavior of UHPFRC beams, specimens with three different height were prepared for each off-set ratios.

To investigate the tensile strength and opening displacement curve, four dog-bone specimens for each mix composition were fabricated and tested by using a specially designed direct tensile test machine. Mix composition A shows tensile hardening behavior with fiber volume fraction of 1.5% and mix composition B shows tensile softening behavior with fiber volume fraction of 0.5% (Fig. 4-30). The compressive strength of material A and B is almost same, bout 180 MPa. To compare the fracture toughness of the material, fracture energy G_f was compared to each other. The fracture energy of material A is about 50 N/mm and that of material B is about 15 N/mm. For reference, the

concrete with compressive strength of 180 MPa is estimated as 0.1~0.2N/mm following the bilinear softening model given *fib* model code 2010. The cracking pattern was shown in Fig. 4-31.

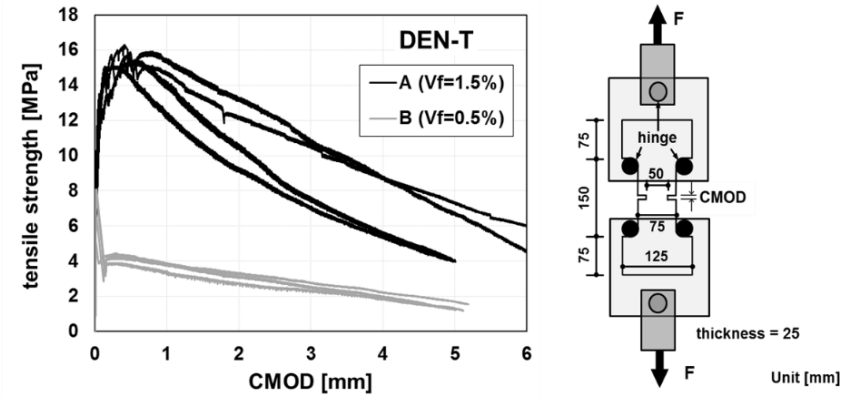

Fig. 4-30. Direct tensile test results on double edge notched plate for UHPFRC

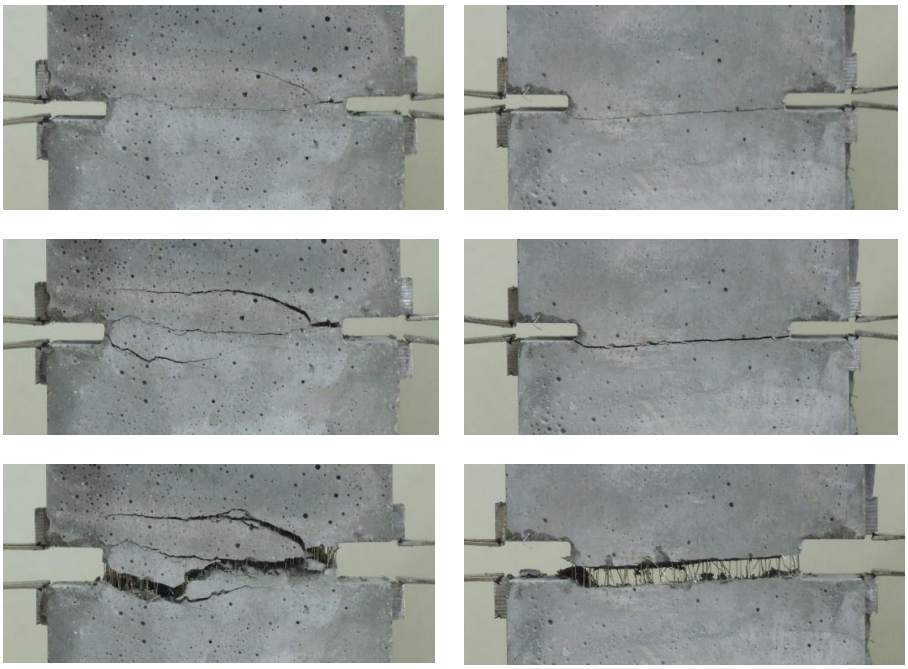

Fig. 4-31. Mode I cracking behavior of UHPFRC A (Left) and UHPFRC B (Right)

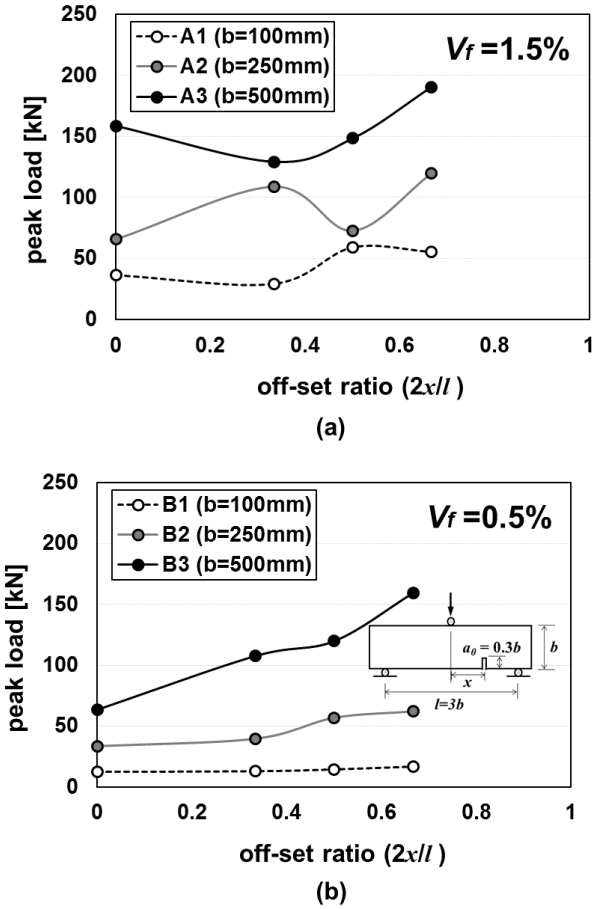

Fig. 4-32. 3-point bending test results on single edge notched prism with different beam size and initial crack location of UHPFRC; (a) A-series and (b) B-series

Three point bend notched beam tests with notches were performed using two parameter fracture model (Shah, 1990). Jenq and Shah (1998) suggested that two fracture mechanics parameters, K_{Ic} and $CTOD_c$, which is the equivalent linear elastic fracture properties can be determined by test results. Compared with the fracture properties for material A and B investigated from the test results, there is a big differences in terms of critical stress intensity factor, critical crack tip opening displacement and fracture energy. It was found

out that K_{Ic} and $CTOD_c$, of material A is greater than three times of the properties of material B. Whereas the equivalent crack length, material length for each material, is similar. This results can be interpreted that the slope of fracture process zone for a material is different although the length of fracture process zone in direction of its growth is similar. This results gives schematic shape and dimension for fracture process zone of the material.

The fracture process zone (FPZ) is a nonlinear zone characterized by progressive softening, for which the stress decreases at increasing deformation. This zone is surrounded by a non-softening nonlinear zone characterized by hardening plasticity or perfect plasticity, for which the stress increases at increasing deformation or remains constant. The relative sizes of two zones defines the fracture behavior (Bazant and Planas, 1998).

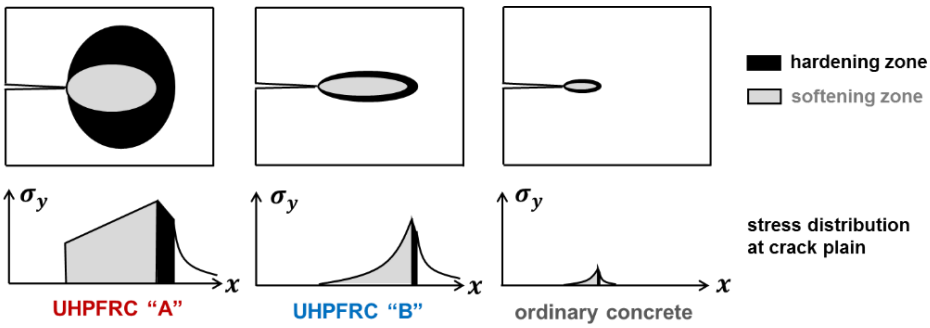

Fig. 4-33. Type of fracture process zone for different UHPFRC

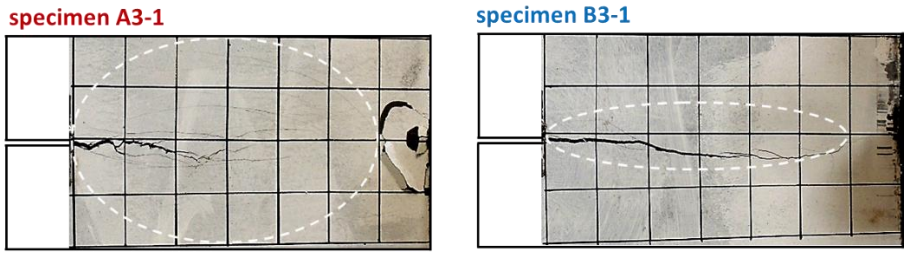

Fig. 4-34. Shape of fracture process zone for different UHPFRC A and B on test results (grid spacing=50 mm)

Right one in Fig. 4-33 shows typical FPZ of quasi-brittle material including concrete. A major part of the nonlinear zone representative equivalent softening zone undergoes progressive damage with material softening due to micro cracking. There is no appreciable plastic deformation takes place, the size of FPZ is large enough to have to take into account in calculations. The differences with the ordinary concrete is that the absolute value is higher and the shape of softening curve is not bilinear, but almost constant within the fracture process zone. Left one in Fig. 4-33 shows the suggested FPZ of UHPFRC with hardening behavior like material A. The length of the FPZ along the crack propagation is almost same as that of material B, but the overall area of FPZ is greater mainly because of the nonlinear hardening zone. The schematic FPZ suggested in Fig. 4-33 can explains the characteristics of flexural behavior and flexural shear behavior of material A and B precisely. Assuming the suggested FPZ for each material, size effect and crack propagation characteristics in flexural shear behavior will be discussed in this research. The cracking pattern shown in Fig. 4-34 supports the suggested FPZ. Hardening zone in material A specimen can be observed in front of the crack tip area as well as the side areas along the localized crack in a wide range. On the other hand, material B specimen shows a clear major crack propagation without visible cracks.

Size effect on ductility for center notched specimens were investigated as shown in Fig. 3. The flexural behavior of UHPFRC does not shows degradation of maximum strength with increase of its size. The maximum strength of center notched specimens for material A in Fig. 4-35 (a) shows no tendency and large deviation because of increase nonlinearity by material heterogeneity. Whereas for B-series specimens in Fig. 4-35 (b), the flexural behavior shows that bigger structure behaves more brittle, but has no greater peak load with increase of its size. Flexural behavior for material B is dominated by brittle failure but the maximum strength is governed by its material tensile strength.

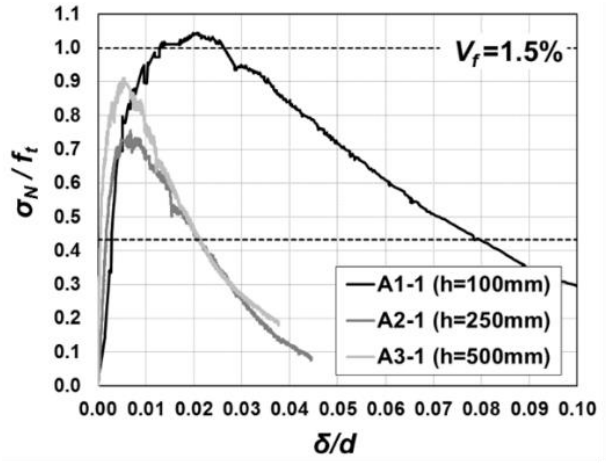

(a)

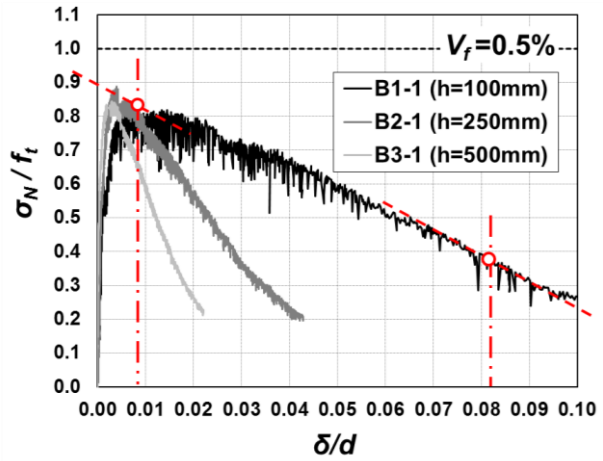

(b)

Fig. 4-35. Size effect on the structural ductility for (a) UHPFRC A, (b) UHPFRC B

For mixed mode failure of concrete, the determination of the final failure path and the criteria for crack instability are more complicated than that of pure mode I failure. Criteria for determining the crack propagation trajectory and crack instability are necessary for mixed mode fracture. There are lots of theories, but all the theories predict that a crack will propagate along its original plane (θ=0°) for pure mode I and will deviate from its own plane (at an angle

of about θ=73°) for pure mode II. In this paper, the maximum stress criterion was used. (Jenq and Shah, 1988) Fig. 4 indicates that the analysis result for flexural behavior on size effect depending on its material characteristics is applicable for flexural shear behavior, too. Flexural shear strength on material A shows nonlinearity with a large deviation and the maximum strength on material B is governed by its tensile strength.

It is important to investigate a direction of crack propagation as well as a stability problem after the peak load in the mixed mode fracture analysis. Likewise mode I fracture, specimens of material A shows that lots of micro cracks accompanies around the major crack. The crack propagation of test specimens are shown in Fig. 4-36. The specimens with a height of 100 mm showed a large difference in crack growth orientation with respect to the fiber volume fraction. The initiation angle of material A is 45° and the propagation angle varied depending on the crack location. The initiation angle of material B is 20° but the propagation is linear and brittle. The major cracks of specimens with a height of 250 mm were relatively scattered and the characteristics of crack propagation is opposite to the specimens with a height of 100 mm. The cracking behavior of material A is more brittle than that of material B for the specimens with a height of 250 mm. The overall cracks propagated in a linear way and it was observed that the angle of crack path is dependent to the initial crack location for the specimens with a height of 500 mm (Fig. 4-36 (b)).

The existing mixed mode failure criteria is the use of stresses expressed in terms of K_I and K_{II} based on crack propagation angle θ. Maximum stress criterion was proposed by Erdogan and Sih (1963) and is based on the assumption that the crack initiates from its tip in a direction normal to the maximum circumferential stress when the circumferential stress σ_θ becomes a principal stress and τ_θ is zero. (Shah, 1991) Crack advance is initiated when the near field stress $\sigma_{\theta,max} = \sigma_\theta(\theta)$ at distance r in front of the crack tip reaches the same critical values as in pure mode I.

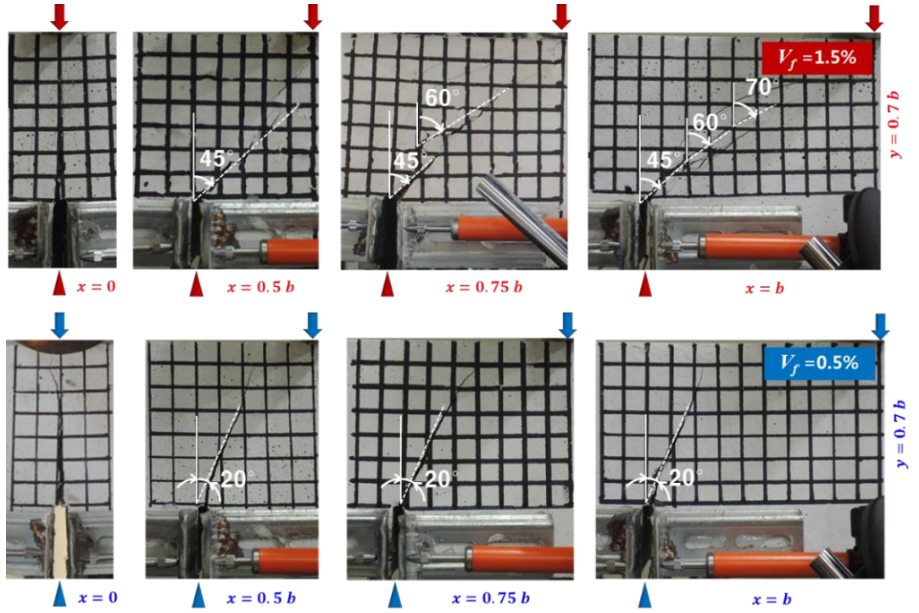

(a) h=100 mm

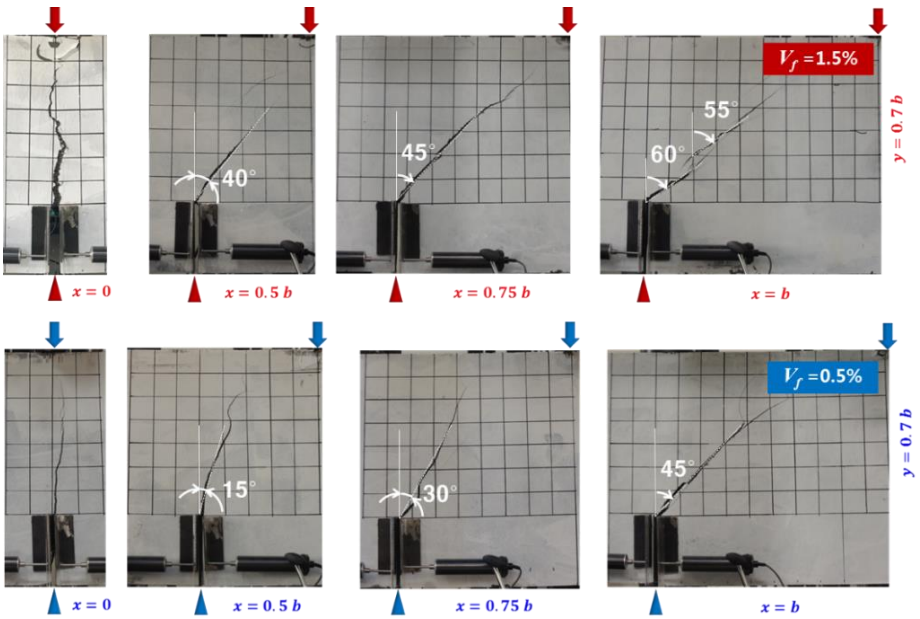

(b) h=500 mm

Fig. 4-36. Crack growth orientation for different heights and initial location

Based on the maximum stress criterion, test results in this research including the test results for ordinary concrete (Jenq and Shah, 1988) were denoted in Fig. 4-37. Assuming that crack initiate and propagate in a straight line, the final crack angle of off-center notches is 20~55°. The ratios of K_{II} / K_I values are relatively high, so mode II behavior of UHPFRC cannot be negligible. Fracture properties of UHPFRC were investigated on three point bending test of twenty-four single notched prisms with varied types of location of notch, height of specimens and fiber volume ratio. Flexural shear strength on material A with tensile hardening behavior shows nonlinearity with a large deviation and the maximum strength on material B with tensile softening behavior is governed by its tensile strength. It can be concluded that size effect on flexural strength of UHPFRC within the depth of 500mm can be negligible with respect to the maximum strength. In addition, the crack propagation angle for flexural shear behavior was investigated and analyzed with respect to the maximum stress criterion. As a result, the ratios of K_{II} / K_I values for material A and B are much higher than ordinary concrete, so the tractions generated through the frictional force and the contribution of the tractions should be considered.

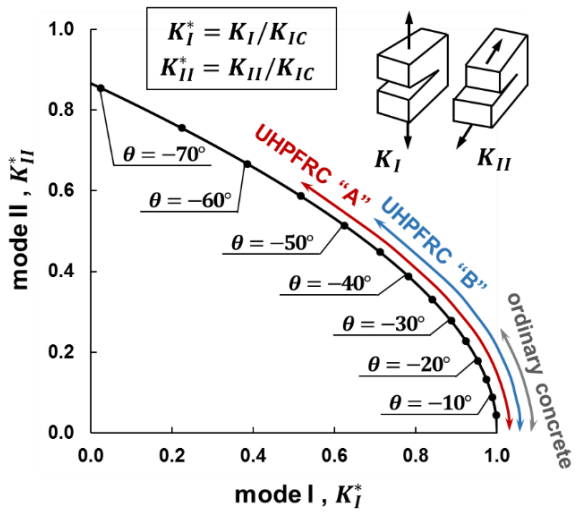

Fig. 4-37. Maximum stress criterion (Erdogan and Sih, 1963) and mode II behavior of UHPFRC

4.5 Summary

Most previous UHPFRC has been investigated by uniaxial tension test regarding to the separation failure. The separation failure observed in uniaxial tension behavior governs a crack localization phase like the tensile behavior of ordinary concrete. However the sliding behavior of UHPFRC with tensile hardening behavior is important in microcracking phase which play a role to increase shear strength of UHPFRC members, and the frictional failure is represented in the Mohr-Coulomb failure theory. The microcracking behavior as a result of fiber reinforcement effect is analyzed with respect to limit analysis for push-off tests assuming that UHPFRC is a composites of cement matrix and fibers. At the same time, the fracture properties of UHPFRC to define microcracking and crack localization are studied three-point bending test and direct tension test on notched specimens. The overall experimental investigations in chapter 4 are indicated in Fig. 4-38.

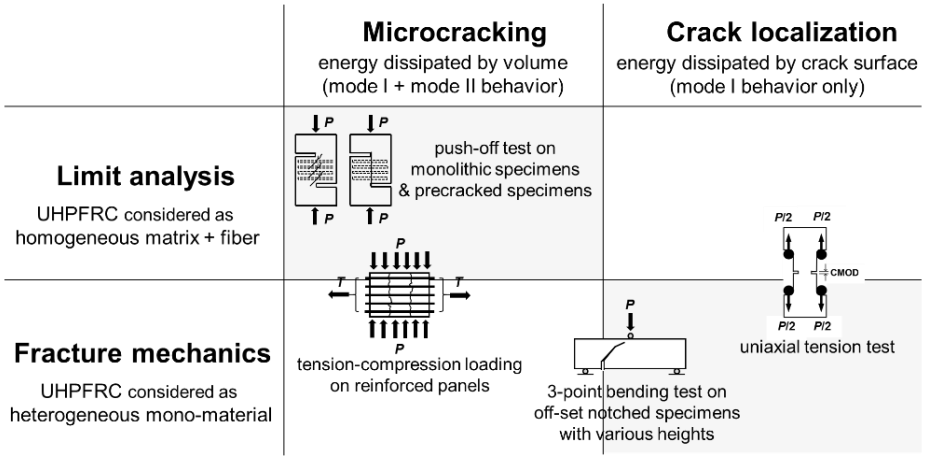

Fig. 4-38. Mapping of material tests for analytical investigation

The experimental investigations to find out UHPFRC mechanical

properties in this dissertation are summarized as follows:

1) The effective tensile strength and the fracture properties of UHPFRC were investigated. To determine the effective tensile strength, three-point bending test and direct tension test on notched specimen were performed. Based on the test results, the definition of UHPFRC with tensile hardening behavior is suggested and the fracture properties of UHPFRC are found out regarding to the given definition of tensile strength and deformation relationship.

2) The failure criterion of UHPFRC was determined assuming the frictional failure based on the Mohr-Coulomb theory and the separation failure based on the effective tensile strength. The frictional angle, which is the important value to explain the fiber reinforcement effect as passive reinforcement, was given by analysing the push-off test results on monolithic specimens.

3) The effective factor to explain compressive softening behavior was determined by the biaxial tension-compression test on reinforced UHPFRC panels. Additionally, tension stiffening behavior and the schematic failure criterion of in-plane behavior were also suggested.

4) The characteristics of UHPFRC microcracking behavior was investigated with respect to the diverse point of view. The push-off test results on pre-cracked specimens were analysed by dilatancy theory, a discrete model, assuming the separation and sliding behavior simultaneously. In addition, at the point of fracture mechanics, the size and shape of fracture process zone of UHPFRC were investigated. The crack growth orientation observed in three point bending test on off-center notched prisms with different sizes shows that the mode II behavior of UHPFRC cannot be negligible for UHPFRC with tensile hardening behavior.

Chapter 5. Shear Strength Evaluation of UHPFRC I-shaped beams

5.1 General Assumptions

The assumptions of the material behavior and the structural shear behavior, especially the assumption of the link between material and structural action, are essential to evaluate the shear strength of UHPFRC beams. Based on the test results in chapter 4, the uniaxial tensile behavior of UHPFRC material is defined in Fig. 5-1. The shear behavior in web of UHPFRC I-shaped beams without stirrups can be represented in Fig. 5-2 depending on the material behavior with the frame of limit analysis coupled to fracture mechanics approach. Segment OA, AB and BC means similar structural behavior defined as elastic part, hardening part after initial cracking and softening part after peak strength in material and structural level. The segments noted by same capital letter in two figures are related to each other directly. The exceptional part, segment BB' is affiliated by material softening behavior when structural confinement is strong enough to increase the shear strength of a member.

Microcracking behavior arises in a wide range of area in a web of I-shaped beams because the energy dissipated by a unit volume. For an element in plane stress, the strain energy density can be obtained by a unit volume of the material. In a segment AB, The material can be assumed to be homogeneous since the stiffness remains constant with increasing its deformation. On the other hand, the ultimate state of UHPFRC shear beams should be related to the crack width of which the crack localization occurs. At failure, the critical crack opens intensively, while the existing microcracks are closed with its own resilience.

In a segment BC, the energy dissipates along the critical crack and the shape of softening curve is determined by the material characteristics.

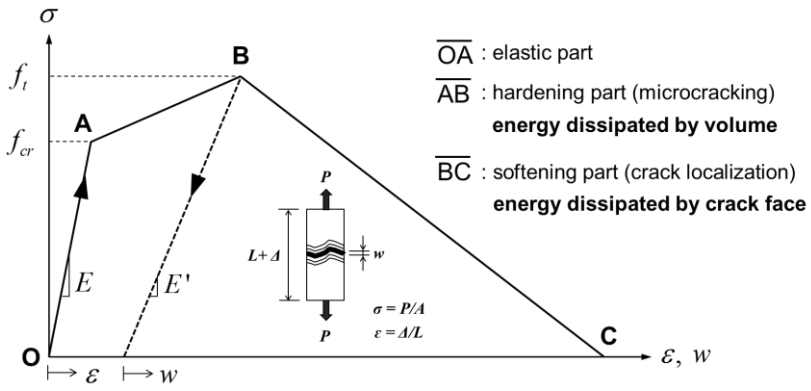

Fig. 5-1. Uniaxial tensile behavior of UHPFRC material

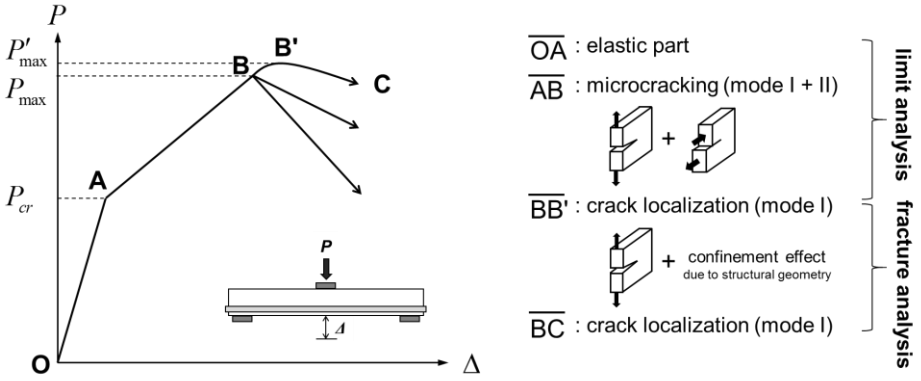

Fig. 5-2. Shear force and deformation relationship in web of UHPFRC I-shaped beams without stirrups

The relationship of shear strength and vertical displacement is more complicated considering the shear design parameters. The material of normal strength concrete (NSC), high-strength concrete (HSC) and UHPFRC are compared in Table 5-1. Table 5-2 shows that general assumptions to shear design for UHPFRC I-shaped beams and RC beams with and without stirrups. The material characteristics can be explained by combination of HSC and fiber

reinforcement effect. The shear strength of UHPFRC shear members is basically quantified by fiber reinforcement effect represented as tensile strength. Comparing the RC beams with stirrups, the reinforcement rebars in RC beams are arranged following the structural design but the tensile strength resists perpendicular to the principal compressive strength in web as the UHPFRC material itself.

Fiber reinforcements are scattered randomly, and the resistance manifests depending on the crack patterns. Hence the summation of the reinforcement contribution and concrete contribution is difficult to explain the physical behavior of the UHPFRC shear structural beams. Instead of the summation form which is adopted in many recommendations, the variable angle truss model is adopted in this dissertation. The range of the inclination of principal compressive strength limited by deformation capacity is important criterion for shear design. The resistance mechanism can be explained by variable angle method based on limit analysis in reference to RC structures, but the final failure should be taken into account in a different way. The failure of RC beams with stirrups is controlled stably because the yielding of steel reinforcement governs the ultimate limit state. However the deformation capacity of UHPFRC shear beams is governed by the crack localization characteristics of UHPFRC material and structural design geometry.

Semi-brittle fracture observed in UHPFRC I-shaped shear beams without stirrups is analyzed by the frame of limit analysis coupled to fracture mechanics. There are two advantages to apply this kind of approach. The diagonal tension failure has to be analyzed corresponding to the deformation capacity represented as the ultimate crack widths of UHPFRC. The concept of brittleness number given by fracture mechanics approach can suggest the size effect correction with respect to the maximum strength given by limit analysis.

Table 5-1. Comparison to material behavior of NSC, HSC and UHPFRC

	NSC	HSC	UHPFRC
Criteria of division	Less than f_c = 60 MPa	greater than f_c = 60 MPa	greater than f_c = 150 MPa (with tensile hardening behavior)
	Quasi-brittle	Brittle	Semi-brittle
Compressive stress-strain relationship	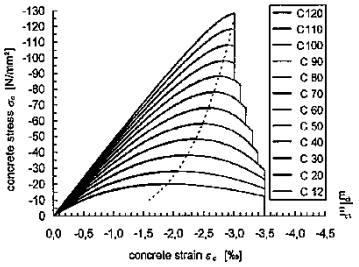 The stiffer and the more brittle in the higher f_c (*fib*, 2012)		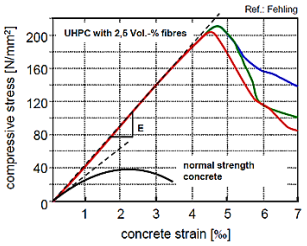 More ductile in the higher volume of V_f in the post-peak behavior
Stress redistribution mechanism	Aggregate interlocking	None	Bond stress between matrix and fiber
Tensile stress-strain relationship	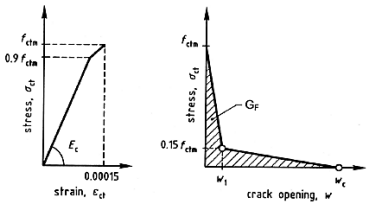 Softening curve is regarded as bilinear shape (*fib*, 2012)		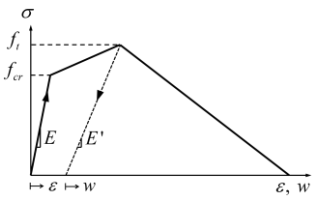 Conspicuous strain hardening part and linear softening curve
Fracture energy G_f	0.1 – 0.2 (N/mm)	-	20 – 25 (N/mm)
Characteristic length	Multiplier of d_{max}	Less than NSC	Multiplier of l_f

Notes: V_f =fiber volume ratio, d_{max} =maximum diameter of aggregates, l_f =length of steel fiber

Table 5-2. Comparison to shear behavior and general assumptions for UHPFRC I-shaped beams and RC beams with and without stirrups

	RC beams without stirrups	UHPFRC beams	RC beams with stirrups
Energy dissipation	Energy dissipates in an elastic part of concrete (plasticity theory assumes $d \rightarrow 0$)	Energy dissipates mainly in a region of microcracks represented as hardening part of UHPFRC	Dissipated energy concentrates steel reinforcement only (assuming rigid-plastic behavior)
	$V = V_{cr}\left(=V_c\right)$	$V = V_f$	$V = V_s$
Governing failure criteria	Concrete failure criterion	HSC+fiber concrete failure criterion	Concrete + steel rebars failure criterion
modelling	Failure line	Failure region (damaged zone)	Truss analogy
Typical failure mechanism	Diagonal tension failure	Diagonal tension failure in a damaged zone	Stirrup yielding or Concrete crushing
	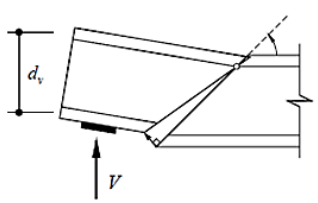	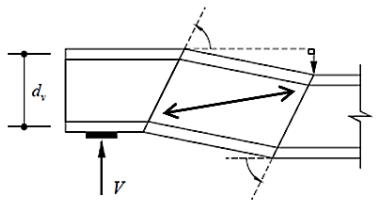	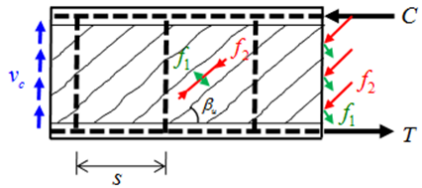
Governing parameter	Concrete characteristics		Steel characteristics
	shear span ratio, effective depth (size effect), longitudinal reinforcement ratio		Shear reinforcement ratio

Notes: V = design shear strength, V_{cr} = initial cracking strength, : V_f = fiber reinforcement shear strength, V_s = stirrup shear strength

First of all, the shear strength of UHPFRC I-shaped beams is evaluated from the material failure criterion with the assumptions of concrete plasticity. Limit analysis focuses on a strength increase due to microcracking in this dissertation. UHPFRC in limit analysis is assumed to be homogeneous material reinforced by steel fiber and the reinforcement effect is represented by UHPFRC tensile strength and the inclination of the principal stress in compression field. The inclination capacity is related to the UHPFRC tensile hardening behavior represented by microcracks development with a relatively constant stiffness. However post-peak behavior of tensile strength gives insufficient ductility so the maximum strength of the structures depends on its structural capability such as effective depth, geometry of cross section and longitudinal reinforcement ratio, etc..

Subsequently, fracture mechanics concentrates on reduced capacity due to material heterogeneity represented as localized crack failure in web. The suggested strength based on limit analysis plays a role as the upper limit value and the brittleness number based on fracture mechanics gives the additional variables. Longitudinal reinforcement ratio and axial forces due to prestressing should be also taken into account. Size effect in ordinary concrete structures generally concentrates on the size range divided by failure criteria governed by limit analysis and LEFM. The critical point D_0 between two failure criteria is about 200 ~ 500 mm, so it is meaningful to compare the test results in laboratory and field application scale. However the characteristic length calculated using equivalent elastic fracture method such as two parameter fracture model of Jenq and Shah is at least 500 ~ 3000 mm for UHPFRC with tensile hardening behavior. Nonlinearity of cracking behavior governs the structural behavior more significantly when the size of fracture process zone is greater. Hence the reduced strength of UHPFRC shear beams with diagonal tension failure should be analyzed with respect to its strength reduction due to inelasticity around the critical point of limit analysis and LEFM.

5.2 Plastic Limit Analysis for Shear Strength of UHPFRC I-shaped beams

5.2.1 Stress Fields and Failure Mechanism

To apply the theory of limit analysis, material yield conditions and applied stress fields should be defined clearly. Based on the assumptions and test results in previous chapters, UHPFRC is homogeneous material followed by Coulomb failure theory before crack localization occurs. The material properties related to Coulomb failure criterion is indicated in Table 5-3. The figure in the Table 5-3 shows a typical stress state at pure tensile failure with sliding behavior.

Table 5-3. Yield conditions of UHPFRC as a Coulomb material

	Material properties	Coulomb failure criterion
Angle of friction	$\varphi = 55^{\circ}$	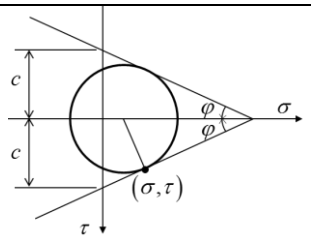
Effectiveness factor	$\nu = 0.7$	
Cohesion	$c = \nu \frac{1-\sin\varphi}{2\cos\varphi} f_c$	

Construction of stress fields and comprehensive and feasible failure mechanics are key issue for limit analysis methods. Inelastic behavior of UHPFRC structural members is governed by micro-cracking which is strongly dependent on material cracking. The load-deformation behavior exhibits a practically constant contribution of the fiber reinforced concrete over large ranges. The shape of stress field in the web of I-shaped shear beam depends on shear span ratio and effective depth d. The extensive number of micro-cracks started to develop from 45° and the crack inclination angle became flatter in a

wide range of the span. At the peak load, one or several diagonal cracks localize in the damage zone (Fig. 5-3).

Limit analysis is applied to the microcracking phase with the assumption of ductile failure, so the stress fields can be regarded as uniform stress field with a well distributed reinforcement. The uniform and discontinuous stress field has been generally accepted to explain the ultimate state behavior of webs of beams as a representative truss models (Sigrist et al., 1995). The discontinuous stress field in RC shear beams with stirrups as shown in Table 5-2 was analyzed with respect to the equilibrium and compatibility condition on the crack faces in many theories, such as cracked membrane model (Kauffmann, 1998) and modified compression field theory (Vecchio and Collins, 1986).

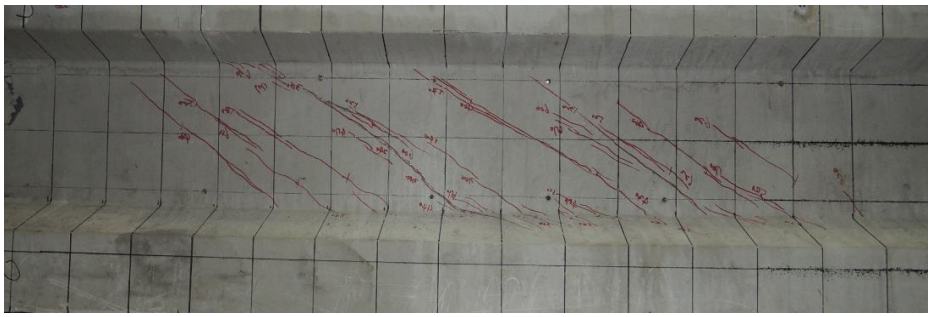

(a)

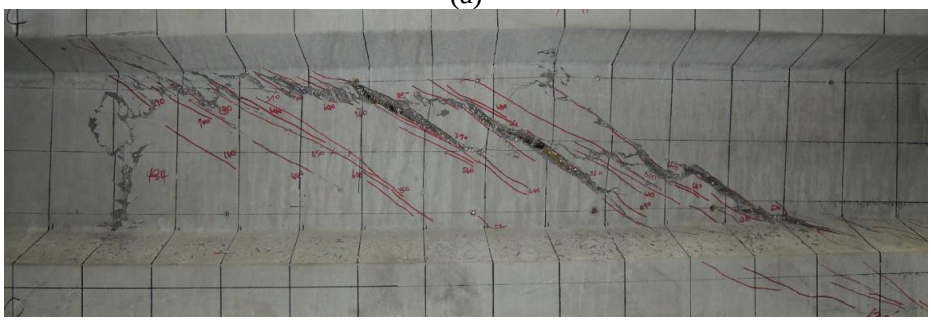

(b)

Fig. 5-3. Cracking behavior in web of UHPFRC I-shaped beam without stirrup: (a) microcracks in web and (b) major cracks at failure

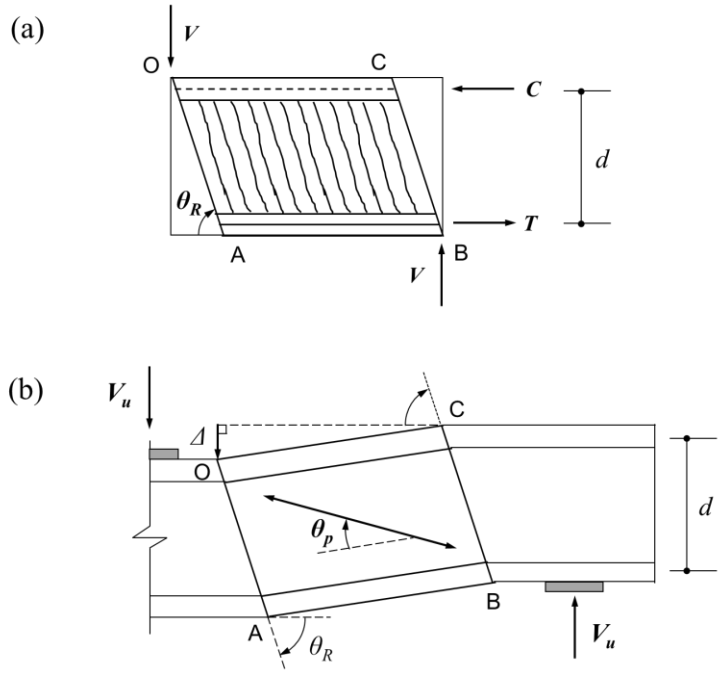

Fig. 5-4. Uniform stress field and failure mechanism in web: (a) splitting cracks with the inclination of θ_R in a microcracking zone ABCD and (b) diagonal tension failure as a result of crack localization with the principal angle θ_p

The crack spacing and the crack width of UHPFRC exhibit much smaller than ordinary concrete, so truss analogy for RC has to be modified. Instead of concrete strut divided by rough crack, the damaged zone with a series of tensile struts with continuous uniform stress field caused by friction along the crack surfaces as shown in Fig. 5-4 is suggested.

The interaction between stress field given by geometry and stress redistribution region given by UHPFRC post-cracking behavior can be assumed to define the size of equivalent panel with relatively uniformly tension-compression stressed field as shown in Fig. 5-4. The hypothetical panel with splitting cracks in uniform stress field can be regarded as widened concrete strut and the damage zone is assumed to be diagonal tension failure by critical crack localization with the angle of θ_p. The structural behavior of shear beam

is modelled by failure of the damaged zone. In this research, the damage zone is regarded as crack band and the dimension of crack band is defined by the location of plastic hinge at the ultimate state and the distribution of micro-cracks in web excluding the area $0.5d$ apart from the loading point and supports. At this point, the most important assumptions to construct damage zone is 1) the definition of physical characteristics of the splitting crack zone and 2) the inclination of splitting cracks.

First, here is the assumption for the inclination of splitting cracks. In RC shear beams with stirrups, the truss analogy gives the inclination of compressive struts 45°. In a strict sense, this value is not correct. However the stirrups in the RC structures are arranged to control the crack width between the concrete struts and the yielding of the stirrups governs the structural failure. In other words, the damaged zone in RC structures that is controlled by steel reinforcement shows much more homogeneous and is easily applied to elastic mechanics. However the damaged zone of UHPFRC shear beams without stirrups caused by fiber reinforcement should take into account of the UHPFRC inherent heterogeneity. The splitting cracks are assumed to have a constant inclination and extend its area called as damaged zone with the inclination towards the support from the loading point. The inclination of the splitting cracks has to be a mean value in the damaged zone rather than the inclination of the initial crack.

In terms of the inclination angle of splitting cracks θ_R, Kupfer and Moosecker (1979) have pointed out that the angle could be up to $5°$ flatter, due to a reduced modulus of elasticity caused by micro-cracking. In other words, θ_R is given by material characteristics with inelastic tensile behavior. Considering the outstanding tensile hardening behavior of UHPFRC, it could be assumed that 1) the inclination angle of the principal stress θ_p decrease till failure and 2) inclination of cracks θ_R are assumed to be $40°$ as a constant and then the area of inclined cracks is widened till failure.

Secondly, the basic assumptions of splitting crack zone for UHPFRC material have to be established. The 'R' of the inclination of splitting crack θ_R stands for Rankine zone. Rankin zone in Fig. 5-5 is the simplest conceivable failure zone for a Coulomb material.

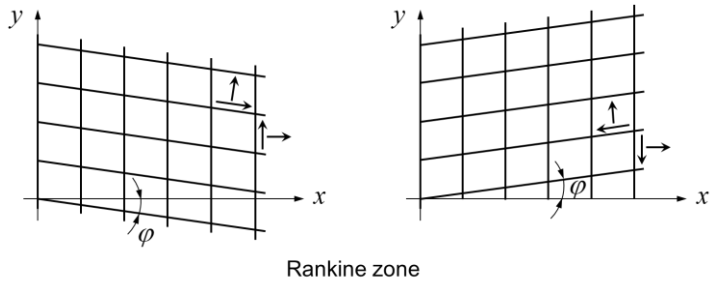

Fig. 5-5. Failure lines in a Rankine zone (Nielsen and Hoang, 2011)

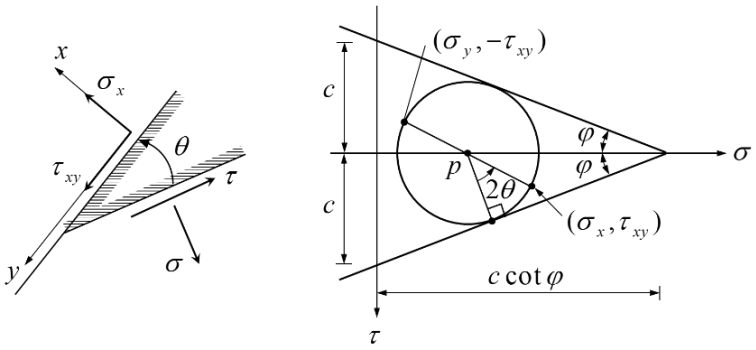

Fig. 5-6. Stress in arbitrary sections determined by Mohr's circle (Nielsen and Hoang, 2011)

A positive direction of rotation, an orientation of the plane, normally counterclockwise, is introduced. In a section, the normal stress σ is assumed positive as a tensile stress, and the shear stress τ is assumed positive when a tensile stress and shear stress, in this order, describe the positive direction of rotation of the plane. Introducing the angle θ between the failure section with positive shear stress and the section with the stresses σ_x, τ_{xy} (Fig. 5-6). The stresses are found by Eq. (5-1).

$$\sigma_x = \sigma$$

$$\sigma_y = \left(1 + 2\tan^2\varphi\right)\sigma - 2c\tan\varphi \tag{5-1}$$

$$\tau_{xy} = \pm\left(c - \sigma\tan\varphi\right)$$

where the upper sign applies to the conditions in Fig. 5-5 to the left, and the lower sign applies to the conditions to the right.

Assuming a weightless material, we have from the equilibrium equations,

$$\begin{gathered}\frac{\partial\sigma}{\partial x} \pm \frac{\partial\left(c - \sigma\tan\varphi\right)}{\partial y} = 0 \\ \frac{\partial\left[\left(1 + 2\tan^2\varphi\right)\sigma - 2c\tan\varphi\right]}{\partial y} \pm \frac{\partial\left(c - \sigma\tan\varphi\right)}{\partial x} = 0\end{gathered} \tag{5-2}$$

Determining $\partial\sigma/\partial x$ and $\partial\sigma/\partial y$ from these equations, we have Eq. (5-3) and (5-4).

$$\frac{\partial\sigma}{\partial x} = \frac{\partial\sigma}{\partial y} = 0 \tag{5-3}$$

$$\sigma = \text{constant} \tag{5-4}$$

The filed is called a Rankine field or a Rankine zone (Nielsen and Hoang, 2011). There is a homogeneous strain field in a Rankine zone for rigid-plastic material. This can be applied where the deformation described is assumed to take place in triangular areas. The change of angle γ means the reduction of the obtuse angle $90^\circ + \varphi$ between the failure sections. The deformation is seen to correspond to a Rankine field. The failure lines of the Rankine field and the sign of the shear stresses are shown in the figure.

5.2.2 Limit Analysis Solution in Rankine Zone

Based on the assumptions of inclination of splitting cracks and a Rankine zone as the homogenous strain field of splitting crack zone, the lower bound solution and upper bound solution are drove, and the governing equation is determined and discussed.

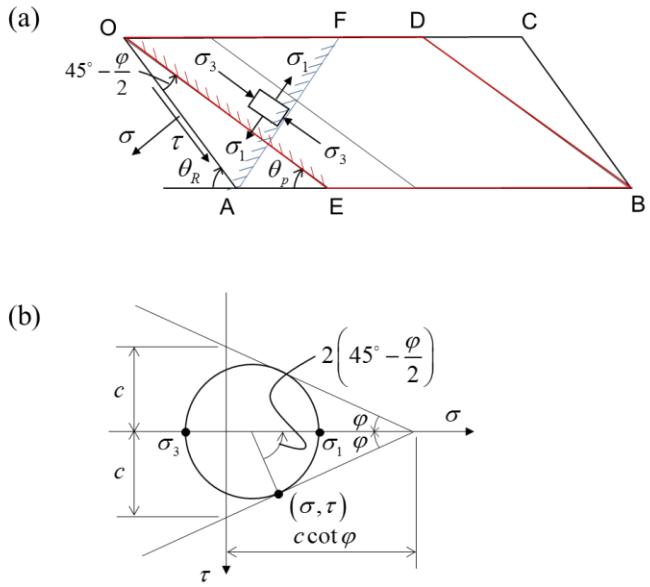

Fig. 5-7. Rankine stress field: (a) Failure line in a Rankine zone, (b) Mohr's circle in a Coulomb material

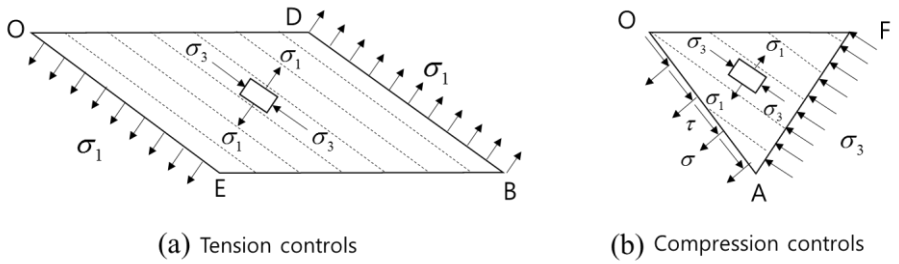

Fig. 5-8. Alternative failure mode according to the internal forces

A uniform stress field in web and material failure criteria for lower bound approach are illustrated in Fig. 5-7. The splitting crack zone of the rectangular OABC is regarded as a Rankine zone. Uniform stresses σ, τ on the failure line OA increase enlarging the diameter of the Mohr's circle and encounter a certain point on the Coulomb failure line at the ultimate state. The ultimate state determined by the given Coulomb criterion can be represented as biaxial stress field with the principal stress σ_1 and σ_3. Fig. 5-8 shows the alternative cases controlled by either σ_1 or σ_3. In principal, the lower bound solution is governed by the maximum strength between Eq. (5-5) and Eq. (5-6).

$$V_u = \sigma_1 \cot\theta \cdot b_w d \tag{5-5}$$

$$V_u = \sigma_3 \tan\theta \cdot b_w d \tag{5-6}$$

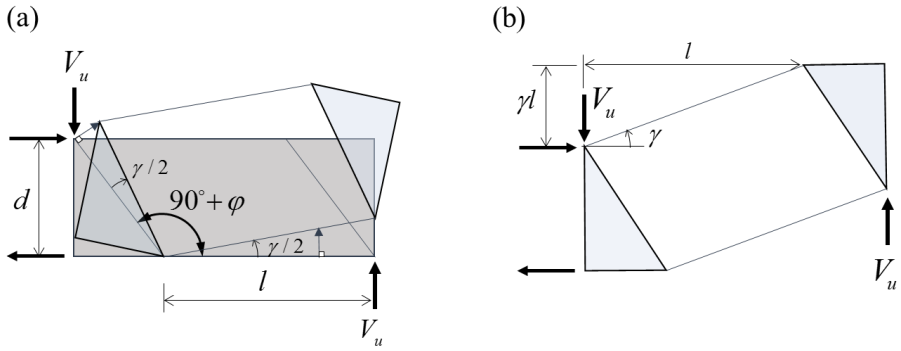

Fig. 5-9. Homogeneous strain field in a Rankine zone

Upper bound solution needs the kinematic condition assumed by an appropriate failure mechanism. Fig. 5-9 is a typical homogeneous strain field of a Rankine zone. Referring the strain field to a rectangular n, t-coordinate system where *t*-axis is identical with one of the failure sections, we have the conditions shown in Fig. 5-10. The change in volume per unit volume $\gamma tan\varphi$ take place, where γ is the numerical value of the change of angle between

line elements in the n- and t-directions. As shown in Fig. 5-10, γ also means the reduction of the angle between the lines of splitting crack zone with inclination of θ_R.

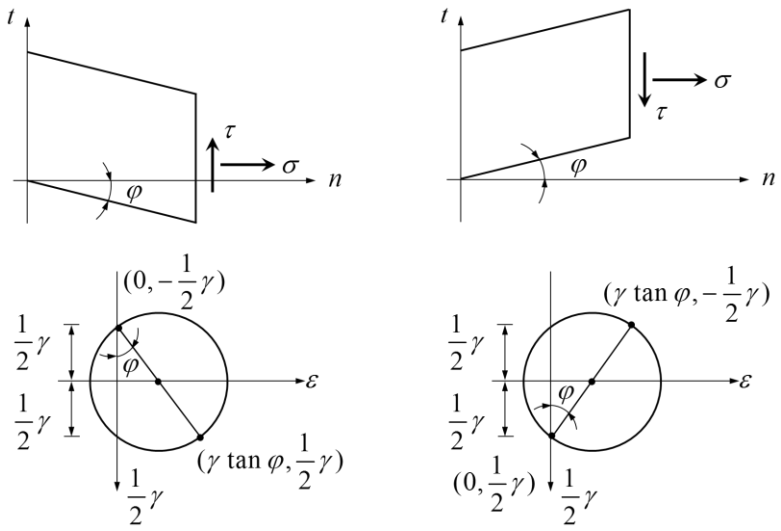

Fig. 5-10. Strains referred to a coordinate system with one coordinate plane parallel to a failure section (Nielsen and Hoang, 2011)

The dissipation in a Rankine field is determined by Eq. (5-7). The dissipation W per unit volume has to be considered by the size of the Rankine zone. Assuming that l is a determinate value when the splitting crack zone spreads to the support homogeneously, l can be regarded as $a - d \cdot cot\left(90^\circ - \varphi\right)$ in Fig. 5-9. Then the ultimate shear strength of Eq. (5-10) is driven by the energy conservation law.

$$W_{d,unit\ voulme} = c\cot\varphi\left(\varepsilon_1 + \varepsilon_3\right) = c\gamma \tag{5-7}$$

$$W_d = c\gamma b_w d\left(a - d\cot\left(90^\circ - \varphi\right)\right) \tag{5-8}$$

$$W_{ext} = V_u\gamma\left(a - d\cot\left(90^\circ - \varphi\right)\right) \tag{5-9}$$

$$V_u = cb_w d = \frac{1}{2} f_c \frac{\cos\varphi}{1+\sin\varphi} b_w d \tag{5-10}$$

To determine the governing equation, several assumptions have to be reminded first. The ultimate strength controlled by UHPFRC compressive strength, such as Eq. (5-6) turns up being overestimated compared to the test results. The reason can be analyzed by several points of view as below.

1) The damaged zone of splitting crack field is homogeneous but anisotropic, so the assumption of Rankine zone could be modified. The splitting cracks are assumed to be arises in the direction of θ_R, which means that the damage zone deforms differently regarding to the perpendicular and parallel to the inclination of splitting cracks. The damage zone is close to be orthotropic, so it would be proper that the stress field is analyzed independently according to the axis rather than a homogeneous strain field.

2) The material compressive strength of UHPFRC is not dependent on the fiber volume content, and the fiber reinforcement only relieves the brittleness near the peak point and in the softening curve. Although the reduction factor evaluated by the test results in this dissertation is applied, the effective compressive strength does not govern the structural failure in this case. Experimental results indicate that the controlling failure in web of UHPFR shear beams is the diagonal tension failure. The assumptions for microcracking behavior does not match the final failure mode, and there are difficulties that the strength depending on the compressive strength is applicable to diagonal tension failure.

Therefore, Eq. (5-5) in a tension controlled failure is adopted as the governing equation as a result of limit analysis theory. The tension strength σ_1

can be replaced by the effective tensile strength.

The lower bound approach with respect to a tension controlled failure is regarded as tension field applied by a variable angle truss model. A variable-angle truss model plasticity has been developed on the basis of the lower bound theory of plasticity (Thürlimann 1979; Nielsen 1984) and is incorporated into the current Eurocode 2 (CEN 2005). The analytical model gives that the designer can choose $cot\theta$ between 1.0 and 2.5, which corresponds to 21.8° $\leq\theta\leq$ 45° where θ is the inclination of struts.

Several assumptions for shear strength model in this paper are made based on the test results. First, the top and bottom chord of a beam is strong enough so that the shear failure in web of the I-shaped beam is only focused. The longitudinal reinforcement does not yield before the beam fails. Secondly, steel fibers are distributed well, so fiber orientation factor is not considered and the average strength and strain concept is applicable, which is similar to smeared crack model. In addition, micro splitting crack spreads in the region after crack initiation starts in the web resulting in a uniform stress field, damaged zone, till crack localization occurs limited by the ultimate strain as an average value of the damaged zone. The damaged zone is defined by the characteristic length of structure as a parameter of stress redistribution capacity. The uniform stress field is postulated as Rankine stress field in Fig. 5-7 (a). Mohr's circle for a stress field causing failure in a Coulomb material is shown in Fig. 5-7 (b). The failure sections, in which the shear stress and the normal stress satisfy the Coulomb failure criterion, form an angle $90^{\circ}-\varphi$ with each other, where φ is the angle of friction (Nielsen, 1999). The inclination angle of the concrete tension tie is defined as $\theta_p=\theta_R-\left(45^{\circ}-\varphi/2\right)$, where φ is the angle of friction. The angle of friction φ and the splitting angle θ_R is considered as 55° and 40° from the previous research and the test results. As a result, the shear capacity V_u from the equilibrium is $\sigma_1 b_w d\,cot\theta_p$, where 22.5° $\leq\theta\leq$ 40°. which is lower bound solution of the theory of plasticity like variable truss model.

The minimum value of principle angle is important for shear design, so it should be verified with experimental results. θ_R can be assumed as the conservative shear capacity relying on the shear transfer capacity of UHPFRC material for safe design for shear. For UHPFRC with tensile hardening behavior, the ratio of tensile strength to compressive strength is about 0.065 conservatively. Applying the reduction factor for cracked compressive strength as 0.7, the equilibrium condition on an imaginary discrete crack face gives θ_p to 5°. With respect to shear transfer capacity limited by ultimate crack width, the displacement ratio defined by the dilatancy model gives the minimum value of $cot\theta_p$=2.45, where w reaches w_u. From the theoretical and experimental analysis, it can be concluded that $1.2 \leq cot\theta_p \leq 2.5°$, which is close to the range of shear design for RC beam with stirrup.

The push-off specimens with transverse reinforcement in the program were tested for different fiber volume ratio and different ratio of reinforced rebar along the shear plane. The shear friction strength for monolithic concrete were suggested by limit analysis of plasticity and verified by test results. It is necessary to define the restricted forces clamping the crack precisely assuming fiber reinforcement contribution. Assuming that fiber reinforcement contribution is the hardening region of tensile strength, normal stress between the crack defines as $\rho f_y + f_t - f_{cr}$. Applying the definition of friction factor, the rate of shear stress to normal stress can be identified as 1.4 and friction angle φ as 55°. The suggested shear friction factor of UHPFRC can be applied to the interface shear design of UHPFRC structural members.

5.2.3 Expanded Failure Mode for UHPFRC Shear Beams

Shear transfer mechanisms in concrete members are more than one and usually developed simultaneously. Traditionally arch action and truss action are considered as representative resistant physical mechanisms depending on the shear reinforcement ratio. Lower bound solution for truss action in Fig. 5-11 (b) assumes that uniformly aligned compressive struts with the inclination of θ. The stress fields is called diagonal compression field. This stress field can be considered as an idealized model for a cracked web, the cracks being parallel to the second principal direction. When the tensile and compression stringers to be strong enough, the best lower bound solution is the largest load satisfying the requirements. It may be shown that θ for the strut with maximum load-carrying capacity is always less than 45°. Additional load-carrying capacity may be obtained by changing the angle θ and letting it approach 45°. This is so because the maximum load-carrying capacity is obtained when $\sigma_c = f_c$ and θ =45°.

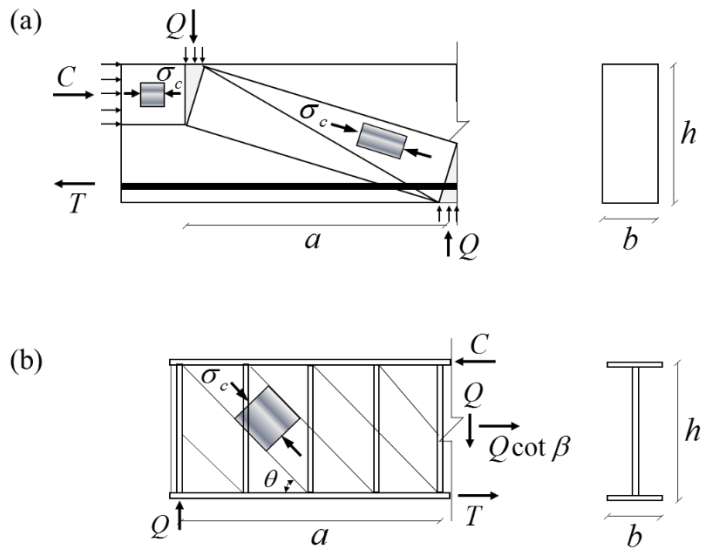

Fig. 5-11. Beam loaded in shear by concentrated forces; (a) arch action for a beam without stirrups, (b) truss action for a beam with stirrups

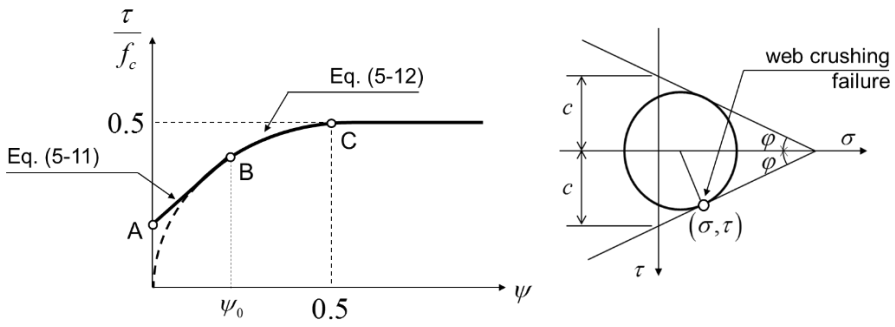

Fig. 5-12. Maximum shear strength versus shear reinforcement degree.

$$\frac{\tau}{f_c} = \frac{1}{2}\left[\sqrt{1+\left(\frac{a}{h}\right)^2} - \frac{a}{h}\right] + \psi\frac{a}{h} \tag{5-11}$$

$$\frac{\tau}{f_c} = \sqrt{\psi(1-\psi)} \tag{5-12}$$

$$\psi_0 = \frac{1}{2}\left(1 - \frac{1}{\sqrt{1+(h/a)^2}}\right) \tag{5-13}$$

If $\sigma_c = f_c$, the web crushing criterion, and shear reinforcement steel yields, Eq. (5-12) can be gotten and expressed by dotted line in Fig. 5-12. The maximum value of τ / f_c is 0.5 for ψ =0.5, when τ is the average shear stress in web and c is the shear reinforcement degree expressed as $A_s f_y / A_c f_c$. Meanwhile the shear stress carried by the strut can be calculated by Eq. (5-11). The line AB in Fig. 5-12 can be represented by Eq. (5-11) and the line BC can be expressed by Eq. (5-12). Point A in Fig. 5-12 indicates a pure arch action with a single strut as shown in Fig. 5-11 (a) and can be represented Eq. (5-11) with ψ =0. The line BC indicates the truss action and the combination of arch and truss action can be expressed by Eq. (5-11). From the given equations, the cross point B which divides arch & truss action and pure truss action is defined by Eq. (5-13).

The UHPFRC shear behavior can be compared to the shear behavior of lightly shear reinforced RC beams. The analytical investigation for direct shear test on Chapter 4.3.2 shows that the tensile strength of UHPFRC can be represented by fiber reinforcement action and this value is great enough to compare with reinforced rebars. If the assumption for reinforcement degree of fiber reinforcement is available for shear beams, the shear reinforcement degree ψ is defined by $\left(f_t - f_{t,el}\right) / f_c$. To apply the typical material properties of UHPFRC which has f_t =11 MPa and f_c =160 MPa, ψ is 0.03125. Based on Eq. (5-13), arch & truss action governs the shear behavior when a/d <2.7, and truss action occurs only when $a/d \geq 2.7$. The specific value can be different, but it still around 2.5 for UHPFRC with tensile hardening behavior.

As a lightly shear reinforced beams, UHPFRC shear beams with $a/d \geq$ 2.7 in this dissertation shows truss action and the assumption for microcracking behavior as Rankine zone is available. On the other hand, the UHPFRC shear beams with a/d <2.7 can shows combined behavior of arch action and truss action and the maximum shear strength can be greater than the suggested equation assuming the truss action only. To investigate arch action of UHPFRC shear beams, the compressive strut has to be analyzed with respect to the different physical mechanism, not Rankine zone. In case of the strut action, the reduction factor 0.7 can be applied. Furthermore, the detailed effectiveness factor for compressive strength according to the tensile strain on the orthogonal direction should be investigated.

5.3 Fracture Mechanics Approach for UHPFRC Shear Design

5.3.1 Application of CDZ model for Semi-Brittle Fracture

Most researches on fracture mechanics for RC structures have been limited to stability problem after peak point which arises with crack localization when cracking behavior of concrete governs the ultimate state of the structures, such as, shear beams without stirrups and lightly reinforced flexural beams. Likewise, the evaluation of UHPFRC member strength with crack localization may require fracture mechanics approach to provide a rational design guidelines for structural concrete made of UHPFRC.

The shear strength of a UHPFRC structure is controlled by material tensile strength which has a great standard deviation due to fiber distribution. The tensile strength should be determined conservatively as a design parameter considering inherent heterogeneity. Fiber orientation factor in the form of reduction factor applies to the characteristic strength. Previous studies deal with the tensile strength corresponding to the fiber distribution assuming the cement matrix and fiber separately in a meso-mechanism. They tried to overcome the gap between the summation of single fiber behavior and the realistic fiber contribution in a structure using probability theory and empirical approaches. Whereas fracture mechanics gives the conversion factor with physical meaning in a structural scale.

The cause of the size effect is the localization of the compression failure of the strut into a fracture band of a fixed width and the growth of this band across the strut. Fracturing truss model (Bazant, 1997) gives the shear strength equation using critical crack width w_{cr} with similar concept (Fig. 5-13). Basically the axial splitting micro-cracking dissipates the energy in stress relief

zone. Many parallel cracks form in the stress redistribution zone, only one of them may open widely while the others unload and close. The equilibrium condition for energy release rate within the crack band and the compatibility condition for tensile strain.

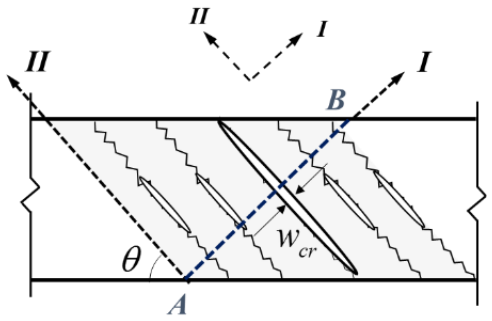

Fig. 5-13. Crack localization in fracturing truss model (Bazant, 1997)

The cause of the size effect is the localization of the compression failure of the strut into a fracture band of a fixed width and the growth of this band across the strut. Fracturing truss model (Bazant, 1997) gives the shear strength equation using critical crack width w_{cr} with similar concept (Fig. 5-13). Basically the axial splitting micro-cracking dissipates the energy in stress relief zone. Many parallel cracks form in the stress redistribution zone, only one of them may open widely while the others unload and close. The equilibrium condition for energy release rate within the crack band and the compatibility condition for tensile strain.

The general assumptions to determine the characteristic length in microcracking zone in web of UHPFRC I-shaped beams without stirrups are modified from the assumptions for fracturing truss model and CDZ model.

1) In a microcracking stage, highly orthtropic panel with tensile cracks of crack band can be assumed. The orthotropic panel is a stress

redistribution zone which is same geometry of the Rankine zone. The inclination of the tensile cracks is assumed to be 40°.

2) Size effect occurs in the orthotropical damaged zone. The damage zone can be analyzed by CDZ model (Markeset and Hillerborg, 1995). The localized deformation is expressed by fracture mechanics term. The only difference is that the failure, diagonal tension failure, is governed by tensile strength.

3) Fracturing truss model assumes that the brittleness factor is constant as a material properties, but in this dissertation the characteristic length of UHPFRC is assumed to be affected by the constraint effect given by the external forces.

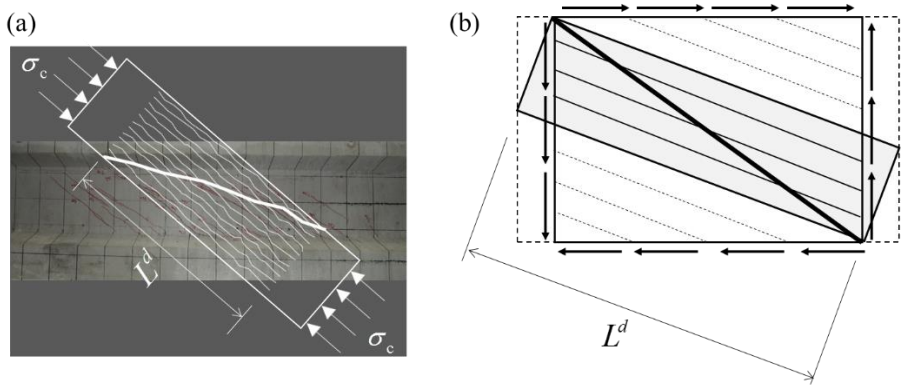

Fig. 5-14. Application of CDZ model for semi-brittle fracture; (a) comparison with test results, (b) idealized stress field and failure mechanism.

One of the conspicuous differences between the fracturing truss model in Fig. 5-13 and the CDZ model in Fig. 5-14 is the geometric assumption for the crack localization. Bazant assumes that the crack localization occurs among the microcracks, but CDZ model considers that the crack localization is defined by the microcracking zone.

The failure mechanism mentioned above concentrates on diagonal tension failure in the uniform stress field, but the idealized stress field and failure mechanism cannot be applied to the limited cases. To expand the suggested model using fracture mechanics approach, CDZ model can be applied. The basic assumptions are similar with respect to the damaged zone composed by initial splitting cracks, but the final failure is different. CDZ model deals with the compressive sliding failure. Despite of the different assumptions, there are several advantages for applying the CDZ model.

1) The damaged zone is defined as a part of compressive strut, so the arch action where the shear span ratio is small can be explained. Arch action is one of the representative physical mechanism for shear beams without stirrups. Rankine zone is isotropic and uniform stress field and the physical mechanism is close to truss action where the shear span ratio is large enough.

2) CDZ model enables to explain the UHPFRC shear failure due to crack localization failure in a microcracked zone using fracture mechanics approach. The length of damaged zone L^d can be regarded that the characteristic length depends on material properties and structural geometry at the same time.

The size of the damaged zone and the critical crack determines the structural characteristics length for UHPFRC shear beams failed in semi-brittle fracture. CDZ model can be applied to compressive failure in case of small shear span ratio directly, but it has to be noticed that the size effect of compressive failure usually governs structural ductility after the peak point, not the peak strength.

5.3.2 Characteristic Length and Size Effect in UHPFRC Structural Design

The post cracking behavior of UHPFRC including micro-cracking and crack localization can be explained by fictitious crack model (Hillerborg, 1992). The specific fracture energy G_f and the characteristic length l_{ch} are two important parameters. G_f is defined as the amount of energy needed to create one unit crack area. Hillerborg and coworkers suggests that l_{ch} is a measure of the brittleness of the concrete. These parameters are basically material properties, which can be determined in a stable displacement controlled in uniaxial tension test. However, the brittleness at material level should be changed to adjusted brittleness factor at structural level for practical design of structural members. In this dissertation, the brittleness factor β_{Rd} for structural design for size effect is suggested as a conversion parameter, which is the ratio of the elastic energy per volume from the inelastic hardening structural behavior and the fracture energy per a surface at failure due to crack localization.

Characteristic length or equivalent length of UHPFRC in current recommendations are ruled to be multiplied by height of the cross section. Characteristic length in AFGC (2013) is given by Eq. (5-14) and equivalent length in JSCE (2008) is given by Eq. (5-15).

$$l_c = \frac{2}{3}h \tag{5-14}$$

$$L_{eq} = 0.8h\left\{1-1/\left(1.05+6h/l_{ch}\right)^4\right\} \tag{5-15}$$

The equivalent length means a conversion factor to tensile strain from the given crack width. It can be interpreted as a physical meaningful parameter of the representative length of stress redistribution due to microcracking. The

equivalent length is governed by the structural size and close to the structural characteristic length suggested in this dissertation.

It is assumed that the damaged zone of UHPFRC consists of series of concrete tension ties, and the failure has to be governed by the longest one as shown in Fig. 5-15. The longest length of damaged zone is defined as the characteristic length of structure, the effective length of concrete tension tie in this research. A structural characteristic length L at structural level is then defined as $L = a\sin\theta - d\cos\theta$. Following the given assumption, the control parameter is shear span ratio, and the effective length is governed by effective depth when shear span ratio is greater than the specific value. The intersection value is calculated to 2.85 where the principal angle of damaged zone is 22.5° based on limit analysis. The a/d should be greater than 2.85.

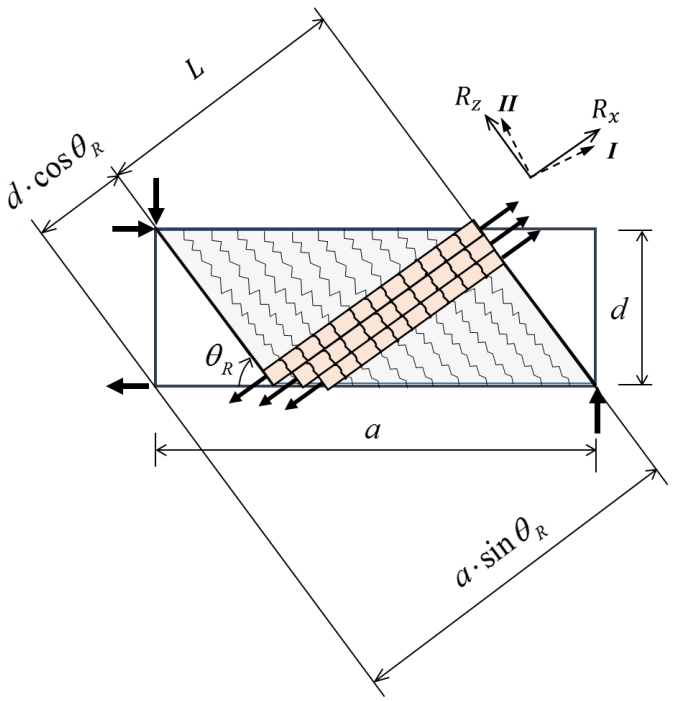

Fig. 5-15. Characteristic length of concrete tension tie

$$l_{ch} = 2g_{f,A} / G_{f,B} \times k \tag{5-16}$$

$$k = 1 + 3\frac{\sigma_{cp} \sin\theta_p}{f_t} \tag{5-17}$$

$$L = a \cdot \sin\theta - d \cdot \cos\theta \tag{5-18}$$

l_{ch} is the material characteristic length which can be increased by the axial constraint. k is the modified by the prestressing effect in AFGC recommendation. The structural characteristics length L is determined by the inclination angle of stress field, in addition of the effective depth which is the characteristic length of ordinary reinforced concrete. The damaged zone can be assumed as series of tension struts, and the failure has to be governed by the longest one. The longest length of damaged zone is defined as characteristic length of structure in this research. L can be a design parameter for semi-brittle failure in UHPFRC structures taking into account the inelastic behavior at structural level of splitting cracked zone.

According to fracture mechanics, the width of the major cracks at failure is approximately proportional to the beam depth, so the failure due to crack localization is strongly affected by size effect, so the strength equation is started from the Eq. (3-21) where v_p is the shear strength calculated by plastic analysis.

The brittleness number of a structure can be defined as L / l_{ch} and the definition can be generally accepted and has been known to be inversely proportional to the strength (Bazant and Planas, 1998). Gustafsson and Hillerborg (1988) suggested that the normalized shear strength f_v / f_t of geometrically similar beams is governed by the dimensionless ratio between absolute structure size d and the characteristic length l_{ch} at material level. This is important ratio d / l_{ch} may be regarded as a measure of the brittleness

of structures sensitive to tensile stress-induced fracture, a higher value of the ratio corresponding to a more brittle structure. Shear strength was suggested by $f_v / f_t = k\left(d / l_{ch}\right)^{-0.25}$ where k is dependent on shear span ratio and percentage of longitudinal reinforcement. Flexural deformation affects the critical crack width in web of shear beam and longitudinal reinforcement ratio has to be design parameter for shear beam without stirrup. König et al. (1993) suggested that the shear strength of RC beam without stirrup is $v_u = Cf_t \sqrt[3]{l_{ch}\rho_l / d}$.

An equation for the shear strength of UHPFRC I-beam without stirrup can be proposed by combining the lower bound approach form the limit analysis and the newly defined brittleness factor based on fracture mechanics approach at structural level. The shear strength is proportional to the brittleness factor β_{Rd} , the shear strength is then suggested as Eq. (5-19).

$$V_u = f_t \cot\theta \cdot b_w d \times \beta_{Rd} \tag{5-19}$$

$$\beta_{Rd} = \frac{1}{\sqrt{1 + l_{ch} / L}} \tag{5-20}$$

The size effect on diagonal crack failure of UHPFRC of I-beam complies with Eq. (3-21) of Bazant's rule. Therefore, the brittleness factor β_{Rd} in Eq. (5-20) involves the size effect and confinement effect to restrain the microcracking behavior.

5.4 Additional Considerations

Previous studies indicates that prestressed UHPFRC shear beams resisted with stable strength increase. Shear contribution of axial forces can be defined as various type of formulation in RC structure recommendation. ACI recommendation regulates the prestressing term separately, and *fib* model code considers the inclination of compressive struts influenced by prestressing forces. AFGC recommendation defines that the prestressing effect term is an amplifying parameter which is subordinate to the tensile strength. In this dissertation, the characteristic length of UHPFRC can be assumed to be affected by the constraint effect given by the external forces. The characteristic length of UHPFRC is assumed to be affected by the constraint effect given by the external forces such as prestressing effect.

Longitudinal reinforcement ratio is used to be important parameter to influence the constraint effect in RC beams of a rectangular cross section without stirrups. However it turns out that the longitudinal reinforcement ratio hardly influences the shear strength of UHPFRC I-shaped beams without stirrups. The fact can be related to that the flexural behavior is also governed by the tensile strength of UHPFRC as well as the yield strength of the longitudinal reinforcement. The influence of the reinforcement ratio is much less than that in RC beams, and the influence of the shape of cross section can be relatively greater.

It is important that the design of prestressing or stirrups in UHPFRC shear beams enhance the shear strength as well as the structural ductility with much less deviation of the peak strength. The heterogeneity due to fiber orientation is struggling issues for UHPFRC shear beams without stirrups because this characteristics gives unexpected shear capacity due to crack localization at

failure. This is why size effect should be considered to design UHPFRC shear beams without stirrups. Therefore, the design of prestressing or stirrups in UHPFRC shear beams can be encouraged with respect to the stable and ductile structural behavior.

The design of shear reinforcement for UHPFRC shear beams has to be investigated with different point of view for RC beams. For instance, the minimum spacing of shear reinforcement for UHPFRC members could be much larger than RC beams, $d/2$. The half of the effective depth can be derived from the assumption of the inclination of 45° compressive strut caused by the initial crack. However, UHPFRC has own stress redistribution ability and the inclination of splitting cracks can be assumed as 40°. Previous test results show that the structural behavior is improved with a ductile manner, but the strength increase is less dependent to the shear reinforcement ratio compared to RC shear beams. It can be explained by the failure mode due to crack localization in UHPFRC shear beams. The bond stress between cement matrix and fiber reinforcement also applies the bond stress between UHPFRC and reinforced rebar even stronger due to large diameter of reinforcement, which means that the failure of UHPFRC members is caused by crack localization inevitably. Although the width of the critical crack is controlled by steel reinforcement for UHPFRC shear beams with stirrups, the tensile strength can be still important.

Chapter 6. Verification of Shear Strength Predictions

6.1 Shear Test on UHPFRC I-shaped beams without Stirrups

Nine I-shaped beam specimens were tested to find out in-plane shear behavior of UHPFRC without conventional reinforcement. The key parameters are shear span-to-depth ratio and effective depth of the specimen to investigate the shear capacity of UHPFRC according to stress field given by geometry. In addition, three types of mix composition with different steel fiber content is additional parameter. The thickness of the web is 40 mm which is much thinner than compression and tension chord to find out in-plane shear behavior in web as uniformly as possible. Specimen S35 and S35-B has same shear span-to-depth ratio, however different effective depth as shown in Fig. 6-1.

The specimens were loaded with vertical forces applied by a hydraulic jack under displacement control with a nominal capacity of 2000 kN. The measurement program is based on the assumptions of uniform stress states and smeared crack concept in the measuring region. In addition to the displacement at the loading point, two types of measurement are installed to investigate the principal strain in the stress field of the web. The dotted lines in Fig. 6-1 shows the location of LVDT, which is about $1.5\,d$ far from the loading point, on one side of the specimens and the shaded rectangles in the opposites indicate the location of the gauges. The principal strain can be calculated using Mohr's circle.

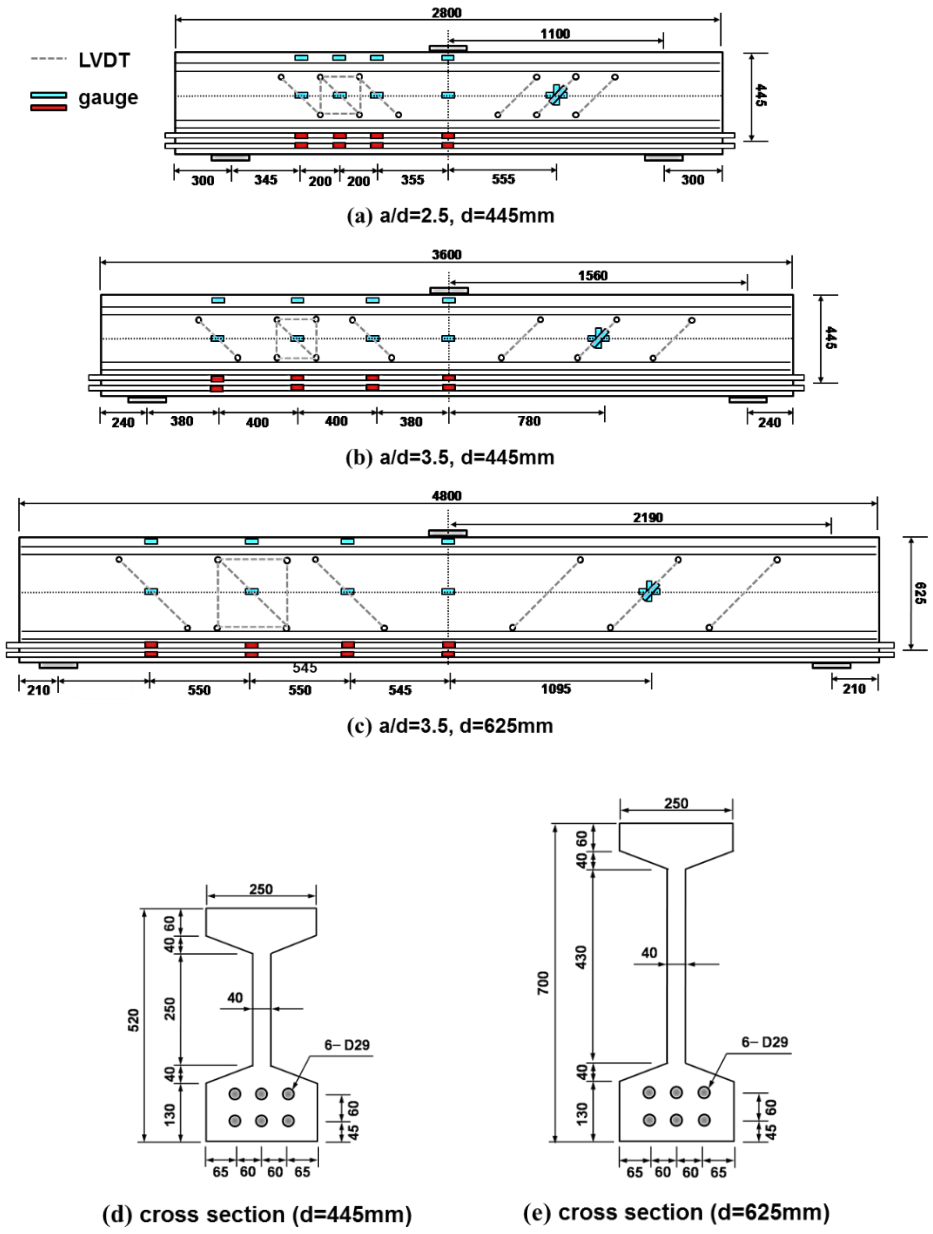

Fig. 6-1. Loading configuration, Measurement plan and Specimen dimension

The load-displacement relationship and the crack patterns of all specimens are shown in Fig. 6-2 ~ Fig. 6-9. The initial crack of S25 and S35 is observed in the middle of the web and the inclination of the crack is 45°. The initial crack of S35-B is observed in the bottom of the web with several flexural cracks. The cracking strength is hardly found out in the load-displacement curves like its material tensile strength tests, but the stiffness after the crack initiation is slightly weakened, but keeps its stiffness constantly till critical crack localization occurs.

Local cracks were observed in the abdomen of all specimens, and the cracks in which the cracks occurred were defined as the main cracks. Fig. The vertical dotted lines in the figures are noted at the spacing of $0.5\,d$ as a reference. The distribution of diagonal cracks in the abdomen is distributed over the range from to when the shear span ratio is 2.5, and the position of the initial cracks and the main cracks are not the same. The major cracks occurred at arbitrary positions in the micro crack region, and the plastic hinge of the upper flange occurred at a point away from the force portion. After reaching the maximum load, the main crack width did not increase continuously, and the member was completely destroyed due to some collapse of the compressive strut which occurred in parallel with the main crack. Also, the range of crack distribution, the number of micro cracks, and the main crack angle were smaller than those of the shear span ratio of 3.5.

In the case of the shear span ratio of 3.5 and the effective height of 445 mm, when the width of the main crack reaches the maximum load and the plastic hinge of the upper flange is largely broken, the main crack width becomes larger than 2 mm. The diagonal cracks were distributed from the beginning to the end, and the position of the main crack occurred at any position in the crack distribution region, but the angle was smaller than that when the shear span ratio was 2.5. The major cracks occurred in the diagonal direction of the abdominal damage zone and the main crack angle was smaller than that

of the shear span ratio of 2.5. The plastic hinge of the upper flange occurred at a position distant from the focal point, and at 1-S35 and 2-S35, the fracture occurred at the hinge located in the top flange.

1-S35-B and 3-S35-B of the case where the shear span ratio is 3.5 and the effective height is 625 mm, the final fracture of the upper flange is largely broken after the width of the main crack reaches the maximum load, And a large deformation was observed in the entire beam as several major cracks occurred at the same time as 1-S35-B. The abdomen diagonal cracks were distributed to the flank, and the plastic hinge of the upper flange was closer to the force field than the case where the effective height was 445 mm within the flank. The abdominal area was observed in the shape of a parallelogram from the hysteresis part to the plastic hinge area. After reaching the maximum load, the diagonal crack gradually widened along the lower flange to the fulcrum, but the height decreased in arch shape. 2-S35-B is widely distributed over the abutment part and the fulcrum part of the abdomen damage part, and the bending crack and the sagittal part crack are connected to the main crack and the deformation is transferred to the lower part, As the crack progressed greatly, the vertical deformation expanded at the focal point in addition to the main crack near the force part at the time of reaching the maximum load, and the final fracture occurred at the same time.

The crack propagation of the specimens explains the stress distribution region obviously. The shape of stress field in web depends on shear span ratio, and especially in case of a / d =2.5, the arch effect with direct concrete strut strengthens shear capacity. In case of a / d =3.5, the specimens with effective depth 445 mm shows arch effect slightly, but the specimens with effective depth 625 mm does not show arch effect at all. The judgement to be arch effect or not is according to whether compressive crushing after the peak load occurs in the middle of the span or not.

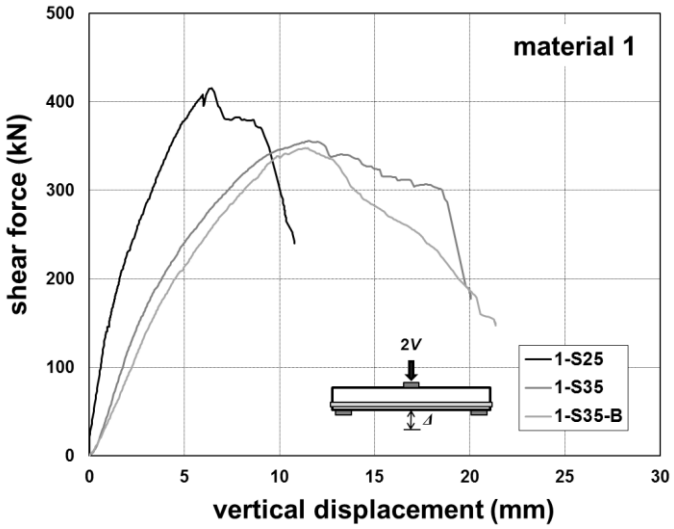

Fig. 6-2. Shear force versus vertical displacement relationship of 1-series specimens

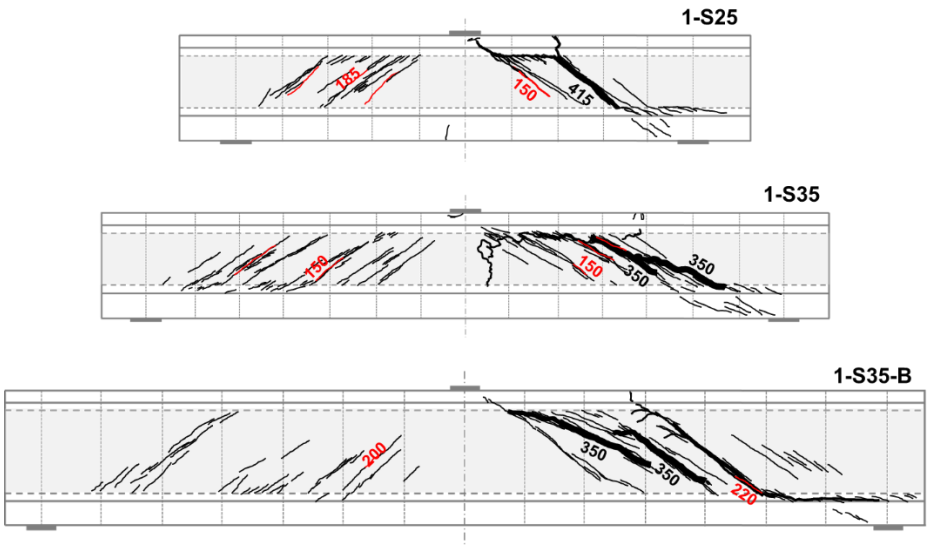

Fig. 6-3. Crack pattern and location of critical shear crack in web of 1-series specimens

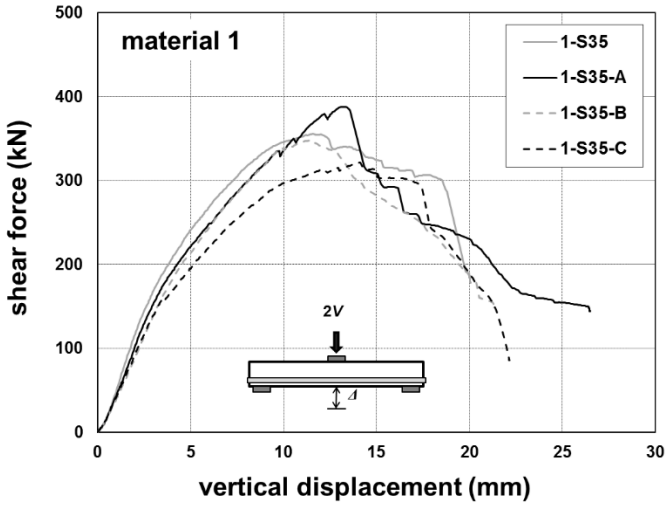

Fig. 6-4. Shear force versus vertical displacement relationship of 1-series specimens regarding to the longitudinal reinforcement ratio

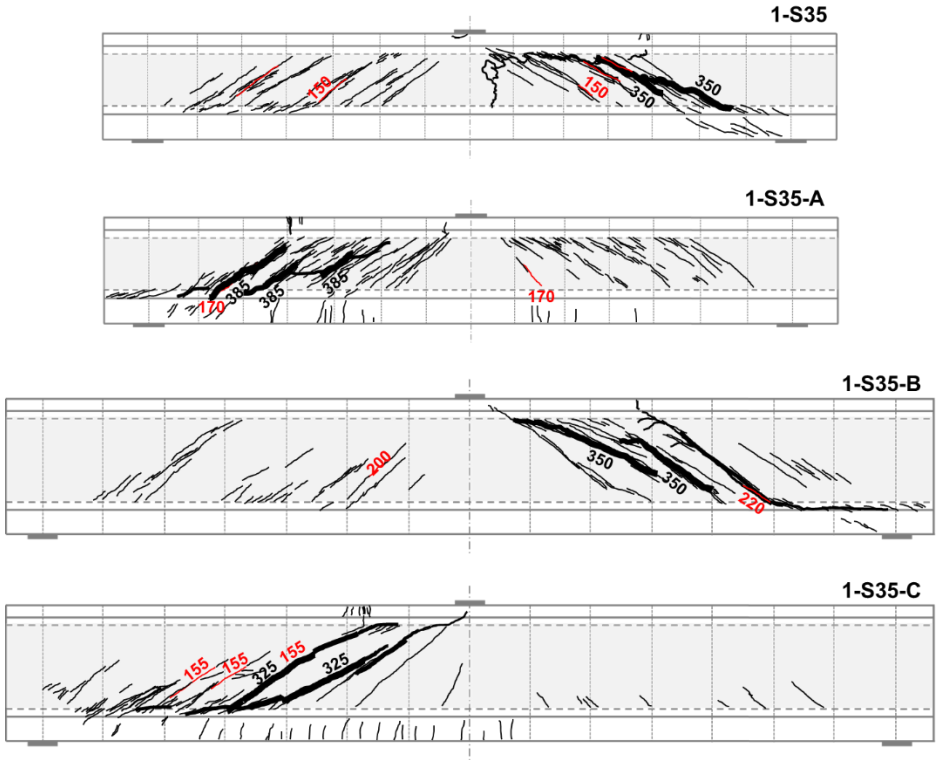

Fig. 6-5. Crack pattern and location of critical shear crack in web of 1-series specimens regarding to the longitudinal reinforcement ratio

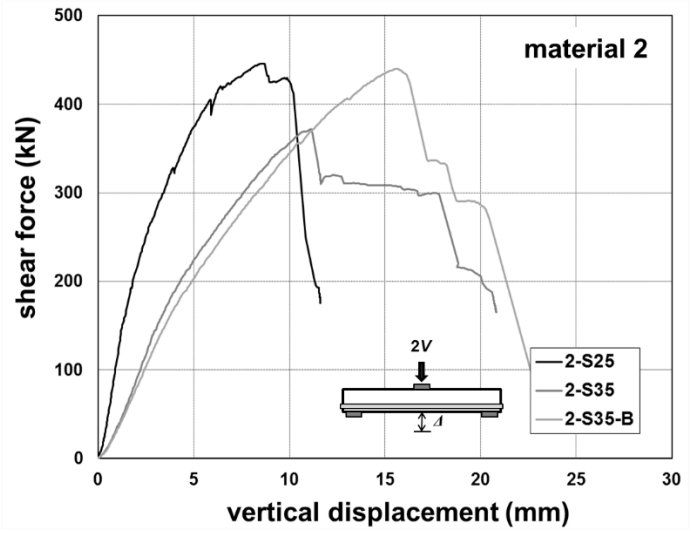

Fig. 6-6. Shear force versus vertical displacement relationship of 1-series specimens of 2-series specimens

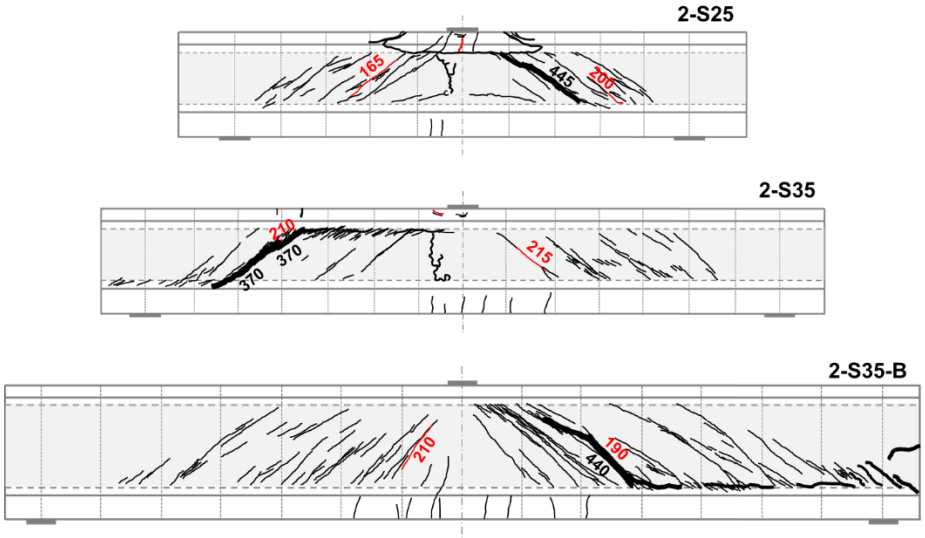

Fig. 6-7. Crack pattern and location of critical shear crack in web of 2-series specimens

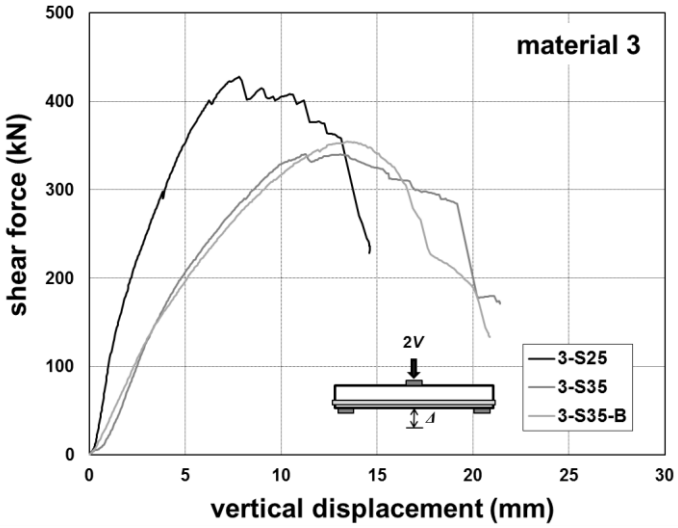

Fig. 6-8. Shear force versus vertical displacement relationship of 1-series specimens of 3-series specimens

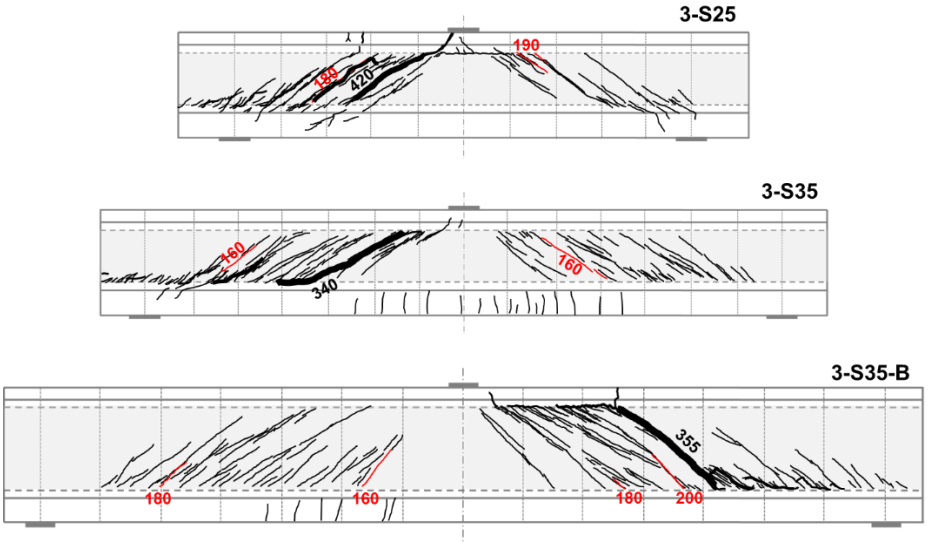

Fig. 6-9. Crack pattern and location of critical shear crack in web of 3-series specimens

The principal stress direction was calculated by Mohr's circle and determined comparing the principal strain direction measured by the LVDT and the triaxial strain gauge in web. In general, it is known that the direction of principal stress is delayed in the principal strain direction. However, the assumption is made that the direction of the principal strain direction is same as the principal stress direction simultaneously. The results measured by LVDT and strain gauges show similar tendency because the microcracks have a small width and therefore the tendency before the main crack can be measured by concrete gauge. S25 and S35 specimens tended to decrease sharply after cracking, whereas S35-B specimens showed a gentle slope even after cracking. At the maximum load, the angle of the S25 specimen was about 25°, which was slightly higher than that of the S35 and S35-B specimens, and the S35 specimen was reduced to about 20° (Fig. 6-10).

The principal direction of stress θ_p can be regarded as the inclination of diagonal line in a parallelogram shape of damaged due to microcracks. For RC members with shear reinforcement, it can be explained that the compressive strut formed in web and the struts rotate. The shear strength of RC members is determined by the ultimate limit state where the compressive struts have its limit value, critical deformation or the maximum strength. Applying this concept to UHPFRC can be explained as follows. The following can be explained as follows: The direction of the stress of the abdomen before crack initiation is constant at 45°. When the crack starts to occur, microcracks are distributed widely in web depending on the capacity of UHPFRC tensile hardening behavior due to fiber reinforcement. In the microcracking stage, the principal stress direction gradually decreases. When the microcracks start to be localized at the deformation limit state, the direction of the principal stress direction in web tends to be kept constant. This can be also explained as a process in which the entire member deformation is transferred to another part such as a flange from the web deformation. Therefore, the maximum strength

due to the critical crack is defined as the ultimate deformation state, and the shear strength is greatly influenced by the material characteristics and the geometric shape of the member.

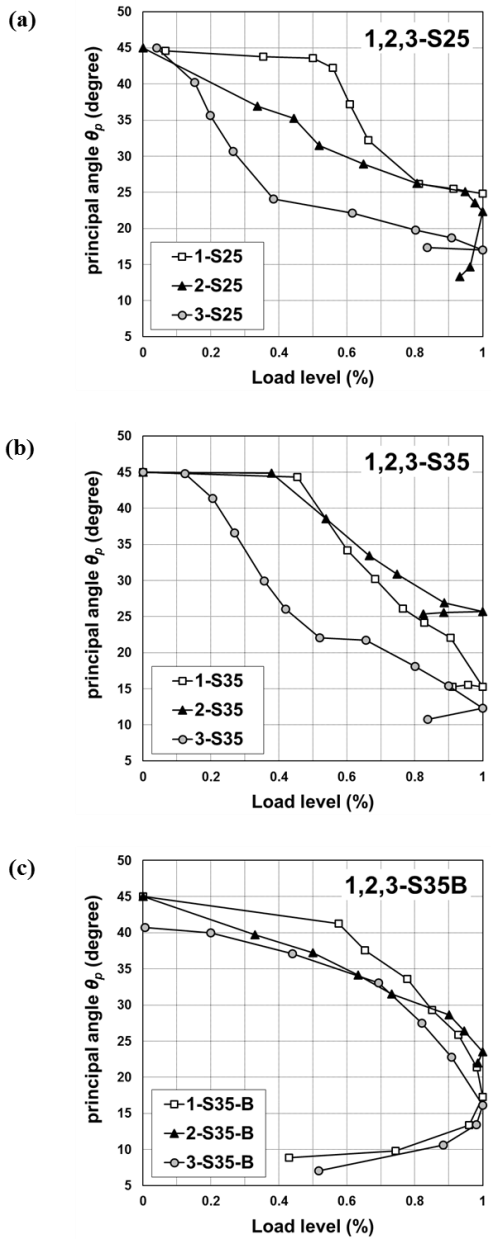

Fig. 6-10. Principal strain of test specimens depending on a / d ratio and effective depth

The number of microcracks started from 45° increases reducing its angle and observed frequently in a wide range of the span. At the peak load, one or several diagonal cracks localize in the damage zone. The distribution of micro-cracks and critical shear cracks are depicted in the figures. The location and the shear strength of the initial crack in web and the maximum shear strength is also denoted. The interaction between stress field given by geometry and stress redistribution region given by UHPFRC post-cracking behavior can be assumed to define the size of equivalent panel with relatively uniformly tension-compression stressed field. The hypothetical panel, shear band, can be regarded as widened concrete strut and the damage panel is assumed to be diagonal tension failure by critical crack localization. In this research, the damage panel is regarded as shear band and the dimension of shear band is deter-mined by the location of plastic hinge at the ultimate state and the distribution of micro-cracks in web excluding the area $0.5d$ apart from the loading point and supports. As a result, the widths of the shear band are approximately $0.5d$ in S25 specimens, $1.5d$ in S35 specimens and 1d in S35-B specimens.

Load-deflection curves with regard to shear span to depth ratio in Fig. 5 shows that the maximum strength and stiffness of the specimens with a/d =2.5 are greater than that of the specimens with a/d =3.5. The specimens of S25-series behaves brittle and the specimens of S35-series shows ductile behavior after the peak load. Load-deflection curves with regard to effective depth in Fig. 6-11 and Fig. 6-12 shows that the maxi-mum strength is almost same and moreover, the behavior with greater depth shows brittle behavior. Most specimens fail to diagonal tension represented as crack localization. After the initial cracking, the stiffness slightly decreases, but still the strength increases stably. Several specimens show flexural shear cracks, but critical crack in localization were extended and connected with diagonal cracks. Exceptionally, the specimen 2-S35-B was failed in anchorage region which

induces higher maxi-mum strength than others. This phenomenon can be occurred when the stress distribution region exceeds the given geometry.

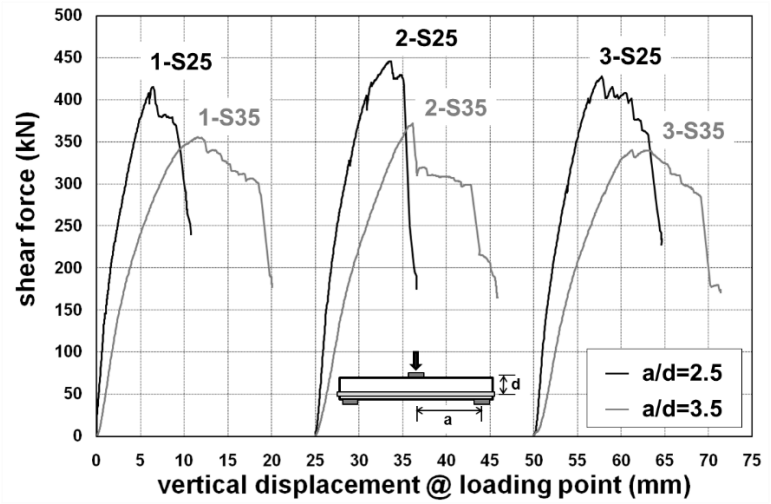

Fig. 6-11. Load-deflection curves with regard to shear span to depth ratio

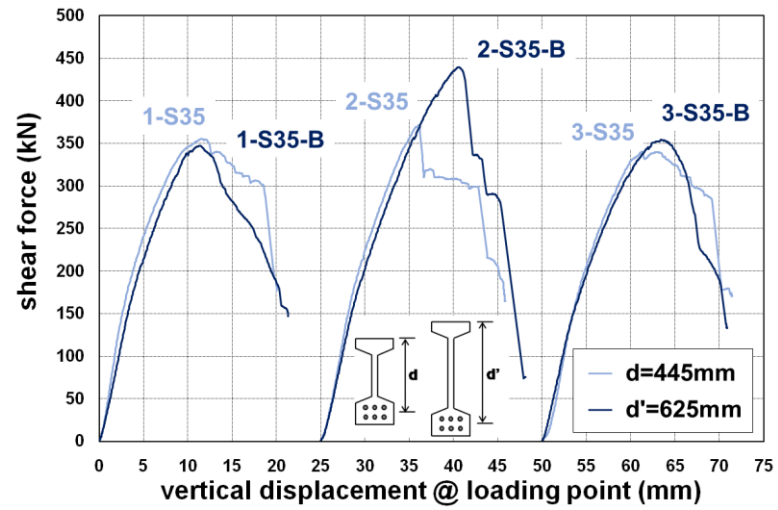

Fig. 6-12. Load-deflection curves with regard to effective depth

6.2 Comparison of Shear Strength

The strength prediction by the proposed equation is compared with those of AFGC recommendation with existing test results. θ is assumed to be differently in each equation. The inclination angle uses the conservative minimum value 25°, in Eq. (5-19), but for the AFGC equation, 40° is applied based on existing researches . The proposed equation can predict the shear strength of UHPFRC shear beam without stirrup more accurately with regard to beam sizes and shear span ratios.

To verify the suggested equation, the data base (JSCE, 2004; Yang et al., 2012; Baby et al., 2014; Randl et al., 2016; Fehling et al., 2016). is collected. The range of design parameters used in the data base are summarized in Table 6-1. The main parameters and test results are presented in Appendix. 1. The verification of proposed shear strength does not included the test results of prestressed UHPFRC shear beams without stirrups.

Table 6-1. Summary of UHPFRC shear beams data base (without stirrups)

Parameter range	44 I-shaped shear beams
Compressive strength f_{cm} (MPa)	147 - 233
Tensile strength f_t (MPa)	6.3 – 17.3
Flexural tensile strength f_r (MPa)	10.4 – 31.5
Volume of steel fiber fraction V_f (%)	0.8 – 4.7
Shear span ratio a / d	2.2 – 6.0
Effective depth d (mm)	170 - 640
Web thickness b_w (mm)	25 - 80
Longitudinal reinforcement ratio ρ_l (%)	4.0 – 24.1

Table 6-2. Comparison of statistical analysis of strength ratio

Strength ratio (V_{test} / V_{pred})	Avg.	Std.	Max.	Min.
AFGC setra recommendation (2013)	1.457	0.457	2.55	0.70
Current study	1.095	0.257	1.70	0.67

Fig. 6-13 shows the correlation between the average shear stress of data base and test variables of effective depth, shear span ratio and longitudinal reinforcement. The test results are collected by the diagonal tension failure in I-shaped beams, and the average shear stress is available to be compared.

The most strong correlation is observed between shear stress and shear span ratio. Comparing the test results in the specimens of shear span of 2.5 and 5, the shear stress of shear span ratio of 2 is almost twice as that of shear span ratio 5. Effective depth has weak correlation, but the data is scattered. However, longitudinal reinforcement hardly affects the shear strength. This results was commented in chapter 5 and the suggested shear strength does not consider the longitudinal reinforcement as a design parameter. The influence of shear span ratio and effective depth are taken into account in a structural characteristic length L which represents the cracking behavior and failure mode.

The collected test results are verified by shear design strength equations. Comparing the current recommendation of AFGC setra, the Eq. (5-19) predicts the shear strength more precisely (Table 6-2).

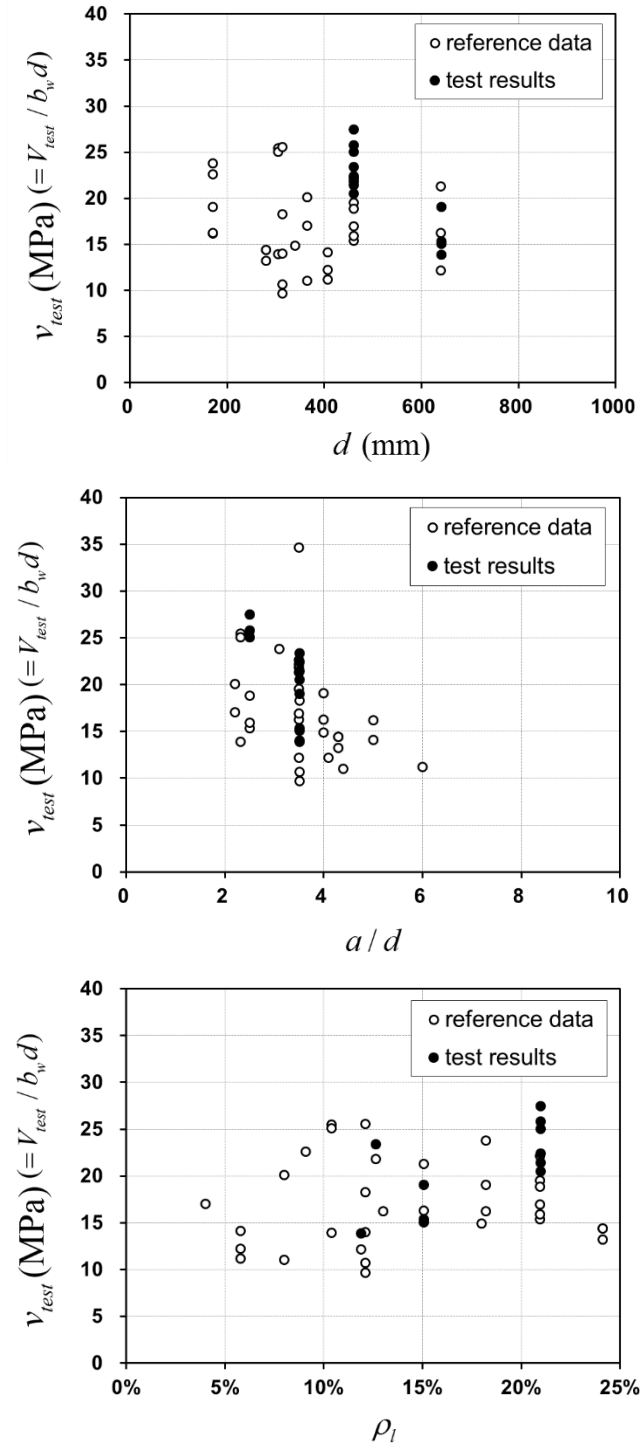

Fig. 6-13. Correlation between average shear stress in web and test variables of effective depth, shear span ratio and longitudinal reinforcement ratio

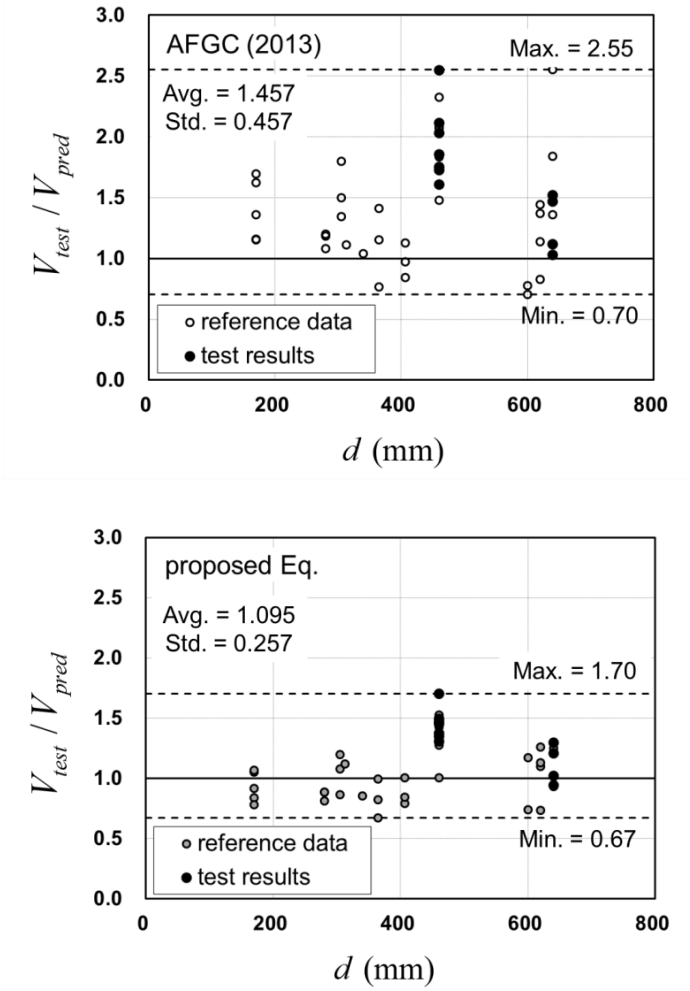

Fig. 6-14. Shear strength predictions for 44 UHPFRC test results without stirrups according to effective depth

Fig. 6-14 shows the shear strength predictions for test results according to effective depth. The AFGC recommendation generally overestimates the shear strength regardless of the size of effective depth, and the suggested equation predicts the strength more precisely.

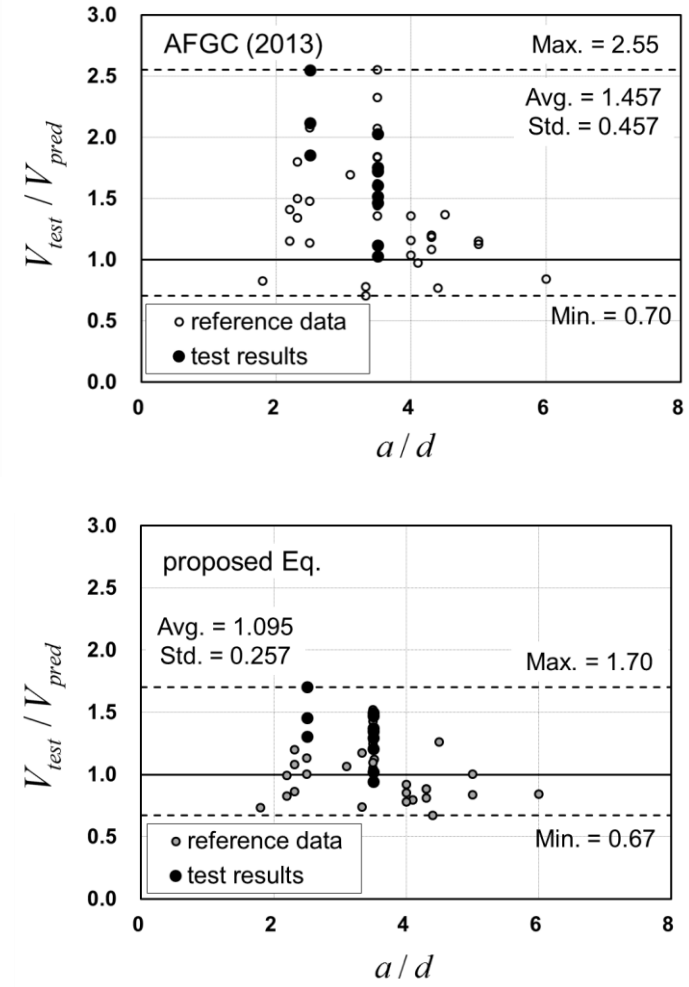

Fig. 6-15 Shear strength predictions for 44 UHPFRC test results without stirrups according to shear span ratio

Fig. 6-15 shows the shear strength predictions for test results according to shear span ratio. Shear span ratio shows clear tendency to shear strength decrease as increase of its value. The proposal in current study loosen the tendency effectively.

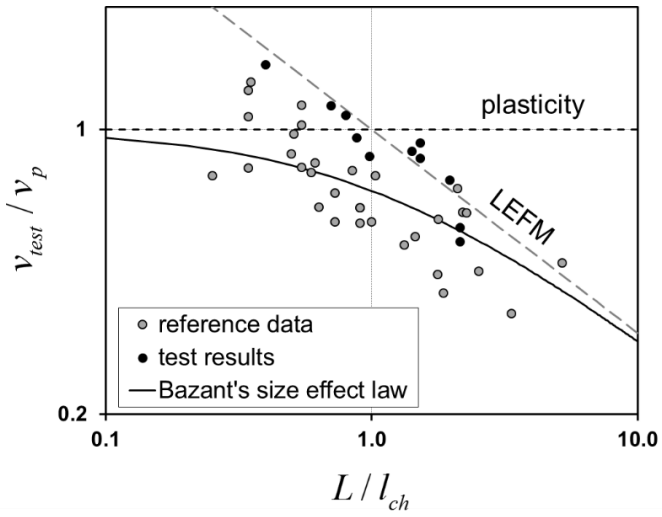

Fig. 6-16. Size effect plot in log scale for current model compared to 44 UHPFRC test results

The size effect plot for current model compared to the limit of plasticity and LEFM in Fig. 6-16. The size effect in shear strength of UHPFRC I-shaped beams without stirrups is clearly observed. The shear strength given by limit analysis is Eq. (5-5) and a -1/2 slope from LEFM are connected by means of asymptotic matching. The solid line is the referred size effect of Bazant's SEL in Eq. (3-21).

The test results larger than the plasticity limit are mainly caused by the evaluation of effective tensile strength. Lots of data were reported as a form of flexural tensile strength, and the estimates by inverse analysis were usually conservative. Despite of the scattered data, it can be concluded that the suggested brittleness factor L / l_{ch} estimates shear strength well and the diagonal tension failure due to UHPFRC crack localization should be analyzed with respect to size effect.

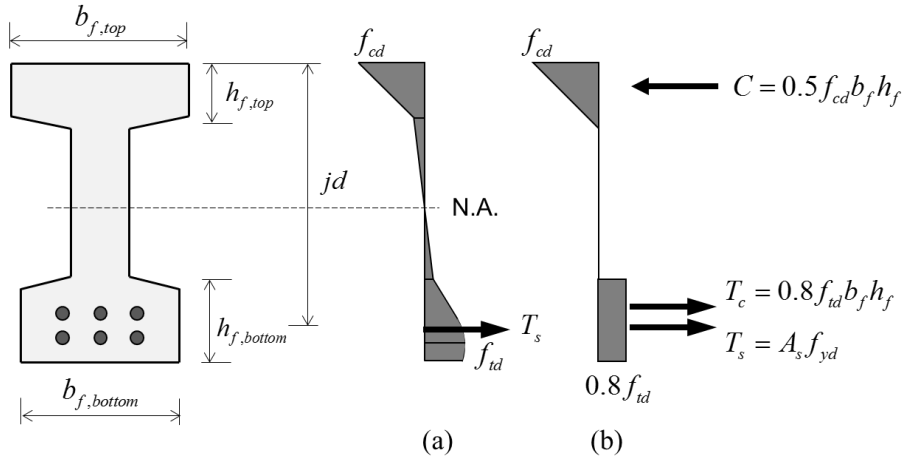

Fig. 6-17. Stress distribution and resultant internal forces for flexural design; (a) the realistic stress distribution and (b) the assumed stress distribution in a cross section

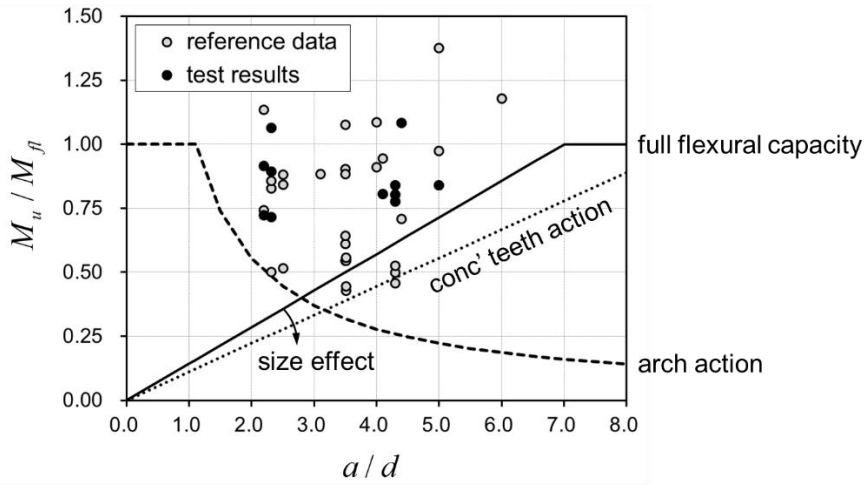

Fig. 6-18. Shear capacity regarding to the flexural capacity influenced by shear span ratio

Assuming the simplified stress distribution for flexural design of UHPFRC I-shaped beams in Fig. 6-17 (b), the relative shear capacity compared to the bending capacity is represented as Fig. 6-18. The full flexural capacity M_{fl} of the member is calculated by the maximum value between the

compression force and the tension force multiplied by the arm length between the two forces in a cross section. The compression force is determined by the equivalent force of the triangular stress distribution in a top flange and the tension force is the summation of fiber reinforcement and longitudinal rebar's contribution. The contribution of fiber reinforcement in a bottom flange is assumed to be equivalent constant tensile stress $0.8 f_{td}$ in this dissertation. The flexural stress in a thin web was neglected for test results of UHPFRC I-shaped shear beams.

The influence of the shear span ratio of Kani's valley (1964) for UHPFRC I-shaped beams is shown in Fig. 6-18. The shear span ratio for the transition point from a shear to a bending failure strongly depends on the depth of the member as well as generally on the reinforcement ratio. As the depth of the member is higher and the longitudinal reinforcement ratio is lower, Shear failure according to concrete teeth action can easily occur. It can be represented by that the slope of the criteria for concrete teeth action is lower due to size effect (Reineck, 1991). The solid line in Fig. 6-18 represents Kani's proposal for RC rectangular beams without stirrups. However the test results of UHPFRC shear beams are depicted below the solid line, which means that the size effect in UHPFRC shear beams is dominant rather than RC shear beams.

The relative shear strength capacity of RC rectangular beams without stirrups is usually depicted along the failure criteria of arch action and concrete teeth action according to the shear span ratio. However, the test results of UHPFRC shear beams are depicted in a diverse range of the Kani's valley, which means that the fiber reinforcement plays a role of shear reinforcement effectively.

Chapter 7. Conclusions

UHPFRC characterizes high strength and fiber reinforcement cement composites. UHPFRC contains steel fibers resulting in superior post-cracking behavior and stress redistribution ability, which gives a ductile failure in compression and tension. For a UHPFRC structural member, a thinner cross section is preferred in practice to compensate the high cost with outstanding strength and durability, and fiber reinforcement enables slender UHPFRC members with little or no reinforcement bar. It is important that the in-plane shear behavior of UHPFRC members be analysed regarding the effect of fiber reinforcement in UHPFRC. The dominant failure mode in UHPFRC I-shaped beams without stirrups has been found as diagonal cracking localized in the web.

The AFGC recommendation advises that shear design strength of UHPFRC is a summation of matrix contribution and fiber contribution. The post-cracking shear strength increase contributes to the shear strength by fiber with the sum of the traditional shear strength for an ordinary concrete beam without stirrups. The fiber contribution is quantified by the UHPFRC tensile strength, and the tensile strength is usually regarded as a residual tensile strength considering the strength reduction as a form of the K factor caused by fiber distribution and orientation. Previous studies including this recommendation tend to consider that the fiber orientation problem in a structural member belongs to the design strength of UHPFRC tensile behavior. K factor is an empirical reduction factor based on test results, and numerous fiber reinforced concrete models employ a probabilistic approach on fiber distribution at a structural level based on bond strength between a single fiber

and the cement matrix at a micro-mechanics level. The shear strength equation misses some points of the physical mechanics of diagonal tension failure, such as the size effect.

In this paper, it is regarded that the heterogeneity due to fiber orientation induces brittle failure represented as crack localization despite of the key role of strength increase interpreted by micro-cracking behavior. The diagonal tension failure within a splitting-dispersed cracked zone in the failure of UHPFRC shear beams can be classified as a 'semi-brittle fracture'. A physical model for shear behavior of UHPFRC beams is proposed by the limit analysis in the framework of the theory of plasticity and fracture mechanics instead of a decomposition of the shear strength contributions of the cement matrix and fiber. A splitting-dispersed cracked zone is assumed a uniform stress field of a damaged zone, which is analysed by plastic limit analysis. Together with the plastic approach for strength estimation, the failure with crack localization should be interpreted by fracture mechanics. Fracture mechanics is able to explain the brittle failure of UHPFRC beams with crack propagation characteristics as a form of the size effect factor included in a shear strength model.

The limit analysis requires the idealization of materials such as a rigid-plastic material. Practical and theoretical application of the limit analysis to structural concrete have shown modified Coulomb failure criteria for concrete has been successful. Based on the adamant assumptions, an appropriate stress field and failure mechanism for a structural behavior provide the lower bound and upper bound solution. These solutions can be then modified by the effective strength parameters determined on the basis of the tests available.

Fiber reinforcement in UHPFRC act as a form of passive confinement and this confinement turns out to be as effective as conventional reinforcement. The characteristic phenomenon of frictional failure is that the yielding failure is

determined by the given pressure, which is usually explained by the confinement effect. The Mohr-Coulomb criterion can explain two physical failure mechanisms, separation failure and sliding failure. The fiber reinforcement effect is taken into account for Coulomb failure criterion with a frictional angle. In this paper, friction angle of UHPFRC is regarded 55° based on push-off test results on monolithic specimens in series of test program for this study.

The tensile strength is an effective strength regarded as the average strength in a tension hardening portion of the stress-crack width relationship. The ultimate crack width has to be determined in a range ensuring the stable strength increase of a structure, and it can be assumed as 0.3 mm conservatively. Similarly, the ultimate crack width plays a key role in performing an inverse analysis for bending test results. Based on the assumptions, UHPFRC material in tensile hardening behavior due to micro-cracking is assumed to be homogeneous. The post-cracking behavior of cementitious materials including micro-cracking and crack localization can be explained by the fictitious crack model. Within nonlinear fracture mechanics, a characteristic length may be defined through a relation between the pre-fracture behavior of the material and its post-fracture tensile softening properties. The load-carrying capacity may be dependent only on the tensile strength and a ratio between the steepness of the stress-strain curve and the steepness of the stress-crack opening curve.

For UHPFRC tensile behavior, the energy dissipation consists of two contributions. Therefore, the problem is identical to that for the cohesive crack with bulk dissipation, which is related to the characteristic length of a material. The critical length of UHPFRC is defined as the ratio of dissipated energy of the pre-peak range to that of the post-peak range. Assuming that the slope in the microcracking phase is almost twice the slope of an equivalent linear elastic phase and the softening curve is linear, the material characteristic length of UHPFRC is defined of twice of the critical length.

Based on the assumptions of the inclination of splitting cracks and a Rankine zone as the homogenous orthotropic strain field of the splitting crack zone, the lower bound solution and upper bound solution are driven, and the governing equation is determined and discussed.

The general assumptions to determine the characteristic length in the micro-cracking zone in the web of UHPFRC I-shaped beams without stirrups are modified from the assumptions for the fracturing truss model. In a micro-cracking stage, a highly orthotropic panel with tensile cracks in the crack band can be assumed. The orthotropic panel is a stress redistribution zone of the same geometry as that of the Rankine zone. The size effect occurs in the orthotropic damaged zone, and the localized deformation is expressed by the fracture mechanics term. The fracturing truss model assumes that the brittleness factor is constant as a material property, but in this paper, the characteristic length of UHPFRC is assumed affected by the confined effect given by the external forces. It is assumed that the damaged zone of UHPFRC consists of series of concrete tension ties, and the failure is governed by the longest one. The longest length of damaged zone is defined as the characteristic length of the structure, which is the effective length of the concrete tension tie in this paper.

The structural characteristics length is determined by the inclination angle of the stress field and the shear span ratio as well as the effective depth which is the characteristic length of ordinary reinforced concrete. The structural characteristics length can be a design parameter for semi-brittle fracturing in UHPFRC structures, taking into account the inelastic behavior at the structural level of the splitting cracked zone. The shear strength of UHPFRC I-beams with crack localization may require a fracture mechanics approach to provide rational design guidelines for structural members made of UHPFRC. A shear strength model of UHPFRC I-beams without stirrups can be proposed by combining the lower bound approach and the newly defined brittleness factor based on the fracture mechanics approach at the structural level.

The brittleness factor involves the size effect. The characteristic length of emerging splitting cracks and the inclination angle of the stress redistribution region of splitting cracks are considered as main parameters for the determination of shear strength of UHPFRC I-beams. The previous studies on the size effect of UHPFRC beams have been interpreted by tensile behavior in flexural members while the size effect in shear behavior have been rarely investigated because the most characteristic length has been derived from the flexural tests in terms of the effective depths of beams. It hereafter is suggested that the brittleness factor at the material level using the ratio of energy release rate be converted into a new brittleness factor at the structural level for the stress redistribution zone in shear beams. The proposed brittleness factor will be able to explain the size effect of the uniform stress field developed in webs of UHPFRC I-beams.

The size effect plot for current model compared to the limit of plasticity and LEFM. The size effect in shear strength of UHPFRC I-shaped beams without stirrups is clearly observed. The shear strength given by limit analysis and a -1/2 slope from LEFM are connected by means of asymptotic matching. The solid line is the referred size effect of Bazant's size effect law. The test results larger than the plasticity limit are mainly caused by the evaluation of effective tensile strength. Lots of data were reported as a form of flexural tensile strength, and the estimates by inverse analysis were usually conservative. Despite of the scattered data, it can be concluded that the suggested brittleness factor estimates shear strength well and the diagonal tension failure due to UHPFRC crack localization should be analysed with respect to the size effect. The diagonal tension failure has to be analysed corresponding to the deformation capacity represented as the ultimate crack widths of UHPFRC. The concept of the brittleness number given by the fracture mechanics approach can suggest the size effect correction with respect to the maximum strength given by limit analysis.

References

AASHTO. (2012). AAHSTO LRFD Bridge Design Specifications. American Association of State Highway and Transportation Officials.

ACI Committee 318. (2011). Building Code Requirements for Structural Concrete (ACI 318M-11) and Commentary. American Concrete Institute.

Assoiation Française de Génie Civil (AFGC). (2013). Ultra High Performance Fiber-Reinforced Concretes Recommendations. French Civil Engineering Association, Paris.

Baby, F., Graybeal, B., Marchand, P., and Toutlemonde, F. (2013). UHPFRC tensile behavior characterization: inverse analysis of four-point bending test results. *Materials and structures, 46*(8), 1337-1354.

Baby, F., Marchand, P., Atrach, M., and Toutlemonde, F. (2013). Analysis of flexure-shear behavior of UHPFRC beams based on stress field approach. *Engineering Structures, 56*, 194-206. doi:10.1016/j.engstruct.2013.04.024

Baby, F., Marchand, P., and Toutlemonde, F. (2013). Shear behavior of ultrahigh performance fiber-reinforced concrete beams. I: Experimental investigation. *Journal of structural engineering, 140*(5), 04013111.

Bažant, Z. P. (1997). Fracturing truss model: Size effect in shear failure of reinforced concrete. *Journal of engineering mechanics, 123*(12), 1276-1288.

Bazant, Z. P., and Gambarova, P. (1980). Rough cracks in reinforced concrete. *Journal of the Structural Division, 106*(ASCE 15330 Proceeding).

Bazant, Z. P., and Planas, J. (1997). *Fracture and size effect in concrete and other quasibrittle materials* (Vol. 16): CRC press.

Belarbi, A., and Hsu, T. T. (1995). Constitutive laws of softened concrete in biaxial tension compression. *Structural Journal, 92*(5), 562-573.

Birkeland, P. W., and Birkeland, H. W. (1966). Connections in precast concrete construction. *ACI Journal Proceedings, 63*(3), 345-368.

Bischoff, P. H. (2003). Tension stiffening and cracking of steel fiber-reinforced concrete. *Journal of materials in civil engineering, 15*(2), 174-182.

Casanova, P., and Rossi, P. (1997). Analysis and design of steel fiber reinforced concrete beams. *ACI Structural Journal, 94*(5), 595-602.

CEN. (2004). EN 1992-1-1 Eurocode 2: Design of Concrete Structures - Part 1-1:General Rules and Rules for Buildings. European Committee for Standardization, Brussels.

CEN. (2005). EN 14651: Test method for metallic fibered concrete – Measuring the flexural tensile strength (limit of proportionality, residual). European Committee for Standardization, Brussels.

Charron, J.-P., Denarié, E., and Brühwiler, E. (2007). Permeability of ultra high performance fiber reinforced concretes (UHPFRC) under high stresses. *Materials and structures, 40*(3), 269-277.

Demeke, A., and Tegos, I. (1994). Steel FiberReinforced Concrete in Biaxial Stress Tension-Compression Conditions. *Structural Journal, 91*(5), 579-584.

Duthinh, D. (1999). Sensitivity of shear strength of reinforced concrete and prestressed concrete beams to shear friction and concrete softening according to modified compression field theory. *Structural Journal, 96*(4), 495-508.

Erdogan, F., and Sih, G. (1963). On the crack extension in plates under plane loading and transverse shear. *Journal of basic engineering, 85*(4), 519-527.

Feenstra, P., De Borst, R., and Rots, J. (1992). Numerical study on crack dilatancy. I: models and stability analysis; II: application. *Journal of Engineering Mechanics ASCE, 117*(4), 733-769.

Fehling, E., Leutbecher, T., and Röder, F.-K. (2008). *Biaxial compression-tension-strength of reinforced concrete and reinforced steel fibre concrete in structural panels* (Vol. 11): kassel university press GmbH.

Fehling, E., Leutbecher, T., Röder, F., and Stürwald, S. (2008). Structural behavior of UHPC under biaxial loading. *Ultra High Performance Concrete (UHPC), 2*, 05-07.

Fehling, E., Schmidt, M., Walraven, J., Leutbecher, T., and Fröhlich, S. (2014a). Ultra-High Performance Concrete UHPC: Wiley Online Library.

Fehling, E., Schmidt, M., Walraven, J., Leutbecher, T., and Fröhlich, S. (2014b). *Ultra-High Performance Concrete UHPC: Fundamentals, Design, Examples*: John Wiley & Sons.

Fehling, E., and Thiemicke, J. (2016). Experimental Investigations on I-Shaped UHPC-Beams with Combined Reinforcement under Shear Load. Proceedings of the HiPerMat, Kassel, Germany.

Fib bulletin 65. (2010a). Model Code 2010 – final, vol 1. fib, switzerland.

Fib bulletin 65. (2010b). Model Code 2010 – final, vol 2. fib, switzerland.

Fib bulletin. (2008). Constitutive modelling of high strength/high performance concrete-state of the art report. switzerland.

Fields, K., and Bischoff, P. H. (2004). Tension stiffening and cracking of high-strength reinforced concrete tension members. *Structural Journal*, *101*(4), 447-456.

Fischer, G., and Li, V. C. (2002). Influence of matrix ductility on tension-stiffening behavior of steel reinforced engineered cementitious composites (ECC). *Structural Journal*, *99*(1), 104-111.

Fischer, G., and Li, V. C. (2007). Effect of fiber reinforcement on the response of structural members. *Engineering Fracture Mechanics*, *74*(1), 258-272.

Graybeal, B. A. (2006). *Material property characterization of ultra-high performance concrete*. Retrieved from

Graybeal, B. A. (2010). *Simultaneous Structural and Environmental Loading of an Ultra-High Performance Concrete Component*: US Department of Transportation, Federal Highway Administration.

Graybeal, B. A., and Baby, F. (2013). Development of Direct Tension Test Method for Ultra-High-Performance Fiber-Reinforced Concrete. *ACI Materials Journal*, *110*(2).

Grob, J. (2013). *Ultimate Strength and Design of Reinforced Concrete Beams under Bending and Shear/Résistance et dimensionnement des poutres en béton armé soumises à la flexion et à l'effort tranchant/Bruchwiderstand und Bemessung von Stahlbetonbalken unter Biegung und Schub* (Vol. 63): Birkhäuser.

Grünberg, J., Ertel, C., Lohaus, L., Wefer, M., Curbach, M., Speck, K., . . . Fitik, B. (2010). Failure models for ultra high performance concrete (UHPC). Proceedings of the 2010 Fib congress and PCI Convention bridge conference, Washington, DC.

Gustafsson, P. J., and Hillerborg, A. (1988). Sensitivity in shear strength of longitudinally reinforced concrete beams to fracture energy of concrete. *Structural Journal, 85*(3), 286-294.

Hegger, J., and Bertram, G. (2008). Shear carrying capacity of ultra-high performance concrete beams. *Tailor Made Concrete Structures. Walraven & Stoelhorst. London*, 341-347.

Hoang, L. C., Jacobsen, H. J., and Larsen, B. (2012). Compressive strength of reinforced concrete disks with transverse tension. *Bygningsstatiske Meddelelser, 83*(2-3), 23-61.

Hofbeck, J., Ibrahim, I., and Mattock, A. H. (1969). Shear transfer in reinforced concrete. *ACI Journal Proceedings, 66*(2), 119-128.

Hsu, T. T., Mau, S., and Chen, B. (1987). Theory on shear transfer strength of reinforced concrete. *Structural Journal, 84*(2), 149-160.

Hussein, A., and Marzouk, H. (2000). Behavior of high-strength concrete under biaxial stresses. *Materials Journal, 97*(1), 27-36.

Jan G.M. Van Mier. (1984). *Strain-softening of concrete under multiaxial loading conditions*: Technische Hogeschool Eindhoven.

Jan G.M. Van Mier. (2012). *Concrete fracture: a multiscale approach*: CRC press.

JCI. (2003). Method of test for fracture energy of concrete by use of notched

beam. Japan Concrete Institute, Japan.

Jenq, Y., and Shah, S. (1988). Mixed-mode fracture of concrete. *International Journal of Fracture, 38*(2), 123-142.

JSCE. (2004). "Design and Construction Guidelines for Ultra High-Performance Concrete (draft). JSCE, Japan.

Jungwirth, J. (2006). *Zum tragverhalten von zugbeanspruchten bauteilen aus ultra-hochleistungs-faserbeton.* Institut de structures SECTION DE GENIE CIVIL ÉCOLE POLYTECHNIQUE FÉDÉRALE DE LAUSANNE POUR L'OBTENTION DU GRADE DE DOCTEUR ÈS SCIENCES PAR Jörg JUNGWIRTH Diplom-Ingenieur, Technische Universität München.

Jungwirth, J., and Muttoni, A. (2004). Structural behavior of tension members in Ultra High Performance Concrete. Proceedings of the International symposium on ultra high performance concrete.

Kani, G. N. J. (1964). The riddle of shear failure and its solution. *ACI Journal Proceedings, 61*(4), 441-468.

KCI. (2012). Design Guidelines for Ultra High Performance Concrete K-UHPC Structure. Korea Concrete Institute.

Koenig, G. (1993). Shear behavior of longitudinally reinforced concrete members of HSC. Proceedings of the JCI International Workshop on Size Effect in Concrete Structures.

Kolleger, J., and Mehlhorn, G. (1987). Material model for cracked reinforced concrete. *IABSE Colloquim on Computational Mechanics of Concrete Structures, Delft*, 63-74.

Kupfer, H., Hilsdorf, H. K., and Rusch, H. (1969). Behavior of concrete under biaxial stresses. *ACI Journal Proceedings, 66*(8), 656-666.

Kupfer, H., and Moosecker, W. (1979). Stress and deformation of the shear zone of the slim profiled steel concrete beam. Proceedings of the Research contributions for building practice, Ernst & Sohn, Berlin, Germany.

Lee, G., and Foster, S. (2008). Modelling of shear-fracture of fibre-reinforced concrete. Proceedings of the Tailor made concrete structures, fib symposium, Amsterdam, The Netherlands.

Lee, J.-H., and Hong, S.-G. (2015a). Constitutive model for shear transfer in Ultra-High Performance Fiber Reinforced Concrete. Proceedings of the fib Symposium Copenhagen.

Lee, J.-H., and Hong, S.-G. (2015b). Shear friction strength based on limit analysis for ultra-high performance fiber reinforced concrete. *Journal of the Korea Concrete Institute, 27*(3), 299-309.

Lee, J.-H., Hong, S.-G., Joh, C., Kwahk, I., and Lee, J.-W. (2017). Biaxial tension–compression strength behaviour of UHPFRC in-plane elements. *Materials and structures, 50*(1), 20.

Lee, J.-Y., and Yoon, S.-H. (2004). Evaluation of the Minimum Shear Reinforcement Ratio of Reinforced Concrete Members. *Journal of the Korea Concrete Institute, 16*(1), 43-53.

Leutbecher, T. (2008). *Rissbildung und Zugtragverhalten von mit Stabstahl und Fasern bewehrtem ultrahochfesten Beton (UHPC)* (Vol. 9): kassel university press GmbH.

Leutbecher, T., and Fehling, E. (2004). Structural behaviour of UHPC under tensile stress and biaxial loading. Proceedings of the International

Symposium on Ultra-High Performance Concrete.

Leutbecher, T., and Fehling, E. (2012). Tensile behavior of ultra-high-performance concrete reinforced with reinforcing bars and fibers: minimizing fiber content. *ACI Structural Journal, 109*(2), 253.

Lim, W. Y. (2012). *Critical crack path dependent shear strength models of concrete beams without web reinforcement*. Ph. D dissertation, Seoul National University.

Mohamed, A. A., and Richard, N. W. (1999). Enhanced contact model for shear friction of normal and high-strength concrete. *ACI Structural Journal, 96*(3), 348-360.

Moreillon, L. (2013). *Shear strength of structural elements in high performance fibre reinforced concrete (HPFRC).* Paris Est.

Naaman, A., Fischer, G., and Krstulovic-Opara, N. (2016). Measurement of tensile properties of fiber reinforced concrete: draft submitted to ACI Committee 544. *Newsletter*.

Ng, T., Htut, T., and Foster, S. (2010). Mode I and II fracture behaviour of steel fibre reinforced high strength geopolymer concrete: an experimental investigation. *Fracture Mechanics of Concrete and Concrete Structures*, 1504-1511.

Ng, T. S., Foster, S. J., Htet, M. L., and Htut, T. N. S. (2014). Mixed mode fracture behaviour of steel fibre reinforced concrete. *Materials and structures, 47*(1-2), 67-76.

Nielsen M.P. (1999). *Limit Analysis and Concrete Plasticity* (2nd ed.): CRC press.

Ottosen, N. S. (1977). A failure criterion for concrete. *American Society of Civil Engineers. Engineering Mechanics Division. Journal*.

Park, S. H., Kim, D. J., Ryu, G. S., and Koh, K. T. (2012). Effect of adding micro fibers on the pullout behavior of high strength steel fibers in UHPC matrix. Proceedings of the Hipermat, Kassel, Germany.

Qi, J., Ma, Z. J., and Wang, J. (2017). Shear Strength of UHPFRC Beams: Mesoscale Fiber-Matrix Discrete Model. *Journal of structural engineering*, *143*(4), 04016209. doi:10.1061/(asce)st.1943-541x.0001701

Randl, N., Mészöly, T., and Harsányi, P. (2016). Load bearing behaviour of slender UHPC beam members in shear. Proceedings of the HiPerMat 2016, Kassel, Germany.

Redaelli, D. (2006). Testing of reinforced high performance fibre concrete members in tension. Proceedings of the 6th Int. Ph. D. Symposium in Civil Engineering, Zurich.

Reineck, K.-H. (1991). Ultimate shear force of structural concrete members without transverse reinforcement derived from a mechanical model (SP-885). *Structural Journal*, *88*(5), 592-602.

Roos, W. (1995). *Zur Druckfestigkeit des gerissenen Stahlbetons in scheibenförmigen Bauteilen bei gleichzeitig wirkender Querzugbeanspruchung.*

Schlaich, J., Schäfer, K., and Jennewein, M. (1987). Toward a consistent design of structural concrete. *PCI journal*, *32*(3), 74-150.

Schnütgen, B., and Vandewalle, L. (2003). Test and design methods for steel fibre reinforced concrete–. *Background and Experience, in proceeding of RILEM TC.*

Shah, S. (1990). Determination of fracture parameters (K Ic s and CTOD c) of plain concrete using three-point bend tests. *Materials and structures, 23*(6), 457-460.

Shah, S. P., Swartz, S. E., and Ouyang, C. (1995). *Fracture mechanics of concrete: applications of fracture mechanics to concrete, rock and other quasi-brittle materials*: John Wiley & Sons.

Sigrist, V., Alvarez, M., and Kaufmann, W. (1995). *Shear and flexure in structural concrete beams*: Institut für Baustatik und Konstruktion, ETH-Hönggerberg.

Speck, K. (2007). *Concrete under multiaxial loading conditions—a constitutive model for short-time loading of high performance concretes.* Dissertation, Technical University of Dresden.

Thiemicke, J., and Fehling, E. (2016). Proposed Model to predict the Shear Bearing Capacity of UHPC-Beams with Combined Reinforcement. Proceedings of the HiPerMat, Kassel, Germany.

Toutlemonde, F., and Resplendino, J. (2011). *Designing and Building with UHPFRC: State of the Art and Development*: ISTE.

Traina, L. A., and Mansour, S. A. (1991). Biaxial strength and deformational behavior of plain and steel fiber concrete. *ACI Materials Journal, 88*(4).

Vecchio, F. J., and Collins, M. P. (1986). The modified compression-field theory for reinforced concrete elements subjected to shear. *ACI J., 83*(2), 219-231.

Voo, J., and Foster, S. (2004). Tensile-fracture of fibre-reinforced concrete: variable engagement model. Proceedings of the 6th International RILEM symposium on fibre reinforced concretes.

Voo, Y. L., Poon, W. K., and Foster, S. J. (2010). Shear strength of steel fiber-reinforced ultrahigh-performance concrete beams without stirrups. *Journal of structural engineering, 136*(11), 1393-1400.

Walraven, J., Belletti, B., and Esposito, R. (2012). Shear capacity of normal, lightweight, and high-strength concrete beams according to Model Code 2010. I: Experimental results versus analytical model results. *Journal of structural engineering, 139*(9), 1593-1599.

Walraven, J. C. (1980). Aggregate interlock: a theoretical and experimental analysis. *Delft University Press*, 197.

Walraven, J. C. (2009). High performance fiber reinforced concrete: progress in knowledge and design codes. *Materials and structures, 42*(9), 1247.

Warner, R. F., and Thürlimann, B. (1963). *Design of stirrup-reinforcement in concrete beams*: na.

Wille, K., El-Tawil, S., and Naaman, A. (2014). Properties of strain hardening ultra high performance fiber reinforced concrete (UHP-FRC) under direct tensile loading. *Cement and Concrete Composites, 48*, 53-66.

Wille, K., Kim, D. J., and Naaman, A. E. (2011). Strain-hardening UHP-FRC with low fiber contents. *Materials and structures, 44*(3), 583-598.

Wille, K., and Naaman, A. (2010). Fracture energy of UHPFRC under direct tensile loading. Proceedings of the FraMCoS-7 international conference, Jeju, Korea.

Yang, I.-H., Kim, K.-C., and Joh, C.-B. (2014). Structural Behavior of Hybrid Steel Fiber-Reinforced Ultra High Performance Concrete Beams Subjected to Bending. *Journal of the Korea Concrete Institute, 26*(6), 771-778.

Yang, I. H., Joh, C., Lee, J. W., and Kim, B. S. (2012). An experimental study on shear behavior of steel fiber-reinforced ultra high performance concrete beams. *Journal of The Korean Society of Civil Engineers, 32*(1A), 55-64.

Appendix 1. UHPFRC Shear Beams Data Base

Eighty-two data are summarized at the Appendix 1. Most of data belongs to UHPFRC I-shaped shear beams without transverse reinforcement, and the main parameters are the fiber type and content, the magnitude of prestressing force and the conventional shear design parameters such as shear span ratio, effective depth. The data summarized at Table A-1 is applied to verify the suggested shear strength equation in this dissertation.

Compressive strength f_{cm} is mean value measured by cylinder compressive test. If there were the test results from cube compressive test only, the conversion factor 0.9 is applied and the revised value is indicated at the tables. Flexural tensile strength f_r is measured by four-point bending test on unnotched prisms. Tensile strength f_t is the indirect value applied the inverse method according to the AFGC recommendation. If there were direct tension test results, the test results are filled out in the f_t column. In case the specific failure mode did not reported, the failure mode are noted as SF, which stands for shear failure.

The prestressing stress is the effective compressive stress assuming that the force presses the cross section uniformly. If the jacking force per a strand was reported only, the effective force is assumed to be 70% of the jacking force. In case the reports do not indicated the yield strength of transverse reinforcement as test results, the characteristic yield strength according to the specification of steel rebar is filled. For example, the yield strength of BSt550 steel rebar is noted as 550 MPa.

Appendix 1. UHPFRC Shear Beams Data Base

Table A-1. Parameters of tested I-shaped UHPFRC beams without transverse reinforcement

No.	Researcher	SP ID	UHPFRC material properties							Dimensions and Reinforcement				Test set-up and results			
			f_{cm} (MPa)	V_f (%)	Fiber type	l_f (mm)	d_f (mm)	f_r (MPa)	f_t (MPa)	b_w (mm)	d (mm)	a/d	ρ_l (%)	σ_n (MPa)	Failure Mode	V_{cr} (kN)	V_{peak} (kN)
1	Baby	A-RC-NS	203.0	2.5	SS	20	0.3	34.5	14.3	65	305	2.3	10.4	0	DT	97	454.5
2	Baby	B-RC-NS	205.0	2.0	SS	13	0.2	28.5	11.1	65	305	2.3	10.4	0	DT	90	447.5
3	Baby	B-OF-RC-NS	157.0	4.7	OF	(n/a)	(n/a)	20.8	7.8	65	305	2.3	10.4	0	DT	70	248.5
4	Baby	A-PC-NS	203.0	2.5	SS	20	0.3	34.5	14.3	30	280	4.3	4.5	12.55	DT	188	430.0
5	Baby	A-PC-NS(2)	203.0	2.5	SS	20	0.3	34.5	14.3	30	280	4.3	4.5	12.55	DT	199	431.0
6	Baby	B-PC-NS	205.0	2.0	SS	13	0.2	28.5	11.1	30	280	4.3	4.5	12.30	DT	125.5	507.0
7	Fehling	Q-F1-1	201.2	1.0	SS	13	0.175	23.2	-	30	280	4.3	24.13	0	DT	-	109
8	Fehling	Q-F1-2	207.9	1.0	SS	13	0.175	23.2	-	30	280	4.3	24.13	0	DT	-	100
9	Fehling	Q2-F1-1	185.6	1.0	SS	13	0.175	23.2	-	30	280	4.3	24.13	0	DT	-	109
10	Hegger	T1a	135.9	0.9	SS	17.5	0.15	22.7	-	60	316	3.8	4.84	13.08	SF	-	234
11	Hegger	T1b	156.6	0.9	SS	17.5	0.15	21.2	-	60	316	3.8	4.84	16.82	SF	-	267
12	Hegger	T3b	145.6	2.5	SS	9	0.15	24.1	-	60	316	3.8	4.84	13.08	SF	-	408
13	Hegger	T4a	158.4	0.9	SS	17.5	0.15	19.1	-	60	316	3.8	4.84	16.82	SF	-	347
14	Hegger	T4b	164.7	0.9	SS	17.5	0.15	20.2	-	60	316	4.4	4.84	16.82	SF	-	292
15	Hegger	T5a	159.3	0.9	SS	17.5	0.15	20.1	-	60	316	3.8	4.84	16.82	SF	-	326
16	Hegger	T5b	161.1	0.9	SS	17.5	0.15	20.1	-	60	316	3.8	4.84	16.82	SF	-	296
17	Hegger	T18a	166.5	0.9	SS	17.5	0.15	34.1	-	60	316	4.1	4.84	16.82	SF	-	301
18	Hegger	T19b	156.6	0.9	SS	17.5	0.15	24.3	-	60	316	3.5	4.84	16.82	SF	-	324
19	Hegger	T22b	170.1	0.9	SS	17.5	0.15	25.6	-	40	316	3.8	4.84	12.03	SF	-	174
20	Hegger	T24b	160.2	0.9	SS	17.5	0.15	29.6	-	40	616	3.8	4.97	18.87	SF	-	316
21	Hegger	T25b	152.1	0.9	SS	17.5	0.15	23.7	-	60	616	3.8	4.97	16.19	SF	-	465
22	Hegger	T26b	154.8	2.5	SS	9	0.15	31.5	-	60	616	3.8	4.97	24.29	SF	-	512
23	Hegger	T29b	164.7	0.9	SS	30	0.4	25.1	-	60	616	3.8	4.97	24.29	SF	-	476
24	Hegger	T30	165.6	0.9	SS	17.5	0.15	23.0	-	40	916	3.8	5.01	23.29	SF	-	371
25	JSCE	BRC1	184.0	2.0	SS	15	0.2	31.5	11.6	40	365	2.2	8.0	0	DT	105	264
26	JSCE	BRC3	212.0	2.0	SS	15	0.2	31.3	11.5	40	365	4.4	8.0	0	DT	59	145

SS=Steel Straight Fibers, OF=Organic Fibers, DT=Diagonal Tension Failure, SF=Shear Failure

Table A-1. Parameters of tested I-shaped UHPFRC beams without transverse reinforcement

No.	Researcher	SP ID	UHPFRC material properties							Dimensions and Reinforcement				Test results			
			f_{cm} (MPa)	V_f (%)	Fiber type	l_f (mm)	d_f (mm)	f_r (MPa)	f_t (MPa)	b_w (mm)	d (mm)	a/d	ρ_l (%)	σ_n (MPa)	Failure Mode	V_{cr} (kN)	V_{peak} (kN)
27	JSCE	BRC4	204.0	2.0	SS	15	0.2	32.7	12.0	80	365	2.2	4.0	0	DT	160	448
28	JSCE	DS-1	202.0	2.0	SS	15	0.2	26.8	9.7	40	407	4.1	5.8	0	DT	70	179
29	JSCE	DS-2	199.0	2.0	SS	15	0.2	26.6	9.7	40	407	5.0	5.8	0	DT	55	207
30	JSCE	DS-3	220.0	2.0	SS	15	0.2	28.2	10.3	40	407	6.0	5.8	0	DT	50	164
31	JSCE	STC1	182.0	2.0	SS	15	0.2	-	11.3	50	170	3.5	9.1	0	DT		173
32	JSCE	3.0_F2_25	195.1	2.0	SS	15	0.2	-	11.3	25	170	3.1	18.2	0	SF	41	91
33	JSCE	4.0_F2_25	195.1	2.0	SS	15	0.2	-	11.3	25	170	4.0	18.2	0	SF	33	73
34	JSCE	5.0_F2_25	195.1	2.0	SS	15	0.2	-	11.3	25	170	5.0	18.2	0	SF	46	62
35	JSCE	4.0_F2_35	195.1	2.0	SS	15	0.2	-	11.3	35	170	4.0	13.0	0	SF	39	87
36	JSCE	4.0_F2_L	232.9	2.0	SS	15	0.2	-	11.3	50	340	4.0	18.0	0	SF	104	228
37	JSCE	BPC1	165	2.0	SS	15	0.2	-	10.7	40	448	3.3	3.5	0.875	DT	135	267
38	JSCE	BPC2	169	2.0	SS	15	0.2	-	10.2	40	448	2.2	3.5	10.0	DT	234	489
39	JSCE	BPC3	163	2.0	SS	15	0.2	-	9.2	40	448	3.3	3.5	10.0	DT	210	420
40	JSCE	BPC4	182	2.0	SS	15	0.2	-	10	40	448	4.5	3.5	10.0	BF	215	358
41	Lee	1-S25	166.6	0.5/1.0	SS-M	16/20	0.2	24.5	11.0	40	460	2.5	20.95	0	DT	141.0	415.1
42	Lee	1-S35	160.2	0.5/1.0	SS-M	16/20	0.2	20.9	10.9	40	460	3.5	20.95	0	DT	189.0	355.6
43	Lee	1-S35-A	160.2	0.5/1.0	SS-M	16/20	0.2	20.9	10.9	40	460	3.5	12.63	0	DT	124.9	387.7
44	Lee	1-S35-B	166.6	0.5/1.0	SS-M	16/20	0.2	24.5	11.0	40	640	3.5	15.05	0	DT	209.3	347.6
45	Lee	1-S35-C	166.6	0.5/1.0	SS-M	16/20	0.2	24.5	11.0	40	640	3.5	11.88	0	FS	156.1	321.1
46	Lee	2-S25	163.3	0.5/1.0	SS-M	16/20	0.2	19.7	10.5	40	460	2.5	20.95	0	DT	155.8	455.9
47	Lee	2-S35	163.3	0.5/1.0	SS-M	16/20	0.2	19.7	10.5	40	460	3.5	20.95	0	DT	180.5	371.8
48	Lee	2-S35-B	163.3	0.5/1.0	SS-M	16/20	0.2	19.7	10.5	40	640	3.5	15.05	0	DT	187.6	439.7
49	Lee	3-S25	170.1	1.0	SS	20	0.2	10.4	7.6	40	460	2.5	20.95	0	DT	113.5	427.7
50	Lee	3-S35	170.1	1.0	SS	20	0.2	10.4	7.6	40	460	3.5	20.95	0	DT	124.3	340.3
51	Lee	3-S35-B	170.1	1.0	SS	20	0.2	10.4	7.6	40	640	3.5	15.05	0	DT	150.2	354.5
52	Randl	B19	150.4	2.0	SS	15	0.2		7.88	58	313	3.5	12.11	0	DT	-	251

SS=Steel Straight Fibers, SS-M=Mixed Steel Straight Fibers, DT=Diagonal Tension Failure, SF=Shear Failure, BF=Bending Failure

Appendix 1. UHPFRC Shear Beams Data Base

Table A-1. Parameters of tested I-shaped UHPFRC beams without transverse reinforcement

No.	Researcher	SP ID	UHPFRC material properties							Dimensions and Reinforcement				Test results			
			f_{cm} (MPa)	V_f (%)	Fiber type	l_f (mm)	d_f (mm)	f_r (MPa)	f_t (MPa)	b_w (mm)	d (mm)	a/d	ρ_l (%)	σ_n (MPa)	Failure Mode	V_{cr} (kN)	V_{peak} (kN)
53	Randl	B25	178.4	2.0	SS	15	0.2	-	7.88	58	313	3.5	12.11	0	DT	-	319
54	Randl	B30	167.5	2.0	SS	15	0.2	-	7.88	58	313	3.5	12.11	0	DT	-	357
55	Randl	B20	151.9	1.0	SS	15	0.2	-	6.25	58	313	3.5	12.11	0	DT	-	266
56	Randl	B24	164.8	1.0	SS	15	0.2	-	6.25	58	313	3.5	12.11	0	DT	-	199
57	Randl	B29	176.5	1.0	SS	15	0.2	-	6.25	58	313	3.5	12.11	0	DT	-	308
58	Sato	NS08	148	0.8	SS	13	0.16	-	7.0	50	340	3.4	4.6	0	DT	-	340
59	Sato	NS16	147	1.6	SS	13	0.16	-	11.2	50	340	3.4	4.6	0	DT	-	531
60	Voo	X-B1	125	1.0	SS	15	0.2	13.0	-	50	620	3.2	2.68	14.15	DT	225	330
61	Voo	X-B2	126	1.0	SS	15	0.2	15.6	-	50	620	3.2	2.68	14.15	DT	225	355
62	Voo	X-B3	135	1.0	SS	15	0.2	13.6	-	50	620	3.2	2.68	14.15	DT	165	360
63	Voo	X-B4	122	1.0	SS	15	0.2	13.6	-	50	620	2.5	2.68	14.15	DT	275	456
64	Voo	X-B5	140	1.0	SS	25	0.2	19.7	-	50	620	3.5	2.68	14.15	DT	250	423
65	Voo	X-B6	140	1.0	SS	25	0.2	19.7	-	50	620	4.5	2.68	14.15	DT	215	391
66	Voo	X-B7	122	1.5	SS	20	0.2	13.6	-	50	620	2.5	2.68	14.15	DT	300	522
67	Voo	X-B8	122	1.0	SS	15	0.2	13.6	-	50	620	1.8	2.68	14.15	SF	350	582
68	Voo	SB1	161	2.5	SS	13	0.2	29.8	11.9	50	600	3.33	5.72	0	DT	150	430
69	Voo	SB2	160	2.5	SS	13	0.2	26.4	11.2	50	600	3.33	5.72	3.6	DT	200	497
70	Voo	SB3	149	2.5	SS	13	0.2	23.2	10.6	50	600	3.33	5.72	7.2	DT	150	428
71	Voo	SB4	164	1.25	SS	13	0.2	14.8	10.3	50	600	3.33	5.72	7.2	DT	150	337
72	Voo	SB5	171	1.5/1.0	SS/EH	13/30	0.2/0.5	26.3	13.6	50	600	3.33	5.72	7.2	DT	200	440
73	Voo	SB6	157	2.5	EH	30	0.5	25.2	10.2	50	600	3.33	5.72	7.2	DT	150	330
74	Voo	SB7	169	1.88/0.62	SS/EH	13/30	0.2/0.5	23.8	11.1	50	600	3.33	5.72	7.2	DT	175	397
75	Yang	S25-F10-P0	174.5	1.0	SS	13	0.2	-	10.1	50	640	2.5	5.3	0	DT	245	488
76	Yang	S25-F15-P0	188.2	1.5	SS	13	0.2	-	14.4	50	640	2.5	5.3	0	DT	280	614
77	Yang	S25-F20-P0	185.5	2.0	SS	13	0.2	-	15.0	50	640	2.5	5.3	0	DT	300	527
78	Yang	S34-F10-P0	168.9	1.0	SS	13	0.2	-	10.1	50	640	3.4	5.3	0	DT	135	279

SS=Steel Straight Fibers, EH=End Hooked Steel Fibers, DT=Diagonal Tension Failure, SF=Shear Failure

Table A-1. Parameters of tested I-shaped UHPFRC beams without transverse reinforcement

No.	Researcher	SP ID	UHPFRC material properties							Dimensions and Reinforcement				Test results			
			f_{cm} (MPa)	V_f (%)	Fiber type	l_f (mm)	d_f (mm)	f_r (MPa)	f_t (MPa)	b_w (mm)	d (mm)	a/d	ρ_l (%)	σ_n (MPa)	Failure Mode	V_{cr} (kN)	V_{peak} (kN)
79	Yang	S34-F15-P0	193.0	1.5	SS	13	0.2	-	13.9	50	640	3.4	5.3	0	DT	270	308
80	Yang	S34-F20-P0	188.5	2.0	SS	13	0.2	-	17.3	50	640	3.4	5.3	0	DT	245	404
81	Yang	S25-F20-PS	185.5	2.0	SS	13	0.2	-	15.0	50	640	2.5	5.3	28.9	DT	-	716.5
82	Yang	S34-F20-PS	185.5	2.0	SS	13	0.2	-	17.3	50	640	3.4	5.3	28.9	DT	-	477

SS=Steel Straight Fibers, DT=Diagonal Tension Failure

초 록

강섬유보강 초고성능 콘크리트(UHPFRC)는 구조적 성능 뿐 아니라 내구성, 시공성이 뛰어나 철근 배근이 없는 세장하고 자유로운 부재 형상의 구현이 가능한 재료이다. 이러한 장점을 활용하기 위해서는 철근 배근이 없는 면내 전단 거동에 대한 연구가 요구된다. 본 연구에서는 전단철근이 없는 UHPFRC I형보의 복부 전단거동을 분석하고 이론적, 실험적 연구를 통해 전단강도 산정식을 제안하였다.

UHPFRC 전단부재는 강섬유 보강효과가 미세균열 확산에 의한 강도증가로 나타나는 특징을 보인다. 강섬유 부피비가 1% 이상인 경우 대부분의 UHPFRC는 휨인장 실험에서 균열 후 경화거동을 보이며, 이러한 UHPFRC 전단부재는 최대 하중이 최초 균열 하중의 2배 이상이며 하중 증가가 일정한 강성을 가지고 안정적으로 발현된다. 현행 UHPFRC 부재 전단강도는 콘크리트 매트릭스에 의한 전단강도와 강섬유 보강에 의한 전단강도를 별도로 산정하여 이를 합하는 방법이 일반적이다. 하지만 이러한 방법은 단일재료로서 UHPFRC의 재료물성을 분리하여 산정하고 있으며 부재의 역학적 거동을 근거로 하지 않는다는 단점이 있다. 실제로 기존 실험결과 대부분의 파괴모드가 복부에서 균열 집중 현상에 의한 사인장 파괴를 보였으며, 사인장 파괴는 일반 철근콘크리트 부재에서는 철근 항복이 아닌 콘크리트 재료성질에 의해 좌우되는 취성적인 파괴로 전단경간비, 유효깊이, 휨철근비 등 다양한 설계변수에 영향을 받는 것으로 알려져 있다.

이 연구에서는 최초 균열 후 미세균열에 확산에 의한 안정적인

하중 증가를 보이지만, 최종 파괴는 미세균열 구간 내에서 발생하는 균열 집중 현상에 발생하는 사인장 파괴를 전단철근이 없는 UHPFRC 부재의 대표적인 파괴모드로서 '준 취성파괴(Semi-Brittle Fracture)'로 정의하였다. 준 취성파괴는 안정적인 하중증가를 보이는 미세균열 구간과 최종파괴로서 균열 집중 현상을 각각 소성이론과 파괴역학을 통해 분석할 수 있다.

재료의 인장거동은 UHPFRC 전단부재의 준 취성파괴를 분석하는데 있어 가장 중요한 부분이다. UHPFRC 강섬유 보강효과에 대한 기존 연구는 재료수준의 단일 강섬유와 매트릭스 부착강도를 기반으로한 재료인장강도를 산정하는데 집중되어 있다. 재료인장강도를 설계인장강도로 부재수준에서 적용시키기 위한 방법은 확률론적인 접근법과 '강섬유 방향성 계수'라는 개념을 적용하여 실험에 의한 계수값을 제안하는 방법이 적용되고 있다. 이 연구에서는 강섬유 보강효과의 재료적 불균질성으로 인한 부재 취성도를 설계인장강도가 아닌, 크기효과를 통해 반영하고자 하였다. 크기효과는 부재의 취성적 거동을 강도식에 반영할 수 있는 효과적인 접근법이다. 소성이론을 통해 부재 전단강도 상한값을 제안하고, 여기에 파괴역학을 기반으로 한 취성계수를 제안하여 이를 크기효과로 전단강도식에 반영하였다. 재료인장강도는 소성이론에 적용 가능한 유효인장강도로 정의하였다.

소성이론을 적용하기 위해서는 유효인장강도와 재료 파괴기준이 제안되어야 하며, 파괴역학 기반 분석을 위해 재료의 파괴역학 변수가 정의되어야 한다. 이 논문에서는 현행 기준에서 제안하고 있는 다양한 형태의 인장실험 및 분석을 비교하여 UHPFRC의 인장거동을 정의하고 파괴역학 변수를 도출하였다. 재료 파괴기준은 일축인장실험에 의한 분리 파괴 외에도 강섬유 보강에 의한 미끄러짐 파괴를 설명하기 위해 모어-쿨롱 파괴기준을 제안하였다. 철근이 배근된 단일부재의 푸시 오프 실험을 통해 쿨롱

파괴기준을 정의하는 데 필요한 마찰각 및 강도저감계수를 도출, 이를 적용하였다. 또한 철근이 배근된 면내 부재의 인장-압축의 이축응력실험을 통해 UHPFRC의 인장강화 및 압축연화 효과를 계수로 정량화하여 도출하였으며, 개략적인 이축 면내 파괴기준을 제안하였다. 균열거동에 대해서도 실험적 연구가 이루어졌다. 또한 노치가 있는 3점 재하 휨실험을 통해 초기 균열 위치 및 부재 크기에 따른 균열 선단에서 미세균열에 의한 비탄성 구간의 크기 및 균열 진전방향, 그리고 크기 효과에 대해 알아보았다.

실험결과에 따른 UHPFRC 재료모델을 적용하여 부재 전단강도식을 유도하였다. 복부 면내 전단거동은 미세균열이 일정한 기울기를 가지고 확산되는 균일한 응력장으로 Rankine 구간으로 가정하였다. Rankine 구간은 쿨롱 파괴기준으로 설명 가능한 균질한 변형을 가지는 형태의 응력장이다. 하한계 이론 중 인장강도에 지배되는 경우를 부재 전단강도로 산정하였다. 사인장 균열에 의한 부재 파괴는 준 취성파괴로서 크기효과로 고려된다. 크기효과를 결정하는 부재 취성도는 부재특성길이와 재료특성길이의 비로 제안되었다. 재료특성길이는 파괴역학 변수로서 재료계수로 제안된 값이고, 부재특성길이는 소성이론에서 가정된 미세균열에 의한 균일한 응력장의 인장지배길이이다. 취성계수는 프리스트레스 등에 의해 부재 단면에 압축력이 작용할 경우 보정될 수 있다. 제안된 식은 직접 수행한 부재 실험결과를 포함하여 전단철근이 없는 UHPFRC I-형 보 44개 데이터를 비교하여 검증하였으며, 현행 전단강도식에 비해 전단경간비, 유효깊이 등의 변수에 대해 정확하게 예측하는 것으로 나타났다.

주요어 : UHPFRC, 전단강도, 준취성파괴, 소성이론, 파괴역학, 크기효과
학 번 : 2012-30151